THE SEQUENCE STRATIGRAPHY OF THE EAST CHINA SEA CONTINENTAL MARGIN (LATE PLEISTOCENE TO PRESENT)

Jeffrey Dennis Warren

A Dissertation submitted to the faculty of the University of North Carolina at Chapel Hill in partial fulfillment of the requirements for the degree of Doctor of Philosophy in the Department of Geological Sciences.

Chapel Hill
2006

Approved by

Advisor: Dr. Louis R. Bartek III

Reader: Dr. John M. Bane

Reader: Dr. Joseph G. Carter

Reader: Dr. Robert V. Demicco

Reader: Dr. Lincoln F. Pratson

Reader: Dr. Paul P. Wang

ABSTRACT

Jeffrey Dennis Warren:
The Sequence Stratigraphy of the East China Sea Continental Margin (Late Pleistocene to Present)
(Under the direction of Dr. Louis R. Bartek III)

The East China Sea continental margin is characterized by abundant sediment supply, high energy, and a unique shelf physiography – a fairly shallow shelf with a low gradient, extreme width, and deep shelf-slope break. Three sequences are chronologically constrained by core data in the shallow strata from the late Pleistocene to present. Regional seismic surveys, collected as part of a broader investigation, provide unique observations unavailable to previous studies. A revised stratigraphy is presented that provides an alternate stratigraphic framework and, in the process, clarifies existing ECS stratigraphic nomenclature. In these strata, the lowstand fluvial systems, prior to oxygen isotope stage 4 do not incise the East China Sea continental margin. Instead, they comprise laterally (>400 km) and vertically (>40 m) extensive sand sheets interpreted as low-energy and low-sinuosity fluvial braidplains dominated by bed load. It is suggested in this paper that the rare nature of lowstand unincised fluvial systems (LUFS) are related to the rare nature of the extreme depositional boundary conditions forming the LUFS on continental margins (i.e., low gradient, deep shelf-slope break, abundant sediment supply). Extensive (>100 km), unincised fluvial sheet sands resembling the LUFS from the ECS margin are preserved in foreland basins throughout the Phanerozoic. Because this stratal architecture is similar to the LUFS preserved on the ECS margin, it may have been created under similar depositional

conditions. In order to better understand stratal sensitivity under these conditions, a three-dimensional, forward simulator (*fuzzy*PEACH) was developed. In this investigation, numerous scenarios of eustasy, tectonic subsidence, and sediment influx were simulated. The various rates and magnitudes of eustatic fluctuations may also be used as a proxy for the effect of margin physiography on stratal geometry, although *fuzzy*PEACH allows the geometry to be user defined. *Fuzzy*PEACH simulations collectively uses only five FISs containing a total of 21 separate rules. These rules incorporate 15 variables and are defined by 47 fuzzy sets. Fuzzy logic was chosen for its ability to quantify subjectivity, by capturing the vagueness of linguistic terms, and assemble a robust fuzzy logic inference system, in relatively short order, that can describe complex, nonlinear relationships.

To Mags – thanks.

If it’s not a good time, it’s good story.

ACKNOWLEDGMENTS

The author would like to thank his advisor, Dr. Louis R. Bartek (LRB), for providing the opportunities to collect seismic data around the world and the provision of seamless financial support. Gratitude is also extended to the author's committee for their time, critical review, and overall support of the investigation. Specifically singled out are Drs. Robert Demicco and Paul Wang for their patience and time teaching fuzzy logic modeling and fuzzy logic theory, respectively. The overall financial support for the regional East China Sea study, of which this dissertation is a subset, was provided by the Office of Naval Research (grants N00014-93-1-0921, N00014-96-0995, N00014-97-1-0382, N00014-99-1-0602, N00014-00-1-0275, N00014-01-1-0918 and N00014-03-1-0190 awarded to the author's advisor LRB). The utilization of the Kingdom Suite seismic interpretation and visualization software was made possible by an additional grant to LRB by Seismic Micro-Technology, Inc. The author was partially funded through the Department of Geological Sciences' Martin Trust Fund and the Graduate School Dissertation Completion Fellowship, both at the University of North Carolina at Chapel Hill. On a more personal note, the author wishes to recognize the many friends and family members who offered support throughout the entire dissertation. Special plaudits are reserved for the author's wife, Missy, who truly made it all possible with her encourgament, patience, selflessness, and love.

PREFACE

In order to facilitate a timely dissemintation of the research presented in this dissertation, each of the three chapters represent a complete manuscript fpr submittal to a peer-reviewed publication. The standalone format requires the citation of figures, tables, and referencesto be specific to that chapter. Because of the inter-related nature of the overall investigation, many of the figures, tables, and references appear in more than one chapter and create minor, internal redundancies in the dissertation as a whole.

TABLE OF CONTENTS

Page

LIST OF FIGURES

LIST OF TABLES

CHAPTER 1

SEQUENCE STRATIGRAPHIC FRAMEWORK AND DEPOSITIONAL PROCESSES OF THE EAST CHINA SEA CONTINENTAL MARGIN (LATE PLEISTOCENE TO PRESENT)

1.0 INTRODUCTION

Recent investigations of the shallow stratigraphy on the East China Sea (ECS) continental margin successfully utilized seismic and sequence stratigraphic concepts (Yang, 1989; Bartek and Wellner, 1995; Saito et al., 1998; Liu et al., 2000; Berne et al., 2002; Yoo et al., 2002; Wellner and Bartek, 2003). Results from these earlier studies provide data on lithofacies, age, and paleoenvironments constrained by fossil content, as well as third-party verification of interpretations presented in this paper. The high-resolution, 2-D seismic survey used in this investigation consisted of 14,000 linear km of profiles across an area of 300,000 km^2, i.e., larger than previous studies combined. The regional extent of this dataset facilitates correlation to oxygen isotope stratigraphy, provides a link to global sea level change, offers an opportunity to determine the relative importance of eustasy and sediment supply, and allows a more comprehensive understanding of the recent geological history of the ECS margin. These observations lead to new interpretations that require stratigraphic revisions of prior studies. This paper introduces a nomenclatorial convention that takes advantage of both sequence stratigraphic and Quaternary oxygen isotope data, in an attempt to create a common nomenclature for the shallow strata on the ECS continental margin. This

approach correlates and unifies previous investigations and facilitates ongoing and future research.

The ECS contains a set of extreme geologic and oceanographic conditions: high sediment supply, high energy, and a unique basin physiography (i.e., wide margin, low gradient, and deep shelf-slope break). Each of these has been a factor in the formation of the stratal surfaces and sedimentary units well preserved in the shallow strata (<100 m) on the ECS margin (late Pleistocene and Holocene). These geologic features are easily imaged using seismic and chirp sonar techniques. Some of the earliest published investigations from the ECS include seismic acquisition and interpretation (e.g., Emery et al., 1969; Wageman et al., 1970). However, it was not until the late 1980s that investigators began integrating sequence stratigraphic concepts with seismic data to better understand the genetic relationships of depositional units and the controlling effects of relative sea level fluctuation. Identification of seismic reflection attributes (e.g., reflection geometry, amplitude, and lateral extent) and stratal termination patterns (e.g., downlap and erosional truncation) facilitates a logical subdivision of stratal units by bounding surfaces (sequence boundary, SB; transgressive surface, TS; maximum flooding surface, MFS). Three nearly complete sequences are observed in this investigation which span the last three sea level cycles (OIS 6 to OIS 1; 186 ka to present; Imbrie et al., 1984). These sequences can be subdivided into three fundamental systems tracts, i.e., lowstand systems tract (LST), transgressive systems tract (TST), and highstand systems tract (HST). In addition, a combination of subsidence and uplift is preserved within these stratal packages which indicates previously unreported, recent tectonism on an otherwise passive margin.

1.1 REGIONAL SETTING

The ECS overlies the eastern margin of the Eurasian plate where it converges with and overrides the Philippine plate. The ECS is an epeiric sea that covers an area of approximately 752,000 km^2, one third of which covers the Okinawa Trough. The Okinawa Trough reaches a maximum depth of 2,719 m and is a back-arc basin formed during the Miocene presently spreading at about 1-2 cm/yr (Park et al., 1998). The ECS continental margin is dominated by exogenic forces and is presently considered to be tectonically inactive (Weiling and Junying, 1989). Together, the continental margin and Okinawa Trough exhibit the fundamental shelf-slope-rise pattern typical of most passive continental margins (Heezen et al., 1959). ECS margin physiography is defined by a low gradient (0.23 m/km or 0.013°) and a deep shelf-slope break that occurs in present water depths between 150 and 192 m deep (average = 170 m; Wong et al., 2000). The portion of the ECS landward (west) of the shelf-slope break (460,000 km^2) is epicontinental with an average water depth of 72 m. The ECS has maximum dimensions of 1,300 km (north-south) by 740 km (east-west), and the underlying continental margin one of the broadest shelves in the world.

The stratal architecture observed in seismic profiles in this investigation indicates that the unique basin physiography of the ECS margin has remained similar throughout the late Pleistocene. For example, the paleo shelf-slope breaks are within 10 km (laterally) of present and indicate a similar width. The lack of major incision at each of these shelf-slope breaks signifies that the edge of the margin was fairly deep (>120 m) and consistently remained submerged during lowstands. A similar gradient is linked to seismic profiles showing stratal architecture with similar low-angle dips in addition to features that require a low gradient for deposition (e.g., lack of incision, lack of sedimentary bypass, homogenous nature in lateral

and vertical extent). These observations are important in that they provide a link between modern and late Pleistocene basin architecture. Further stratigraphic evidence, provided by a strong correlation between the vertical succession of seismic attributes and vertically repetitive seismic reflection attributes, also suggests a link between current and past depositional processes. Features such as tidal ridges present on the modern seafloor, as well as throughout the geological record imaged in seismic profiles (e.g., transgressions between OIS 2 and 1, 4 and 3, 6 and 5, and older), denote oceanographic and geologic conditions during the late Pleistocene were similar to those observed in the present. Therefore, a solid understanding of modern processes (e.g., fluvial input, ocean currents, sediment distribution), how they operate on the margin, and the stratigraphic response to these conditions, is helpful in deciphering the nature of depositional environments on the ECS margin during the late Pleistocene.

Variations in climate and RSL in the ECS region during late Pleistocene and Holocene glacial maxima, when the margin was subaerially exposed, also created depositional conditions that were distinctly different from those observed today. Correlation of the high-resolution seismic and core data from the ECS margin with regional (e.g., Yangtze River coastal plain and the Loess Plateau) and global (e.g., Greenland ice core) high-resolution, paleoclimate data also allows the reconstruction of depositional environments. It is important to distinguish between these two extreme depositional environments when interpreting the shallow ECS stratigraphy (i.e., warm and wet climate with an epicontinental sea versus cold and dry exposed margin), realizing that not all of these strata form under conditions similar to present. However, for those strata that do, the knowledge gained from the understanding of modern conditions, and the ability to extrapolate these observations into

the geologic record, is a valuable tool for understanding the stratigraphic response to depositional processes.

The high-energy environment of the present-day ECS is a complex interaction of oceanic and tidal currents as well as frequent, intense storm events. The general oceanic circulation pattern of the ECS and the adjoining Yellow Sea (YS) and Bohai Sea (BS) is driven by the warm (T=20° to 27° C; Yu and Hong, 1992) and highly saline (S=33 ‰ ; Yu and Hong, 1992) Kuroshio western boundary current, its offspring (e.g., Taiwan Warm Current, Tsushima Current, Jiangsu Warm or Yellow Sea Warm Current, Shandong Coastal Current, Jiangsu or Yellow Sea Coastal Current, and Changjiang Coastal Current), and a minor thermohaline component from the colder, sediment-laden freshwater discharge of the Yellow and Yangtze Rivers. The ECS, YS, and BS are geographically and hydrodynamically inseparable and are, therefore, considered one system (Bingxian and Hanli, 1982). Semidiurnal tidal currents between 20 cm/sec (weakest in BS) and 100 cm/sec (strongest near mouth of Yangtze River) are sufficiently strong in some areas to cause localized resuspension or bedload transport (Choi, 1980; Milliman et al., 1985). Approximately 7% of the global dissipation of tidal energy presently occurs in the shallow ECS/YS/BS system (Choi, 1980) and causes sea level fluctuations from 5 to 6 m in Taiwan and up to 11 m in Hangchow Bay southwest of Shanghai (Fairbridge, 1966).

The Asian monsoon draws in winds and moisture from the tropical Pacific and Indian oceans during the summer and exports very cold, strong winds from the Asian interior during the winter (Sarnthein and Wang, 1999). This weather system is responsible for a partial seasonal reversal of coastal currents in the ECS (Kang, 1984; Yanagi and Takahashi, 1993; Yanagi et al., 1996) as well as development of the region's frequent summer typhoons (storm

surges reaching 5 m above mean water level; Wang, 1980; Wang and Aubrey, 1987) and winter storms where winds and waves are intensified (wave heights reaching 4 m; Alexander et al., 1991). Storm-generated surface waves have the potential to rework (i.e., resuspend and redistribute) finer-grained sediments in water depths up to 100 m (Graber et al., 1989). Milliman et al. (1985) attributed winter storms as a major agent of resuspension for sediments from the Yangtze River.

The ECS receives an enormous sediment influx from the Yellow (a.k.a. Huanghe) and Yangtze (a.k.a. Changjiang) Rivers. The Yellow and Yangtze Rivers are the second and fourth largest river systems in the world, respectively, in terms of sediment discharge. Combined, these rivers deliver approximately 1.6×10^9 tons of sediment per year (Yellow = 1.08×10^9 tons/yr, Yangtze = 4.78×10^8 tons/yr), 10% of the total suspended sediment delivered by all rivers to oceans worldwide (Milliman and Meade, 1983). Transport of these sediments is aided by the Shandong and Jiangsu (Yellow) longshore (coastal) currents and the Changjiang (Yangtze) Coastal Water (Milliman et al., 1985). In addition to the Yellow and the Yangtze Rivers, many other smaller rivers flow into the ECS/YS/BS system from China, Korea, and Taiwan. Together, these rivers contribute approximately 5×10^8 t/yr (Figure 1.1; Qian and Dai, 1980; Chough and Kim, 1981; Milliman and Meade, 1983; Wang and Aubrey, 1987; Lee and Chough, 1989; Congxian et al., 1991; Milliman and Syvitski, 1992; Zhang and Li, 1996; Water Resources Bureau, 1997).

Figure 1.1. Geographic map of the East China Sea region with study area outlined by circle. Also shown (inset) are locations for geotechnical boreholes DZQ4 and YQ1 with respect to seismic profiles from survey grid as well as additional seismic profile locations and their respective figures. Bathymetry modified from Quanxing (1990). Major fluvial systems and current annual depositional rates into the East China, Yellow, and Bohai Seas. Data compiled from: a) Milliman and Meade, 1983; b) Qian and Dai, 1980; c) Wang and Aubrey, 1987; d) Zhang and Li, 1996; e) Congxian et al., 1991; f) Milliman and Syvitski, 1992; g) Chough and Kim, 1981; h) Lee and Chough, 1989; I) Water Resources Bureau, 1997.

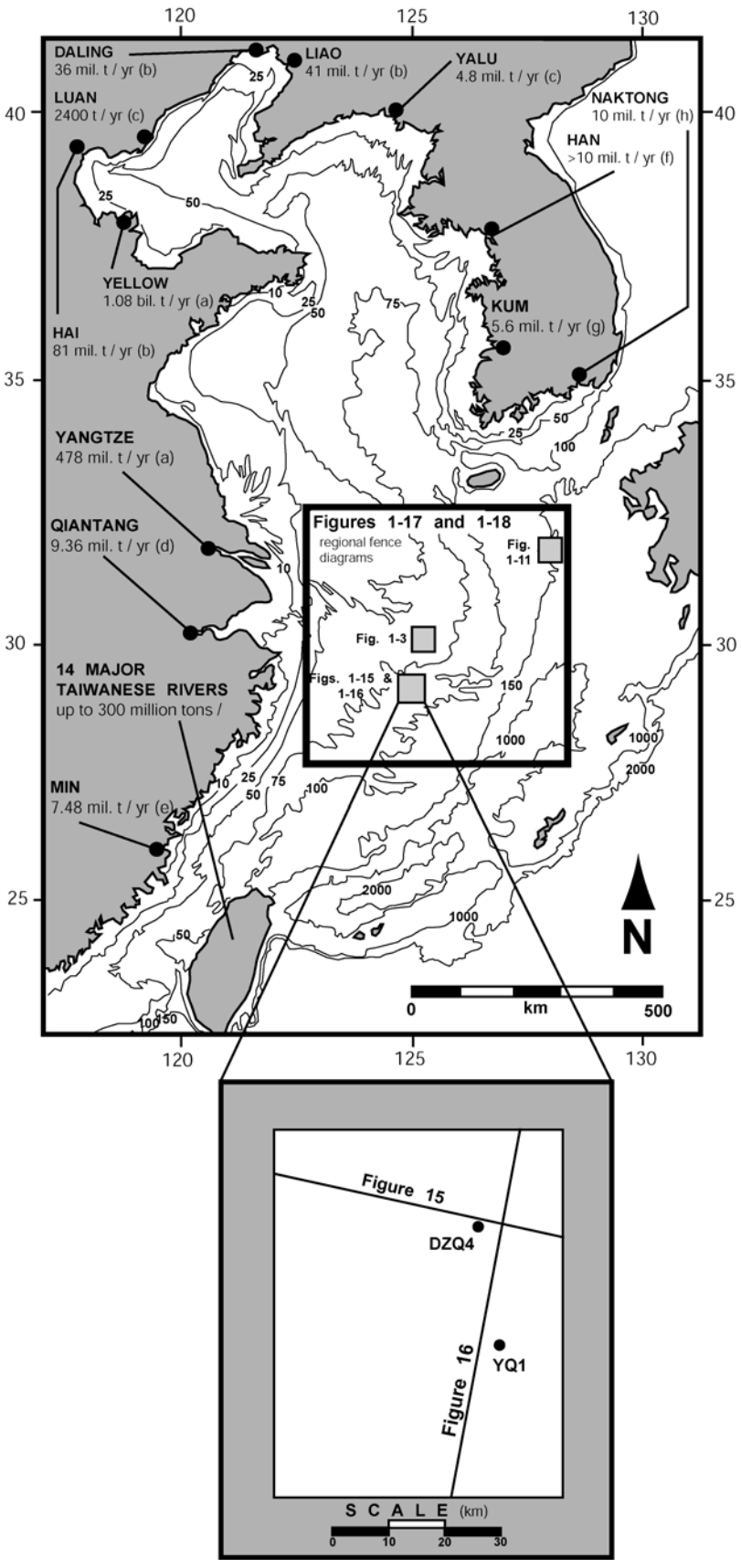
120
125
130
40
35
30
25
DALING
36 mil. t / yr (b)
LIAO
41 mil. t / yr (b)
YALU
4.8 mil. t / yr (c)
LUAN
2400 t / yr (c)
NAKTONG
10 mil. t / yr (h)
HAN
>10 mil. t / yr (f)
YELLOW
1.08 bil. t / yr (a)
KUM
5.6 mil. t / yr (g)
HAI
81 mil. t / yr (b)
YANGTZE
478 mil. t / yr (a)
QIANTANG
9.36 mil. t / yr (d)
14 MAJOR
TAIWANESE RIVERS
up to 300 million tons /
MIN
7.48 mil. t / yr (e)
Figures 1-17 and 1-18
regional fence
diagrams
Fig.
1-11
Fig. 1-3
Figs. 1-15 &
1-16
N
0
km
500
Figure 15
DZQ4
Figure 16
YQ1
S C A L E (km)
0
10
20
30

1.2 METHODS

Four seismic surveys conducted in the ECS (ca. 1993, 1996, 1999, 2000) acquired an overlapping grid of approximately 14,000 km of 2-D, high-resolution, single-channel seismic profiles. These data cover a 300,000 km^2 study area extending from 28° to 33° N latitude and 123° to 128° 30' E longitude (Figure 1.1). In addition to seismic acquisition, approximately 10,000 km of higher-frequency chirp sonar profiles were collected concurrently over portions of the same grid. These data provide sub-meter resolution of the uppermost strata that are often masked in seismic profiles by the acoustic source signature (i.e., bubble pulse). This extensive, nested-frequency dataset (i.e., 100 to 2,000 Hz for seismic and 2,000 to 16,000 Hz for chirp) facilitates a regional, seismic- and sequence-stratigraphic analysis of shallow subsurface strata (up to 150 m deep) deposited during the Holocene and late Pleistocene back to OIS 12 (approximately 500 ka). However, this investigation focuses on the strata from OIS 6 and younger and spans the past 186 ky (Figure 1.2).

Seismic data were acquired using a number of acoustic sources. Depending on sea state and/or water depth, sources varied between high-frequency boomer systems (500 to 2,000 Hz, up to 350 Joules), generator-injector (GI) air guns (50 in^3 and 210 in^3; 10 to 2,000 Hz), and water guns (15 in^3; 100 to 4,000 Hz). Shot intervals varied between 0.5 and 4 seconds depending on source and water depth. Single-channel hydrophone arrays were employed, and they contained between 10 to 20 elements with an average spacing interval of 1 meter. The average ship speed during acquisition was no faster than 5 knots. Digital data were recorded using the DelphSeismic acquisition system from Triton Elics International. Paper records (thermal plots) were also generated in real time from analog data that underwent

Figure 1.2. A) Primary eustatic sea level curve used in this study (from Pillans et al., 1998) based on duration proximity of the $\partial^{18}O$ core data on which the curve is based to the ECS (western Pacific, offshore Papua New Guinea; Shackleton, 1987). B) Relative sea level curve specific to ECS (from Saito et al., 1998). Both curves correlate well where they overlap but limited time span of ECS RSL data makes the use of this curve secondary.

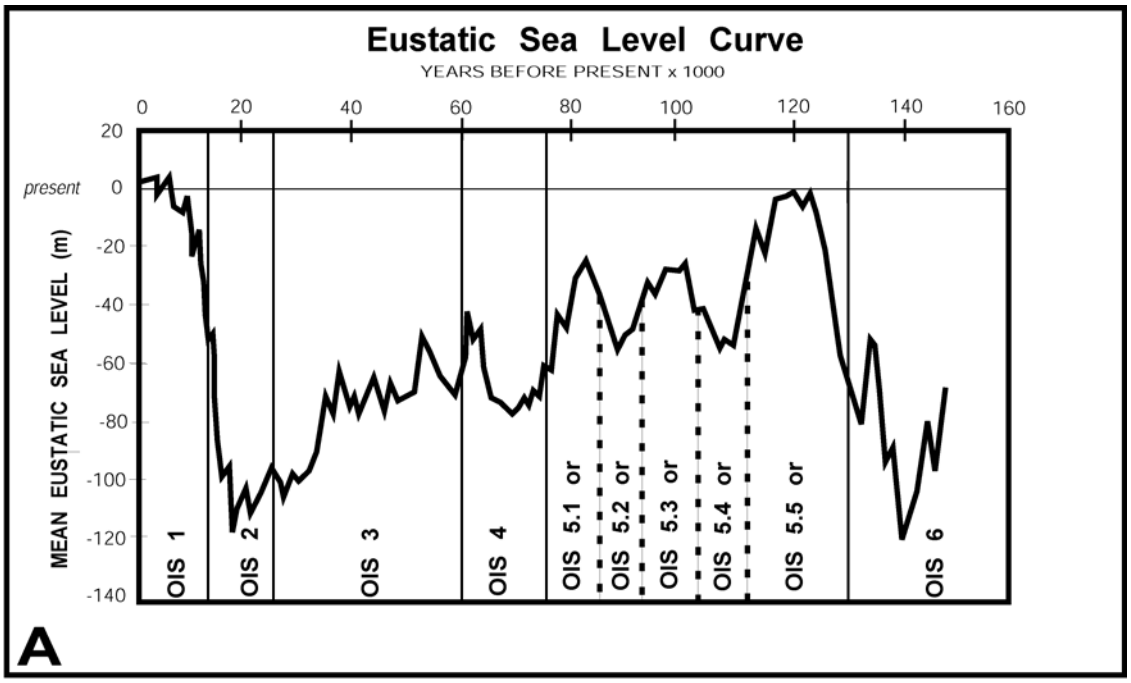
Eustatic Sea Level Curve
YEARS BEFORE PRESENT x 1000
0
20
40
60
80
100
120
140
160
20
present
0
-20
-40
-60
-80
-100
-120
-140
MEAN EUSTATIC SEA LEVEL (m)
OIS 1
OIS 2
OIS 3
OIS 4
OIS 5.1 or
OIS 5.2 or
OIS 5.3 or
OIS 5.4 or
OIS 5.5 or
OIS 6
A

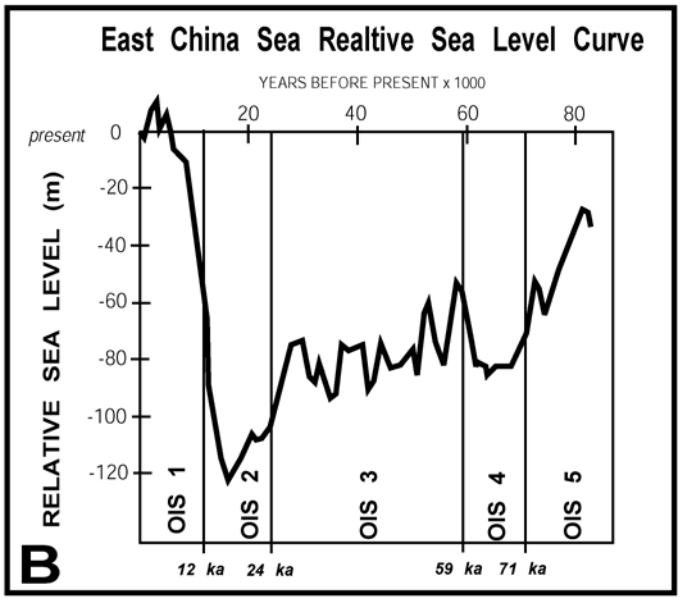
East China Sea Realtive Sea Level Curve
YEARS BEFORE PRESENT x 1000
20
40
60
80
present
0
-20
-40
-60
-80
-100
-120
RELATIVE SEA LEVEL (m)
OIS 1
OIS 2
OIS 3
OIS 4
OIS 5
12 ka
24 ka
59 ka
71 ka
B

minimal filtering and amplification. Digital data were processed with standard techniques such as bandpass filtering and gain using both DelphSeismic and ProMax (Landmark Graphics Corporation) software packages and interpretation was done both on paper and digital sections, the latter using the Kingdom Suite software package from Seismic-Micro Technology, Inc.

Velocity models were constructed in order to correlate the two-way travel time (TWT) of seismic stratigraphy to depth in cores. Due to the absence of borehole velocity data within the study area, approximate time-depth conversions use an average sediment velocity of 1,600 m/sec based on shallow (0 to 4 m) core velocities (Jim Miller, pers. comm.) and least square regression plots of a regional borehole sonic (acoustic velocity) dataset (Kong, 1998). Other investigations within the ECS use velocities ranging from 1,500 m/sec (Saito et al., 1998) to 2,000 m/sec (Wageman et al., 1970). Water column velocity of 1,500 m/sec is based on empirical data (Bark et al., 1964) for expected salinity and temperature distributions during acquisition (Yanagi et al., 1996).

The seismic survey geometries in this study were designed to incorporate two published borehole locations spaced within 20 km of each other: DZQ4 and YQ1 (Figure 1.1). These data provide the chronostratigraphic control to which the sequence stratigraphic framework is tied. Core DZQ4 was acquired by the Shanghai Marine Geology Bureau from the middle shelf region (29° 24.75' N, 125° 21.85' E) in 88.7 m of water. The borehole penetrated to a depth of 51.65 m below the seafloor (mbsf). A summary of the sedimentology, microfossils (foramanifera), nannofossils (coccolithophores), sporo-pollen assemblages, and oxygen isotope and thermoluminescence (TL) dates was originally reported by Tang (1996) and summarized by Saito et al. (1998), Liu et al. (2000) and Berne et al. (2002). Core YQ1 was

acquired by the Bureau of the Marine Geological Survey, Ministry of Geology and Mineral Resources of China on the middle shelf region in approximately 90 m of water. The core penetrated to a depth of 25.75 mbsf. The authors have been unable to locate published coordinates for the exact location of YQ1 but graphical approximations from published figures have placed it on the middle shelf region (29° 14' N, 125° 24' E; Yang, 1989; Berne et al., 2002). A summary of the sedimentology, microfossils (foraminifera), and sporo-pollen assemblages is presented by Yang (1989) and Berne et al. (2002).

Seismic facies attributes (*sensu* Mitchum et al., 1977), including the amplitude and lateral continuity of reflection geometries, and seismic termination patterns (i.e., downlap and erosional truncation) are used to create a sequence stratigraphic framework based on the three major bounding surfaces (SB, TS, and MFS) found within each sequence (e.g., Payton, 1977; Vail, 1987; Wilgus et al., 1988; Van Wagoner et al., 1988; Posamentier and Allen, 1999). The ages of the stratigraphic subdivisions are constrained by biostratigraphy and thermoluminescence dates from borehole DZQ4. The primary sea level reference used is from Pillans et al. (1998). The sea level curve was chosen based on its time span (0 to 150 ka) and the geographic proximity to the ECS of the core on which it is based (i.e., western Pacific, offshore Papua New Guinea; Shackleton, 1987). The relative sea level (RSL) curve of Saito et al. (1998) is specific to the ECS, correlates well to the curve presented by Pillans et al. (1998), but it spans a shorter interval of time (0 to 80 ka). Both curves are presented in Figure 1.2.

1.3 RESULTS

1.3.1 Stratigraphic Framework

Subsidence on the ECS margin varies between outer margin rates of 0.3 mm/yr (Quaternary; Berne et al., 2002) and inner margin rates of up to 4.4 mm/yr at the Yangtze delta depocenter (Holocene; Stanley and Chen, 1993). Aggradational stacking patterns of strata on the southern, outermost margin (see Figure 1.3) also indicate subsidence (rate of sedimentation < rate of accommodation; Van Wagoner et al., 1990). Uplift rates on northern and northwestern portions of the margin vary between 1.1 and 1.4 mm/yr along the east coast of the Korean peninsula (Quaternary; Kim, 1973) and 3 mm/yr in the YS (Holocene; Wang and Wang, 1982; Kim and Kucera, 2000). Progradational stacking patterns of strata on the northern, outermost margin (see Figure 1.3) are most likely related to lower rates of subsidence in this area (rate of sedimentation < rate of accommodation; Van Wagoner et al., 1990). High-frequency glacio-eustatic fluctuations during this same period are often greater than 1 cm/yr (Pillans et al., 1998; Saito et al., 1998). The low gradient of the ECS margin (0.013°) amplified the rapid Quaternary sea level fluctuations that translated into shoreface advance/retreat rates in the ECS greater than 3 m/yr. Together, these data illustrate the eustatic domination of the RSL signal on the ECS margin during the Quaternary.

The stratigraphic signatures associated with these sea level fluctuations are laterally extensive stratal termination patterns. Primarily erosional truncation and downlap, these surfaces are traceable in seismic profiles throughout the study area. Much of the stratigraphy on northern portions of the margin is uplifted and truncated by erosion. Furthermore, the shallow nature of the ECS (average depth = 72 m; Yunshan et al., 1996) creates a shallow seafloor multiple that obscures the seismic reflections of deeper strata. This limits the depth

Figure 1.3. High-resolution seismic profile illustrating the three seismic sequences and associated systems tracts (LST, TST, and HST) preserved in the strata on the central portion of the ECS margin. Sequences are referred to here as Seq 3 (oldest), Seq 2, and Seq 1 (youngest). See Figure 1 for location of seismic profile within study area.

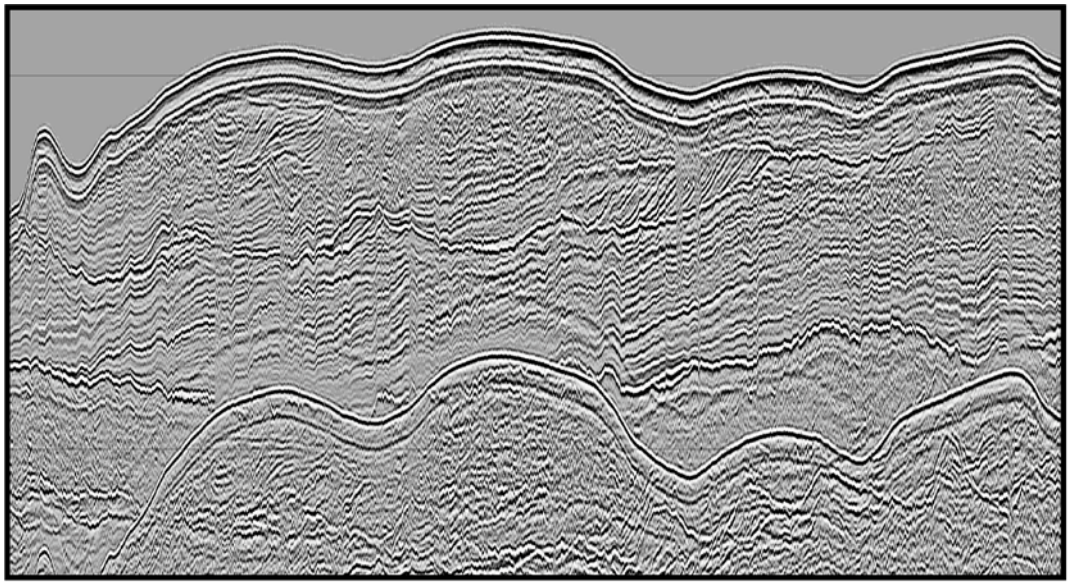

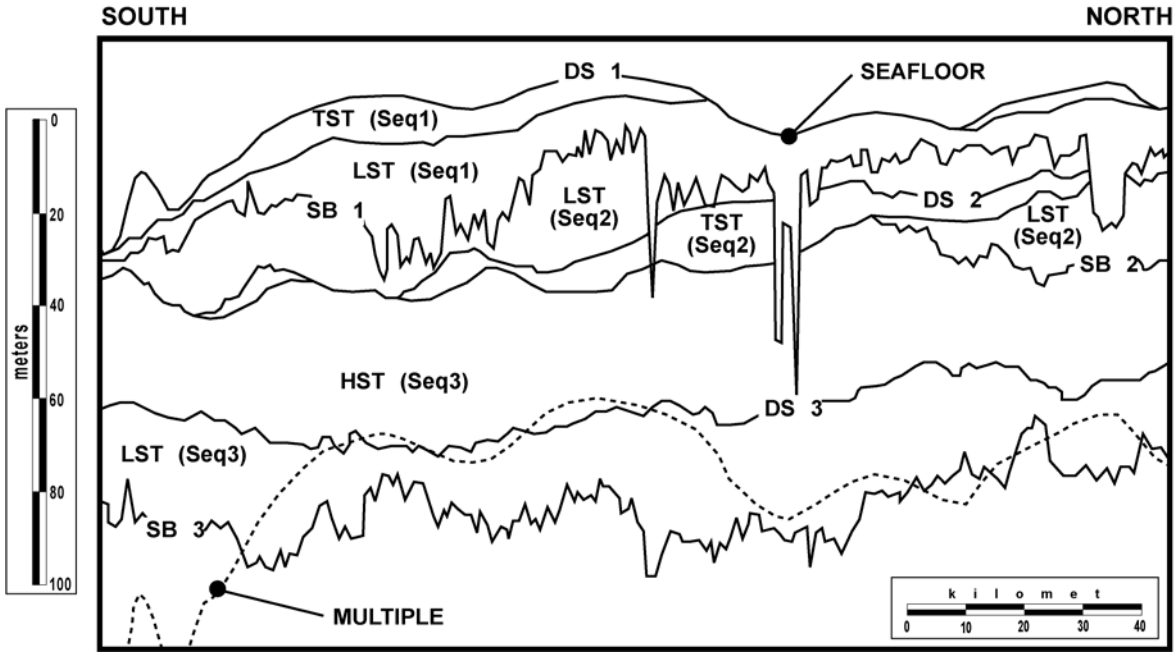
SOUTH
NORTH
DS 1
SEAFLOOR
TST (Seq1)
LST (Seq1)
SB 1
LST (Seq2)
TST (Seq2)
DS 2
LST (Seq2)
SB 2
HST (Seq3)
DS 3
LST (Seq3)
SB 3
MULTIPLE
meters
0
20
40
60
80
100
k i l o m e t
0
10
20
30
40

of investigation, especially on the inner margin where waters are often less than 40 m deep (i.e., multiple occurs <40 m below seafloor). Therefore, the most complete observations of the stratigraphy are from the southwestern portion of the study area, on the central and outer margin, where three complete sea level sequences are identified in the upper 50 m of strata as Seq 3, Seq 2, and Seq 1 (Figure 1.4).

Seq 3. The deepest sequence analyzed in this study (initially referred to here as Seq 3) is bound at its base by a relatively flat erosional surface that is initially identified here as erosional discontinuity 3 (ED 3), at least on inner and central portions of the margin (Figure 1.5). On the outer margin, the seismic unit directly above ED 3 thins and grades laterally into downlapping reflections that offlap in a basinward direction below ED 3 (Figure 1.6). Therefore, ED 3 on the inner and central margin is equivalent to the SB of Seq 3 (i.e., SB 3). The correlative conformity of SB 3 is the downlap surface (DS) underlying ED 3 on the outer margin (Figure 1.6). The upper boundary of the seismic unit above SB 3 is a high-amplitude DS (i.e., DS 3). This surface is the most laterally extensive seismic reflection in the dataset and extends across the margin (strike and dip profiles) for hundreds of kilometers (Figure 1.7). However, the downlapping reflections above DS 3, but below the overlying Seq 2, are confined to the inner and central portions of the margin and do not appear on the outer margin (Figure 1.7). Seq 3 is truncated by erosion on the inner margin as well as northern portions of the margin by the overlying SB 1. On portions of the inner margin, SB 3 becomes indistinguishable from SB 1.

Seq 2. The next significant stratal termination above DS 3 (and above Seq 3) is an erosional surface observed only on the central portion of the margin (initially referred to here as SB 2). The seismic unit here is on average 14 m thick, extends for approximately 50 km

Figure 1.4. Two dip-oriented seismic profiles from northern (top) and southern (bottom) portions of the margin. The stratal stacking patterns in the north are progradational and provide evidence of uplift. On the other hand, the stratal stacking patterns in the south are aggradational and provide further evidence of subsidence. While not the case here, these stratal patterns can also be indicative of a change in sediment supply (progradation = increase, aggradation = decrease).

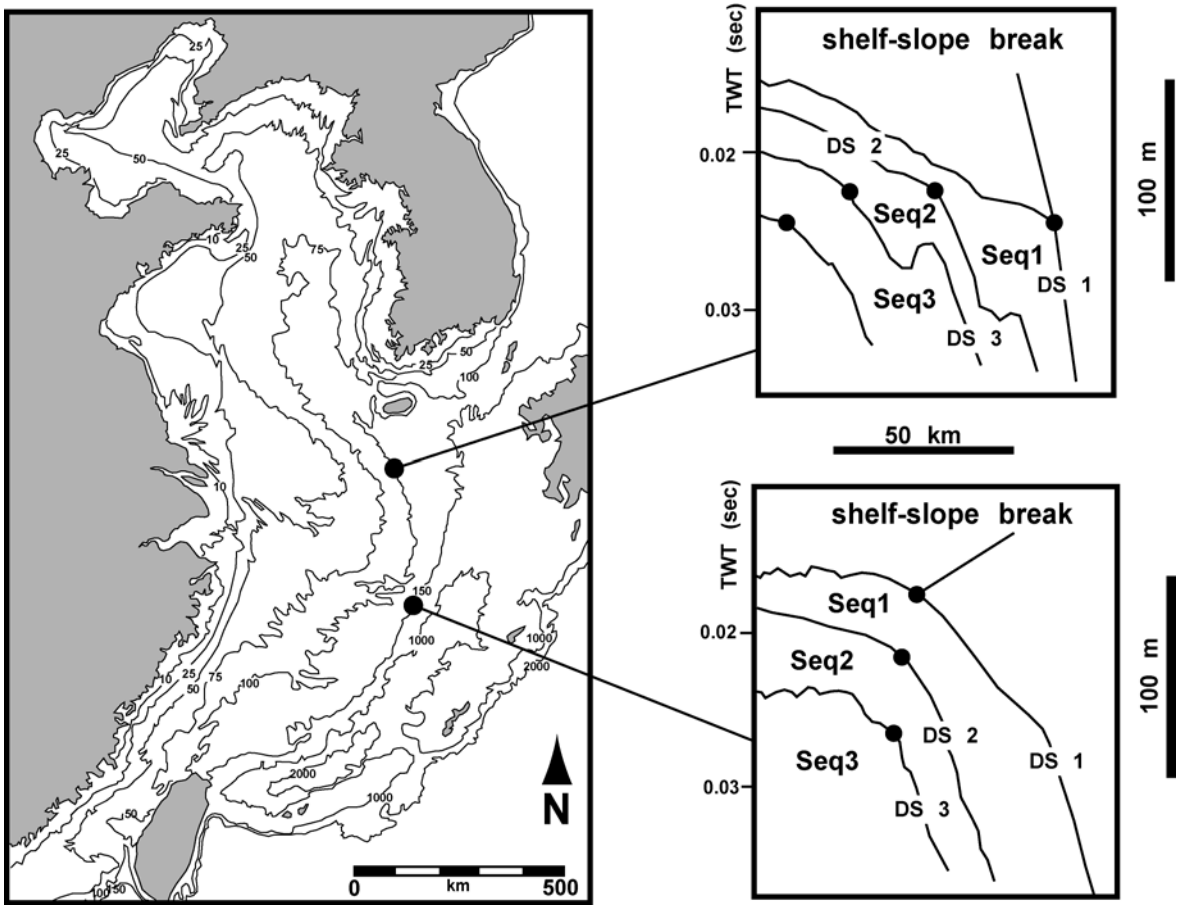
shelf-slope break
TWT (sec)
0.02
0.03
DS 2
Seq2
Seq1
Seq3
DS 1
DS 3
100 m
50 km
shelf-slope break
TWT (sec)
0.02
0.03
Seq1
Seq2
Seq3
DS 2
DS 1
DS 3
100 m
N
0
km
500

Figure 1.5. Structure map of SB 3 at the base of Seq 3 (also referred to as LST 6). On inner and central portions of the margin, this SB is an erosional disconformity (identitifed as ED 3) formed by extensive subaerial exposure of the margin and the fluvial processes that ensued. This SB grades laterally into a DS that is a correlative conformity on the outer margin found at the base of the submarine deltaic component of the fluvial system. Note the flat, planar nature of this SB and the lack of incision across the entire margin.

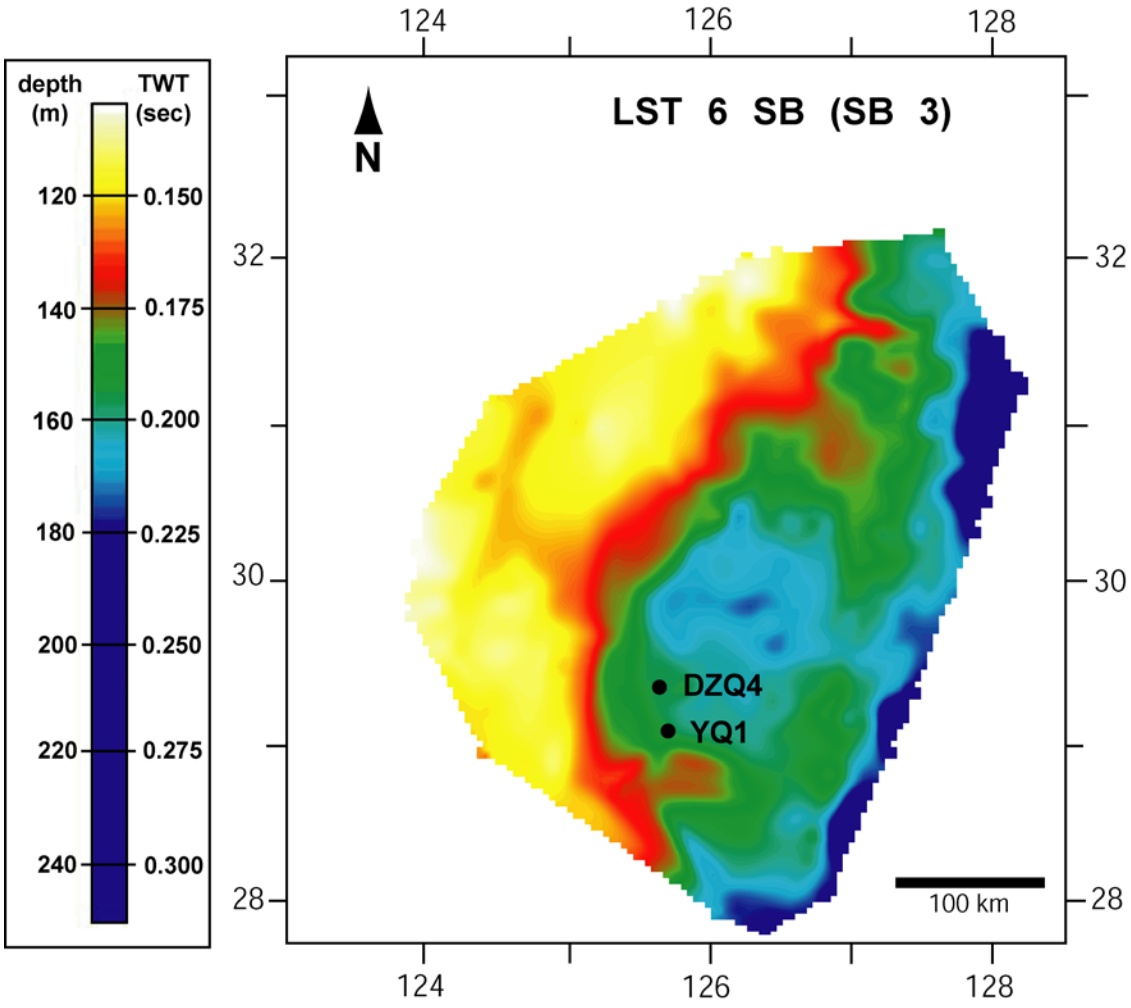
depth (m)
TWT (sec)
120
0.150
140
0.175
160
0.200
180
0.225
200
0.250
220
0.275
240
0.300
124
126
128
N
LST 6 SB (SB 3)
32
30
28
DZQ4
YQ1
100 km

Figure 1.6. A) Isopach map of SF CHAO for Seq 3 (also referred to as LST 6). Note the lateral extent of the strata across the margin in both strike and dip directions as well as how the unit thins basinward. B) Isopach map of SF DIP for Seq 3 (also referred to as LST 6). Note distinct concentration of sediment suggesting deltaic depocenters. Also note how this unit thins landward. C) Idealized lateral transition between landward SF CHAO (fluvial) and basinward SF DIP (deltaic) in Seq 3. These two units are stratigraphically equivalent.

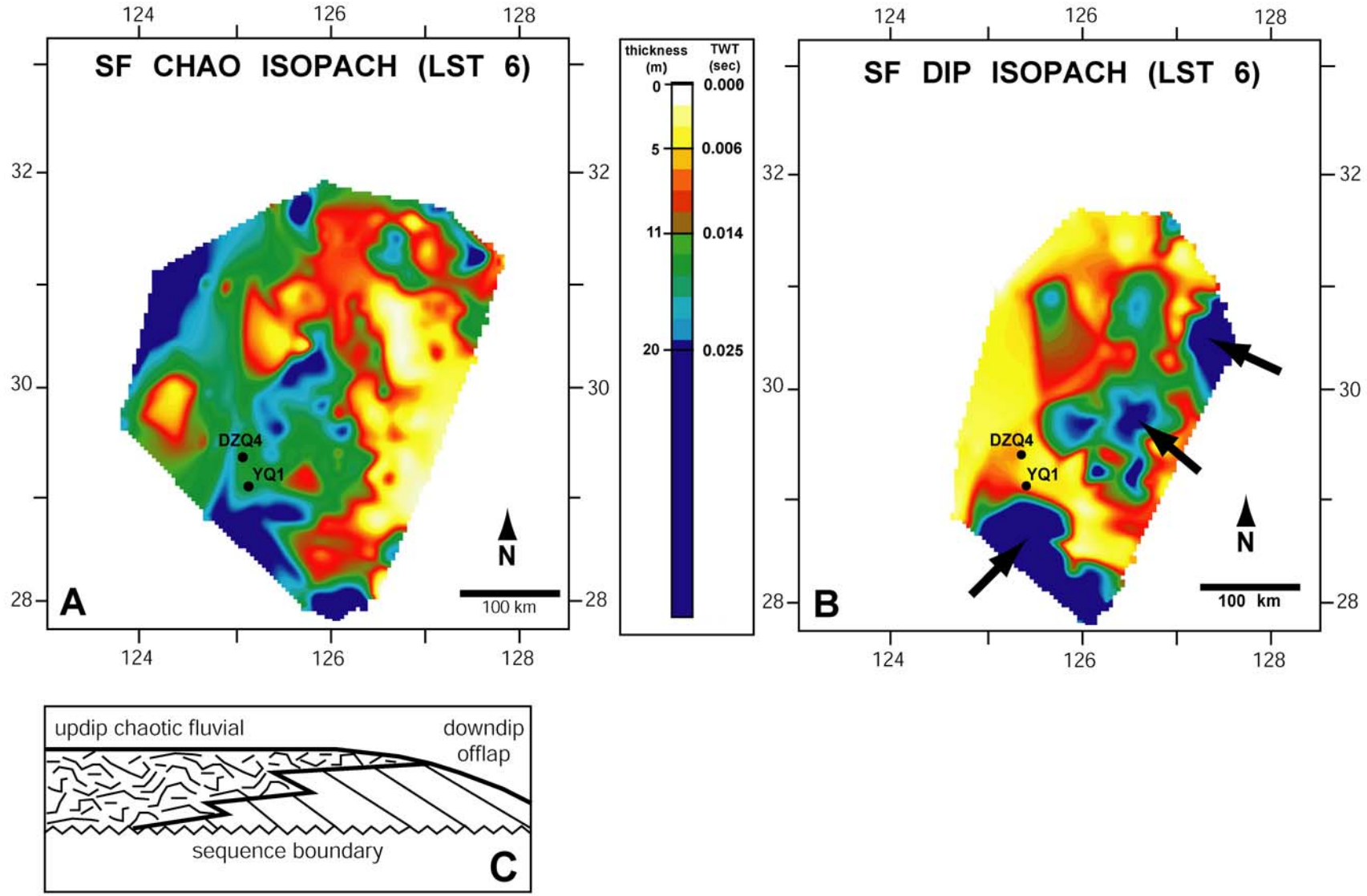
SF CHAO ISOPACH (LST 6)
SF DIP ISOPACH (LST 6)
thickness (m)
TWT (sec)
0
5
11
20
0.000
0.006
0.014
0.025
124
126
128
32
30
28
DZQ4
YQ1
N
100 km
A
B
updip chaotic fluvial
downdip offlap
sequence boundary
C

Figure 1.7. A) Structure map of DS 3 in Seq 3 (also referred to as the MFS at the base of HST 5). Note the flat nature, planar nature of this surface across the entire margin. B) Isopach map of HST 5. SF FLAT dominates inner portions of the margin and SF DIP dominates central portions of the margin. Note lobate structure of HST and how it pinches out to the east and south. Thinning and disappearance of this unit to the north and west is due to erosional truncation from the overlying SB from LST 2.

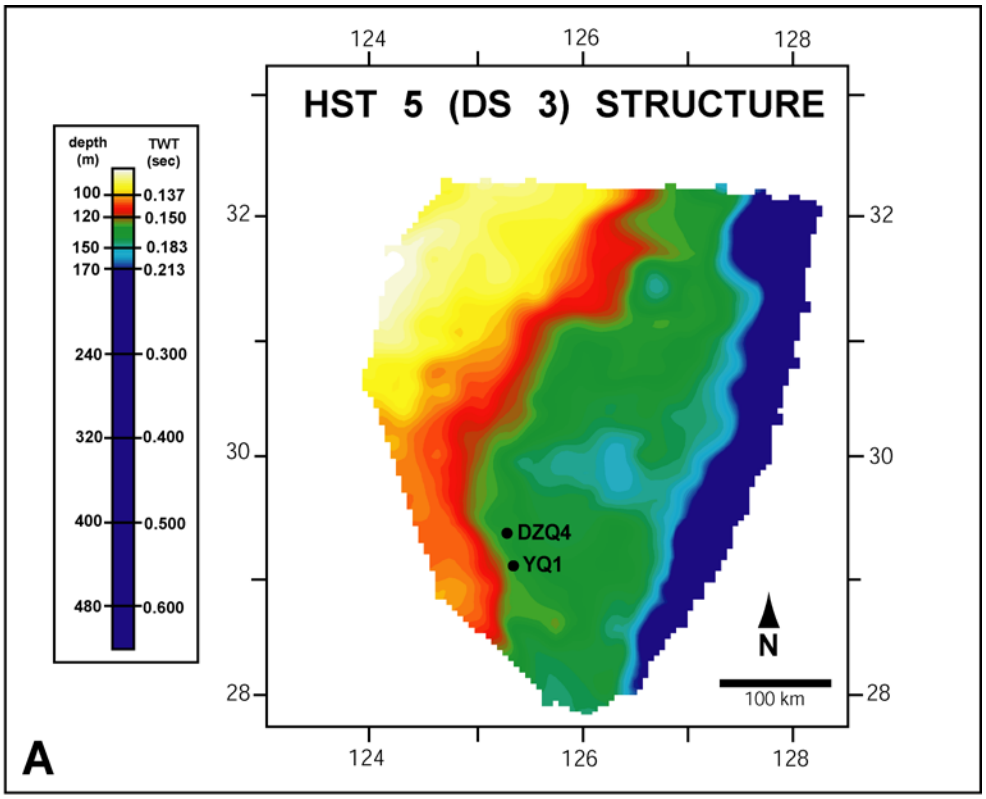
HST 5 (DS 3) STRUCTURE
depth (m)
TWT (sec)
100 0.137
120 0.150
150 0.183
170 0.213
240 0.300
320 0.400
400 0.500
480 0.600
124
126
128
32
30
28
DZQ4
YQ1
N
100 km
A

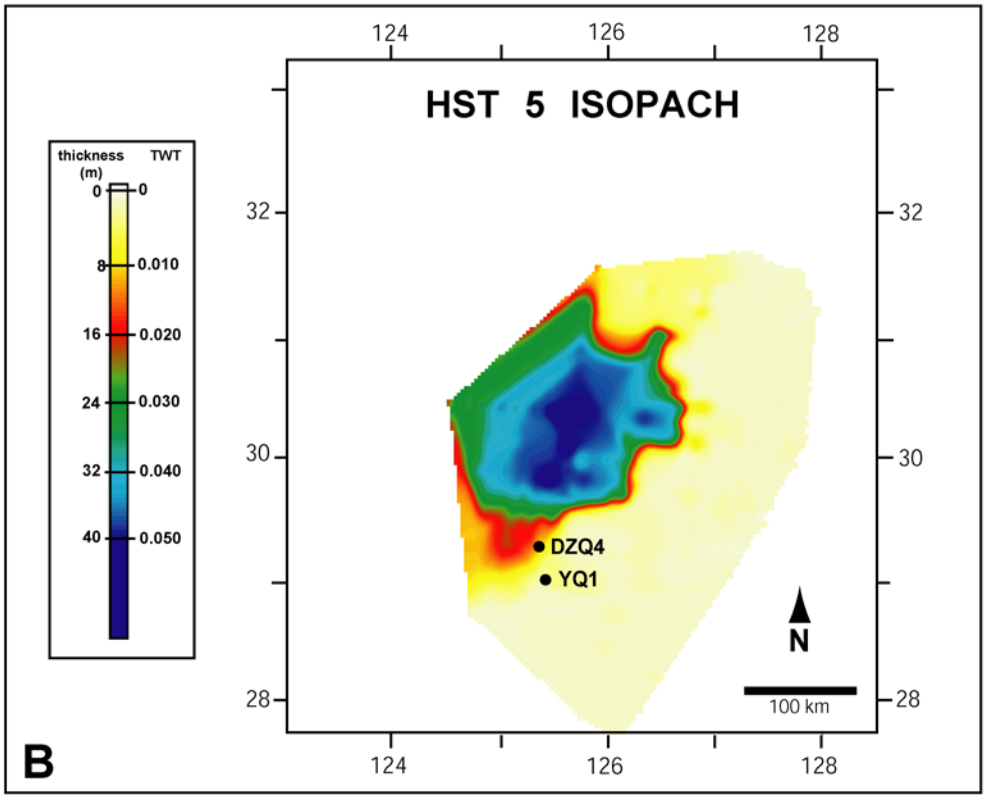
HST 5 ISOPACH
thickness (m)
TWT
0 0
8 0.010
16 0.020
24 0.030
32 0.040
40 0.050
124
126
128
32
30
28
DZQ4
YQ1
N
100 km
B

in all directions, and then thins rapidly to the point where they are resolved seismically as a single, high-amplitude reflection. Where it is of consistent thickness, this seismic unit (Seq 2) is bound on top by a high-amplitude DS (DS2). Where the unit pinches beneath DS 2, both SB 2 and DS 2 merge into an amalgamated, high-amplitude reflection that extends laterally across the margin for hundreds of kilometers (Figure 1.8). The seismic unit of downlapping reflections above DS 2, but below the overlying Seq 1, is thin on the central margin, primarily from erosional truncation by the overlying SB 1, and thickens (on average to 30 m) on the outer margin (Figure 1.9). Seq 2 also thins to the north where it is erosionally truncated by SB 1. On large portions of the innermost margin, Seq 2 is completely absent and Seq 1 sits directly atop Seq 2, many times with SB 3 and SB 1 virtually indistinguishable.

Seq 1. The youngest erosional surface in the dataset (initially referred to here as SB 1) occurs above DS 2 (and above Seq 2) but below the present-day seafloor. Unlike the flat nature of the erosional portion of SB 3 (i.e., ED 3), SB 1 is irregular and has extreme vertical fluctuations in depth (>50 m) that channelizes overlying seismic reflections of Seq 1 across the majority of the margin (Figure 1.10). On the innermost margin, Seq 1 truncates Seq 3, the stratal units become amalgamated, and the respective SBs become virtually indistinguishable. The seismic unit above SB 1 thins basinward, and the reflection of SB 1 becomes indistinguishable from the overlying seafloor on the outer margin. A high-amplitude DS 1 is observed above SB 1 on the inner and central margin but also becomes amalgamated with the seafloor on the outer margin. On the outermost portion of the margin (at the present-day shelf-slope break), a secondary DS not associated with an older sequence (i.e., Seq 2 or Seq 3) occurs below DS 1 and SB 1 (there, both amalgamated with the

Figure 1.8. A) Structure map of SB 2 at the base of Seq 2 (also referred to as LST 4). Note the deep relief on the central portions of the margin and the flat, planar nature of the surface across the rest of the margin. B) Isopach map of LST 4. The thick portion of this unit on the central portion of the margin corresponds to the incised valley fill of SF CHAO. Note that this is the only portion of the margin where the SB from LST 4 (a.k.a. SB 2) is overlain by SF CHAO. This thick unit has not been observed in prior investigations of the shallow strata on the ECS margin.

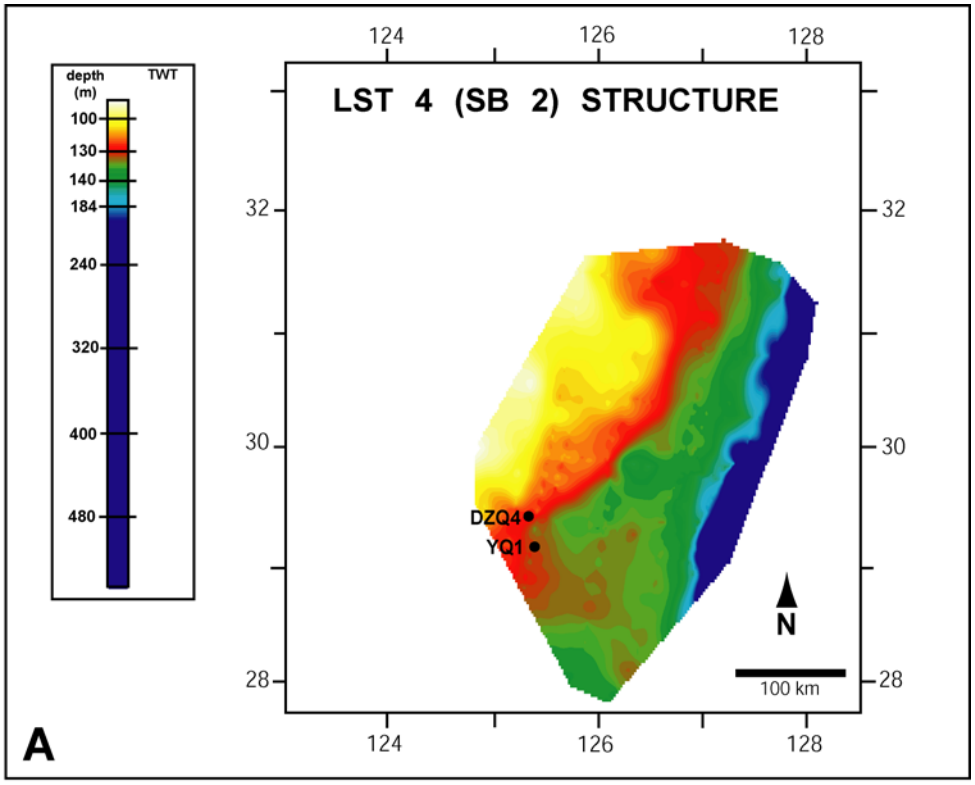
depth (m)
TWT
100
130
140
184
240
320
400
480
LST 4 (SB 2) STRUCTURE
124
126
128
32
30
28
DZQ4
YQ1
N
100 km
A

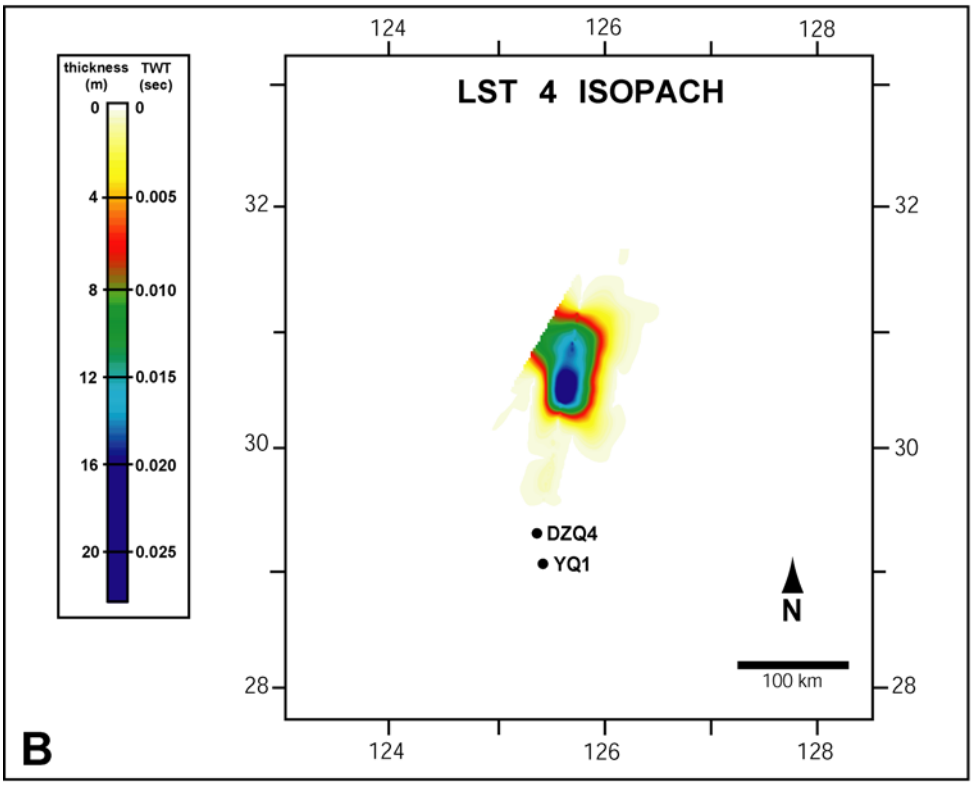
thickness (m)
TWT (sec)
0
0
4
0.005
8
0.010
12
0.015
16
0.020
20
0.025
LST 4 ISOPACH
124
126
128
32
30
28
DZQ4
YQ1
N
100 km
B

Figure 1.9. A) Structure map of DS 2 in Seq 2 (also referred to as the MFS at the base of HST 3). Note the horizon's progressively increasing depth on the outer margin, basinward of the underlying HST 5. B) Isopach map of HST 3. SF FLAT dominates the inner margin overlying HST 5, and SF DIP dominates the outer margin past the shelf-slope break. Note the majority of this unit is deposited basinward of the underlying HST 5 lobe.

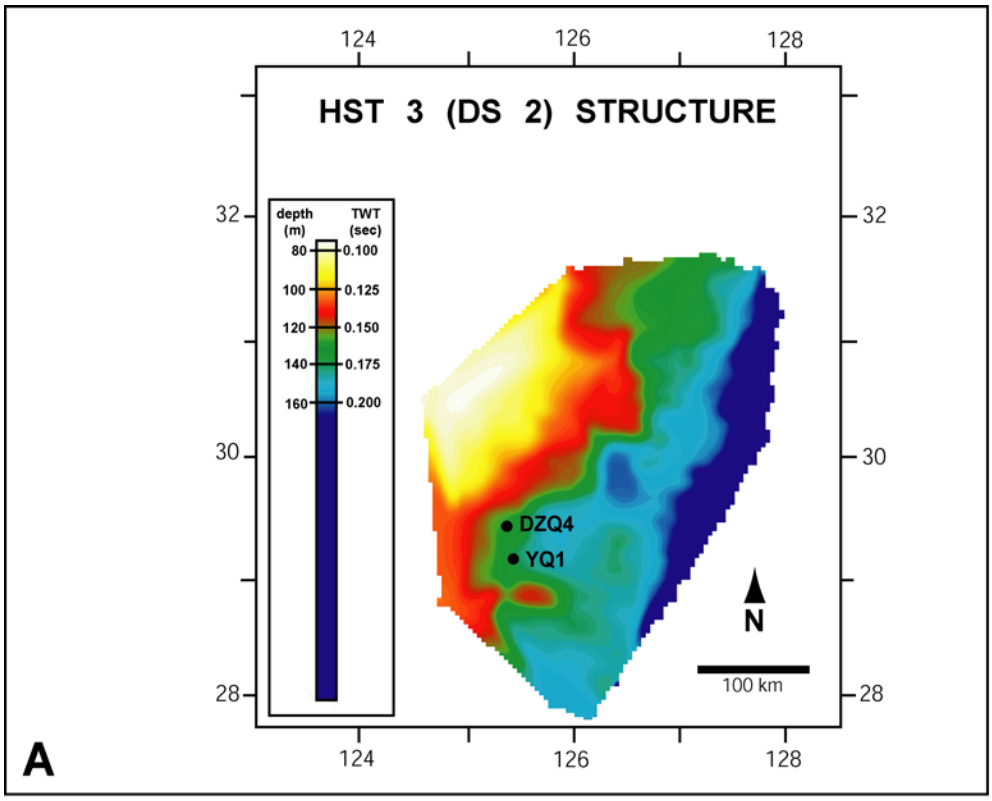
HST 3 (DS 2) STRUCTURE
124
126
128
32
30
28
depth (m)
TWT (sec)
80
100
120
140
160
0.100
0.125
0.150
0.175
0.200
DZQ4
YQ1
N
100 km
A

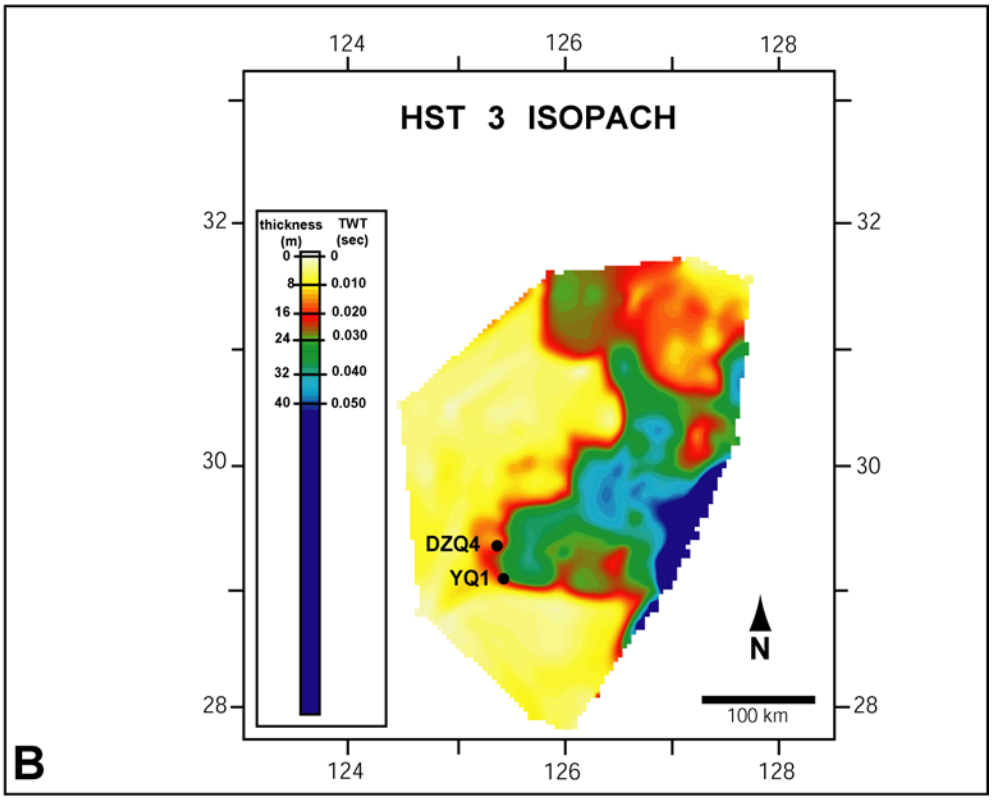
HST 3 ISOPACH
124
126
128
32
30
28
thickness (m)
TWT (sec)
0
8
16
24
32
40
0
0.010
0.020
0.030
0.040
0.050
DZQ4
YQ1
N
100 km
B

Figure 1.10. A) Structure map of SB 1 in Seq 1 (also referred to as LST 2). On inner and central portions of the margin, this SB is an erosional disconformity created by extensive subaerial exposure of the margin and the incisive fluvial processes that ensued. Similar to Seq 3, this SB grades laterally into a DS that is a correlative conformity on the outer margin found at the base of the submarine deltaic component of the fluvial system. Note the incised nature of this surface across the margin and how the depth of these incisions shallows on the outer margin. B) Isopach map of SF CHAO and SF MOUND in Seq 1 (also referred to as LST 2). SF CHAO dominates the reflection attributes across the entire shelf with the exception of the outermost margin. The two large, mounded complexes at the shelf-slope break are composed of SF FLAT and SF DIP (depending on whether a strike- or dip-oriented profile is observed).

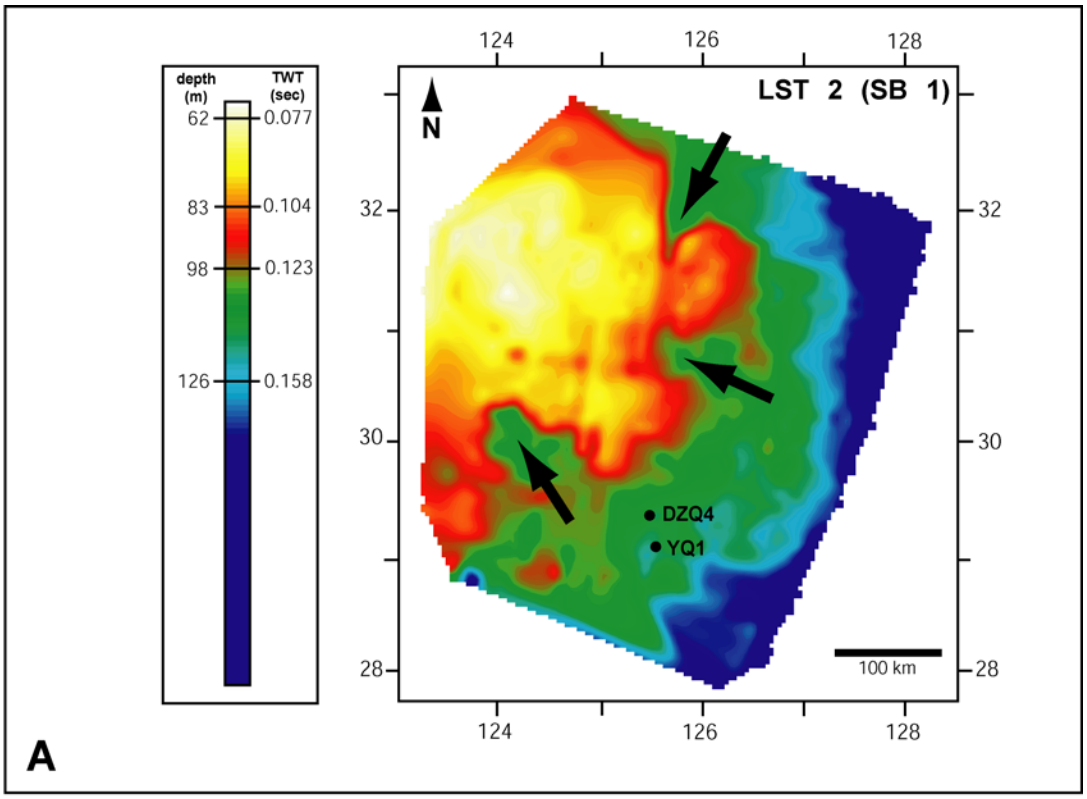
depth (m)
TWT (sec)
62
0.077
83
0.104
98
0.123
126
0.158
LST 2 (SB 1)
N
124
126
128
32
30
28
DZQ4
YQ1
100 km
A

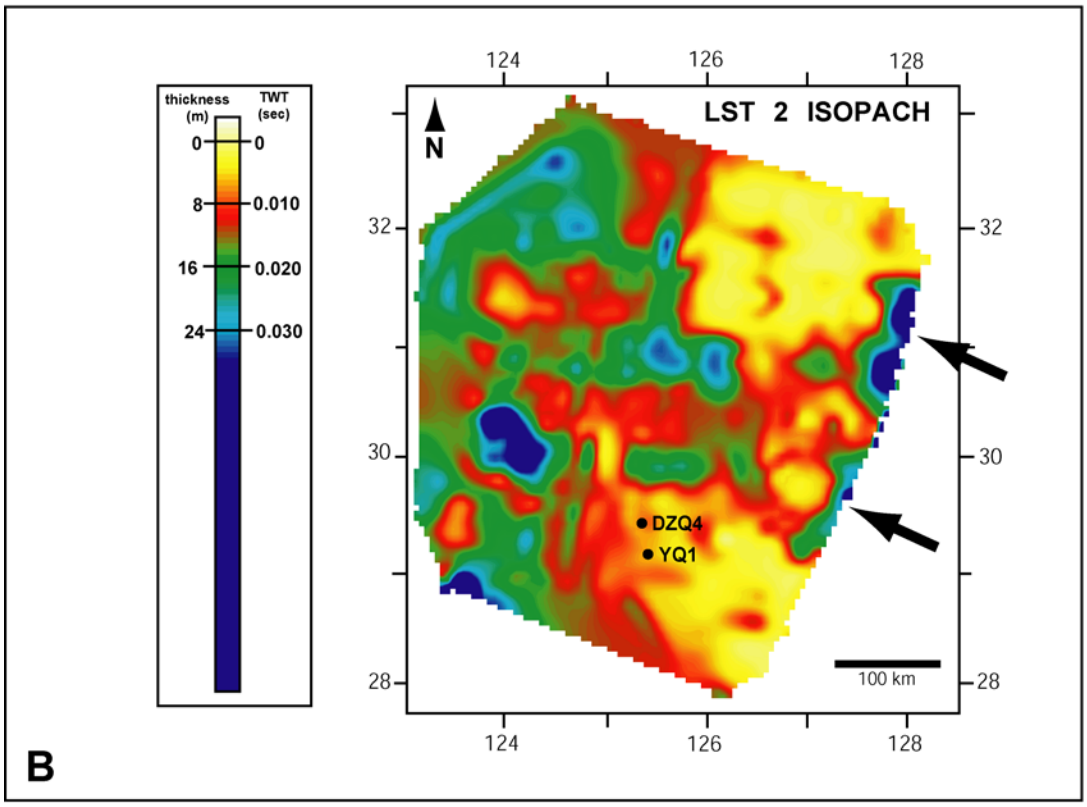
thickness (m)
TWT (sec)
0
0
8
0.010
16
0.020
24
0.030
LST 2 ISOPACH
N
124
126
128
32
30
28
DZQ4
YQ1
100 km
B

seafloor). At that location, the seismic unit (i.e., between this secondary DS and the seafloor) thickens into two mounded packages of downlapping reflections, each of which extends for approximately 100 km at an average thickness of 20 m (Figure 1.11). Similar to the basinward occurrence of the DS below ED 3 (the correlative conformity of SB 3 in Seq 3), this DS associated with Seq 1 is a candidate for the correlative and conformable portion of SB 1.

1.3.2 Seismic Facies

Lateral continuity, amplitude, and vertical frequency of reflections are used to classify seismic facies observed in the shallow seismic profiles from the ECS continental margin and are quantified in Table 1.1. Variations in these reflection attributes are subdivided into four distinct seismic facies (SF) categories: 1) chaotic (i.e., random and unorganized) reflections (CHAO), 2) flat-lying reflections (FLAT), 3) dipping reflections (DIP), and 4) mounded external geometries (MOUND). Idealized examples of each of these SF are shown in Figure 1.12. Other investigations in the ECS yielded similar observations classifying as few as three SF categories (Liu et al., 1998; Berne et al., 2002) and as many as eight SF categories (Yang, 1989).

SF CHAO exhibits variable reflection orientation, low and/or variable amplitude, and low lateral continuity for individual reflections. This facies reaches more than 50 m in thickness, but averages 15 m and has a high lateral continuity across the entire ECS margin. SF CHAO is underlain by an erosional surface (i.e., SB 1, 2, and 3) everywhere it is observed in the data. SF CHAO thins on the outer margin, sometimes becoming unidentifiable, yet it thickens on the innermost margin where the majority of the seismic reflections appear as SF CHAO and become vertically indistinguishable from younger and older seismic strata.

Figure 1.11. Detailed view of SF MOUND of Seq 1 (also referred to as LST 2) at the present-day shelf-slope break in both thickness (isopach) and cross section (seismic profile). These strata are equivalent to the SF CHAO strata of Seq 1 (LST 2) on the central and inner margin.

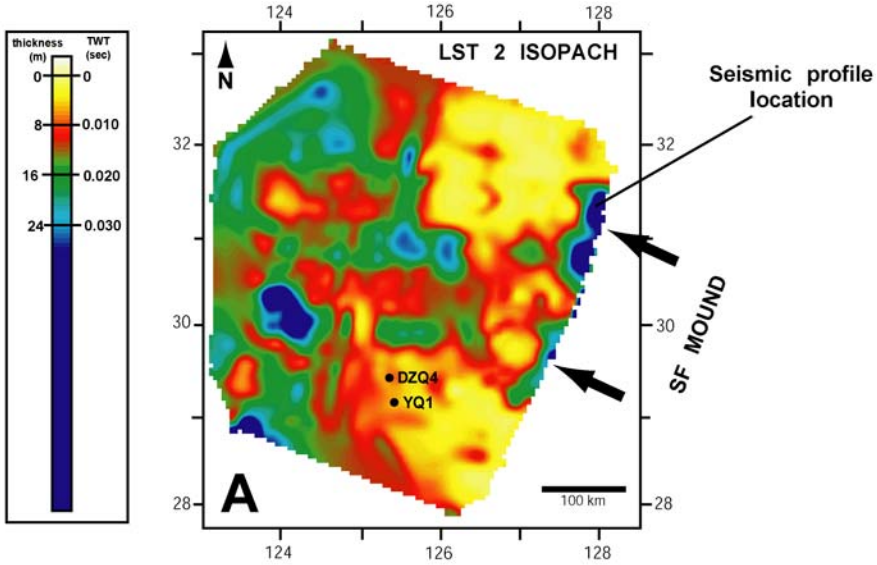
thickness (m)
TWT (sec)
0
0
8
0.010
16
0.020
24
0.030
124
126
128
LST 2 ISOPACH
N
Seismic profile location
32
30
28
SF MOUND
DZQ4
YQ1
A
100 km

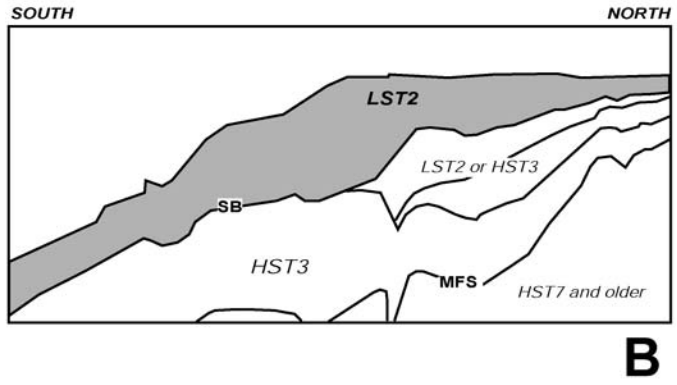
SOUTH
NORTH
LST2
LST2 or HST3
SB
HST3
MFS
HST7 and older
B

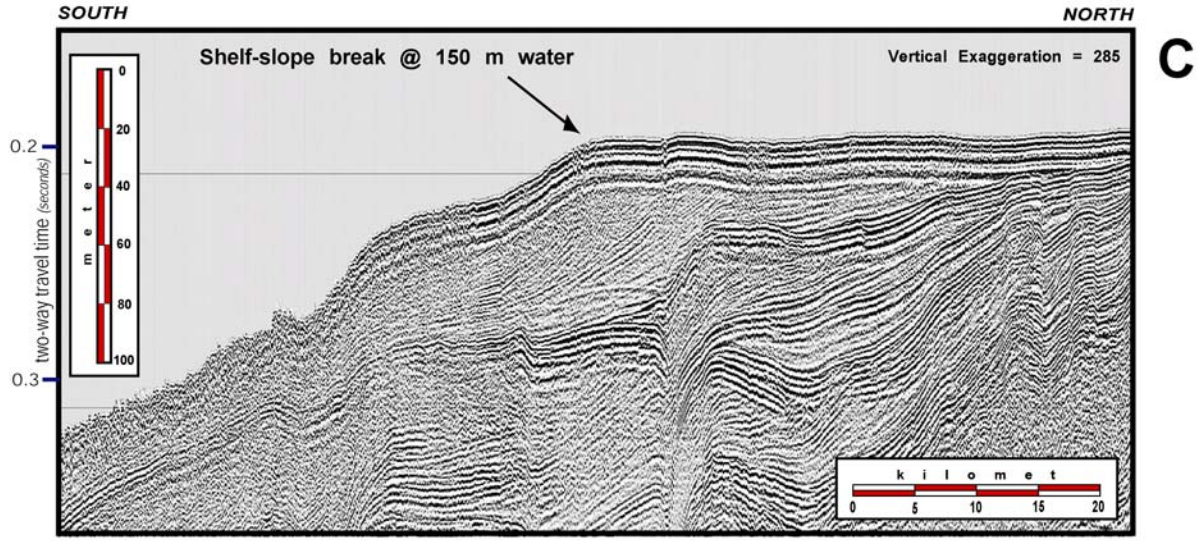
SOUTH
NORTH
Shelf-slope break @ 150 m water
Vertical Exaggeration = 285
C
0.2
0.3
two-way travel time (seconds)
meter
0
20
40
60
80
100
kilometer
0
5
10
15
20

Table 1.1. Quantification of three seismic facies attributes: 1) lateral continuity, 2) amplitude, and 3) frequency. This classification scheme was modified from Bartek et al. (1997).

LATERAL CONTINUITY STANDARDS	
(length reflection can be traced)	
HIGH	>200 km
MODERATE	10 to 200 km
LOW	<10 km

REFLECTION AMPLITUDE	
(GSA color scale)	
HIGH	black to dark gray
MODERATE	med to black
LOW	very light gray to med gray

VERTCIAL FREQUENCY STANDARDS	
(number of reflections in 10 msec)	
HIGH	6 and above
MODERATE	4-5
LOW	0-3

Figure 1.12. Examples of the four seismic facies (SF) types found in the shallow strata on the East China Sea continental margin: A) unconfined chaotic and confined chaotic (SF CHAO), B) dipping reflections (SF DIP), C) horizontally oriented reflections (SF FLAT), and D) mounds containing inclined reflections (SF MOUND).

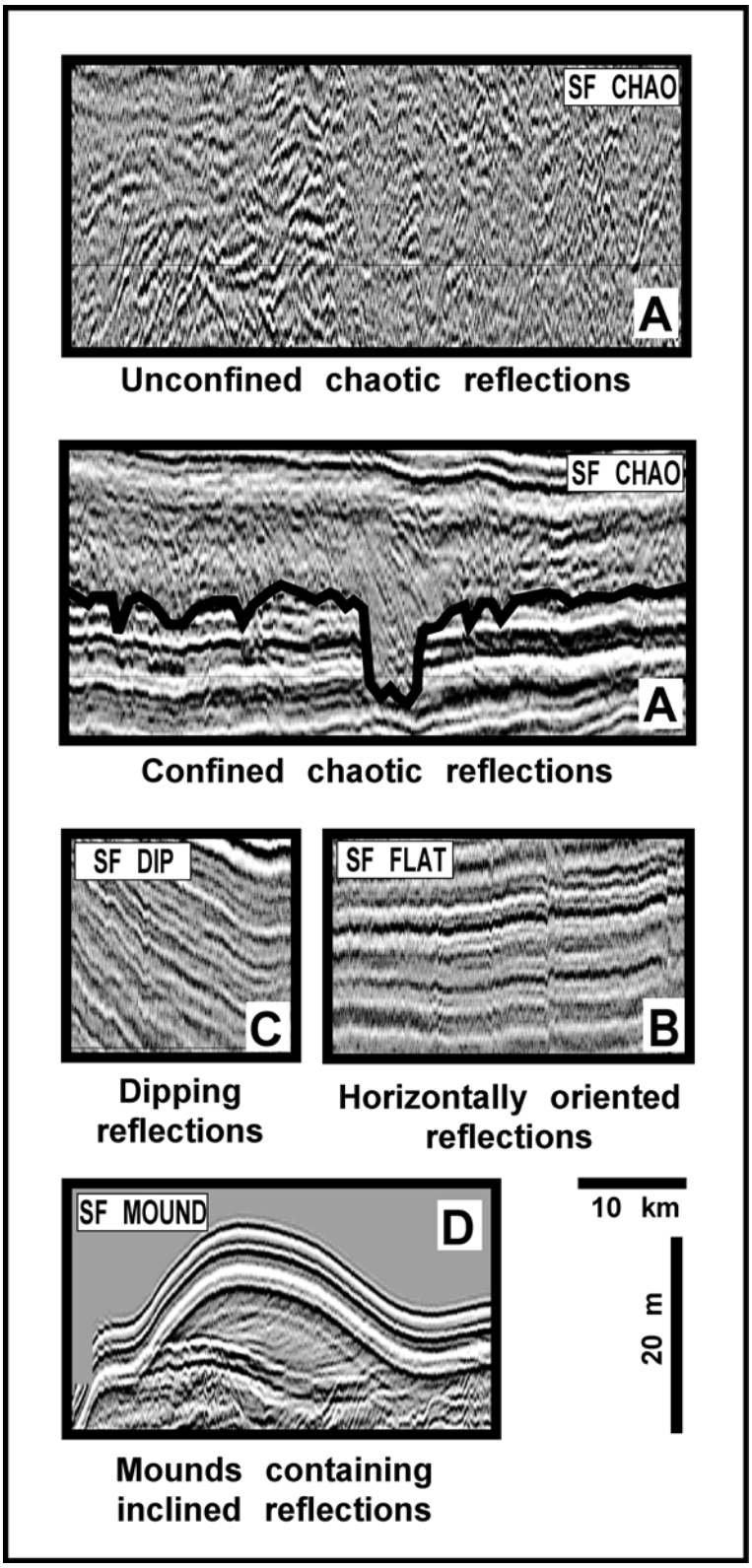
SF CHAO
A
Unconfined chaotic reflections
SF CHAO
A
Confined chaotic reflections
SF DIP
C
Dipping reflections
SF FLAT
B
Horizontally oriented reflections
SF MOUND
D
Mounds containing inclined reflections
10 km
20 m

The second seismic facies, SF FLAT, is characterized by horizontal and nearly horizontal (dip < 1°) reflections of moderate to high amplitude. These reflections have a moderate to high vertical frequency and a high lateral continuity. This facies reaches over 50 m in thickness, with an average thickness of 20 m, and has a moderate to high lateral continuity across the margin.

Reflections of SF DIP, the third seismic facies, exhibit the same attributes (amplitude, frequency, and continuity) as SF FLAT with the exception of higher dips that range between 1 and 5°. Overall, reflections tend to dip south and east and magnitudes generally increase basinward (east). Thickness of SF DIP can exceed 130 m on the outermost margin near the paleo shelf-slope break, but average 20 m. SF FLAT occurs landward (west) of, and grades laterally into, SF DIP. A lateral transition also occurs as SF CHAO thins basinward and grades laterally into SF DIP. SF FLAT and DIP are always underlain by a downlap surface (i.e., DS 1, 2, and 3).

External geometries of these three SF (CHAO, FLAT, and DIP) are fairly tabular and laterally extensive (> 100 km) across the ECS margin. However, there is also a fourth seismic attribute category that has a distinctive external morphology, consisting of externally mounded ridges, up to 25 km long and 30 m thick (SF MOUND). This facies is distributed primarily on inner and middle portions of the margin with extremely rare occurrence on the outer portion of the margin. SF MOUND also appears to be more extensive on the present-day seafloor, relative to deeper units. Yang (1989) reports that sand ridges on the modern seafloor trend ESE-WNW (NNE stoss dips of NNE of 0.5 ° and ESW lee dips of 2°) and are limited to water depths between 45 and 115 m. Internal reflections of SF MOUND are primarily dipping reflections that resemble clinoforms. Therefore, SF MOUND is always

underlain by a downlap surface (i.e., DS 1, 2, and 3). Berne et al. (2002) report dip magnitude calculations of internal reflections up to 6°, but we have only observed angles on the order of 2 to 3°. Internal reflections also contain a minor component of chaotically oriented reflections that resemble SF CHAO. Due to the bi-directional orientation bias associated with the survey grid geometry (i.e., profiles are either strike or dip oriented, generally north-south and east-west, respectively), it is difficult to assess whether these ridges, or their internal dipping reflections, exhibit any preferred orientation. The ridges of this seismic facies were addressed by Yang and Sun (1988), Saito et al. (1998), Liu et al. (2000), Li et al. (2001), and Park et al. (2003). Additionally, three unique occurrences of SF MOUND occur on a larger scale along the outermost portion of the margin. At this location, thickness exceeds 80 m, averages 30 m, and the upper boundary of these mounded units is the present-day seafloor. These external forms extend laterally for >100 km and internal reflections offlap basinward.

1.3.3 Chronostratigraphy

Numerous cores have been collected in the ECS, but many are poorly documented and/or lack detailed lithologic descriptions and reliable chronological data. Therefore, the two published boreholes used to constrain this study, DZQ4 and YQ1, are also those used to constrain the major seismic- and sequence-stratigraphic studies in the ECS during the past decade (e.g., Yang, 1989; Saito et al., 1998; Liu et al., 2000; Berne et al., 2002; Wellner and Bartek, 2003). Borehole DZQ4 lies within 1 km of dip-oriented seismic profile and within 4 km of a strike-oriented seismic profile. Borehole YQ1 lies within 20 km of a dip-oriented seismic profile and within 10 km of a strike-oriented seismic profile. These two locations are

located on the central portion of the margin approximately 20 km apart and project into seismic profiles well (Figure 1.1).

Core DZQ4. Descriptions of the 51.65 m core acquired from borehole DZQ4 and subsequent studies of lithology, micropaleontology, pollen and spores, as well as oxygen isotope and TL dating were reported by Tang (1996). A limited summary of these data were presented by Liu et al. (2000) and Berne et al. (2002). The stratigraphy in this area on the ECS margin is fairly simple and consists of six major stratigraphic divisions (Unit 6 to Unit 1, oldest to youngest). Correlation between core units and seismic profiles is relatively straightforward (Figure 1.13). For reasons discussed earlier, thickness and depth are converted from TWT using a velocity constant of 1600 m/sec (see Methods). Other constant velocity models of similar values (1600 m/sec, Liu et al., 2000; 1650 m/sec, Berne et al., 2002) also tie well to seismic data. Descriptions of these six core units presented in this paper are a compilation of observations from both Liu et al. (2000) and Berne et al. (2002) and are summarized in Figure 1.14.

Age constraints for Units 5 (87,764 ±4,388 at 35 meters below seafloor, or mbsf) and 3 (50,246 ±2,512 at24.4 mbsf and 46,903 ±2,313 at 20.9 mbsf) are provided by three thermoluminscence (TL) dates. The principle of TL dating is based on the ability of imperfections in the lattices of inorganic crystals, in this case mineral grains, to trap electrons and store absorbed radiation. Upon thermal stimulation, this energy is released in the form of thermoluminescent light. However, if a solid with occupied electron traps and the potential to produce TL is exposed to elevated temperatures or light, electrons can escape from their traps. This electron escape causes the latent TL signal to fade partially or completely (Wagner, 1998). The accuracy of this dating technique is sensitive to the influence of

Figure 1.13. The correlation between the six units from core DZQ4 and a nearby, dip-oriented seismic profile. Units 1 through 3 are stratigraphically equivalent in core YQ1. See Figure 1 for location within study area of core and adjacent seismic profile.

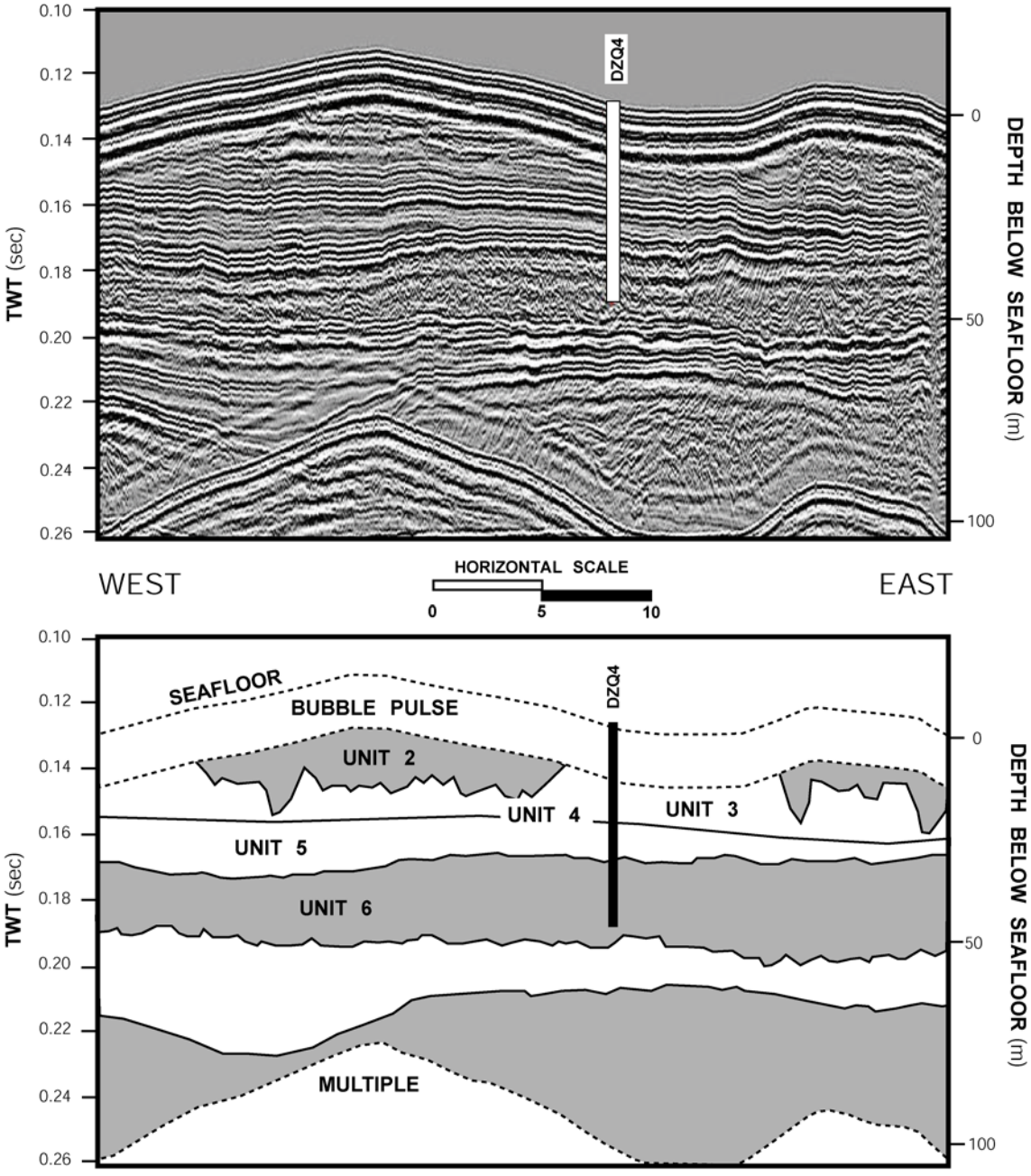
0.10
0.12
0.14
0.16
0.18
0.20
0.22
0.24
0.26
TWT (sec)
DZQ4
0
50
100
DEPTH BELOW SEAFLOOR (m)
WEST
HORIZONTAL SCALE
0
5
10
EAST
SEAFLOOR
BUBBLE PULSE
UNIT 2
UNIT 4
UNIT 3
UNIT 5
UNIT 6
MULTIPLE

Figure 1.14. Description of core DZQ4 compiled from Liu et al. (2000) and Berne et al., 2002 (stratigraphic column) with comparisons of stratal units and sequence stratigraphic interpretation.

BOREHOLE DZQ4

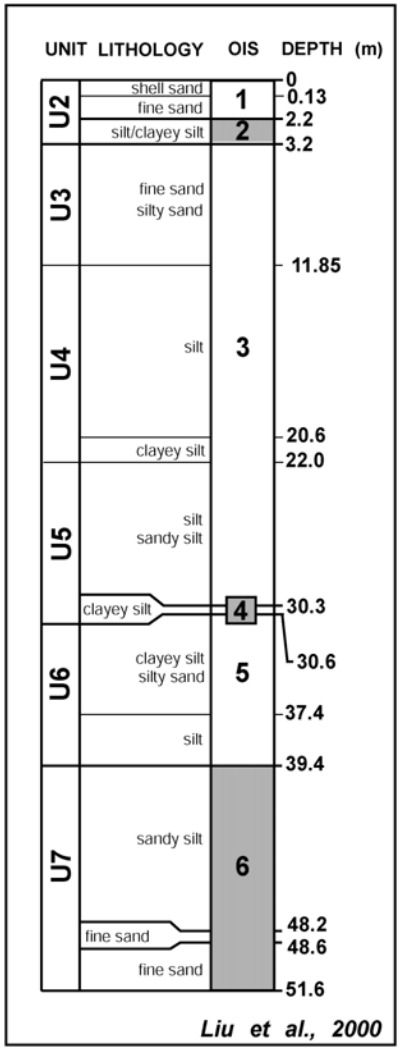

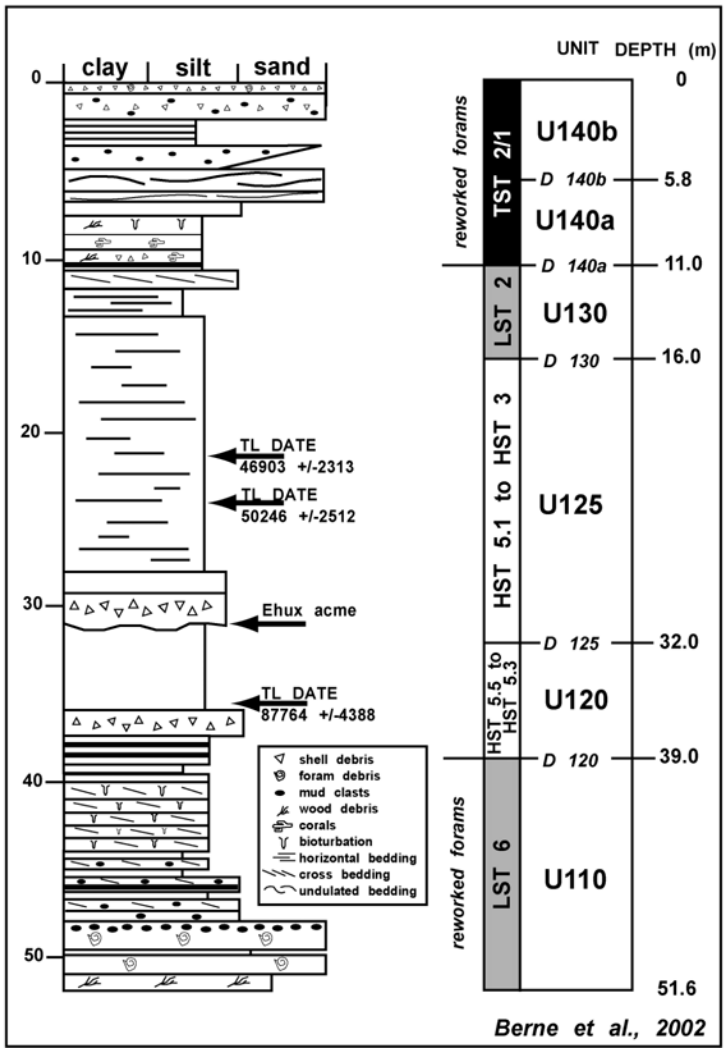

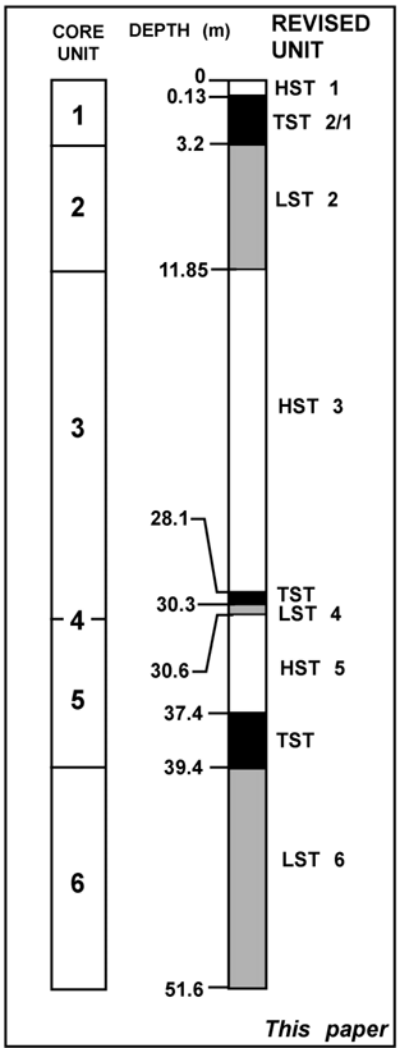

sunlight on grains after initial environmental exposure (Forman et al., 2000). To eliminate the impact of reworking and post-depositional exposure, Berne et al. (2002) only consider TL dates from stratigraphic units associated with high sedimentation rates. Therefore, only three of the TL dates reported by Tang (1996) are used, and only these three TL dates, associated with Units 5 (core DZQ4) and 3 (cores DZQ4 and YQ1), are presented in this paper. These strata are fine-grained intervals from the middle margin. Saito et al. (1998) provide multiple ^{14}C dates (between 25 and 50 ka) from piston cores throughout the ECS. These additional age constraints correlate to Unit 3 (DZQ4 and YQ1).

One additional chronostratigraphic datum exists at the *Emiliania huxleyi* (Ehux) acme biomarker, observed in core DZQ4 at 30.8 mbsf. This acme is time transgressive and occurred between 73 and 85 ka, based on latitude. Transitional zones are associated with 73 ka, and low-latitudes are associated with 85 ka (OIS 5.2 and 5.1 a.k.a. 5b and 5a). The first concern resides with data from Wang (1999) who calculated that the strengthening of winter monsoons during glacial times (i.e., OIS 4) reorganized sea circulation in the marginal seas of the western Pacific. In response, sea surface temperatures in both summer and winter months decreased, providing environments more similar to higher latitudes (i.e., earlier acme). Second, the open-ocean flora dataset of Thierstein et al. (1977), used to define the reversal in dominance between *Gephyrocapsa caribbeanica* and *Emiliania huxleyi,* is distinctly different from the flora found in the neritic environment of the marginal ECS. Both Okada and Honjo (1975) and Wang and Samtleben (1983/4) showed the floral assemblage in the ECS to be dominated by *Gephyrocapsa oceanica,* with *Emiliani huxleyi* of secondary importance. This is the opposite trend of the open ocean (i.e., Ehux dominates; Hine, 1990). Liu et al. (2000) and Berne et al. (2002) interpret the Ehux acme in core DZQ4

to occur between 80 and 85 ka. This 5-ky span occurs on the rising limb of sea level between OIS 5.2 (5b) and OIS 5.1 (5a). Using the same data of Thierstein et al. (1977), as well as that of Wang (1999), we interpret a transitional latitude and one closer to 73 ka. This age falls on the falling limb of sea level between the HST of OIS 5.1 (5a) and the LST of OIS 4. However, we also point out the nature of this boundary is tenuous at best. The questionable nature suggests further research is needed to constrain the relationship of the diachronous Ehux acme in the ECS.

Core YQ1. Descriptions of the 25.75 m core acquired from borehole YQ1 and subsequent studies of lithology, sporo-pollen and foraminifera analyses are originally presented by Yang (1989). No absolute age data such as TL and biozones are associated with this core. The stratigraphy in this area on the ECS margin is fairly simple and consists of three major stratigraphic divisions (Unit 3 to Unit 1, oldest to youngest). These numbered units correlate to, and correspond with, Units 1-3 in core DZQ4. In addition, correlation between units from core YQ1 and seismic profiles is relatively straightforward (Figure 1.15). For reasons discussed earlier, thickness and depth are converted from TWT using a velocity constant of 1600 m/sec (see Methods). Similar to DZQ4, correlation to nearby seismic profiles is still possible with relative ease even when higher-value velocity models are used (1700 m/sec; Yang, 1989). Descriptions of these three core units presented in this paper are a compilation of observations from Yang (1989) and are summarized in Figure 1.16.

1.3.4 Revised Stratigraphic Nomenclature

Results from earlier studies of the ECS continental margin provide data on lithofacies, age and paleoenvironments constrained by fossil content, as well as third-party verification of present interpretations. However, the regional extent of the present seismic dataset used in

Figure 1.15. The correlation between the three units from core YQ1 and a nearby, strike-oriented seismic profile. Units 1 through 3 are stratigraphically equivalent in core DZQ4. See Figure 1 for location within study area of core and adjacent seismic profile.

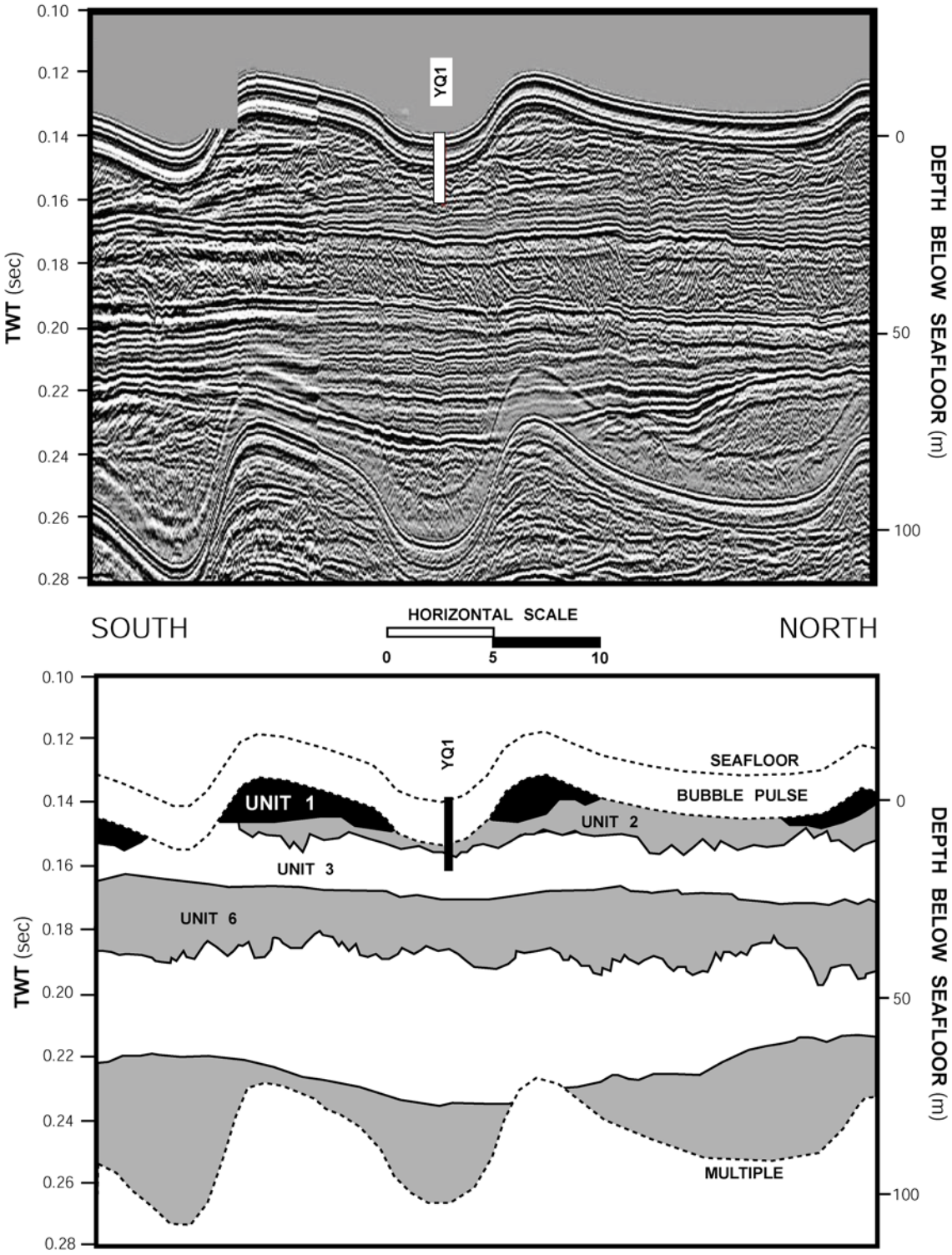
0.10
0.12
0.14
0.16
0.18
0.20
0.22
0.24
0.26
0.28
TWT (sec)
YQ1
0
50
100
DEPTH BELOW SEAFLOOR (m)
SOUTH
HORIZONTAL SCALE
0
5
10
NORTH
SEAFLOOR
BUBBLE PULSE
UNIT 1
UNIT 2
UNIT 3
UNIT 6
MULTIPLE

Figure 1.16. Summarized core description of core YQ1 from Yang (1989) with interpretive comparisons from this paper and Berne et al. (2002).

BOREHOLE YQ1

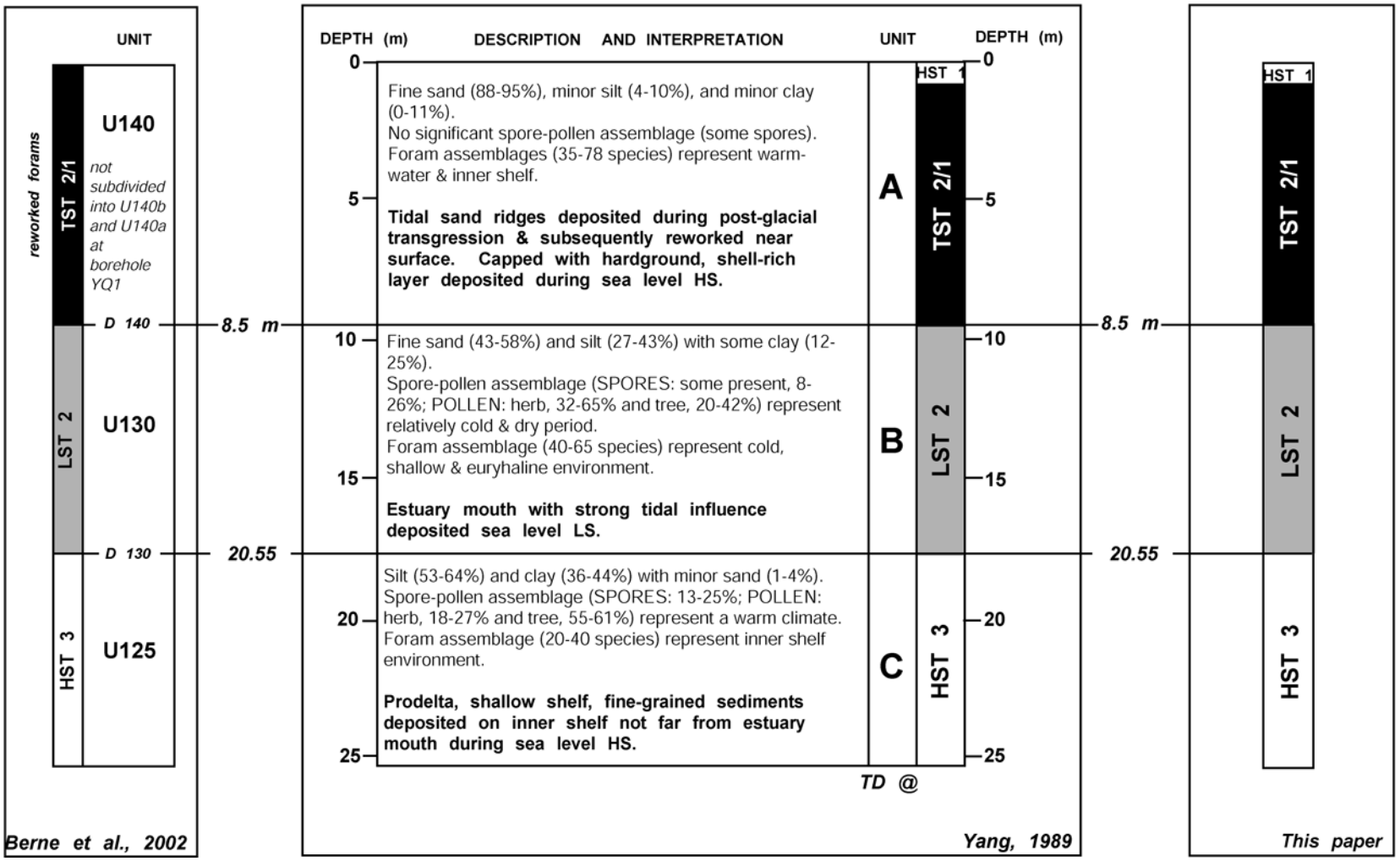

this investigation facilitates correlation to oxygen isotope stratigraphy and provides a link to global sea level change and an opportunity to determine the relative importance of eustasy and sediment supply. Prior to this project, the most extensive seismic stratigraphic dataset from the ECS was presented Liu et al. (2000) and later revised by Berne et al. (2002). These two studies based the position of stratigraphic boundaries on core data from DZQ4 and YQ1 and discussed a sequence stratigraphic framework tied to OIS dates from OIS 6 (186 ka) to present. However, neither the systems tract or OIS age are incorporated into associated unit classifications. For example, Liu et al. (2000) subdivided core DZQ4 into 7 major units (U7 to U1; listed oldest to youngest). Berne et al. (2002) revised interpretations and identified six units (U=unit; U110, U120, U125, U130, U140, and U145; listed oldest to youngest) and corresponding basal bounding surfaces (D=discontinuity; D110, D120, D125, D130, D140a, and D140b). A comparison of the revised nomenclature used herein and how it relates to Liu et al. (2000) and Berne et al. (2002) as well as Yang (1989) is shown in Figures 1.13 and 1.16, respectively.

The stratigraphic units from cores DZQ4 (Units 1 to 6) and YQ1 (Units 1 to 3) and their associated ages and systems tracts form the basis of the present nomenclature: LST 6 (Unit 6), TST 6/5 (lowermost Unit 5), HST 5 (Unit 5), LST 4 (Unit 4), TST 4/3 (lowermost Unit 3), HST 3 (Unit 3), LST 2 (Unit 2), TST 2/1 (Unit 1), HST 1 (uppermost Unit 1). The component systems tracts also correlate well to the four seismic facies (SF) observed in the shallow strata of the ECS (i.e., SF CHAO, SF MOUND, SF FLAT, and SF DIP). Lithologic data (grain size, sedimentary structures, sorting) that correspond to these seismic facies allow further insight into depositional environments and their vertical and lateral distributions across the margin.

1.3.5 Synthesis of Seismic and Core Data

Correlation between cores and adjacent seismic profiles provides age constraints on seismic surfaces and units, thereby permitting correlation of seismic facies and lithofacies, identification of systems tracts, and tie of overall sequence stratigraphic framework to the Quaternary sea level curve (Figure 1.2). A compilation and synthesis of these data are presented below. Organization of the data is based on the six major stratigraphic subdivisions related to the units from cores DZQ4 (Units 6 to 1, oldest to youngest, respectively) and YQ1 (Units 3 to 1, oldest to youngest, respectively). Units 3, 2 and 1 in core DZQ4 correlate to their namesake Units 3, 2, and 1 in core YQ1.

Unit 6. This unit extends for approximately 12 m in core DZQ4 from a total depth (TD) of 51.65 m to 39.4 m below seafloor (mbsf). Based on nearby seismic profiles, the total thickness of this unit is 16 m at the borehole. Elsewhere on the margin, this package is up to 46 m thick and averages between 10 and 20 m. Unit 6 contains cross-bedded sands with terrestrial components such as pollen from land plants and wood debris. Pollen assemblages indicate a warm and humid climate transitional to a colder, drier climate toward the top of the interval. Nannofossil assemblages (coccolithophores) are, however, indicative of cold environments throughout the entire interval. This unit correlates to SF CHAO at borehole DZQ4 and extends in both strike- and dip-oriented profiles for hundreds of kilometers. Across the entire margin, SF CHAO is bound at its base by a fairly flat erosional surface previously identified as ED3 and SB3 on the inner and central margin. SF CHAO also grades laterally into basinward dipping, downlapping seismic reflections (SF DIP) on the outer margin. There, SF DIP is bound at its base by a DS previously identified as SB3 (i.e., the correlative conformity of ED3). Based on absolute age data from OIS 5 in the overlying

stratal Unit 5 and the overall sequence stratigraphic framework (i.e., overlying HST and underlying SB), Unit 6 correlates to the LST of OIS 6 (LST 6) that spanned 186 to 128 ka (Imbrie et al., 1984).

Unit 5. The lowermost 2 m of Unit 5 in core DZQ4 (39.4 to 37.4 mbsf) lies above LST 6 and below absolute ages tied to the overlying HST 5. Primarily composed of silt, there is also abundant shell debris and a sharp, basal lithologic contact that shows an abrupt deepening upward sequence. This unit correlates to the TST between LST 6 and HST 5 (i.e., TST 6/5), approximately 133 to 123 ka (Figure 1.2). At the borehole, this portion of Unit 5 is resolved in seismic profiles as a single, thick (low frequency), high-amplitude reflection and represents the TST as well as its upper and lower bounding surfaces (MFS of HST 5 and TS between LST 6 and TST 6/5, respectively). This reflection is also traceable across the entire margin and frequently thickens into the externally mounded units of SF MOUND. Thicker portions of this unit are easily resolvable in seismic profiles and are bound at the base by the high-amplitude reflection of the TS and bounded at the top by the high-amplitude MFS of HST 5. The ridges of TST 6/5 are distributed across the inner and central margin but do not appear on the outer margin. They are on average 4 m thick with an observed maximum of 13 m, and their preservation is attributed to a high subsidence rate and subsequent burial by prodeltaic muds (Berne et al., 2002). Berne et al. report a preferred orientation of internal reflections offlapping to the SW.

The upper portion of Unit 5 in core DZQ4 (39.4 to 30.6 mbsf) contains interbedded clays, silts, and sands. The sediments are much finer than the underlying LST 6 and lack the shell hash found in the underlying TST 6/5. Fossil assemblages are indicative of warm water and middle-to-outer shelf environments (specifically the planktonic foraminifera *Globigerina*

ruber). A TL date of 87,764 years (±-4,388 years) collected at approximately 35 mbsf corresponds to HST 5 that spanned 128 to 71 ka (Imbrie et al., 1984). The Ehux acme biozone at 30.8 mbsf may also provide an additional age around 73 ka (Thierstein et al., 1977) also tying this unit to the HST 5. These sediments correlate to SF FLAT at the borehole, across the inner and central margin, and laterally grade into SF DIP to the south and east. While Unit 5 is almost 9 m at the core location, this upper portion of the unit 5 averages between 15 and 30 m across central portions of the margin where it reaches up to 53 m in thickness. Maps and cross-sections of this unit show a perched lobe that pinches out to the south and east on the central to outer margin and does not reach the paleo shelf-slope break (Figures 1.7, 1.17, and 1.18).

Unit 4. This thin stratigraphic package from core DZQ4 spans 30.6 to 30.3 mbsf. It lies 1 cm above the Ehux acme biozone from HST 5. This 3 cm interval consists of a coarse shell lag as well as sporo-pollen content and fossil indicators that, while limited, are consistent with a cold and dry terrestrial climate with a high oxygen isotopic ratio. Absolute ages bracket Unit 4 by TL dates from HST 5 and HST 3. In addition, the Ehux acme (around 73 ka; Thierstein et al., 1977) is 2 cm below the lower boundary of this stratigraphic unit. This stratal package is resolved in seismic profiles as a single, thick (low frequency), high-amplitude reflection. Therefore, this LST is indistinguishable from its lowermost and uppermost boundaries, the SB of OIS 4 (previously referred to as SB 2) and the TS of TST 4/3, respectively. Towards the north, however, this single reflection expands to a package of SF CHAO over 20 m thick and about 50 km long in both strike- and dip-oriented seismic profiles (Figure 1.8). This thicker portion of the LST 4 unit is easily resolvable on both strike and dip-oriented seismic profiles within our dataset. To the best of our knowledge, the

Figure 1.17. Strike-oriented stratigraphic profile across the East China Sea continental margin. Note uplift and erosional truncation of older strata in the north and subsidence in the south. Seismic profiles are spread across the study area identified in Figure 1.1.

STRIKE-ORIENTED SHELF PROFILE

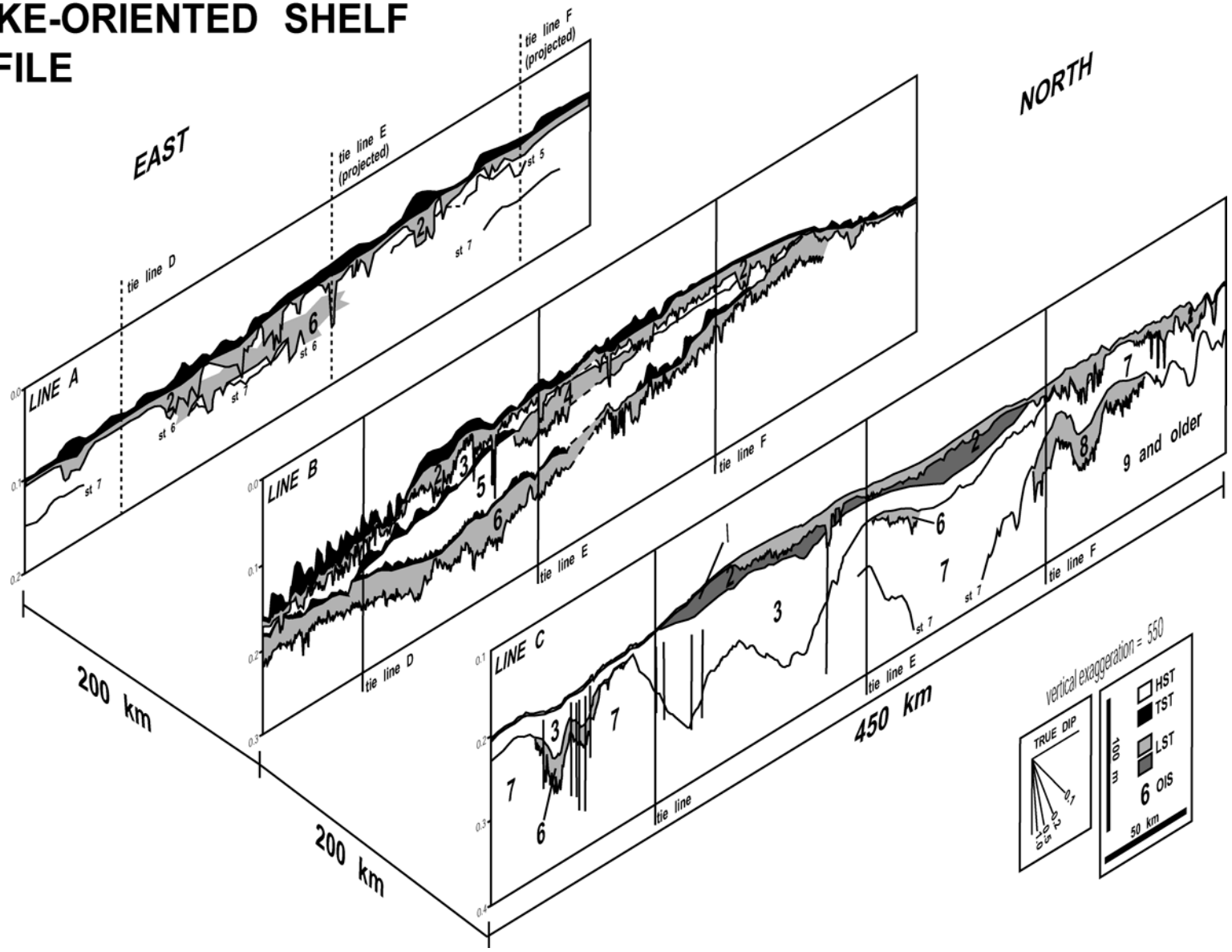

Figure 1.18. Dip-oriented stratigraphic profile across the East China Sea continental margin. Note stratal stacking patterns at shelf-slope break on northern margin are progradational and indicative of uplift. Stratal stacking patterns at the shelf-slope break on the southern margin are aggradational and indicative of subsidence. Seismic profiles are spread across the study area identified in Figure 1.1.

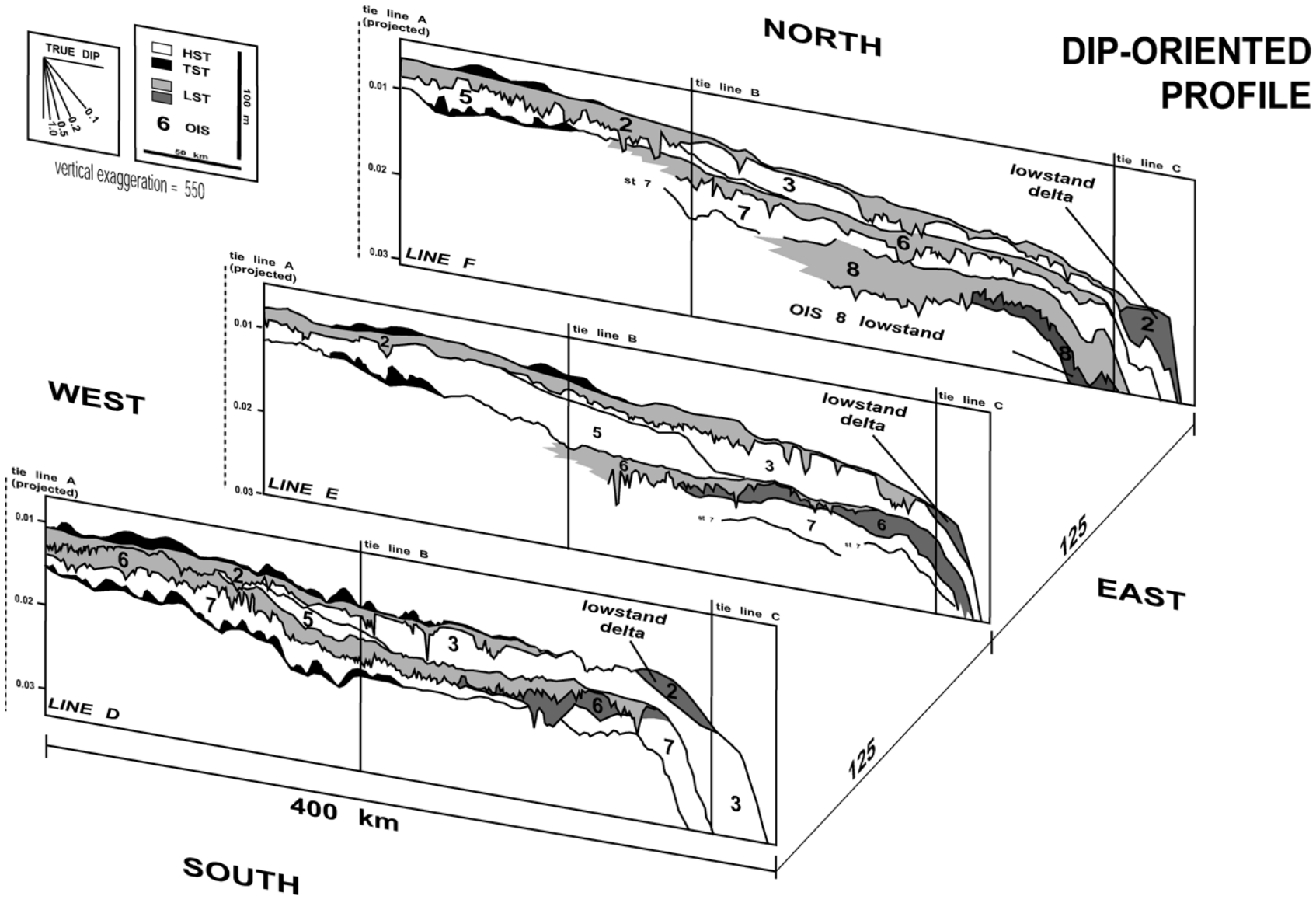
DIP-ORIENTED
PROFILE
NORTH
WEST
EAST
SOUTH
TRUE DIP
0.1
0.2
0.5
1.0
HST
TST
LST
6 OIS
100 m
50 km
vertical exaggeration = 550
tie line A
(projected)
tie line B
tie line C
LINE F
LINE E
LINE D
lowstand
delta
OIS 8 lowstand
st 7
0.01
0.02
0.03
125
400 km

thicker portion of LST 4 has not been identified in previous studies of the ECS and is unique to this investigation. Based on these data, as well as absolute ages from both the underlying and the overlying units (HST 5 and 3, respectively), and the overall sequence stratigraphic framework (i.e., position between two HSTs and a basal SB), Unit 4 correlates to the LST of OIS 4 (LST 4) that spanned 71 to 59 ka (Imbrie et al., 1984).

Unit 3. The lowermost portion of Unit 3 in core DZQ4 (30.3 to 28.1 mbsf) is composed of sandy and clayey silt. This 2.2 m unit is resolved in almost every seismic profile as a single, thick (low frequency), high-amplitude reflection traceable across the entire margin. At the borehole location, this unit cannot be differentiated from the reflection representing underlying unit (i.e., LST 4). With one exception, this reflection expands into multiple occurrences of SF MOUND in one strike-oriented seismic profile from the central portion of the margin (Figure 1.17). Based on these data, in addition to absolute ages in the overlying unit (HST 3) and the general sequence stratigraphic framework (i.e., position between LST 4 and HST 3), this 2-m portion of Unit 3 correlates to TST 4/3 that occurred between LST 4 and HST 3 (approximately 61 to 57 ka; Figure 1.2). In TST 4/3, SF MOUND is bound at the bottom by the TS and at the top by a DS, in this case the MFS, of the overlying HST 3 (previously referred to as DS 2). In the majority of seismic profiles, SF MOUND is not present and the single, high-amplitude reflection is resolved as an amalgamation of both LST 4 (3 cm) and TST 4/3 (2.2 m). This single reflection, therefore, represents the LST 4 SB, the TS, and the overlying MFS of HST 3.

The remainder, and majority, of Unit 3 in core DZQ4 is 16.25 m thick and extends from 28.1 to 11.85 mbsf. It consists of well-bedded clayey silts and fine sands with an overall shallowing upward trend. Two TL dates at approximately 20.9 and 24.4 mbsf indicate ages

of 46,903 years (± 2,313) and 50,246 years (±2,512), respectively. Saito et al. (1998) provide additional ^{14}C dates for this unit from shallow piston cores. These dates range from 25 to 50 ka. Five meters of Unit 3 is also penetrated by core YQ1 (25.75 to 20.55 mbsf). This shorter core contains silts and clays as well as a sporo-pollen assemblage indicative of a warm climate. Foraminifera species suggest an inner shelf environment. In light of these data, this portion of Unit 3 in both cores correlates to OIS 3 and the associated HST that spanned 59 to 24 ka (Imbrie et al., 1984). Thin occurrences of (i.e., < 10 m) of SF FLAT appear on landward portions of the margin above HST 5. There, the bottom boundary of HST 3 is the MFS (previously identified as DS 2) and the upper boundary is the SB of the overlying LST 2 (previously identified as SB 1). However, the majority of HST 3 occurs basinward of the HST 5 lobe on central and outer portions of the margin. There, the majority of HST 3 is composed of SF DIP with an upper boundary composed of the SB of the overlying LST 2. The lower boundary is more complex as it is basinward of HST 5 deposition and HST sits directly over LST 6 making the lower bounding MFS (previously identified as DS 2) an amalgamation of the HST 3 MFS, the TST 4/3 TS, the conformable portion of the LST 4 SB, the HST 5 MFS, and the TST 6/5 TS. Thicknesses of SF DIP on the outer portion of the margin consistently reach between 30 and 50 m thick and averages between 15 and 20 m thick. Basinward of the shelf-slope break there is massive progradation of SF DIP that exceeds 130 m in thickness.

Unit 2. This unit extends for 8.65 m in core DZQ4 (11.85 to 3.2 mbsf) and for 12.05 m in core YQ1 (20.55 to 8.5 mbsf). Grain sizes are consistently fine sand and silt and coarser than the underlying unit (abrupt shallowing upward sequence). The sporo-pollen assemblages indicate a relatively cold and dry period. Shell and wood debris present in the

bottom portion of core DZQ4 also indicate a terrestrial component. Based on these data and the overall sequence-stratigraphic framework, this unit correlates to the LST that occurred during OIS 2 between 24 and 12 ka (Imbrie et al., 1984). This stratal package is primarily composed of SF CHAO with a laterally extensive lower boundary that is an erosional discontinuity (previously identified as SB1). On the inner and central margin this unit averages between 10 and 20 m with a maximum thickness of 52 m. SF CHAO thins basinward and LST 2 is resolved seismically as a single, thick (low frequency), high-amplitude reflection that extends laterally across the outer margin for hundreds of kilometers in both strike- and dip-oriented seismic profiles. On the outer margin this reflection sometimes becomes indistinguishable from the high-amplitude seafloor but is often resolvable with higher-frequency chirp sonar. Where this surface truly becomes amalgamated, it represents the present-day highstand (i.e., HST 1), the underlying SB, the overlying TS, TST 2/1, MFS, HST 1, and the seafloor. However, on the outermost portion of the margin (at the present-day shelf-slope break), LST 2 abruptly thickens laterally into two mounded packages of SF MOUND. The scale of these external geometries is much larger than previous SF MOUND from TST 6/5 and TST 4/3. Each of these two SF MOUND units extends for approximately 100 km at an average thickness of 20 m and a maximum of 87 m (Figure 1.11). Similar to the basinward occurrence of the LST 6 SB, the DS at the base of SF MOUND is most likely the correlative SB for LST 2. The upper boundary of these SF MOUND complexes is a single, thick (low frequency), high-amplitude reflection that is an amalgamation of the present-day seafloor as well as the overlying TS, TST 2/1, MFS, and present-day HST 1.

Unit 1. The majority of this stratal package in cores DZQ4 (3.2 to 0.13 mbsf) and YQ1 (8.5 to <1 mbsf) consists of fine sand with minor silts and clays. Shell debris and mud clasts are reported in the upper portion of this unit in DZQ4. Limited spores were found in YQ1. Both units are composed of SF MOUND and the external morphology of these ridges is observable in present-day bathymetry. Thickness of these ridges varies between 5 and 22 m. Stratigraphically equivalent examples of SF MOUND are found across the inner and central margin and thin laterally into a single, thick (low frequency), high-amplitude reflection that is indistinguishable from the seafloor. This single reflection is often resolvable with higher-frequency (2 to 16 kHz versus ≤2 kHz for seismic sources) chirp sonar due to the higher resolution capability of the device (i.e., optimal resolution of beds as thin as 10 cm). By nature, this higher resolution (and, therefore, frequency) limits the depth of study to about 20 m. Because of the stratigraphic occurrence of Unit 1 above LST 2 and the similarity of SF MOUND to deeper ridges associated with TSTs, this stratal package correlates to TST 2/1 (approximately 7 to 17 ka; Figure 1.2). Therefore, the upper bounding surface is an amalgamation of the MFS, HST 1, and the seafloor. Yang (1989) notes that the TST 2/1 SF MOUND occur in present-day water depths of 45 to 115 m with the following spatial parameters: 10-50 km long, 3-5 km wide, 5-20 m high, spaced on average between 8-14 km apart, and usually oriented parallel to each other with an ESE-WNW trend. Yang and Sun (1988) note that the majority of these mounded ridges occur in the submerged paleovalley of the Yangtze River (still evident in present-day bathymetry; Figure 1.1).

The top interval of Unit 1 is a very thin layer in both cores DZQ4 (0.13 mbsf to seafloor) and YQ1 (<1 mbsf to seafloor). It is characterized by a high sand content with shell debris and an extremely high content of foraminifera. Because it is the youngest unit is the

stratigraphic section and appears at the seafloor just above TST 2/1, this portion of Unit 1 correlates with the present-day HST 1 (12 ka to present; Imbrie et al., 1984). This unit is resolved in seismic data as a single, thick (low frequency), high-amplitude reflection that is indistinguishable from the seafloor but often resolvable with higher-frequency chirp sonar. Therefore, the lateral continuity of this unit is extremely high.

1.3.6 Summary

Borehole DZQ4 on the central margin of the ECS sampled six lithologic units (Units 6 to 1, oldest to youngest). These units correlate with the upper three lithologic units in core YQ1 (also acquired on the central margin). Also present in the six units from the 51.6 m vertical section of DZQ4 are three sea level cycles that span OIS 6 (128 to 186 ka; Imbrie et al., 1984) to present. In each of these three cycles, the three major component systems tracts (i.e., LST, TST, and HST) can be identified in core and seismic profiles, and a nomenclature that takes advantage of both sequence stratigraphic and Quaternary oxygen isotope data is introduced: LST 6 Unit 6), TST 6/5 (lowermost Unit 5), HST 5 (Unit 5), LST 4 (Unit 4), TST 4/3 (lowermost Unit 3), HST 3 (Unit 3), LST 2 (Unit 2), TST 2/1 (Unit 1), HST 1 (uppermost Unit 1). This is an attempt to create a common nomenclature for the shallow strata on the ECS continental margin which unifies contributions of previous investigations while facilitating ongoing and future research.

Multiple trends exist between seismic facies and each of the three component systems tracts (i.e., LST, TST, HST). SF CHAO is always related to a LST and bound at its base by an ED. On inner and central portions of the margin this ED is the SB. On the outer margin, this ED is underlain by SF DIP. There, the basal boundary of SF DIP (overlain by SF CHAO) is a DS that is most likely the correlative SB. SF MOUND is always related to the

TST. The HST is always represented by SF FLAT and SF DIP. When stratal units are thin they are resolved in seismic data as single, thick (low frequency), high-amplitude reflections. Finally, the general structural trends of shallow strata across the ECS continental margin are uplift in the north and subsidence in the middle shelf region. LST 2 is fairly flat lying and truncates the underlying strata to the north creating a regional angular unconformity. Therefore, strata underlying LST 2 get progressively older to the north (Figure 1.17). The stratal stacking patterns on the outermost portions of the margin also suggest uplift (north) and subsidence (south). In the north, strata prograde basinward in relation to their respective shelf-slope break. In the south, strata aggrade in relation to their respective shelf-slope break (Figure 1.18). These trends suggest a gradual and consistent subsidence and uplift prior to OIS 6 through the present. This observation supports various regional subsidence and uplift values reported by Kim (1973), Wang and Wang (1982), Stanley and Chen (1993), Kim and Kucera (2000), and Berne et al. (2002).

1.4 DISCUSSION

Chronostratigraphic data (TL and ^{14}C dates, possibly the Ehux biozone) and paleoclimate indicators (sporo-pollen and foraminiferal assemblages) from cores DZQ4 and YQ1 allow sequence stratigraphic correlation to both the sea level and oxygen isotope curves (Pillans et al., 1998 and Shackleton, 1987, respectively) of the past 186 ky (i.e., OIS 1 to 6). Our revised stratigraphy for the ECS strata is based on these relationships. Results from earlier studies of the ECS continental margin are critical to our understanding of the shallow strata (<100 m). However, the regional extent of the seismic dataset used in this investigation provides unique observations unavailable to these previous studies. Many of these observations require a revised stratigraphic framework. This is an effort to unify previous nomenclature associated with shallow strata on the ECS margin and provides a link to global sea level change that allows for an assessment of the relative importance of sea level, sediment supply, and tectonics in shaping ECS margin stratigraphy. This investigation also provides an opportunity to characterize the stratigraphy evolving as a consequence of extremely high sediment supply over a shelf margin with very minimal physiographic relief.

1.4.1 Late Pleistocene Depositional History

LST 6. Liu et al. (2000) correlated this unit to OIS 6 and interpreted the depositional environments as a combination of terrestrial, river mouth, and shallow (5-20 m) sea (their Table 1). Berne et al. (2002) also correlated this unit to OIS 6 and interpreted the depositional environment as fluvial changing upward into pro-deltaic and then back into fluvial/estuarine. In addition, they classified the lower bounding unconformity as a regressive surface of marine erosion. The Berne et al. (2002) model suggested that characteristics of Unit 6 are associated with a forced regressive deposit (*sensu* Posamentier et

al., 1992). Therefore, Berne et al. (2002) placed the fluvially incised SB near the top of Unit 6 (forced regressive systems tract of Hunt and Tucker, 1995; falling stage systems tract of Plint and Nummedal, 2000) but did not identify this SB in their seismic data. Berne et al. (2002) attributed the majority of the laterally and vertically extensive sediments of LST6 to a deltaic/estuarine environment during the late LST with only a minor fluvial component (their Figure 1.16).

Whereas both the Liu et al. (2000) and the Berne et al. (2002) models are plausible, a third model is that Unit 6 represents a massive, unconfined fluvial system formed during LST 6. Instead of producing a narrow incised valley and estuarine system, this fluvial system deposited a laterally and vertically extensive sand sheet with little to no sedimentary bypass over the shelf-slope break (Figure 1.6). Sea level during LST 6 is estimated to have been approximately 120 m below present (Pillans et al., 1998; Figure 1.2). A sea level drop of this magnitude exposed the majority of the margin subaerially (approximately 1.0×10^6 km^2 presently covered by the ECS/YS/BS). Because a prominent basal unconformity most likely formed during this subaerial exposure and subsequent erosion, the fluvial interpretation places the bounding discontinuity at the base of the fluvial strata (SF CHAO). In this interpretation, widespread erosion occurs because the rate of eustatic fall exceeded the rate of subsidence. Posamentier and Vail (1988) initially classified this type of SB as type 1. Due to widespread misuse and confusion, Posamentier and Allen (1999) later suggested the elimination of this terminology (i.e., type 1 and type 2). However, regardless of whether or not the type 1 classification is considered current or archaic, the processes controlling the formation of the LST 6 SB remain the same (i.e., rate of eustasy > rate of subsidence).

The basinward component of this erosional surface is a correlative conformity that underlies the deltaic component of this system that also lies basinward (downlapping reflections that dip and offlap basinward; SF DIP). The youngest (shore proximal) deltaic deposits were subsequently removed by fluvial and subaerial erosion and are overlain by the sediments of SF CHAO as sea level continued to drop across the margin (Figure 1.6). SF CHAO of LST 6 does not offlap over the shelf-slope break but remains perched on the margin. There is a minor amount of offlap in SF DIP beyond the shelf-slope break. Based on these observations, three major factors provide evidence in support of a fluvial origin and discount the aforementioned estuarine hypothesis. First, a lack of incision observed in the LST 6 SB suggests the embayments needed for estuarine development did not exist (Figure 1.5). Second, the TST overlaying LST 6 is a distinct transition from a fluvial- to a tidal-dominated regime (see TST 6/5 discussed later in this section). This TST occurs as a single, high-amplitude reflection that expands laterally into the ridge morphology of SF MOUND. Third, the basinward deltaic component (SF DIP) is stratigraphically equivalent to the landward occurrence of SF CHAO, supporting a lateral transition from terrestrial fluvial to submarine deltaic.

Warren and Bartek (2002a, 2002b) also presented this unit (Unit 6 or LST 6) as completely fluvial, describing it as a metastable fluvial shelf system (MFSS). They defined the MFSS as a laterally extensive, unincised lowstand fluvial deposit with little or no associated sedimentary bypass (i.e., progradation over the shelf-slope break). It was attributed to metastable conditions created within fluvial systems by high sedimentation rates that caused the fluvial system to avulse rather than incise. The fluid dynamics of these metastable conditions could have been created primarily by the low gradient of the margin

(i.e., 0.013°) and, less so, by an abundant sediment supply. Over time, deposition caused channel bottom elevation to exceed the elevation of the surrounding area adjacent to river levees, and the system avulsed (*sensu* Thorne, 1994). Over time, avulsion and aggradation formed a sediment sheet similar to a braid plain.

An example of the MFSS as defined above, and an analog to the ECS LST 6 deposits, is found on the Canterbury Plains, east coast of the South Island, New Zealand. The Canterbury Plains are approximately 70 km wide, up to 150 km wide, 185 km long with a gradient of 0.006 or 0.3°, and a shelf-slope break at –145 m. The Canterbury Plains are bounded by the Southern Alps on the north and west and the Pacific Ocean on the east and southeast (Lecke, 1994; Browne and Naish, 2003). The large, coarse-grained, braided fluvial systems of the Canterbury Plains (presently the Rangitata, Ashburton, Rakaia, and Waimakariri rivers) shed significant volumes of sediment (50,000 km^3) eastward onto a low-gradient margin (6 m/km or 0.3°) that is subsiding between 0.2 and 0.5 m/ka (Leckie, 1994; Browne and Naish, 2003). Underlying the Canterbury Plains are cyclically stacked fluvio-deltaic gravel, sand, and mud deposits associated with the glacio-eustatic sea-level fluctuations of the Quaternary (Brown and Wilson, 1988; Brown and Weeber, 1992). With the exception of minor incision during the late LST at the exposed shelf-slope break, Browne and Naish (2003) observed an overall lack of incision across the exposed Canterbury shelf during regressions into LSTs. They attribute the unincised nature of these lowstand fluvial deposits to an abundant and continual supply of sediment delivery to the shoreline by braided rivers. These rivers, in turn, formed broad, unconfined, sheet-like deposits across the entire regressive braidplain. Woolfe et al. (1998), Posamentier (2001), and Browne and Naish (2003) suggested that rivers do not necessarily incise during glacio-eustatic lowstands on

margins where they are able to flow out onto a coastal plain flanked by a broad, low-gradient shelf. The stratigraphic evidence from LST 6 of the ECS lends additional support to this model.

Browne and Naish (2003) did not elaborate on sediment supply rates for the Canterbury Plains and how they may fluctuate during late Pleistocene climate fluctuations. Similarly, Warren and Bartek (2002a, 2002b) did not elaborate on how much sediment is needed in tandem with a low gradient with respect to the MFSS model for the ECS. This is important because fluvial sediment influx (primarily from the Yellow and Yangtze Rivers), while presently abundant, is not necessarily extrapolated back in time due to changes in climate regime, erosional and depositional patterns, and anthropogenic influences (Saito et al., 2001). Fortunately, the Loess Plateau in central China offers an excellent terrestrial record of the late Pliocene and Pleistocene climate to assess paleoprecipitation trends (e.g., Xiao et al., 1999; An, 2000). The loess from the plateau is associated with the domination of the cold and dry northerly winter monsoon during glacial periods. The development of interbedded paleosols is associated with the domination of the southerly, moisture-bearing summer monsoon during stadials (An, 2000). Liu et al. (1995) calculated a precipitation rate of only 200 mm/yr (compared to a present rate of about 500 mm/yr for the study area) during OIS 6 from the Xifeng section of the Loess Plateau. Evans and Heller (2001) compiled multiple datasets from the Luochuan section of the Loess Plateau that indicate somewhat higher paleoprecipitation rates (between 300 and 400 mm/yr for OIS 6), but still less than present day for this region (600 and 650 mm/yr). Thus, data from these two sites suggest precipitation trends during OIS 6 to be about half of what they are today.

It is assumed that decreased precipitation during glacials yields a decrease in fluvial sedimentation as well. However, the LST 6 strata are extensive across the ECS margin (up to 30 m thick and over 400 km wide). Hypotheses explaining this observation include: 1) decreased precipitation rates are still adequate to carry abundant sediment load, 2) increased erosion of unconsolidated loess and transport (fluvial and eolian) of sediments from the Loess Plateau to exposed margin with subsequent fluvial erosion and deposition, and 3) margin exposure during LST 6 added significant drainage area (approximately 1 x 10^6 km^2; Yunshan et al., 1996; Kim and Kucera, 2000; Li et al., 2003) thereby providing more sediment and compensating for decreased erosion and runoff from decreased precipitation. Hypothesis #2 seems unlikely due to a disparity in grain size between the Loess Plateau and core DZQ4. Lanying et al. (1991) report that 84% of the grains analyzed for an OIS 6 loess horizon are no larger than coarse silt (0.05 mm) whereas core DZQ4 contains fine sand (>0.125 mm) for LST 6. Initially, hypothesis #3 (i.e., increased drainage basin via subaerial exposure and increased erosion, transport, and deposition) seems plausible. In this scenario, an exposure of the shelf under the ECS/YS/BS system represents a 40% increase of the present-day drainage basin (2.6 x 10^6 km^2; Saito et al., 2001), and sediment yields are strongly dependent on the size of the drainage basin (Milliman and Syvitski, 1992). Sediment yields are also proportional to topography – high yields equate to mountainous regions and low yields equate to lowlands (Milliman and Meade, 1983; Walling, 1987). However, Milliman and Syvitski (1992) also identified trends within these data that show runoff is inversely proportional to basin area (i.e., decreased runoff with increased basin area). Decreased runoff is likely caused by decreased precipitation and increased evapotranspiration across lowland regions (D. Walling written comm., 1991 *in* Milliman and

Syvitski, 1992). Runoff is expected to decrease across the emergent seafloor from the ECS/YS/BS and, therefore, limit the contribution of sediment by erosion of shelf strata exposed during the LST. The sandy, fluvial sediments from LST 6 do not suggest a cannibalization of the underlying finer-grained silts and clays (HST 7). The third hypothesis, while plausible, is not considered to be a major factor for increased sediment supply during glacial periods prior to OIS 4 on the ECS margin. However, hypothesis #1 (i.e., decreased precipitation rates still adequate to carry an abundant sediment load) is still a viable explanation for extensive LST 6 sedimentation. Even though this hypothesis stands on its own without further comment, precipitation during glacial periods and its effect on both large (Yellow and Yangtze) and small (mountainous regions along present-day coast) rivers is not documented well. Westhoff and Bartek (2001) suggested the domination of small coastal rivers on southern portions of the exposed margin during lowstands, specifically OIS 6, although further research on provenance of these sediments seems warranted.

While this first hypothesis addresses the amount of sediment supplied to the margin, additional factors unrelated to sediment supply offer further insight into the volume of LST 6 sediment perched on the margin. These two additional hypotheses, listed here as fourth and fifth, are: 4) an exposed margin decreases fluvial gradient even further, which leads to greater deposition and 5) oceanic (coastal) currents that currently transport sediment south along the Chinese coast are non-existent during a major lowstand like LST 6 and sediment remains in system. Hypothesis #4 suggests that as margin exposure occurred during LST 6, the widening coastal plain, which extends onto a continental shelf with a lower gradient, created a lower fluvial gradient, thus causing fluvial systems to become overextended. The result of this leads to power loss and deposition. As a result, a greater percentage of sediments were

deposited (i.e., reduced velocity leads to higher deposition rates) and "apparent" sediment supply would be increased. Similar to the third hypothesis, this explanation also compensates for decreased erosion and runoff from decreased precipitation. This idea was presented by Holbrook (1996) to explain the broad, fluvial sand sheet of the Cretaceous Mesa Rica Sandstone (Dakota Group, late Albian) of the U.S. Western Interior Basin. Similar to the MFSS presented by Warren and Bartek (2002 a; 2002 b), the Mesa Rica experienced frequent avulsion in conjunction with a low gradient that, in turn, caused regional scouring of a flat, planar, sequence-bounding unconformity (Holbrook and Dunbar, 1992; Holbrook, 1996).

The fifth, and final, hypothesis addresses the effect of oceanic (coastal) currents on the transport of fluvial sediments south and potentially out of the ECS system (e.g., Hung and Chung, 1994; Chung and Chang, 1995; Tamburini et al., 2003). Of the 4.78×10^8 tons of sediment presently transported by the Yangtze River each year, 30% (1.46×10^8 tons/year) is carried south by the Changjiang (Yangtze) Coastal Water (Milliman et al., 1985). During lowstands, especially major ones (>100 m drop), these currents are attenuated or non-existent (Jun et al., 1995). Without these currents, the entire sediment load of the Yangtze, Yellow, and other river systems remains in the system available for deposition.

In summary, the laterally and vertically extensive fluvial sands from LST 6 seem inconsistent with the cooler and drier climate during that period, a climatic signal preserved both locally (core DZQ4) and regionally (Loess Plateau). Decreased precipitation and runoff during this glacial period suggests decreased sediment loads in the fluvial systems that transport sediment to the ECS margin. Even under these conditions, it appears that the fluvial systems were still capable of transporting abundant sediment. One mechanism may

be the domination of small coastal rivers in comparison to the major systems of today (i.e., the Yellow and Yangtze rivers). Additional factors, unrelated to sediment supply, have the potential to increase "apparent sediment supply" through higher rates of deposition. Underpowered fluvial systems flowing across the wide, exposed margin further decrease an already low gradient and lead to greater rates of deposition. In addition, the absence of the ECS during the extreme RSL lowstand from LST 6 means the absence of the high-energy coastal current system that presently removes 30% of the Yangtze sediments from the study area. Potentially, it is a combination of all three of these factors (ample fluvial transport, underpowered fluvial systems, and the absence of sediment export via oceanic currents) that explains the abundant fluvial sediments perched on the ECS margin during the dry climate of the LST 6 glacial period.

TST 6/5. Primarily composed of silt, there is also abundant shell debris in this 2-m-thick unit that was most likely material reworked and winnowed during transgressive ravinement. This thin horizon is interpreted as a thin veneer of sand deposited during a rapid rise in RSL. This is analogous to the interpretations of Bartek and Wellner (1995) that was based on observations of the most recent TST, between the last glacial maximum and the present-day highstand. This single reflection is also the stratigraphic equivalent to the externally mounded ridges on inner and central portions of the margin. These ridges occur throughout the shallow stratigraphic record in the ECS and are the focus of many recent investigations (e.g., Yang, 1989; Saito et al., 1998; Liu et al., 2000; Li et al., 2001; Berne et al., 2002) and are considered to represent concentrations of sediments reworked by the flow field of tidal currents during marine transgressions. The youngest of these ridges, observed on the present-day seafloor of the ECS (i.e., from TST 2/1), are also linked to shallow-water tidal

currents. Ridges on the outer and middle portions of the present-day shelf are moribund while those on the inner shelf in the ECS as well as the YS are presently active and in equilibrium with current oceanographic conditions (Yang and Sun, 1988; Yang, 1989; Bartek and Wellner, 1995). Both Liu et al. (2000) and Berne et al. (2002) also interpret this 2-m interval of Unit 5 as TST 6/5, but Berne et al. (2002) specify a basal tidal ravinement surface (TRS) in lieu of a transgressive surface (TS). Both groups of authors also suggested that two factors led to the preservation of the morphology of these ridges across the margin: 1) a rapid sea level rise that provided a rapid burial by prodeltaic muds in conjunction with 2) a subsidence rate of 0.3 mm/yr (30 cm/ky). Berne et al. (2002) attributed ample subsidence as an integral part of sand ridge preservation, citing low subsidence in the Celtic Sea (lower than the ECS by an order of magnitude) as the sole reason buried Pleistocene sand ridges do not exist, even though they are prominent on the present-day seafloor (Berne et al., 1998; Evans, 1990). Galloway and Hobday (1996) noted that tidal ridges from the ECS and YS, as well as the North Sea, Bering Sea, and Gulf of Mexico, are conspicuous in transgressive settings. The ridges from the North Sea are similar in size, shape, as well as internal structure and are considered to be modern analogs to the sand ridges in the ECS (Stride et al., 1982).

HST5. The lobate morphology of this unit, along with the smaller grain size and warm-water, middle-to-outer shelf fossil assemblages (specifically the planktonic foraminifera *Globigerina ruber*) suggest a deltaic environment deposited on the middle to outer portion of the margin during a warm and humid climate. A TL date of 87,764 years (±-4,388 years) collected at approximately 35 mbsf corresponds to the beginning of the HST of OIS 5.1 (a.k.a. 5a). During the span of HST 5 (128 to 71 ka; Imbrie et al., 1984), sea level fluctuated

between 0 and 60 m below present (Pillans et al., 1998; Figure 1.2). Basinward of the HST 5 lobe pinchout, on the outer margin, HST 3 sits directly over TST 6/5. HST 5 at borehole DZQ4 may or may not include all of the sub-stages spanning 128 to 71 ka (5.5 to 5.1 a.k.a. 5e to 5a ; Imbrie et al., 1984; Figure 1.2). Parasequences and/or hiatuses caused by autocyclic processes such as lobe switching (i.e., shifting of depocenter) are not present within the dataset used in this investigation, which is far more extensive than other published reports on OIS 5 in the ECS.

Liu et al. (2000) do not address the sub-stages of OIS 5, but they do offer a similar interpretation of Unit 5 as a subfluvial delta in a shallow sea (their Table 1). Berne et al. (2002), however, do address the sub-stages of OIS 5. Based heavily on the interpretation of the Ehux acme (30.8 mbsf) occurring between 80 to 85 ka, Berne et al. (2002) interpret this unit at borehole DZQ4 as a regressive prodeltaic deposit formed during overall base-level fall between OIS 5.5 and 5.2, downlapping onto a surface formed during the sea level fall into OIS 5.2. A time discrepancy arises as this RSL fall occurs at about 95 ka (Figure 1.2; Pillans et al., 1998) yet overlies the Ehux acme zone (their interpretation = 80 to 85 ka) by 2 cm. Use of the Ehux acme as an age indicator is tenuous at best (see previous comments in Results). However, if it is used, it has an age of about 73 ka (Thierstein et al., 1977) at this latitude and is not consistent with the interpretations of Berne et al. (2002). Just above this horizon is Unit 4, a 3 cm interval associated with a cold and dry interval consistent with a LST (OIS 4, this paper), rather than a warm and wet interval associated with a HST (time period of 80-85 ka for OIS 5.1; Berne et al., 2002).

LST 4. Liu et al. (2000) limit their interpretation of the single reflection at borehole DZQ4 as “terrestrial” associated with OIS 4 (their Table 1). Berne et al. (2002) interpret this

single reflection at borehole DZQ4 as the base level fall between OIS 5.3 (5c) and 5.2 (5b) (Figure 1.14). Neither Liu et al. (2000) or Berne et al. (2002) identify the thicker portion of this unit north of core DZQ4 or the SF MOUND TST tidal ridges (TST 4/3) bounding the top of this thicker SF CHAO portion of LST 4. The thicker portion of LST 4 has not been identified in previous studies of the ECS and is unique to this investigation. Like the underlying LST 6, this package of SF CHAO is interpreted as a fluvial deposit. This thicker portion of LST 4 was not cored, so lithologic comparison is made through the similarity of seismic attributes between the SF CHAO units of LST 4 and 6 (penetrated by core DZQ4). Therefore, the thick portion of LST 4 is inferred to have a composition similar to cross-bedded sands with terrestrial components such as pollen from land plants and wood debris. Like the thin LST 4 interval observed in core DZQ4, sporo-pollen and nannofossil assemblages from LST 4 SF CHAO are also expected to be indicative of the cold and dry environment that existed between 74 and 59 ka (Imbrie et al., 1984). Because LST 4 (80 m below present) was not as extreme as LST 6 or LST 2 (120 m below present), much of the margin remained submerged and fluvial deposition appears to be limited to the 50 km wide incised valley observed in strike-oriented seismic profiles. Therefore, the correlative high-amplitude reflection observed at DZQ4 is interpreted as terrestrial flood plain or a shallow (20-50 m), inner-shelf environment.

TST 4/3. At DZQ4, Liu et al. (2000) interpreted this as a separate unit related to the TST. Berne et al. (2002) do not differentiate the TST from the overlying HST 3. As stated earlier, the tidal ridges that are present between LST 4 and HST 3 are limited to one strike-oriented seismic profile. There, six tidal ridges occur at the upper boundary of the southern portion of the LST 4 incised valley and continue south for 100 km down the sloping toe of

the underlying HST 5 delta lobe. Tidal ridges from TST 4/3 may be preserved elsewhere on the margin and were not imaged during our study based on survey geometry. However, it is certainly feasible that these ridges are limited to this locale and associated with the sediment supply of the LST 4 incised valley. Yang and Sun (1988) present evidence that the tidal ridges that formed during the transgression between LST 2 and the present-day highstand (i.e., TST 2/1) occur primarily in the submerged paleovalley of the Yangtze River formed during LST 2. It is hypothesized that the limitation of tidal rivers to the incised valleys is associated with a combination of reworking of trapped fluvial sediment into ridges by tidal currents that were amplified by estuary geometry during transgression. However, Yang and Sun (1988) also identified TST 2/1 tidal ridges in locations across the margin besides the Yangtze paleovalley. Minor sets of TST 2/1 ridges are also present on northern portions of the margin (see Figures 1.17 and 1.18) outside the Yantze paleovalley, incision still evident in modern bathymetry (Figure 1.1). These tidal ridges appear to be related to other incised valleys across the margin (Figure 1.10A).

In comparison, tidal ridges from TST 6/5 are present across the entire margin during a time when no incision is present in the seismic record (Figure 1.5). Tidal ridges from TST 4/3 are only located within the incised LST 4 paleovalley. Assuming the presence of the critical tidal velocity to create these ridges (Yang and Sun, 1988; Zhu and Chen, 2005), their formation may also be dependent on sediment supply. During times of decreased precipitation (i.e., glacials) and a possible decrease in sediment supply, it is not surprising that tidal ridges are proximal to one or more fluvial sediment supplies (e.g., TST 4/3 and TST 2/1). Lateral constraint of a fluvial system (i.e., incised valley) produces a focused depocenter and reduces the extent of sediment on the rest of the margin. The isolation of

tidal ridges to sites within the incised valleys of LST 4 and 2 may therefore be significant. While tidal ridges also are present outside the LST 2 Yangtze paleovalley on northern portions of the margin, there are multiple secondary incised systems across the central and northern margin to which these TST 2/1 ridges could be related (Figure 1.10). The widespread tidal ridges of TST 6/5 have no preferential location on the margin. The apparent lack of an incised fluvial system during LST 6 explains the lack of a focused depocenter. The widespread fluvial sheet sands of LST 6 provide a widely distributed sediment supply that may explain the widespread tidal ridges of the overlying TST 6/5.

A modern example that links the ECS/YS tidal ridges to the presence of an unconsolidated sediment source, and one not associated with an incised valley, is found in the Jianggang radial sand ridge field 100 km north of the mouth of the Yangtze River. While tidal currents are requisite to rework these submarine sediments, there must be sediment to rework. In this case, an abandoned delta of the Yellow River supplies ample sediment for the ridges. An amphidromic point for multiple tidal components (e.g., M2 or principal lunar, K1 or luni-solar diurnal) is probably responsible for the radial pattern of this ridge field (Choi, 1980; Larsen et al., 1985; Yang, 1989; Congxian et al., 2001; Zhu and Chen, 2005). While these tidal currents are an important factor in tidal ridge development, this particular ridge field owes its existence to a pre-existing sediment supply from an abandoned delta of the Yellow River (Yang, 1989; Li et al., 2001).

HST 3. HST 3 in both cores is interpreted as deltaic silts and sands deposited on the central to outer margin during OIS 3 (i.e., HST 3). During this time (59 to 24 ka; Imbrie et al., 1984) sea level averaged 80 m below present, but gradually fell from its high of 60 m to its low of 100 m below present, signaling the beginning of LST 2. Precipitation rates during

OIS 3 were interpreted to be a little less than they are today (Liu et al., 1995; Evans and Heller, 2001). Unlike the HST 5 deltaic perched lobe that occupied middle and inner shelf accomodation, the majority of HST 3 deltaic deposits were forced basinward and offlap over the paleo shelf-slope break into the Okinawa Trough. SF FLAT is found on the middle margin and SF DIP is found on the outer margin and uppermost continental slope. Yang (1989) interpreted this interval at borehole YQ1 as prodeltaic, fine-grained sediments on the shallow, inner shelf not far from an estuary mouth. Liu et al. (2000) suggested a suite of environments at borehole DZQ4 (subfluvial delta, shallow sea, terrestrial river mouth, and poorly preserved tidal sand ridge; their Table 1). Berne et al. (2002) interpreted this unit at borehole DZQ4 as shallowing upward, well-bedded, prodeltaic silts.

LST 2. LST 2 is the only stratigraphic unit that experiences major incision. Infill of these channels varies between SF FLAT, SF DIP, and SF CHAO. This incised system was not completely filled during LST 2, TST 2/1, and HST 1 and is present in modern bathymetry (Wang, 1980; Hori et al., 2001; 2002a; 2002b; 2002c). The incised valley complex dissects the shelf and terminates basinward into distinct units of SF MOUND that are interpreted as lowstand deltas perched at and offlapping over the shelf-slope break. Wellner and Bartek (2004) contrasted the ECS incised valley system from OIS 2 with the Rhone incised valley on the Rhone Shelf (Gensous and Tesson, 1996) and the Brazos-Trinity incised valley complexes in the Gulf of Mexico (Anderson et al., 1996; Badalini et al., 2000). The incised valleys of both the Rhone and Brazos-Trinity maintain a constant width or become narrower and deeper offshore, and feed lowstand deltas at the shelf-slope break. The ECS incised valley complex, however, becomes shallower and broader offshore. In addition, Wellner and Bartek (2004) contend that the ECS also lacks lowstand deltas. However, examination of

isopach maps, produced with data collected for this investigation, reveals the presence of thick packages of SF MOUND at the terminus ofat least two LST 2 incisions (Figure 1.10). In some areas, the basinward-stepping clinoforms of these units offlap over the shelf-slope break (Figure 1.11). These units at the present-day shelf-slope break are interpreted as the deltaic component of the LST 2 incised valley system. While Chung and Chang (1995) also proposed direct sediment discharge onto the continental slope in the southernmost part of the ECS shelf basin into the Okinawa Trough via incised channels, they did not identify or suggest lowstand delta complexes. Aside from preliminary work with this dataset (Miller, 2002; Warren and Bartek, 2002b), this is the first time lowstand deltas associated with LST 2 are identified on the ECS continental margin.

LST 2 thins dramatically on the interfluves, often to a single reflection. The base of this unit is the SB at the beginning of OIS 2 and the upper boundary is the transgressive surface of TST 2/1. Yang (1989) interpreted this unit at YQ1 as a LST in an estuary mouth with strong tidal influence. Liu et al. (2000) interpreted this unit at borehole DZQ4 as riverine, but noted the zone is beyond recognition at only 1 m thick (their Table 1). Berne et al. (2002) interpreted this unit at borehole DZQ4 as a deepening from reworked fluvial sediments to an inner shelf facies (20-50 m deep) and into the tidal sand ridge facies. The correlation in this unit (LST 2) is the poorest tie between this paper and Berne et al. (2002). There are many possible reasons for this. First, much of the summarized core description contains interpretation, rather than just simple observation of the variation in lithologic attributes. Second, seismic profiles are most likely not from exactly the same location as the core site. Core DZQ4 is projected into seismic profiles analyzed in this investigation to within 1 km of the borehole, and the bathymetry in this area varies widely due to a

concentration of tidal ridges on the seafloor. Third, the velocity model is approximate and assumed to be constant rather than tied to the borehole with a sonic survey and a synthetic seismogram. Finally, discrepancies in correlation and interpretation exist because the acoustic masking from the source signature at and near the seafloor makes interpretation difficult, and Berne et al. (2002) did not use higher resolution chirp sonar in their interpretation.

TST 2/1. The tidal ridges preserved from the last transgression are evident in present-day bathymetry. These sand ridges in particular, while closely related to transgressions and the flow field of tidal currents, are moribund on the outer and middle margin and in equilibrium with current oceanographic conditions on the inner margin (Bartek and Wellner, 1995; Yang, 1989). Yang (1989) identified this interval at borehole YQ1 as transgressive tidal sand ridges reworked near their surface. Liu et al. (2000) interpreted this unit at borehole DZQ4 as an estuary mouth with strong tidal influence. Berne et al. (2002) classified this unit at borehole DZQ4 as another separate tidal sand ridge facies separated from the underlying sand ridge facies by a sharp erosional boundary. Therefore, similar to older TSTs previously identified in this investigation, the TST between OIS 2 and 1 is represented by either a thin sand veneer or a stratigraphically equivalent tidal ridge. The thin nature of the TST is represented by a single high-amplitude reflection that is also an amalgamation of the underlying TS in seismic profiles. The thicker portion of the TST appears in seismic profiles as mounded ridges (SF MOUND) bounded at its base by the TS. As mentioned previously, these tidal ridges are distributed across the margin and are prominent in present-day bathymetry. The majority of ridges are found within the Yangtze paleovalley. Minor occurrences of these ridges outside this location may also be related to

secondary incisions across the northern and central portions of the margin (Figure 1.10). The sediments accumulated in these incised valley complexes during the LST, and subsequently reworked by tidal currents during rising sea level, may be a crucial component to tidal ridge formation.

HST 1. The tidal sand ridges at the seafloor were formed during TST 2/1 and are now moribund. In addition, ECS sea level reached or approached its present level around 6 to 7 ka. At which point the current HST (HST 1) began. Therefore, it can be argued that the current depositional condition of the ECS represents that of a highstand (HST 1). Yang (1989) noted a hardground capping the tidal ridges at the seafloor at boreholeYQ1 with a shell-rich layer containing foraminifera deposited during the current HST. Yang (1989) and Liu et al. (2000) identified this thin veneer of sediments related to HST 1 in their core summaries, but Berne et al. (2002) did not. The present-day HST 1 is preserved as a thin veneer (< 1m) of sand draped over the entire margin at the present-day seafloor or a thin wedge of mud that downlaps the TST in the central and northern portions of the study area (Bartek and Wellner, 1995; Miller, 2002; Wellner and Bartek, 2004). Sands are primarily attributed to the Yangtze River and muds to the Yellow River (Suk, 1989; their Figure 3). Because the HST is thin (< 1 m) across the majority of the margin, it is resolved in seismic profiles as a single, high-amplitude reflection at the seafloor. Where the underlying TST is a thin sand veneer, the HST and TST appear amalgamated in seismic profiles and are only identifiable in higher resolution chirp profiles. With this resolution (≥10 cm) and the sharp impedance contrast generated between underlying TST sands and overlying HST silts and clays, the thin HST is easily imaged across the margin (e.g., Bartek and Wellner, 1995; Wellner and Bartek, 2004). The representation of HST 1, which is essentially at or near the

modern seafloor, in seismic profiles as a single, high-amplitude reflection illustrates the inadequacy of seismic acoustic sources to investigate this unit.

1.5 CONCLUSIONS

The ECS continental margin is characterized by abundant sediment supply, high energy, and unique shelf physiography – a fairly shallow shelf with a low gradient, extreme width, and deep shelf-slope break. These factors facilitated preservation of nearly complete stratigraphic sequences in the shallow strata (<100 m) from the late Pleistocene to present. These sequences offer an excellent opportunity to study the stratigraphic response to extreme depositional conditions. The regional extent of the seismic dataset used in this investigation is larger than all previous studies combined and provides unique observations not available to earlier investigators. A revised stratigraphic framework clarifies existing ECS stratigraphic nomenclature and provides a link to global sea level change. The latter offers an opportunity to assess the relative importance of sea level, sediment supply, and tectonics in shaping ECS margin stratigraphy.

Sedimentation on the ECS margin has been controlled primarily by fluvial depositional processes. Evidence of this is present in the deltaic components that exist during both highstand (e.g., HST 5, HST 3) and lowstand (e.g., LST 6 and LST 2). Further, regional stratigraphic trends and stacking patterns indicate syndepositional tectonic activity. With subsidence dominating the southern portion of the margin and uplift dominating the north, previous hypotheses of tectonic inactivity and passive regional subsidence of this portion of the margin are too simplistic. The combination of all these factors, however, was overwhelmed by the magnitude of high-frequency, glacio-eustatic fluctuations during the Quaternary. Eustatic dominance over subsidence rates is also responsible for the sequence boundaries on the ECS margin that are characterized by widespread erosion during periods of RSL fall (type 1 SB; Posamentier and Vail, 1988). In addition, the rapid transgressions that

spread a thin veneer across the low-gradient shelf also illustrate eustatic dominance over sediment supply and tectonics. Therefore, in light of these observations, eustasy, and not sediment supply or tectonics, is the dominant influence on RSL on the ECS margin during the late Pleistocene and Holocene.

A synopsis of our interpretation of the depositional history on the ECS continental margin during the past 186 ky is as follows:

Seq 3. During the extreme lowstand of OIS 6 (-120 m), the massive fluvial sand sheet of LST 6 was deposited for hundreds of kilometers across the subaerially exposed, low-gradient margin. These unconfined fluvial deposits (SF CHAO) grade laterally into a marine deltaic component (SF DIP) that was truncated by advancing LST 6 fluvial deposits (SF CHAO) as sea level continued to fall. Paleoprecipitation rates are estimated to be about half of present-day values. Intuitively, it seems that decreased precipitation, and subsequent drops in runoff and erosion, would decrease sediment supply to the margin. However, one or more of a combination of factors may explain the massive LST 6 fluvial sand sheet (and ensuing glacial lowstands) in light of decreased precipitation: 1) rates were still adequate to transport abundant sediment load, 2) overextension of fluvial systems across decreased gradient (wider coastal plain) incited deposition, and 3) loss of coastal current system during falling sea level significantly reduced transport of sediment out of the ECS system. The tidal ridges of TST 6/5 (SF MOUND) were created during the subsequent RSL rise. Where tidal ridges are not present, thin sand veneers are stratigraphically equivalent and are evidence of a rapid transgression. These thin (2 m) veneers are resolved in seismic profiles as a single, high-amplitude reflection. The widespread distribution of TST 6/5 tidal ridges may be related to a lack of major, widespread incision observed during LST 6. Without an incised valley to

focus sediment accumulation (and sequester it from interfluves), ample sediment was widely available from the underlying substrate. As RSL reached its highest point, during OIS 5 (similar to present), the interbedded silts and clays of the HST 5 deltaic lobe (SF DIP and SF FLAT) were deposited on the inner and central margin. There, they remained perched, in that they pinched out on the outer margin and did not offlap over the shelf-slope break into the Okinawa Trough.

Seq 2. During the lower magnitude RSL fall into OIS 4 (-80 m), the central portion of HST 5 was exposed. The gradient differential between the delta plain and delta front allowed fluvial processes to incise and create a 50-km-wide incised valley in which LST 4 (SF CHAO, most likely fluvial sands) was deposited. Outside of this incised system and across the rest of the margin, LST 4 is only a very thin (3 cm) unit that represents either an interfluve or a shallow marine environment. A brief RSL rise (-50 m) created a small collection of tidal ridges within the LST 4 incised valley, possibly related to the focused and limited supply of fluvial sediments (SF CHAO) and tidal amplification, as the incision was flooded. Elsewhere on the margin, similar to TST 4/3, these ridges are absent and correlate to a thin veneer of sand. This thin unit (2 m) is resolved seismically as a single, high-amplitude reflection. During the ensuing HST of OIS 3, RSL averaged –80 m, but possessed and overall falling trend heading into OIS 2 at approximately –100 m. Therefore, the majority of the interbedded silts and clays of the HST 3 delta (SF DIP) were deposited on the outer margin, basinward of the HST 5 lobe, and continued to offlap over the shelf-slope break with massive bypass into the Okinawa Trough (thicknesses up to 130 m).

Seq 1. As RSL continued to fall heading into the high-magnitude OIS 2 LST (-120 m), the majority of the margin was again exposed and dissected by a highly incisive LST 2.

Fluvial sediments (SF CHAO) were deposited within these incised valley complexes and grade laterally into floodplain deposits on the interfluves. In some interfluve locales, the LST is thin and resolved in seismic profiles as a single, high-amplitude reflection. Only minor incision occurred on the outermost margin and these fluvial deposits (SF CHAO) are terminated at the shelf-slope break by two, large lowstand delta complexes (SF MOUND). The rapid RSL rise of TST 2/1 again created a numerous tidal ridges (SF MOUND). In areas where ridges are absent, the TST is a thin veneer of sand that is resolved in seismic profiles as a single, high-amplitude reflection. The majority of TST 2/1 tidal ridges are found within the paleovalley of the Yangtze River. The remaining ridge distribution is probably related to secondary incised valley sediment sources across the margin. The present-day HST 1 is preserved as a thin veneer (< 1 m) of sand draped over the entire margin at the present-day seafloor or a thin wedge of mud that downlaps the TST in the central and northern portions of the study area (Bartek and Wellner, 1995; Miller, 2002; Wellner and Bartek, 2004).

Results from earlier studies of the ECS continental margin provide data on lithofacies, age and paleoenvironments constrained by fossil content, as well as verification of present interpretations. However, many of the alternate hypotheses presented in this study require stratigraphic revision of these prior results. Therefore, new stratigraphic framework is presented which utilizes both sequence stratigraphic and Quaternary oxygen isotopic data. This methodology creates a common nomenclature for the shallow strata on the ECS continental margin that correlates and unifies the contributions of previous investigations and facilitates ongoing and future research.

Understanding the interaction between depositional processes and stratigraphic response on the ECS margin has implications for similar strata throughout the geologic record.

Extensive investigations provide an understanding of the formation and distribution of surface and near-surface lithologic (transgressive sands and shell lags as well as highstand silts and clays) and stratigraphic (transgressive tidal ridges) features, both of which occur in the deeper strata within high-resolution core data and seismic profiles. Even though present conditions do not reflect those active during glacial times, an extensive understanding of the last glacial maximum in and around the ECS, in conjunction with the high-resolution core data and seismic profiles used in this investigation, places constraints on those depositional processes as well.

The combination of depositional processes that shape the strata of the ECS margin – high sediment supply, high energy, wide margin, low-gradient margin, deep shelf-slope break – are unique when compared to the spectrum of conditions in modern depositional basins. For example, the Brazilian margin, in close proximity to the Amazon River, has a similar gradient (0.013°) and receives an abundant influx of sediment (1.2 billion tons per year; Milliman and Syvitski, 1992). However, it has a shallow shelf-slope break of about -82 m and a moderate width of 225 km. The Pakistani margin near the Indus River has a deep shelf-slope break at –167 m, but it is much narrower (110 km), it has a steeper gradient (0.08°), and it receives less sediment (pre-dam value of 250 million tons per year; Milliman and Syvitski, 1992). Indeed, many basins share one or more depositional conditions that are similar to the ECS but none share them all. This is not the case throughout the geologic record. For example, most ancient foreland basin systems possess a low-gradient, wide shelf with minimal incision and ample sediment influx. It is possible that stratal architecture within these basins may be formed under depositional processes analogous to the ECS continental margin.

The Eastern Venezuela foreland basin (Miocene) contains many components that are similar to the ECS, including transgressive sand ridges, lowstand deltaic lobes, and sequence boundaries overlying offshore muds (Picarelli et al., 2001; Picarelli et al., 2000). Further, in the upper part of the section, a decrease in lowstand valley incision is attributed to greater accommodation space hypothesized to be driven by a lower gradient (Picarelli et al., 2001). Strata similar to the extensive lowstand unincised fluvial systems active on the ECS margin are found in foreland basin settings from the Mesozoic Castlegate Formation and Mesa Rica Sandstone, both preserved within the U.S. western interior. The Desert Member of the Blackhawk Formation and the Castlegate Formation (late Campanian) exhibit extensive, continuous cliff face exposures attributed to lowstand and transgressive non-marine fluvial deposits formed by vigorous braided river systems on a foreland basin ramp (Miall and Arush, 2001). Van Wagoner (1995) suggests a depositional environment wherein a fluvial complex formed a mega fan complex that did not connect to the sea but died out in a broad, swampy complex of shallow lakes. The Mesa Rica Sandstone (Dakota Group, Albian) is a broad sandstone sheet of similar thickness deposited across the alluvial and/or coastal plain during the maximum Kiowa-Skull Creek regression (late Albian). During this time, the Dalhart Basin maintained a low offshore gradient and gradient reduction in the adjacent coastal plain forced both stream straightening and storage of coarser (non-transportable) sediments in channels. The stable baselevel conditions only allowed minimal channel aggradation, and frequent avulsion and minor lateral migration spread excess sediment and caused regional scouring of a sequence-bounding unconformity (Holbrook and Dunbar, 1992; Holbrook, 1996). Further examples of strata similar to the ECS can also be found in Paleozoic foreland basins. The Devonian Catskill Delta of the northeastern U.S.

Appalachian Basin consists of an abundant clastic influx from the Acadian mountains attributed to alluvial processes with braided streams depositing the coarsest sediments on the fans (Ettensohn, 1985; Woodrow, 1985). Sevon (1985) presents a simplified description of the non-marine portion of the Catskill coastal alluvial plain and represents an orderly vertical progression of delta plain meandering streams to alluvial plain braided streams to alluvial plain meandering streams. Similarly, fluvial morphology on the ECS margin is directly affected by an abundant sediment supply while also being gradient dependent.

A complete interpretation of these ancient rocks requires a thorough understanding of these depositional conditions. This is particularly challenging when many ancient basins lack extensive outcrop, have limited core and well data, and/or are constrained by low-resolution dating techniques (e.g., K-Ar and biostratigraphy) and low-resolution seismic techniques. Because many foreland basins, such as those discussed above, contain stratigraphic architecture similar to the ECS margin, it is quite possible that the strata were created under similar depositional conditions, many of which are observed in the modern system. Therefore, an understanding of the process-response relationship of the ECS margin, both present and recent, offers a tool for to better understand the depositional conditions in similar basinal conditions preserved throughout the geologic record.

1.6 REFERENCES CITED

An, Z., 2000, The history and variability of the East Asian paleomonsoon climate. Quaternary Science Reviews, v. 19, p. 171-187.

Anderson, J.B., Abdulah, K., Sarzalejo, S., Siringin, F., Thomas, M.A., 1996, Late Quaternary sedimentation and high-resolution sequence stratigraphy of the East Texas Shelf. In De Batist, M. and Jacobs, P. (eds.), Geology of Silicilcastic Shelf Seas, Geological Society Special Publication no. 117, London Geological Society, p. 95-124.

Alexander, C.R., DeMaster, D.J., Nittrouer, C.A., 1991, Sediment accumulation in a modern epicontinental-shelf setting: The Yellow Sea. Marine Geology, v. 98, p. 51-72.

Badalini, G., Kneller, B., Winker, C.D., 2000, Architecture and processes in the Late Pleistocene Brazos-Trinity turbidite system, Gulf of Mexico continental slope. Gulf Coast Section of the Society of Economic Paleontologists and Mineralogists, 20th Annual Conference Report, p. 16-33.

Bark, L.S., Ganson, P.P., and Meister, N.A., 1964, Tables of the Velocity of Sound in Sea Water: Pergamon Press, Oxford, England, 182 p.

Bartek, L.R., and Wellner, R.W., 1995, Do equilibrium conditions exist during sediment transport studies on continental margins? An example from the East China Sea. Geo-Marine Letters, v. 15, p. 23-29.

Bartek, L.R., Anderson, J.L.R., Oneacre, T.A., 1997, Substrate control on distribution of subglacial and glaciomarine seismic facies based on stochastic models of glacial seismic facies deposition on the Ross Sea continental margin, Antarctica. Marine Geology, v. 143, p. 223-262.

Berne, S., Lericolais, G., Marsset, T., Bourillet, J.F., de Batist, M., 1998, Erosional shelf sand ridges and lowstand shorefaces: Examples from tide and wave dominated environments of France. Journal of Sedimentary Research, v. 68, p. 540-555.

Berne, S., Vagner, P., Guichard, F., Lericolais, G., Liu, Z., Trentesaux, A., Yin, P., and Yi, H.I., 2002, Pleistocene forced regressions and tidal sand ridges in the East China Sea: Marine Geology, v. 188, p. 293-315.

Bingxian, G. and Hanli, M, 1982, A note on the circulation of the East China Sea. Chinese Journal of Oceanology and Limnology, v. 1, p. 5-16.

Brown, L.J. and Weeber, J.H., 1992, Geology of the Christchurch urban area. Institute of geological and Nuclear Sciences Geological Map 1, 1:25,000, Institute of Geological and Nuclear Sciences, 1 sheet, 104 p.

Brown, L.J. and Wilson, D.D., 1988, Stratigraphy of the late Quaternary deposits of the northern Canterbury Plains New Zealand. New Zealand Journal of Geology and Geophysics, v. 31, p. 305-335.

Browne, G.H. and Naish, T.R., 2003, Facies development and sequence architecture of a late Quaternary fluvial-marine transition, Canterbury Plains and shelf, New Zealand: implications for forced regressive deposits. Sedimentary Geology, v. 158, p. 57-86.

Choi, B.H., 1980, A tidal model of the Yellow Sea and the Eastern China Sea: KORDI Report 80-82, Korea Ocean Research and Development Institute, Seoul, 72 p.

Chough, S.K. and Kim, D.C., 1981, Dispersal of fine-grained sediments in the southeastern Yellow Sea: A steady-state model: Journal of Sedimentary Petrology, v. 51, no. 3, p. 721-728.

Chung, Y. and Chang, W.C., 1995, Pb-210 fluxes and sedimentation rates on the lower continental slope between Taiwan and the South Okinawa Trough. Continental Shelf Research, v. 15, p. 149-164.

Congxian, L., Gang, C., Ming, Y., Ping, W., 1991, The influences of suspended load on the sedimentation in the coastal zones and continental shelves of China. Marine Geology, v. 96, p. 341-352.

Ettensohn, F.R., 1985, Controls on development of Catskill Delta complex basin-facies. In Woodrow, D.L. and Sevon, W.D. (eds.), The Catskill Delta. Special Paper 201, Geological Society of America, Boulder, p. 65-77.

Evans, C.D.R., 1990, The geology of the western English Channel and its western approaches. United Kingdom Offshore Regional Approach, HMSO for the British Geological Survey, London, 94 p.

Evans, M.E. and Heller, F., 2001, Magnetism of loess/paleosol sequences: recent developments. Earth-Science Reviews, v. 54, p. 129-144.

Fairbridge, R.W. (ed.), 1966, The Encyclopedia of Oceanography. Encyclopedia of Earth Sciences, Volume I, Reinhold Publishing Corporation, New York, p. 242.

Forman, S.L., Pierson, J., Lepper, K., 2000, Luminescence geochronology. In: Noller, J.S., Sowers, J.M., Lettis, W.R. (eds.), Quaternary Geochronology, Methods and Applications. American Geophysical Union, Washington, DC, p. 157-176.

Galloway, W.E. and Hobday, D.K., 1996, Terrigenous Clastic Depositional Systems. Springer, Berlin, 489 p.

Gensous, B. and Tesson, M., 1996, Sequence stratigraphy, seismic profiles, and cores of Pleistocene deposits on the Rhone continental shelf. Sedimentary Geology, v. 105, p. 183-190.

Graber, H.C., Beardsley, R.C., Grant, W.D., 1989, Storm-generated surface waves and sediment resuspension in the East China and Yellow Seas. Journal of Physical Oceanography, v. 19, p. 1039-1059.

Han, J.M., Lu, H.Y., Wu, N.Q., Guo, Z.T., 1996, The magnetic susceptibility of moern soils in China and its use for paleclimate reconstruction. Stduies in Geophysics and Geodesy, v. 40, p. 262-275.

Heezen, B., Tharp, M., and Ewing, M., 1959, The floors of the oceans: I. The North Atlantic. Geological Society of America Special Paper 65, 122 p.

Heller, F., Shen, C.D., Beer, J., Liu, X.M., Liu, T.S., Bronger, A., Suter, M., Bonani, G., 1993, Quantitative estimates and paleoclimatic implications of pedogenic ferromagnetic mineral formation in Chinese loess. Earth and Planetary Science Letters, v. 114, p. 385-390.

Hine, N., 1990, Late Cenozoic calcareous nannoplankton from the northeast Atlantic: PhD thesis, University of East Anglia, 339 p.

Holbrook, J., 1996, Complex fluvial response to low gradients at maximum regression: a genetic link between smooth sequence-boundary morphology and architecture of overlying sheet sandstone. Journal of Sedimentary Research, v. 66, p. 713-722.

Holbrook, J.M. and Dunbar, R.W., 1992, Depositional history of Lower Cretacoues strata in northeastern New Mexico: Implications for regional tectonics and depositional sequences. Geological Society of America Bulletin, v. 104, p. 802-813.

Hori, K., Saito, Y., Zhao, Q., Cheng, X., Wang, P., Sato, Y., Li, C., 2001, Sedimentary facies of the tide-dominated paleo-Changjiang (Yangtze) estuary during the last transgression. Marine Geology, v. 177, p. 331-351.

Hori, K., Saito, Y., Zhao, Q., Wang, P., 2002a, Control of incised-valley fill stacking patterns by accelerated and decelerated sea level rise: the Changjiang example during the last deglaciation. Geo-Marine Letters, v. 22, p. 127-132.

Hori, K., Saito, Y., Zhao, Q., Wang, P., 2002b, Evolution of the coastal depositional systems of the Changjiang (Yangtze) River in response to Late Pleistocene-Holocene sea level changes. Journal of Sedimentary Research, v. 72, p. 884-897.

Houthuys, R., Trentesaux, A., De Wolf, P., 1994, Storm influences on a tidal sandbank's surface (Middelkerke Bank, southern North Sea). Marine Geology, v. 121, p. 23-41.

Hung, G.W. and Chung, Y.C., 1994, Sedimentation rates on the continental slope off eastern Taiwan: Marine Geology, v. 119, p. 99-109.

Hunt, D. and Tucker, M.E., 1995, Stranded parasequences and the forced regressive wedge systems tract: deposition during base-level fall – reply. Sedimentary Geology, v. 96, p. 147-160.

Imbrie, J., Hays, J.D., Martinson, D.G., McIntyre, A., Mix, A.C., Morley, J.J., Pisias, N.G., Prell, W.L. and Shackleton, N.J., 1984, The orbital theory of Pleistocene climate: support from a revised chronology of the marine $\partial^{18}O$ record. In, Berger A.L., Imbrie, J., Hays, J., Kukla, G., and Saltzman, B. (eds.), Milankovitch and Climate: Understanding the Response to Astronomical Forcing, Part I. NATO ASI Series, series C, mathematical and physical sciences, v. 126, D. Reidel Publishing Company, Dordrecht, Holland, p. 269-305.

Jun, Y., Shuxi, C., and Healy-Williams, N., 1995, Evolution of the paleo-Kuroshio system and its relation to climate changes since the last interglacial. Marine Geology and Quaternary Geology (Haiyang Dizhi Yu Disiji Dizhi), v. 15, p. 26-40.

Kang, Y.Q., 1984, An analytic model of wind-driven currents in the Yellow, the East China and the South China Seas. In Ichiye, T. (ed.), Ocean Hydrodynamics of the Japan and East China Seas, Elsevier Oceanography Series v. 39, Elsevier, Amsterdam, p. 143-154.

Kim, S.W., 1973, A study on the terraces along the southeastern coast (Bang-eojin-Pohang) of the Korean Peninsula. The Journal of Geological Society of Korea, v. 9, no. 2, p. 89-121.

Kim, J.-M. and Kucera, M., 2000, Benthic foraminifer record of environmental changes in the Yellow Sea (Hwanghae) during the last 15,000 years. Quaternary Science Reviews, v. 19, p. 1067-1085.

Kong, F., 1998, Continental margin deformation analysis and reconstruction – evolution of the East China Sea Basin and adjacent plate interaction: PhD dissertation, University of Texas at Austin, 263 p.Lee, H.J. and Chough, S.K., 1989, Sediment distribution, dispersal, and budget in the Yellow Sea: Marine Geology, v. 119, p. 99-109.

Lanying, W., Jiuxu, C., Yanchou, L., 1991, A preliminary study of the physicomechanic properties of loesses and paleosols of different ages at Weibei Yuan, Shaanxi Province. In, Tungsheng, L. (ed.), Loess, Environmnet and Global Change, Science Press, Beijing, China, p. 245-259.

Larsen, L.H., Cannon, G.A., Choi, B.H., 1985, East China Sea tide currents. Continental Shelf Research, v. 4, p. 77-103.

Leckie, D.A., 1994, Canterbury Plains, New Zealand – Implications for Sequence Stratigraphic Models. American Association of Petroleum Geologists Bulletin, v. 78, p. 1240-1256.

Lee, H.J. and Chough, S.K., 1989, Sediment distribution, dispersal and budget in the Yellow Sea. Marine Geology, v. 87, p. 195-205.

Li, C.-X., Zhang, J.Q., Fan, D.D., Deng, B., 2001, Holocene regression and the tidal radial sand ridge system formation in the Jiangsu coastal zone, east China. Marine Geology, v. 173, p. 97-120.

Li, S., Pang, X., Li, M., Jin, Z., 2003, Geochemistry of petroleum systems in the Niuzhuang South Slope of Bohai Bay Basin – part 1: source rock characterization. Organic Geochemistry, v. 34, p. 389-412.

Liu, X., Rolph, T., Bloemendal, J., Shaw, J., Liu, T., 1995, Quantitative estimates of paleoprecipitation at Xifeng, in the Loess plateau of China. Palaeogeography, Palaeoclimatology, Palaeoecology, v. 113, p. 243-248.

Liu, Z.X., Berne, S., Saito, Y., Lericolais, G., Marsset, T., 2000, Quaternary seismic stratigraphy and paleoenvironments on the continental shelf of the East China Sea: Journal of Asian Earth Sciences, v. 18, p. 441-452.

Maher, B.A., and Thompson, R., 1995, Paleorainfall reconstructions from pedogenic magnetic susceptibility variations in the Chinese loess and paleosols. Quaternary Research, v. 44, p. 383-391.

Miall, A.D. and Arush, M., 2001, The Castlegate Sandstone of the Book Cliffs, Utah: sequence stratigraphy, paleogeography, and tectonic controls. Journal of Sedimentary Research, v. 71, p. 537-548.

Miller, K.M., 2002, Paradoxical sediment starvation in the East China Sea and Okinawa Trough region. Unpublished Master's Thesis, University of North Carolina at Chapel Hill, 140 pp.

Milliman, J.D. and Meade, R.H., 1983, World-wide delivery of river sediments to the oceans: Journal of Geology, V. 91, no. 1, p. 1-21.

Milliman, J.D., Shen, H-.T., Yang, Z-.S., Meade, R.H., 1985a, Transport and deposition of river sediment in the Changjiang estuary and adjacent continental shelf. Continental Shelf Research, v. 4, p. 37-45.

Milliman, J.D. and Syvitski, J.P.M., 1992, Geomoprhic/tectonic control of sediment discharge to the ocean: The importance of small mountainous rivers: Journal of Geology, v. 100, p. 525-544.

Mitchum, R.M., Vail, P.R., Sangree, J.B., 1977, Seismic stratigraphy and global changes of sea level, part 6: stratigraphic interpretation of seismic reflection patterns in depositional sequences. In Payton, C.E. (ed.), Seismic Stratigraphy – applications to hydrocarbon exploration, AAPG Memoir 26, American Association of Petroleum Geologists, Tulsa, p. 117-133.

Okada, H and Honjo, S., 1975, Distribution of coccolithophores in marginal seas along the western Pacific Ocean and in the Red Sea: Marine Biology, v. 31, p. 271-285.

Park, S.-C., Han, H.-S., Yoo, D.-G., 2003, Transgressive sand ridges on the mid-shelf of the souther sea of Korea (Korea Strait): formation and development in high-energy environments. Marine Geology, v. 193, p. 1-18.

Park, J.-O., Tokuyama, H., Shiohara, M., Suyehiro, K., Taira, A., 1998, Seismic record of tectonic evolution and backarc rifting in the southern Ryukyu island arc system. Tectonophysics, v. 294, p. 21-42.

Payton, C.E. (ed.) 1977, Seismic Stratigraphy – applications to hydrocarbon exploration, AAPG Memoir 26, American Association of Petroleum Geologists, Tulsa, 516 p.

Picarelli, A.T., Savini, R.R., Selva, C., 2000, Tectonic and eustatic controls on reservoir architecture on the distal zone of foreland basins: shallow marine Cenozoic sediments in eastern and western Venezuela. Annual Meeting Extended Abstracts, American Association of petroleum Geologists, v. 2000, p. 116.

Picarelli, A.T., Arguello, J., Abreu, V., 2001, High resolution sequence stratigraphy and reservoir characterization applied to mature fields: example from the Eastern Venezuela Basin (Mata-Araibel Field). Annual Meeting Extended Abstracts, American Association of petroleum Geologists, v. 2001, p. 158.

Pillans, B., Chappell, J., Naish, T.R., 1998, A review of the Milankovitch climatic beat: template for Plio-Pleistocene sea level changes and sequence stratigraphy. Sedimentary Geology, v. 122, p. 5-21.

Plint, A.G., and Nummedal, D., 2000, The falling stage systems tract: Recognition and importance in sequence stratigraphy. In: Hunt, D., Gawthorpe, R.L. (eds.), Sedimentary Responses to Forced regressions. Geolgoical Society, London, p. 1-17.

Posamentier, H.W., 2001, Lowstand alluvial bypass systems: Incised vs. unincised. American Association of Petroleum Geologists Bulletin, v. 85, p. 1771-1793.

Posamentier, H.W. and Vail, P.R., 1988, Eustatic controls on clastic deposition II – sequence and systems tracts models. In Wilgus, C.K., Hastings, B.S., Kendall, C.G.St.C., Posamentier, H.W., Ross, C.A., Van Wagoner, J.C. (eds.), Sea level Changes: An Integrated Approach. SEPM Special Publication 42, Society of Exonomic Paleontologists and Mineralogists, Tulsa, p. 125-154.

Posamentier, H.W. and Allen, G.P., 1999, Siliciclastic Sequence Stratigraphy – Concepts and Applications. SEPM Concepts in Sedimentology and Paleontology #7, Tulsa, 210 p.

Posamentier, H.W., Allen, G.P., James, D.P., Tessno, M., 1992, Forced regressions in a s equence stratigraphic framewrok: concepts, examples and exploration significance. AAPG Bulletin, v. 76, p. 1687-1709.

Qian, N. and Dai, D.-Z., 1980, Problems of river sedimentation and the present status of its research in China: Chinese Society Hydraulic Engineers, Proceedings of the International Symposium on River Sedimentation, v. 1, p. 1-39.

Saito, Y., Katayama, H., Ikehara, K., Kato, Y., Matsumoto, E., Oguri, K., Oda, M., Yumoto, M., 1998, Transgressive and highstand systems tracts and post-glacial transgression, the East China Sea: Sedimentary Geology, v. 122, p. 217-232.

Saito, Y., Yang, Z., Hori, K., 2001, The Hunaghe (Yellow River) and Changjiang (Yangtze River) deltas: a review on their characteristics, evolution and sediment duscharge during the Holocene. Geomorphology, v. 41, p. 219-231.

Sarnthein, M. and Wang, P., 1999, Response of West Pacific marginal seas to global climatic change. Marine Geology, v. 156, p. 1-3.

Sevon, W.D., 1985, Nonmarine facies of the Middle and Late Devonian Catskill coastal alluvial plain. In Woodrow, D.L. and Sevon, W.D. (eds.), The Catskill Delta. Special Paper 201, Geological Society of America, Boulder, p. 79-90.

Shackleton, N.J., 1987, Oxygen isotopes, ice volume and sea level. Quaternary Science reviews, v. 6, p. 183-190.

Stanley, D.J. and Chen, Z., 1993, Yangtze delta, eastern China: 1. Geometry and subsidence of Holocene depocenter. Marine Geology, v. 112, p. 1-11.

Stride, A.H., Belderson, R.H., Kenyon, N.H., and Johnson, M.A., 1982, Offshore tidal deposits: sand sheets and sand bank facies. In, Stride, A.H. (ed.), Offshore Tidal Sands: Processes and Deposits, Chapman and Hall Limited, London, p. 95-125.

Suk, B.-C., 1989, Sedimentology and history of sea level changes in the East China Sea and adjacent seas. In Asahiko, T. and Fujio, M. (eds.), Sedimentary Facies in the Active Plate Margin, Terra Scientific Publishing Company, Tokyo, p 215-231.

Tang, B.G., 1996, Quaternary stratigraphy in the shelf of the East China Sea in Yang, Z.G. and Lin, H.M. (eds.), Quaternary Stratigraphy in China and its International Correlation: Geology Press, Beijing, China, p. 56-75 (in Chinese).

Tamburini, F., Adatte, T., Föllmi, Bernasconi, S.M., Steinmann, P., 2003, Investigating the history of East Asian monsoon and climate during the last glacial-interglacial (0-140,000 years): mineralogy and geochemistry of ODP Sites 1143 and 1144, South China Sea. Marine Geology, v. 201, p. 147-168.

Thierstein, H.R., Geitzenauer, K.R., Molfino, B., Shackleton, N.J., 1977, Global synchroneity of late Quaternary coccolith datum levels: Validation by oxygen isotopes: Geology, v. 5, p. 400-404.

Thorne, J., 1994, Constraints on riverine valley incision and the response to sea level change based on fluid mechanics. In: Dalrymple, R.W., Boyd, R., Zaitlin, B.A. (eds.), Incised-Valley Systems: Origin and Sedimentary Sequences, SEPM Special Publication no. 51, Society for Sedimentary Geology, Tulsa, p. 29-43.

Vail, P.R., 1987, Seismic stratigraphic interpretation procedure. In: Bally, A.W., (ed.), Atlas of Seismic Stratigraphy: AAPG Studies in Geology no. 27, p. 1-10.

Van Wagoner, J.C., 1995, Sequence stratigraphy and marine to nonmarine facies architecture of foreland basin strata, Book Cliffs, Utah, U.S.A. In Van Wagoner, J.C. and Bertram, G.T. (eds.), Sequence Stratigraphy of Foreland Basin Deposits: Outcrop and Subsurface Examples from the Cretaceous of North America. AAPG Memoir 64, American Association of Petroleum Geologists, Tulsa, p. 137-223.

Van Wagoner, J.C., Posamentier, H.W., Mitchum, R.M., Vail, P.R., Sarg, J.F., Loutit, T.S., and Hardenbol, J., 1988, An overview of the fundamentals of sequence stratigraphy and key definitions. In: Wilgus, C.K., Hastings, B.S., Kendall, C.G.S.C., Posamentier, H.W., Ross, C.A., Van Wagoner, J.C. (eds.), Sea level Changes: An Integrated Approach, SEPM Special Publication no. 42, Tulsa, p. 39-46.

Van Wagoner, J.C., Mitchum, R.M., Campion, K.M., Rahmanian, V.D. (eds.), 1990, Siliciclastic Sequence Stratigraphy in Well Logs, Cores, and Outcrops: Concepts for High-Resolution Correlation of Time and Facies. AAPG Methods in Exploration Series #7, American Association of Petroleum Geologists, Tulsa, 55 p.

Wageman, J.M., Hilde, T.W.C., Emery, K.O., 1970, Structural framework of the East China Sea and Yellow Sea: AAPG Bulletin, v. 54, no. 9, p. 1611-1643.

Wagner, G.A., 1998, Age Determination of Young Rocks and Artifacts: Physical and Cemical Clocks in Quaternary Geology and Archaeology. Springer-Verlag, Berlin, 466 p.

Walling, D.E., Rainfall, runoff, and erosion of the land: a global view. In Gregory, K.J. (ed.), Energetics of Physical Environmnet. Wiley, London, p. 89-117.

Wang, Y., 1980, The Coast of China. Geoscience Canada, v. 7, p. 109-113.

Wang, P., 1999, Response of Western Pacific marginal seas to glacial cycles: paleoceanographic and sedimentological features. Marine Geology, v. 156, p. 5-39.

Wang, J. and Wang, P., 1982, Relationship between sea level changes and climatic fluctuations in East China since last Pleistocene. The Quaternary Research, v. 21, p. 101-114 (in Japanese).

Wang, P. and Samtleben, C., 1983/4, Calcareous nannoplankton in the surface sediments of the East China Sea: Marine Micropaleontology, v. 8, p. 249-259.

Wang, Y. and Aubrey, D.G., 1987, The characteristics of the China coastline: Continental Shelf Research, v. 7, no. 4, p. 329-349.

Warren, J.D. and Bartek, L.R., 2002a, The Metastable Fluvial Shelf System (MMFS): An alternative hypothesis to lowstand unincised fluvial bypass on the East China Sea continental margin: SEPM Research Conference: Incised Valleys: Images and Processes, August 18-23, 2002, Casper and Newcastle, WY.

Warren, J.D. and Bartek, L.R., 2002b, The Sequence Stratigraphy of the East China Sea: Where are the incised valleys? GCSSEPM Foundation Bob F. Perkins Research Conference: Sequence Stratigraphic Models for Exploration and Production: Evolving Methodology, Emerging Models and Applications History, December 8-11, Houston, TX, p. 729-738.

Water Resources Bureau, 1997, Hydrological Year Book of Taiwan, Republic of China, 1995: Ministry of Economic Affairs, Report 00-H-30-26, 400 p.

Weiling, X. and Junying, L., 1989, Structural history of the East China Sea. China Earth Sciences, v. 1, no. 1, p. 59-73.

Wellner, R.W. and Bartek, L.R., 2003, The effect of sea level, climate, and shelf physiography on the development of incised valley complexes: a modern example from the East China Sea. Journal of Sedimentary Research., v. 73, p. 926-940.

Westhoff, K.M. and Bartek, L.R., 2001, Stratigraphy produced by small coastal rivers on the East China Sea continental margin. Abstracts with Programs, v. 33, Geological Society of America, Boulder, p. 80.

Wilgus, C.K., Hastings, B.S., Kendall, C.G.St.C., Posamentier, H.W., Ross, C.A., Van Wagoner, J.C. (eds.), 1988, Sea level Changes: An Integrated Approach. SEPM Special Publication 42, Society of Exonomic Paleontologists and Mineralogists, Tulsa, 407 p.

Wong, G.T.F., Chao, S.-Y., Li, Y.-L., Shiah, F.-K., 2000, The Kuroshio edge exchange process (KEEP) study – an introduction to hypotheses and highlights. Continental Shelf Research, v. 20, p. 335-347.

Woodrow, D.L., 1985, Paleogeography, paleoclimate, and sedimentary processes of the Late Devonian Catskill Delta. In Woodrow, D.L. and Sevon, W.D. (eds.), The Catskill Delta. Special Paper 201, Geological Society of America, Boulder, 246 p. 51-63.

Woolfe, K.J., Larcombe, P., Naish, T., Purdon, R.G., 1998, Lostand rivers need not incise the shelf: An example from the Great Barrier Reef, Australia, with implications for sequence stratigraphic models. Geology, v. 26, p. 75-78.

Xiao, J.L., An, Z.S., Liu, T.S., Inouchi, Y., Kumai, H., Yoshikawa, S., Kondo, Y., 1999, East Asian monsoon variation during the last 130,000 years: evidence from the Loess Plateau of central China and Lake Biwa of Japan. Quaternary Science Reviews, v. 18, p. 147-157.

Yanagi, T. and Takahashi, S., 1993, Seasonal variation of circulations in the East China Sea and the Yellow Sea. Journal of Oceanography, v. 49, p. 503-520.

Yanagi, T., Takahashi, S., Hoshika, A., and Tanimoto, T., 1996, Seasonal variation in the transport of suspended matter in the East China Sea: Journal of Oceanography, v. 52, p. 539-552.

Yang, C.S., 1989, Active, moribund and buried tidal sand ridges in the East China Sea and the southern Yellow Sea: Marine Geology, v. 88, p. 97-116.

Yang, C.S. and Sun, J.S., 1988, Tidal sand ridges on the East China Sea shelf. In: de Boer, P.L., van Gelder, A., Nio, S.D. (eds.), Tide-influenced Sedimentary Environments and Facies. Dordrecht, The Netherlands, D. Reidel, p. 23-38.

Yongqi, Z., Chengkai, A., Yun, F., 1983, The geomorphic types and origin of the East China Sea continental shelf. In: Proceedings of International Symposium on Sedimentation on the Continental Shelf with Special Reference to the East China Sea, April 12-16, Hangzhou, China, China Ocean Press, Beijing, p. 593-601.

Yu, H.-S. and Hong, E., 1992, Physiographic characteristics of the continental margin, northeast Taiwan. TAO (Terrestrial, Atmospheric, and Oceanic Sciences), v. 3, p. 419-434.

Yunshan, Q., Yiyang, A., Lirong, C., Songling, A. (eds.), 1996, Geology of the East China Sea. Science Press, Beijing, 357 p.

Zhang, G. and Li, C., 1996, The fills and stratigraphic sequences in the Qiantangjiang incised paleovalley, China. Journal of Sedimentary Research, v. 66, p. 406-414.

Zhiwu, Z., Jinhai, Z., Peiling, Y., 1989, Characteristics and tectonic evolution of the East China Sea. In: Zhu, X. (ed.), Chinese Sedimentary Basins, Sedimentary Basins of the World, v. 1, chapter 14, p. 165-179.

Zhu, Y. and Chen, Q., 2005, On the origin of the radial sand ridges in the southern Yellow Sea: Results from the modeling of the paleoradial tidal current fields off the paleo-Yangtze River estuary and northern Jiangsu Coast. Journal of Coastal Research, v. 21, p. 1245-1256.

CHAPTER 2

SEQUENCE STRATIGRAPHIC IMPLICATIONS OF THE LOWSTAND UNINCISED FLUVIAL SYSTEM: A CASE STUDY FROM THE EAST CHINA SEA CONTINENTAL MARGIN (LATE PLEISTOCENE)

2.0 INTRODUCTION

Fluvial systems that do not incise the continental margin during relative sea level (RSL) lowstands are rare in the geologic literature. Known examples of lowstand unincised fluvial systems (LUFS) occur during the Quaternary on the continental margins of Australia (Woolfe et al., 1998), Java (Posamentier, 2001), and New Zealand (Browne and Naish, 2003). In addition, based on preliminary observations of the seismic data utilized in this investigation, Warren and Bartek (2002a; 2002b) and Warren et al. (2002) identified laterally and vertically extensive LUFS deposits (>400 km and >40 m, respectively) on the East China Sea (ECS) continental margin prior to oxygen isotope stage (OIS) 4. The limited number of published examples of these unincised strata may reflect their true distribution within the recent geologic record. However, if these unincised lowstand deposits are more widespread than current observations suggest, it begs the question why they have gone unnoticed.

In this paper, a complete characterization of the ECS LUFS are presented, and processes associated with the formation of this stratigraphic element are explored. These observations are based on an extensive, high-resolution 2D seismic dataset containing 14,000 linear km of core-constrained (e.g., lithofacies, age, and paleoclimatic indicators) seismic profiles over a

300,000 km^2 study area (Figure 2.1). The shallow stratigraphy (<150 m) is well preserved on the ECS continental margin and imaged well using these geophysical techniques. Three nearly complete stratigraphic sequences are observed and span the last three sea level cycles

Figure 2.1. Geographic map of the East China Sea region with study area outlined by circle. Also shown (inset) are locations for geotechnical boreholes DZQ4 and YQ1 with respect to seismic profiles from survey grid. Bars mark locations of seismic profiles displayed in this paper. Major fluvial systems and current annual depositional rates into the East China, Yellow, and Bohai Seas. Data compiled from: a) Milliman and Meade, 1983; b) Qian and Dai, 1980; c) Wang and Aubrey, 1987; d) Zhang and Li, 1996; e) Congxian et al., 1991; f) Milliman and Syvitski, 1992; g) Chough and Kim, 1981; h) Lee and Chough, 1989. Bathymetry modified from Quanxing (1990). In the line drawings of stratal unit boundaries on the righthand side of the map, note the aggradational stacking patterns to the south and the progradational stacking patterns to the north, which suggest syn-depositional subsidence and uplift, respectively.

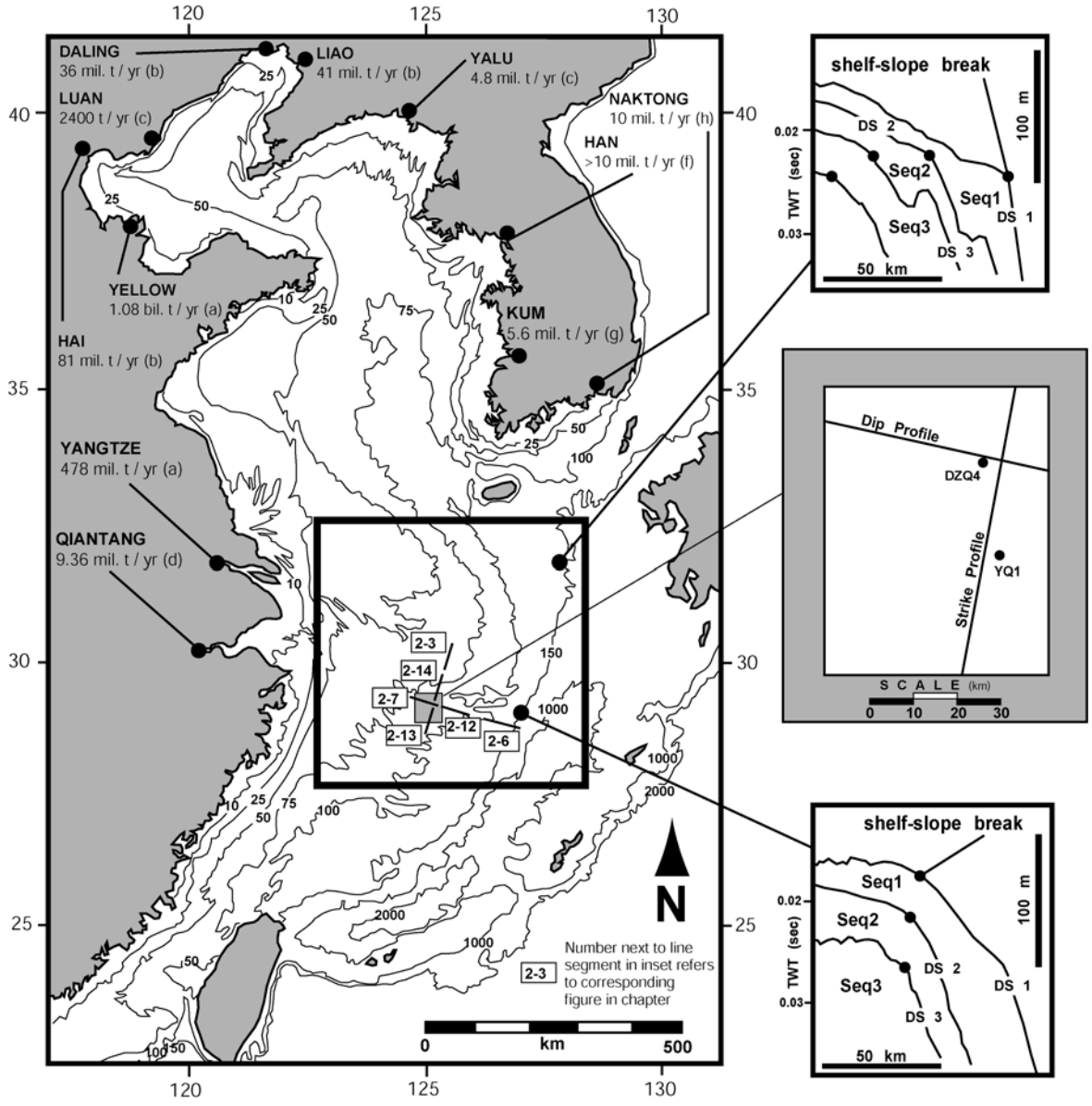
DALING
36 mil. t / yr (b)
LIAO
41 mil. t / yr (b)
YALU
4.8 mil. t / yr (c)
LUAN
2400 t / yr (c)
NAKTONG
10 mil. t / yr (h)
HAN
>10 mil. t / yr (f)
YELLOW
1.08 bil. t / yr (a)
KUM
5.6 mil. t / yr (g)
HAI
81 mil. t / yr (b)
YANGTZE
478 mil. t / yr (a)
QIANTANG
9.36 mil. t / yr (d)
2-3
2-14
2-7
2-13
2-12
2-6
N
Number next to line segment in inset refers to corresponding figure in chapter
0 km 500
120
125
130
40
35
30
25
shelf-slope break
DS 2
Seq2
Seq1
DS 1
Seq3
DS 3
TWT (sec)
0.02
0.03
100 m
50 km
Dip Profile
DZQ4
Strike Profile
YQ1
S C A L E (km)
0 10 20 30
shelf-slope break
Seq1
Seq2
DS 2
Seq3
DS 1
DS 3
TWT (sec)
0.02
0.03
100 m
50 km

(i.e., oxygen isotope stages, or OIS, 6 to 1) from 186 ka to present (Imbrie et al., 1984; Figure 2.2). The present physiography of the ECS margin – an average width of 500 km, an extremely low gradient of 0.013°, and a deep shelf-slope break (between 150 and 192 m below sea level) – is unique and causes the ECS margin to behave like a ramp (i.e., no discrete shelf edge). The gradients of the Yangtze coastal plain (0.003°) and the lower reaches of the Yangtze River (between 0.0002° and 0.0005°; Saito et al., 2001) were even less. Evidence is presented herein that the ECS margin maintained similar physiographic and depositional (i.e., abundant sediment supply) boundary conditions throughout the late Pleistocene and Holocene.

During rapid relative sea level (RSL) fall (i.e., rate of eustatic fall > rate of subsidence) and lowstand (stillstand) on both typical passive continental margins (i.e., shelf-slope-rise morphology of Heezen et al, 1959) and ramp margins, the sequence stratigraphic model predicts cessation of widespread fluvial deposition across the exposed margin, along with stream rejuvenation, subsequent sediment bypass, and incision (Posamentier et al., 1988; Van Wagoner et al., 1988). Therefore, the application of sequence stratigraphic concepts by geologists unfamiliar with an alternate, unincised response to RSL lowstand, may lead to misinterpretation of the LUFS. Posamentier (2001) noted that unincised fluvial systems are difficult to distinguish from highstand alluvial systems. In addition, he postulated that, since their presence is unanticipated, they may be mistaken for a large-scale incised valley system. If Posamentier's (2001) hypothesis is correct, and the LUFS deposits are taken out of stratigraphic context and genetically misunderstood, then the lack of documented examples may reflect a bias due to consistent misidentification. To test this hypothesis, a re-evaluation of continental margin stratigraphy throughout the geologic record may yield evidence that the

Figure 2.2. A) Primary eustatic sea level curve used in this study (from Pillans et al., 1998) based on duration proximity of the $\partial^{18}O$ core data on which the curve is based to the ECS (western Pacific, offshore Papua New Guinea; Shackleton, 1987). B) Relative sea level curve specific to ECS (from Saito et al., 1998). Both curves correlate well where they overlap but limited time span of ECS RSL data makes the use of this curve secondary.

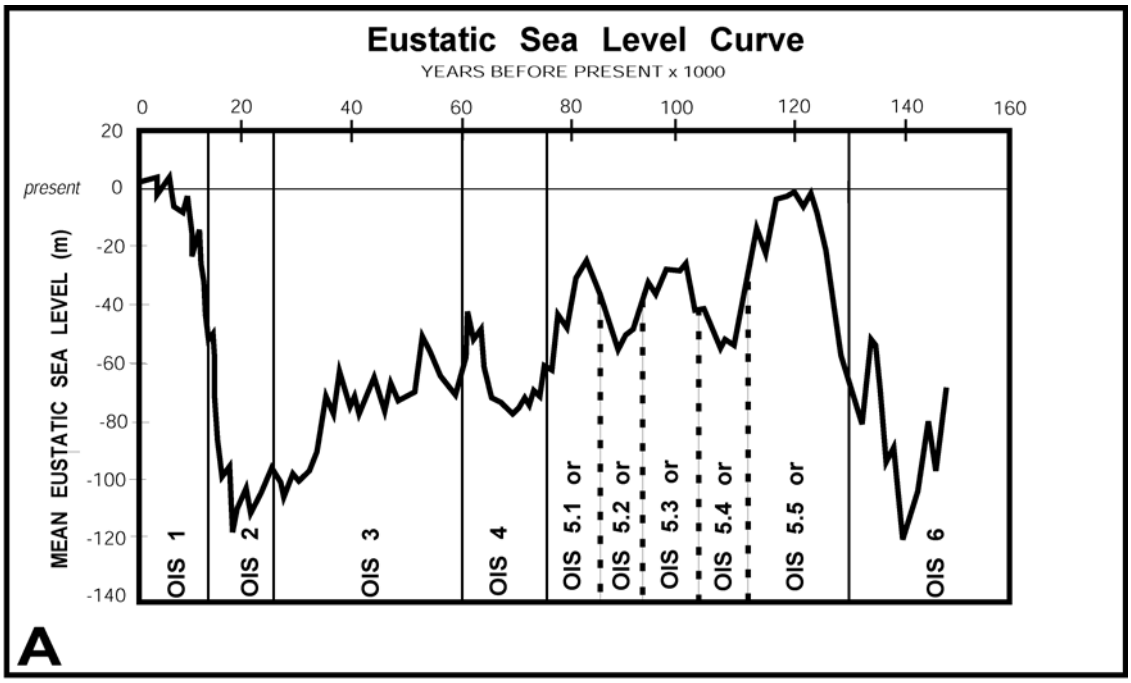
Eustatic Sea Level Curve
YEARS BEFORE PRESENT x 1000
0
20
40
60
80
100
120
140
160
20
present
0
-20
-40
-60
-80
-100
-120
-140
MEAN EUSTATIC SEA LEVEL (m)
OIS 1
OIS 2
OIS 3
OIS 4
OIS 5.1 or
OIS 5.2 or
OIS 5.3 or
OIS 5.4 or
OIS 5.5 or
OIS 6
A

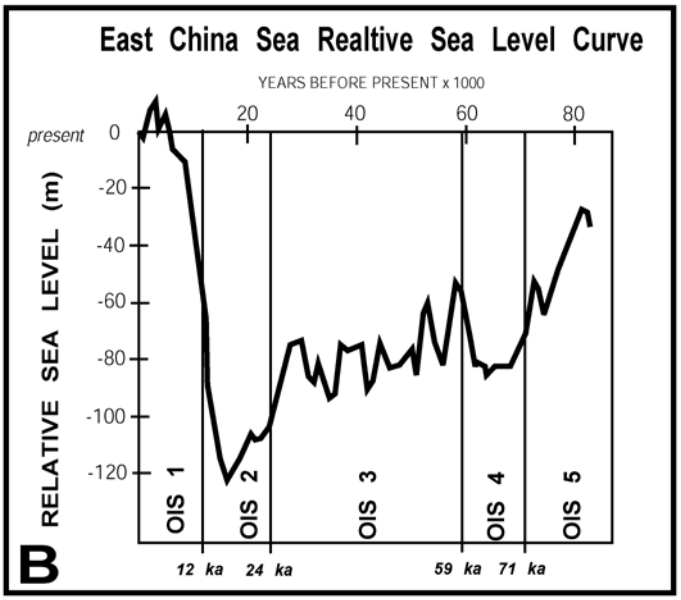
East China Sea Realtive Sea Level Curve
YEARS BEFORE PRESENT x 1000
20
40
60
80
present
0
-20
-40
-60
-80
-100
-120
RELATIVE SEA LEVEL (m)
OIS 1
OIS 2
OIS 3
OIS 4
OIS 5
12 ka
24 ka
59 ka
71 ka
B

LUFS are more widespread than currently suspected. Potential margin candidates probably exhibit similar features of those margins where the LUFS are observed, namely a low gradient (i.e., coastal plain / exposed shelf gradient < fluvial gradient), possibly a deep shelf-slope break, and an abundant sediment supply. This combination of conditions, while rare on passive continental margins, is common in foreland basins throughout the Phanerozoic, where deposits contain extensive fluvial sand sheets that aggrade and avulse instead of incise. The similar stratal geometry of foreland basin lowstand deposits may signifiy formation under a comparable set of depositional processes. This link establishes a process-response relationship that allows a more comprehensive understanding of ancient basins, many of which lack extensive outcrop, have limited core and well data, and/or are constrained by low-resolution dating techniques (e.g., K-Ar and biostratigraphy) and low-resolution seismic techniques.

2.1 GEOLOGIC SETTING

The ECS overlies the eastern margin of the Eurasian plate where it converges with and overrides the Philippine plate. The ECS is an epeiric sea that covers an area of approximately 752,000 km^2, one third of which overlies the Okinawa Trough. The Okinawa Trough is a back-arc basin formed during the Miocene, presently spreading at about 1-2 cm/yr and reaching a maximum depth of 2,719 m (Park et al., 1998). The ECS continental margin is dominated by exogenic forces and is presently considered to be tectonically inactive (Weiling and Junying, 1989). Together, the continental margin and Okinawa Trough exhibit the fundamental shelf-slope-rise pattern typical of most passive continental margins (Heezen et al., 1959). ECS margin physiography is defined by a low gradient (0.23 m/km or 0.013°) and a deep shelf-slope break that occurs in present water depths between 150 and 192 m deep (average = 170 m; Wong et al., 2000). The portion of the ECS landward (west) of the shelf-slope break (460,000 km^2) is epicontinental with an average water depth of 72 m. The ECS has maximum dimensions of 1,300 km (north-south) by 740 km (east-west) making the underlying continental margin one of the broadest shelves in the world.

The ECS offers a set of extreme geologic and oceanographic conditions: high sediment supply, high energy, and a unique basin physiography that consists of a wide, low-gradient continental margin with a deep shelf-slope break. This suite of depositional conditions is rare in modern environments but has occurred throughout the geologic record and has often been associated with foreland basins, including the Cenozoic Ebro basin (Spanish Pyrenees; e.g., Bentham et al., 1993; Jones et al., 2001), the Mesozoic U.S. western interior (e.g., Holbrook and Dunbar, 1992; Van Wagoner, 1995; Holbrook, 1996; Yoshida, 2000; Miall and Arush, 2001), and the Paleozoic Bowen basin (Queensland, Australia; e.g., Fielding et al.,

1993) (the similar characteristics of the lowstand fluvial deposits in these basins are presented in the discussion section of this paper). A better understanding of the stratigraphic response to the depositional processes presently and recently active on the ECS margin (e.g., fluvial input, oceanographic currents, sediment distribution) might, in turn, provide a viable analog for similar elements in ancient basins.

Interpreting the process-response relationship on the ECS margin is fairly straightforward. A strong correlation between vertically repetitive seismic attributes and systems tracts indicates that similar depositional processes were also active during the late Pleistocene and Holocene. Stratal features at or near the modern seafloor, such as tidal ridges (see Discussion), are identical to those observed deeper in the seismic profiles and suggest similar oceanographic and geologic conditions. In addition, the stratal architecture observed in seismic profiles in this investigation also indicates similar physiographic conditions throughout the late Pleistocene and provides a potential link between basin architecture and depositional processes. For example, the paleo shelf-slope breaks are within 10 km (laterally) of present and indicate a similar width (Figure 2.1). The lack of major incision at both the modern and paleo shelf-slope breaks signifies that the edge of the margin remained submerged during even high-magnitude lowstands (i.e., 120 m below present; Pillans et al., 1998; Figure 2.2). Throughout this same time interval, glacial maxima created geologic and oceanographic conditions distinctly different from today. Core data presented in this study verify cool, dry climates and subaerial depositional environments across an exposed margin (i.e., decreased baselevel). These data correlate well with the seismic profiles used in this investigation and indicate a distinct, and different, stratigraphic response

between highstand (stadial) and lowstand (glacial) strata. Based on these process-response relationships, the depositional processes active during glacial maxima can be inferred.

2.2 DATA AND METHODS

The seismic data utilized in this investigation were acquired in the ECS during the past decade. These surveys consist of an overlapping grid of approximately 14,000 km of 2-D, high-resolution, single-channel seismic profiles and cover a 300,000 km^2 study area extending from 28° to 33° N latitude and 123° to 128° 30' E longitude (Figure 2.1). Survey geometries consist of an even distribution of strike- and dip-oriented profiles where strike is considered to trend parallel to the shelf-slope break (approximately N 12° E). Survey lines are spaced between 10 and 20 km on the inner margin and between 20 and 50 km on the outer margin. In addition to seismic data, approximately 10,000 km of higher-frequency chirp sonar profiles were collected concurrently over portions of the same grid. These data provide sub-meter resolution of the uppermost strata that are often masked in seismic profiles by the acoustic source signature (i.e., bubble pulse). This extensive, nested-frequency dataset (i.e., 100 to 2,000 Hz for seismic and 2,000 to 16,000 Hz for chirp) facilitates a regional, seismic- and sequence-stratigraphic analysis of shallow subsurface strata (up to 150 m deep) deposited during the Holocene and late Pleistocene back to OIS 12 (approximately 500 ka). However, this investigation primarily focuses on the strata from the sea level lowstand associated with the glacial period during OIS 6.

Seismic data were acquired using a number of acoustic sources. Depending on sea state and/or water depth, sources varied between high-frequency boomer systems (500 to 2,000 Hz, up to 350 Joules), generator-injector (GI) air guns (50 in^3 and 210 in^3; 10 to 2,000 Hz), and water guns (15 in^3; 100 to 4,000 Hz). Shot intervals varied between 0.5 and 4 seconds depending on source and water depth. Single-channel hydrophone arrays were employed, and they contained between 10 to 20 elements with an average spacing interval of 1 meter.

The average ship speed during acquisition was no faster than 5 knots. Digital data were recorded using the DelphSeismic acquisition system from Triton Elics International. Paper records (thermal plots) were also generated in real time from analog data that underwent minimal filtering and amplification. Digital data were processed with standard techniques such as bandpass filtering and gain using both DelphSeismic and ProMax (Landmark Graphics Corporation) software packages and interpretation was done both on paper and digital sections, the latter using the Kingdom Suite software package from Seismic-Micro Technology, Inc.

Velocity models were constructed in order to correlate the two-way travel time (TWT) of seismic stratigraphy to depth in cores. Due to the absence of borehole velocity data within the study area, approximate time-depth conversions use an average sediment velocity of 1,600 m/sec based on shallow (0 to 4 m) core velocities (Jim Miller, pers. comm.) and least square regression plots of a regional borehole sonic (acoustic velocity) dataset (Kong, 1998). Other investigations within the ECS use velocities ranging from 1,500 m/sec (Saito et al., 1998) to 2,000 m/sec (Wageman et al., 1970). Water column velocity of 1,500 m/sec is based on empirical data (Bark et al., 1964) for expected salinity and temperature distributions during acquisition (Yanagi et al., 1996).

The seismic surveys include profiles proximal to a 52-meter-deep coring location to take advantage of published data. Core DZQ4 was acquired by the Shanghai Marine Geology Bureau on the central portion of the margin (29° 24.75' N, 125° 21.85' E) in 88.7 m of water (Figure 2.1). This core penetrated to a depth of 51.65 m below the seafloor (mbsf). A summary of the sedimentology, microfossils (foramanifera), nannofossils (coccolithophores), sporo-pollen assemblages, and oxygen isotope and thermoluminescence (TL) dates was

originally reported by Tang (1996) and subsequently presented in English by Saito et al. (1998), Liu et al. (2000) and Berne et al. (2002). These data and provide the chronostratigraphic control to which the sequence stratigraphic framework is tied. Confident correlations exist between the core strata and the seismic profiles.

Seismic reflection attributes (*sensu* Mitchum et al., 1977), including the amplitude and lateral continuity of reflection geometries, and seismic termination patterns (i.e., downlap and erosional truncation) are used to create a sequence stratigraphic framework based on the three major bounding surfaces (SB, TS, and MFS) found within each sequence (e.g., Vail, 1987; Posamentier and Vail, 1988; Posamentier et al., 1988; Van Wagoner et al., 1988; Van Wagoner et al., 1990; Posamentier and Allen, 1999). The ages of the stratigraphic subdivisions are constrained by biostratigraphy and thermoluminescence dates from borehole DZQ4. The primary sea level reference used is from Pillans et al. (1998). The sea level curve was based on the interval of time it spans (0 to 150 ka) and the geographic proximity to the ECS of the core on which it is based (i.e., western Pacific, offshore Papua New Guinea; Shackleton, 1987). The relative sea level (RSL) curve of Saito et al. (1998) is specific to the ECS and correlates well to the curve presented by Pillans et al. (1998), but it spans an interval too short (i.e., 0 to 80 ka) to include the main stratigraphic interval from OIS 6 presented in this investigation (Figure 2.2).

2.3 RESULTS

The stratal surfaces and sedimentary units from the late Pleistocene and Holocene are well preserved in the shallow strata (<100 m) on the ECS margin. Furthermore, they are easily imaged using seismic and chirp sonar techniques. Identification of seismic reflection attributes (e.g., reflection geometry, amplitude, and lateral extent) and stratal termination patterns (e.g., downlap and erosional truncation) facilitates a logical subdivision of stratal units by bounding surfaces (sequence boundary, SB; transgressive surface, TS; maximum flooding surface, MFS). Three nearly complete stratigraphic sequences (i.e., lowstand systems tract, LST; transgressive systems tract, TST; highstand systems tract, HST) are constrained chronologically by core data for the last three sea level cycles that span the past 186 ky (OIS 6 to OIS 1; Imbrie et al., 1984). Ages of units deeper than OIS 6, due to their similar seismic reflection attributes and sequence stratigraphic framework, are estimated using downward extrapolation of correlation between the OIS and sequence stratigraphy.

Results from earlier studies of the ECS continental margin (e.g., Yang, 1989; Bartek and Wellner, 1995; Saito et al., 1998; Liu et al., 2000; Berne et al., 2002; Yoo et al., 2002; Wellner and Bartek, 2003) provide data on lithofacies, age, and paleoenvironments constrained by fossil content, as well as third-party verification of interpretations. However, the high-resolution, 2-D seismic survey from this investigation is larger, in terms of linear length of acquired seismic profiles, than all of the aforementioned studies combined. This regional dataset facilitates observations of strata relationships that were not possible using datasets of the earlier investigations.

2.3.1 Seismic and Sequence Stratigraphy

The shallow nature of the ECS (average depth = 72 m; Yunshan et al., 1996) creates a shallow seafloor multiple that obscures the seismic reflections of deeper strata. These factors limit the depth of investigation, especially on the inner margin where the sea is often less than 40 m deep (i.e., seafloor multiple occurs in seismic data <40 m below seafloor). Further, much of the stratigraphy on the inner margin is truncated by erosion. Therefore, the most vertically extensive and complete observations are from the southwestern portion of the study area, on the central and outer margin, where three complete sea level sequences are identified in the upper 50 m of strata as Seq 3, Seq 2, and Seq 1 (Figure 2.3).

The deepest of these three sequences, the lower portion of which is the focus of this investigation (i.e., the LST), is initially referred to as Seq 3. It is bound at its base, on the inner and central portions of the margin, by a relatively flat erosional surface that is the sequence boundary (i.e., SB 3). This high-amplitude surface exhibits high lateral continuity and extends across the margin for hundreds of kilometers in both strike- and dip-oriented seismic profiles (Figure 2.4). On the outer margin, the LST directly above SB 3 thins and grades laterally into downlapping reflections that offlap in a basinward direction (Figures 2.5 and 2.6). Where this occurs, the sequence boundary becomes a correlative, conformable surface onto which the downlapping reflections offlap, and the erosional surface that overlies these downlapping reflections becomes an erosional disconformity (i.e., ED 3). The upper boundary of the LST is also a high-amplitude downlap surface (i.e., DS 3) and the most laterally extensive seismic reflection in the dataset. This downlap surface is relatively flat and extends across the margin for hundreds of kilometers in both strike- and dip-oriented seismic profiles. However, the downlapping reflections above DS 3, but below the overlying

Figure 2.3. High-resolution seismic profile illustrating the three sea level sequences and their systems tracts (LST, TST, and HST) preserved in the strata on the central portion of the ECS margin. Sequences are referred to here as Seq3 (oldest), Seq2, and Seq1 (youngest). The location of this profile with respect to the ECS margin is identified in Figure 2.1.

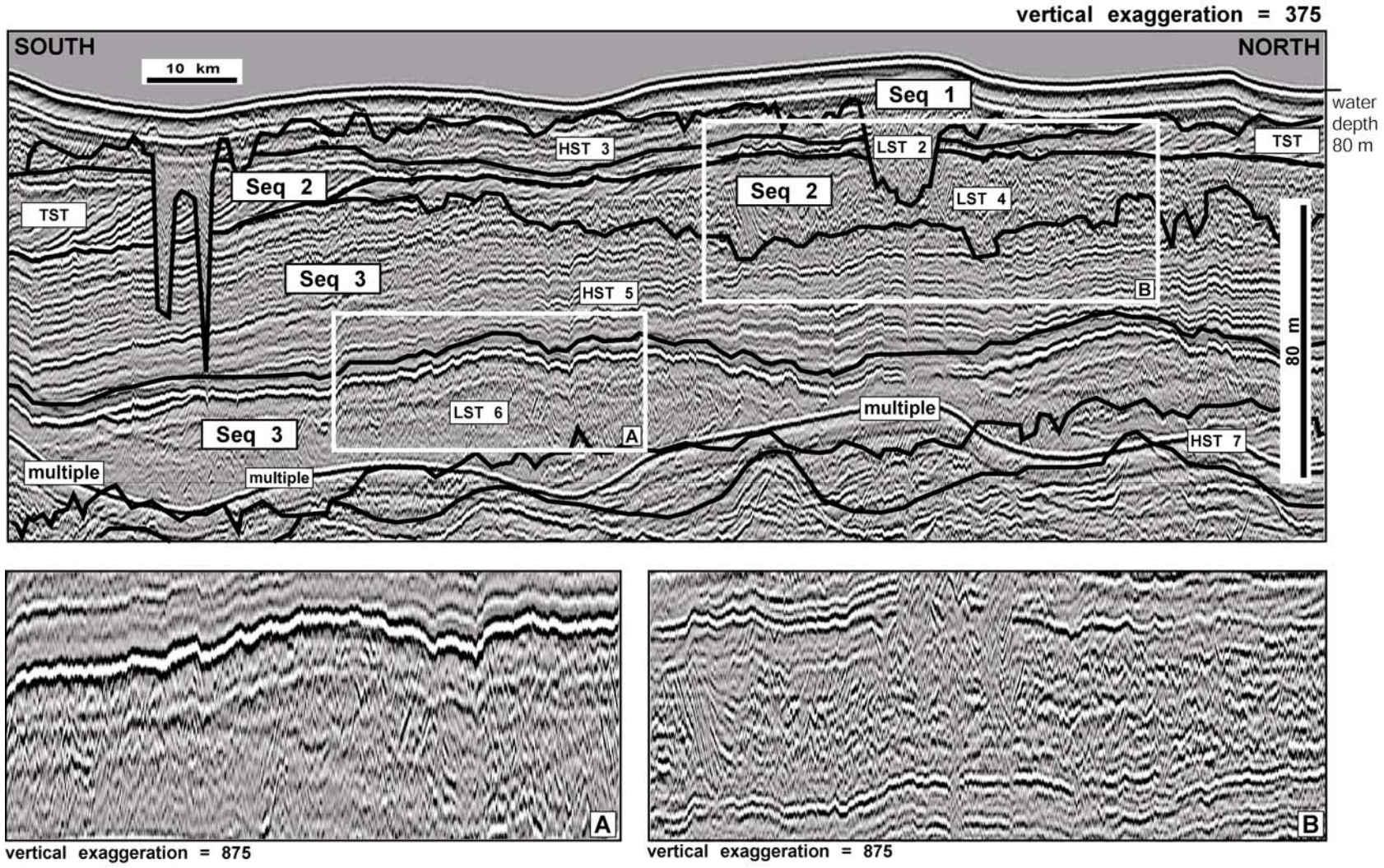
vertical exaggeration = 375
SOUTH
NORTH
10 km
water
depth
80 m
Seq 1
Seq 2
Seq 3
Seq 2
Seq 3
TST
TST
HST 3
HST 5
LST 2
LST 4
LST 6
HST 7
multiple
multiple
multiple
A
B
80 m
A
B
vertical exaggeration = 875
vertical exaggeration = 875

Figure 2.4. Structure map of SB 3 at the base of Seq 3 (also referred to as LST 6). On inner and central portions of the margin, this SB is an erosional disconformity (identitifed as ED 3) formed by extensive subaerial exposure of the margin and the fluvial processes that ensued. This SB grades laterally into a DS that is a correlative conformity on the outer margin found at the base of the submarine deltaic component of the fluvial system. Note the flat, planar nature of this SB and the lack of incision across the entire margin.

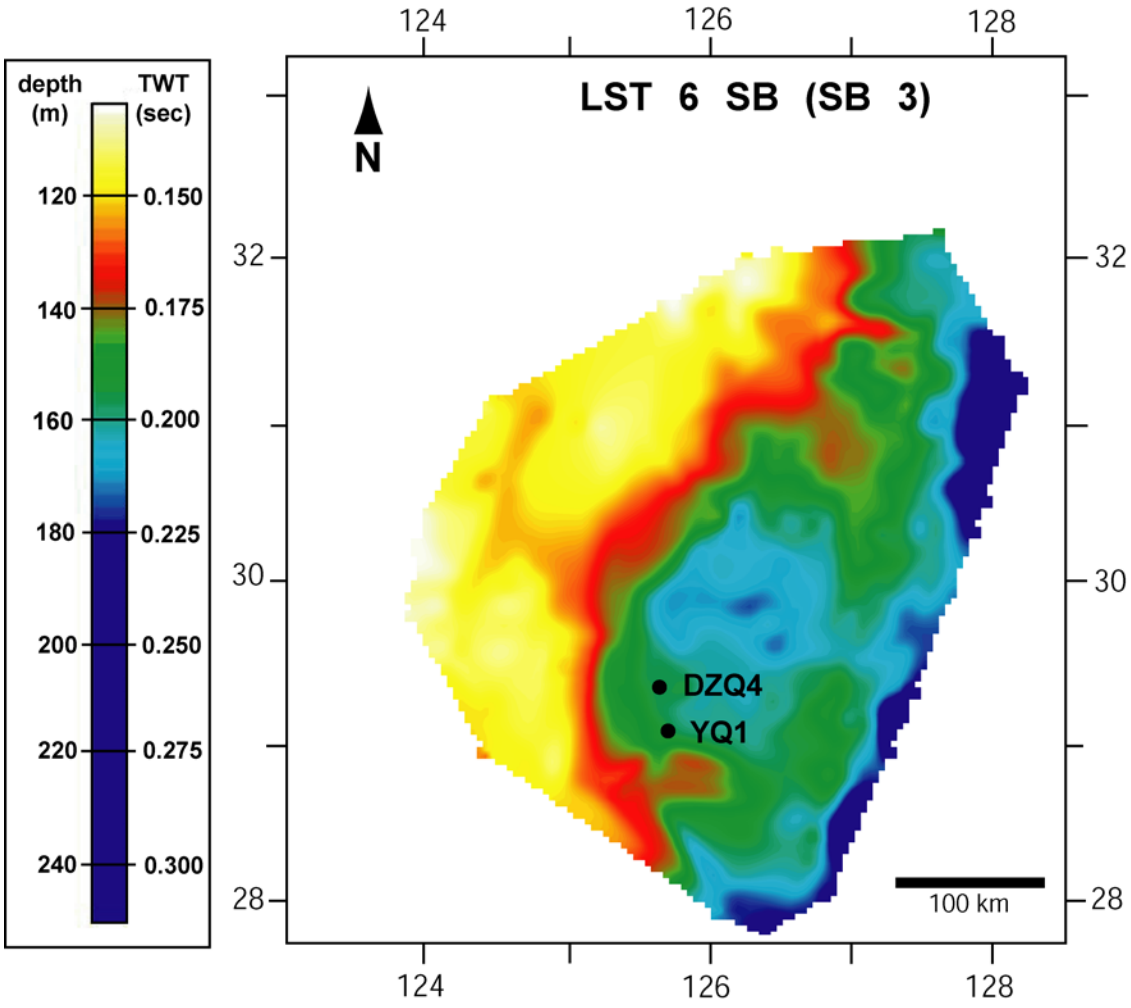
depth (m)
TWT (sec)
120
0.150
140
0.175
160
0.200
180
0.225
200
0.250
220
0.275
240
0.300
124
126
128
LST 6 SB (SB 3)
N
32
30
28
DZQ4
YQ1
100 km

Figure 2.5. A) Isopach map of SF CHAO for Seq3 (also referred to as LST 6). Note the lateral extent of the strata across the margin in both strike and dip directions as well as how the unit thins basinward. B) Isopach map of SF DIP for Seq 3 (also referred to as LST 6). Note distinct concentration of sediment suggesting deltaic depocenters. Also note how this unit thins landward. C) Idealized lateral transition between landward SF CHAO (fluvial) and basinward SF DIP (deltaic) in Seq3. These two units are stratigraphically equivalent.

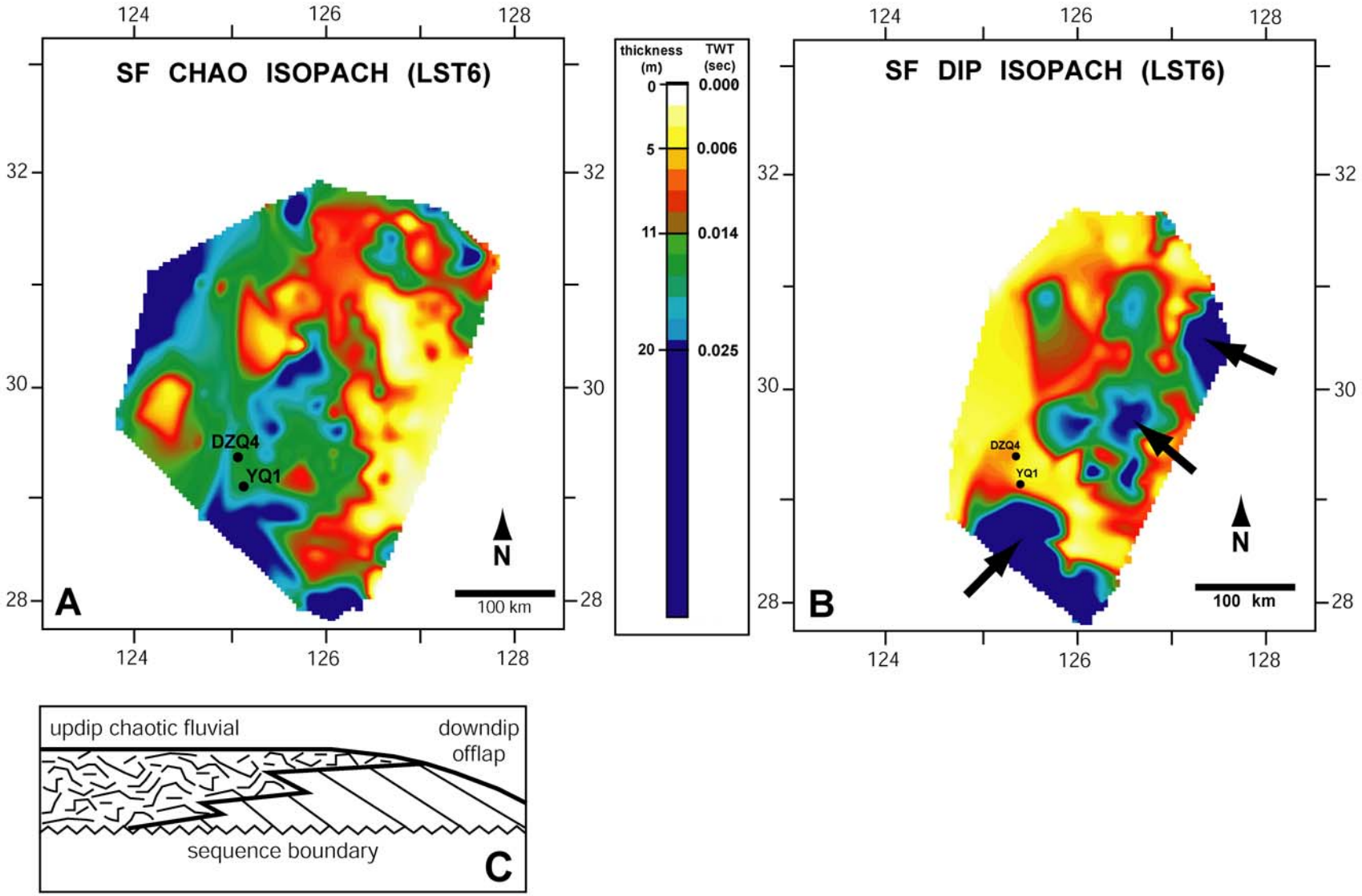
SF CHAO ISOPACH (LST6)
SF DIP ISOPACH (LST6)
thickness (m)
TWT (sec)
0
5
11
20
0.000
0.006
0.014
0.025
124
126
128
32
30
28
DZQ4
YQ1
N
100 km
A
B
updip chaotic fluvial
downdip offlap
sequence boundary
C

Figure 2.6. Dip-oriented seismic profile from the outer margin illustrating the lateral gradation from SF CHAO (landward) to SF DIP (basinward). The location of this profile, with respect to the ECS margin, is identified in Figure 2.1. An idealized cartoon of this transition is presented in Figure 2.5C.

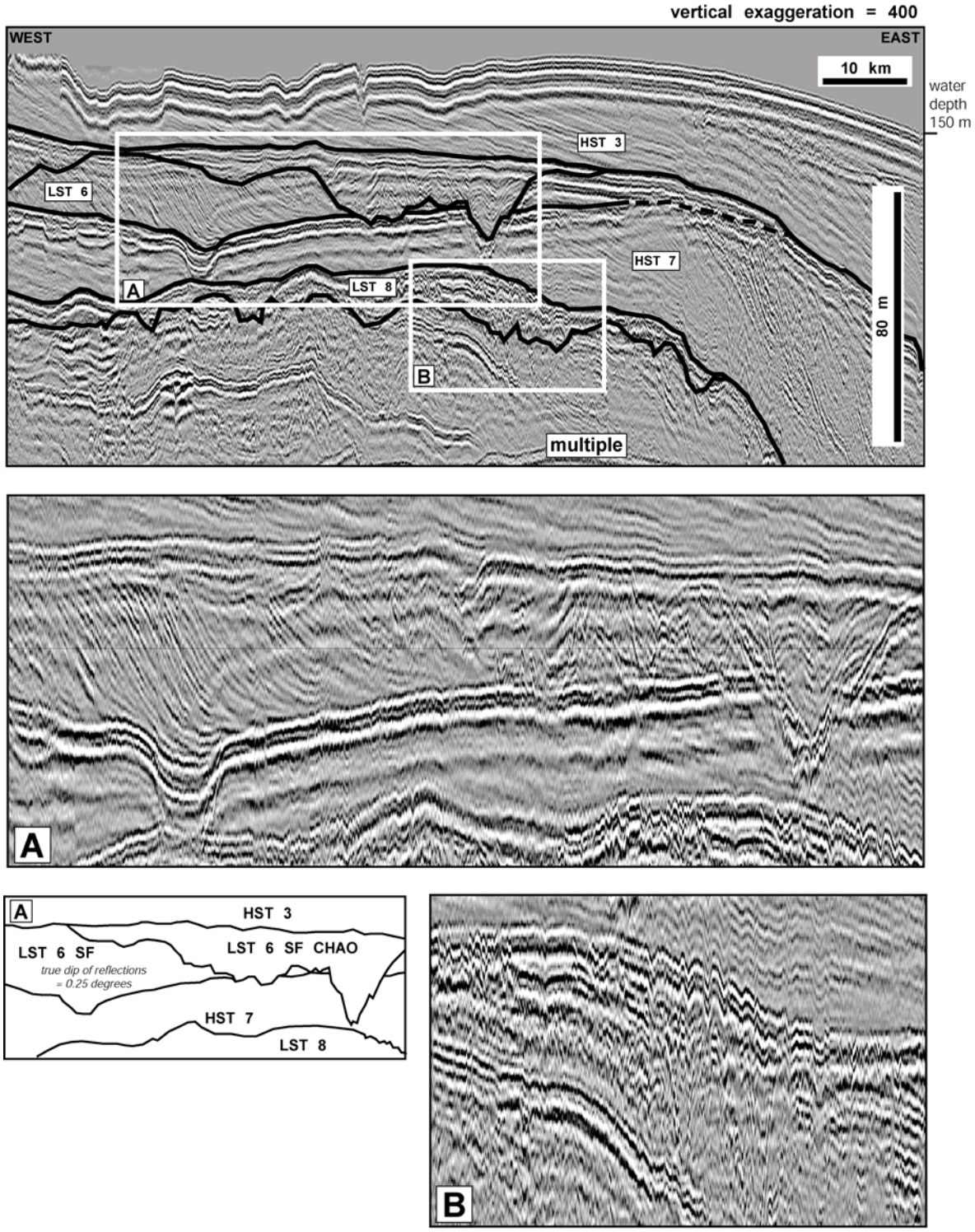
vertical exaggeration = 400
WEST
EAST
10 km
water depth 150 m
HST 3
LST 6
HST 7
LST 8
A
B
80 m
multiple
A
A
HST 3
LST 6 SF
LST 6 SF CHAO
true dip of reflections = 0.25 degrees
HST 7
LST 8
B

Seq 2, pinch out on central portions of the margin and form a lobate geometry. These reflections are considered to be the HST of Seq 3. On the outer margin, DS 3 becomes amalgamated with the younger DS 2 where the overlying reflections are associated with the HST from the younger Seq 2 (Figure 2.7). Seq 3 is truncated by erosion on the inner margin, as well as northern portions of the margin, by the overlying SB 1. On portions of the inner margin, Seq 3 becomes amalgamated with the overlying Seq 1 (Seq 2 is absent on the inner margin) and SB 3 becomes indistinguishable from the SB at the base of Seq 1 (i.e., SB 1).

2.3.2 Chronostratigraphy

Numerous cores have been collected in the ECS, but many are poorly documented and/or lack detailed lithologic descriptions and reliable chronological data. Few penetrate further than 50 m below seafloor (mbsf). Only one published borehole (borehole DZQ4) is available to constrain this study. Similarly, DZQ4 is also used to constrain other seismic- and sequence-stratigraphic studies deep enough to include Seq 3 (e.g., Saito et al., 1998; Liu et al., 2000; Berne et al., 2002; Warren and Bartek, 2002a; 2002b; Warren et al., 2002; Wellner and Bartek, 2003). Borehole DZQ4 lies within 1 km of dip-oriented seismic profile and within 4 km of a strike-oriented seismic profile (Figure 2.1). A shallower, 25 m borehole (YQ1) does not penetrate the bottom sequence of this study (i.e., Seq 3). However, YQ1 was utilized to constrain younger units on the margin (i.e., Seq 2 and Seq 1). For a description of borehole YQ1 and subsequent studies of lithology, sporo-pollen and foraminifera analyses, readers are referred to Yang (1989).

Descriptions of the 51.65 m core acquired from borehole DZQ4, and subsequent studies of lithology, micropaleontology, pollen and spores, as well as oxygen isotope and TL dating, were originally reported by Tang (1996). A limited summary of these data was presented by

Figure 2.7. The correlation between the six units from core DZQ4 projected less than 1 km into a nearby, dip-oriented seismic profile. The location of this profile, with respect to the ECS margin, is identified in Figure 2.1.

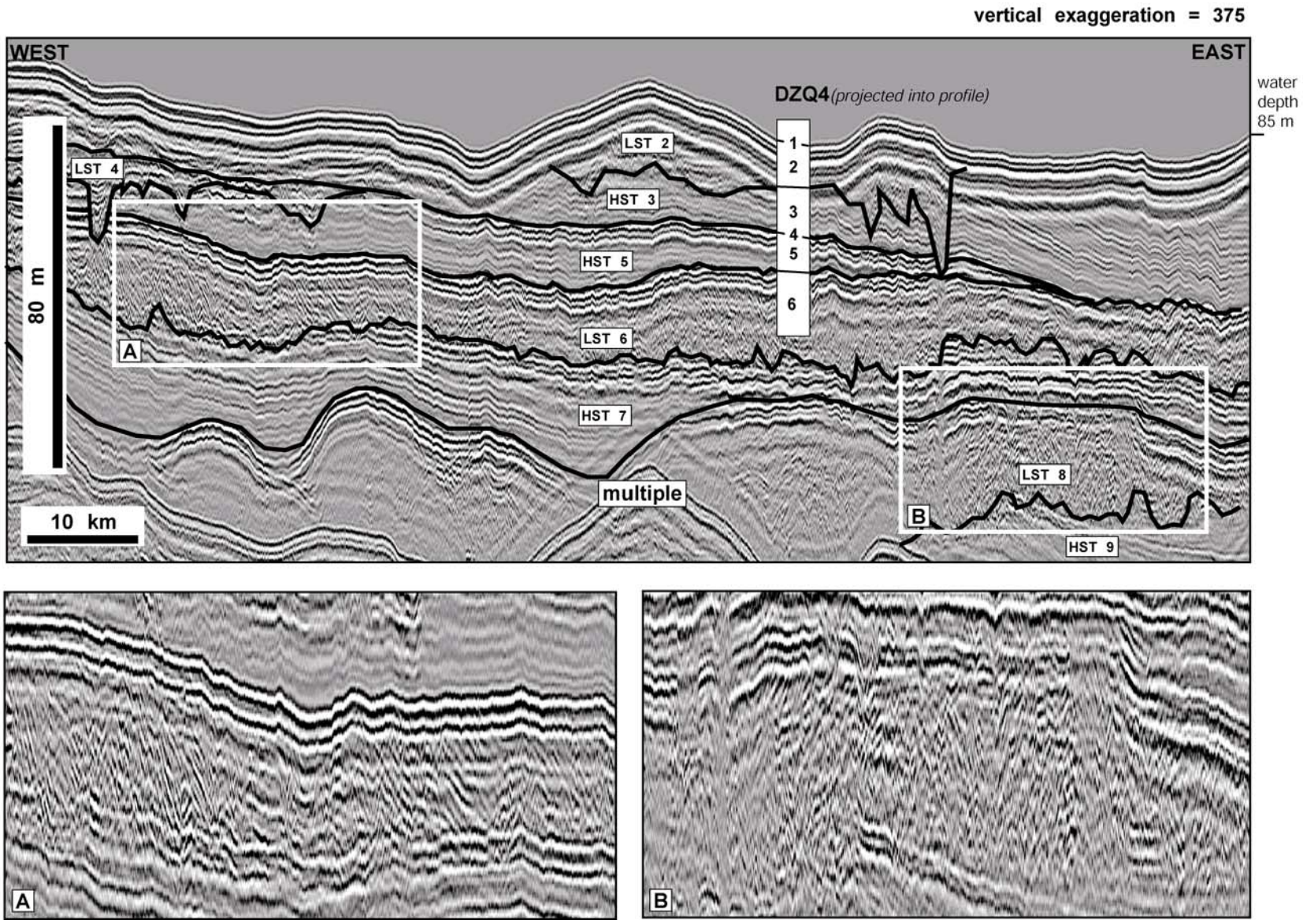
vertical exaggeration = 375
WEST
EAST
DZQ4 (projected into profile)
water depth 85 m
LST 2
LST 4
HST 3
HST 5
LST 6
HST 7
LST 8
HST 9
multiple
1
2
3
4
5
6
80 m
10 km
A
B
A
B

Liu et al. (2000) and Berne et al. (2002). The stratigraphy in the area of the ECS margin near borehole DZQ4 is fairly simple and consists of six major stratigraphic divisions (Unit 6 to Unit 1, oldest to youngest). Unit 6 is the primary stratal package investigated in this study. Correlation between core units and seismic profiles is relatively straightforward (Figure 2.7). For reasons discussed earlier, thickness and depth are converted from TWT using a velocity constant of 1600 m/sec (see Methods). Other constant velocity models of similar values (1600 m/sec, Liu et al., 2000; 1650 m/sec, Berne et al., 2002) also tie well to seismic data. Descriptions of the six core units presented in this paper are a compilation of observations from both Liu et al. (2000) and Berne et al. (2002) and are summarized in Figure 2.8.

The age of Seq. 3, which consists of core units 5 (younger) and 6 (older), is constrained by dates from within the sequence as well as overlying stratigraphic units (Unit 3 is the uppermost portion of Seq. 2). Primary age constraints for Unit 5 (87,764 ±4,388 at 35 meters below seafloor, or mbsf) and 3 (50,246 ±2,512 at24.4 mbsf and 46,903 ±2,313 at 20.9 mbsf) are provided by three thermoluminscence (TL) dates. The principle of TL dating is based on the ability of imperfections in the lattices of inorganic crystals, in this case mineral grains, to trap electrons and store absorbed radiation. Upon thermal stimulation, this energy is released in the form of thermoluminescent light. However, if a solid with occupied electron traps and the potential to produce TL is exposed to elevated temperatures or light, electrons can escape from their traps. This electron escape causes the latent TL signal to fade either partially or completely (Wagner, 1998). The accuracy of this dating technique is sensitive to the influence of sunlight on grains after initial environmental exposure (Forman et al., 2000). To eliminate the impact of reworking and post-depositional exposure, Berne et al. (2002) only considered three TL dates from stratigraphic units associated with high sedimentation rates as

Figure 2.8. Description of core DZQ4 compiled from Liu et al. (2000) and Berne et al., 2002 (stratigraphic column) with comparisons of stratal units and sequence stratigraphic interpretation.

BOREHOLE DZQ4

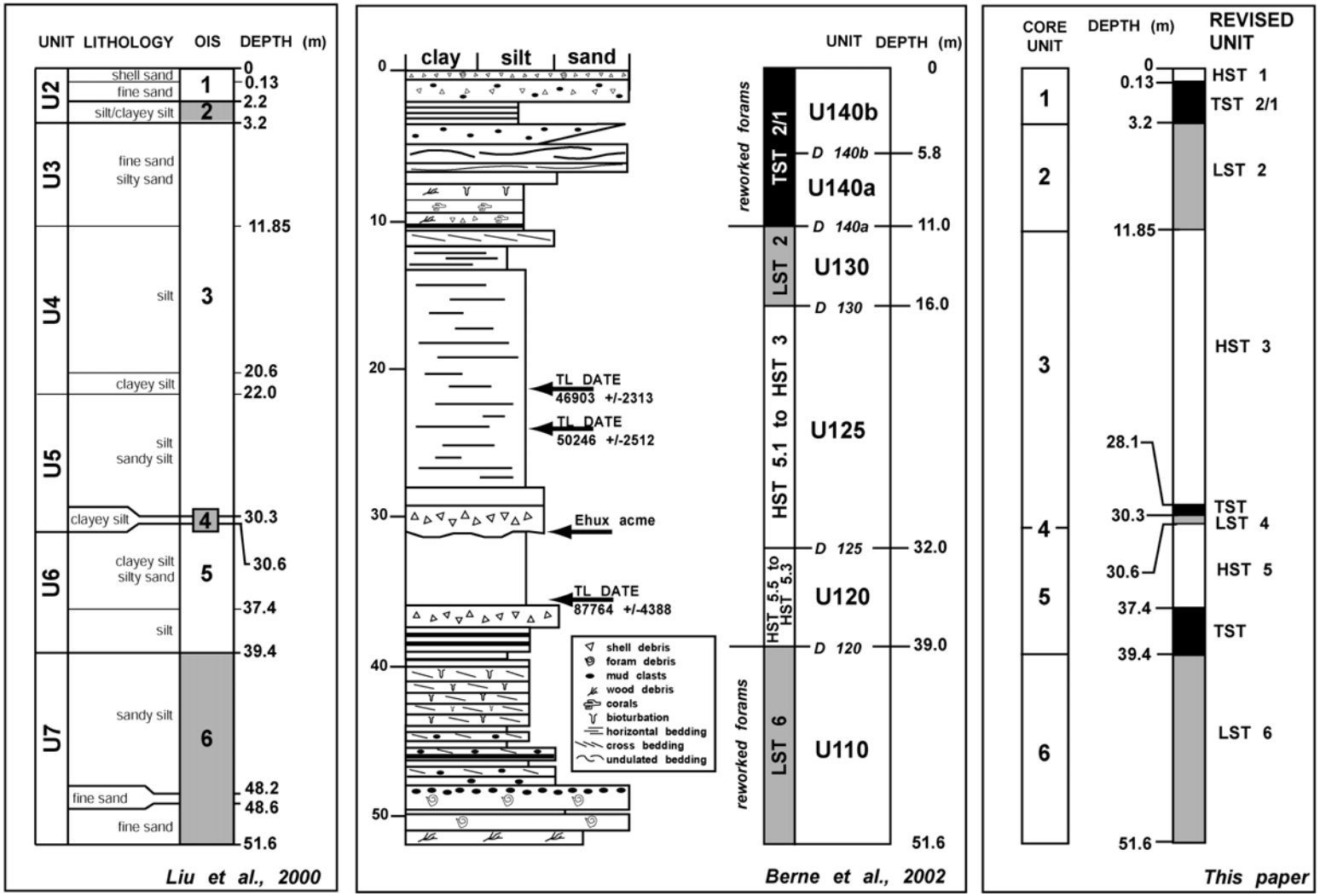

completely valid. This procedure is scientifically valid in that it eliminates the incorporation of inaccurate dates (i.e., skewed too young). Therefore, the same three TL dates utilized by Berne et al. (2002) from Tang (1996), those associated with units 5 and 3, are presented in this paper. These strata are fine-grained intervals from the middle margin. In addition, two additional dating methods are used to verify these TL dates and further constrain the ages of shallow ECS strata. First, the appearance of the *Emiliania huxleyi* (Ehux) acme biomarker at 30.8 mbsf in core DZQ4 occurred around 73 ka at mid latitudes (Thierstein et al., 1977). Second, Saito et al. (1998) provide multiple ^{14}C dates (between 25 and 50 ka) from piston cores throughout the ECS that correlate to Unit 3.

2.3.3 Seismic Facies

Lateral continuity, amplitude, and vertical frequency of reflections are used to classify seismic facies observed in the shallow seismic profiles from the ECS continental margin. Variations in these attributes are subdivided into four, distinct seismic facies (SF) categories: 1) chaotic reflections (CHAO), 2) dipping reflections (DIP), 3) flat-lying reflections (FLAT), and 4) mounded external geometries (MOUND). Examples of each of these SF are shown in Figure 2.9. Other investigations in the ECS used seismic reflection classification schemes to yield similar observations (e.g., Yang, 1989; Liu et al., 1998; Berne et al., 2002). While Yang (1989) reported using seismic facies to help infer five distinct sedimentary facies (i.e., estuarine channel facies, lacustrine and swamp facies, tidal sand ridge facies, shelf mud facies, and deltaic facies), the seismic facies parameters used for their classification scheme were not described. Liu et al. (1998) identified three distinct seismic facies (chaotic, gently oblique, and externally mounded units with internal clinoforms) as did Berne et al. (2002) (chaotic and channelized, very low-angle clinoforms, and high-angle clinoforms). The

Figure 2.9. Examples of the four seismic facies (SF) types found in the shallow strata on the East China Sea continental margin: A) unconfined chaotic and confined chaotic (SF CHAO), B) dipping reflections (SF DIP), C) horizontally oriented reflections (SF FLAT), and D) mounds containing inclined reflections (SF MOUND).

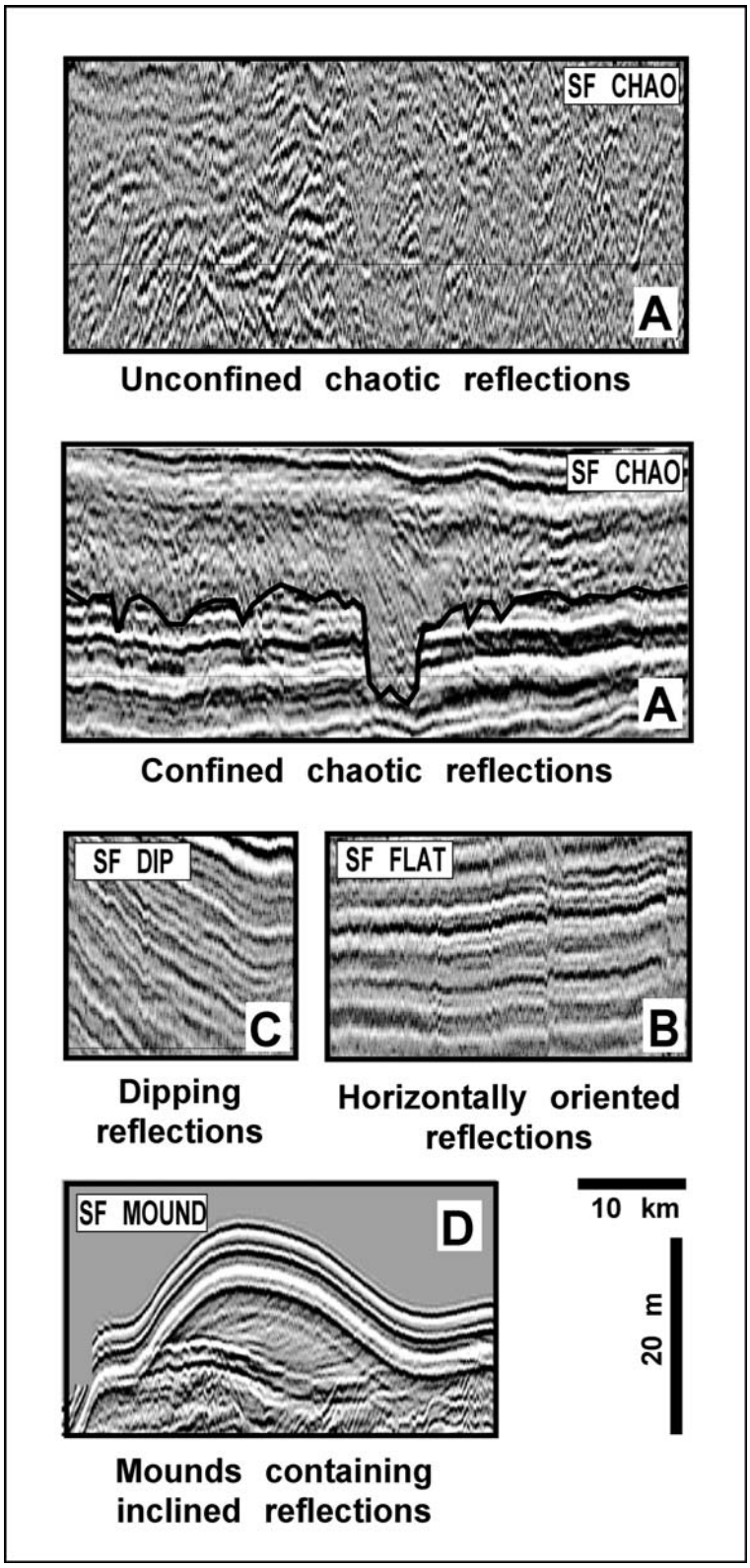
SF CHAO
A
Unconfined chaotic reflections
SF CHAO
A
Confined chaotic reflections
SF DIP
C
Dipping reflections
SF FLAT
B
Horizontally oriented reflections
SF MOUND
D
Mounds containing inclined reflections
10 km
20 m

seismic facies classifications used in this investigation encompass both the Liu et al. (1998) and Berne et al. (2002) schemes by merging them into four separate and distinct seismic facies categories.

The first of these categories is SF CHAO. The LST is the only systems tract to contain this chaotic facies, which exhibits variable reflection orientation, low and/or variable amplitude, and low lateral continuity for individual reflections. This seismic facies can be more than 50 m thick, but averages 15 m and has a high lateral continuity across the entire ECS margin (>200 km). SF CHAO is always underlain by an erosional surface (i.e., SB 1, 2, and 3 on the inner margin and ED 1, 2, and 3 on the outer margin). SF CHAO thins on the outer margin, sometimes becoming unidentifiable. On the innermost margin, the majority of the seismic reflections appear as SF CHAO and become vertically amalgamated and indistinguishable from each other. On the outer margin, the lateral, stratigraphic equivalent to SF CHAO are the dipping reflections of SF DIP. However, this dipping facies is non-unique and also correlates to the HSTs in Seq 3 and Seq 2 (Figure 2.6). In general, SF DIP contains reflections that have a moderate to high vertical frequency (≥6 reflections per 10 msec) and a high lateral continuity (>200 km). This dipping facies, with magnitudes between 1 and 5°, reaches over 50 m in thickness, with an average thickness of 20 m, and has a moderate (10 to 200 km) to high lateral (>200 km) continuity across the margin. Overall, reflections tend to dip south and east and magnitudes generally increase basinward (east). Thickness of SF DIP can exceed 130 m on the outermost margin near the paleo shelf-slope break, but average 20 m.

The third facies, SF FLAT, is characterized by horizontal and nearly horizontal (dip < 1°) reflections of moderate to high amplitude. This facies correlates to the HST that overlies

portions of the LST (SF CHAO), when SF MOUND is absent (see below). The reflections of SF FLAT have a moderate to high vertical frequency (≥6 reflections per 10 msec) and a high lateral continuity (>200 km). This facies reaches over 50 m in thickness, with an average thickness of 20 m, and has a moderate (10 to 200 km) to high lateral (>200 km) continuity across the margin. SF FLAT occurs landward (west) of, and grades laterally into, SF DIP. SF FLAT and DIP are always underlain by a downlap surface (i.e., DS 1, 2, and 3).

External geometries of these three SF (CHAO, FLAT, and DIP) are fairly tabular and laterally extensive (> 100 km) across the ECS margin. This contrasts with the fourth seismic facies, SF MOUND, that has a distinctive external morphology of limited lateral extent, consisting of externally mounded ridges, up to 25 km long and 30 m thick. In many locations, SF MOUND is the upper boundary of SF CHAO in LST 6. Distribution of this facies is primarily on inner and middle portions of the margin with extremely rare occurrence on the outer portion of the margin where it correlates with the TST that directly overlies many portions of the LST (SF CHAO). The ridges of this seismic facies were the subject of additional work by Yang and Sun (1988), Yang (1989), Saito et al. (1998), Liu et al. (2000), Li et al. (2001), Park et al. (2003), and Zhu and Chen (2005).

2.3.4 Lithostratigraphy

The correlation between cores and adjacent seismic profiles assigns age constraints to seismic surfaces and units, specifically OIS 5 and 3. This ground truth correlates seismic facies and lithofacies, identifies systems tracts, and ties the overall sequence stratigraphic framework to its appropriate position on the Quaternary sea level curve (Figure 2.2). The complete shallow stratigraphy of the ECS margin (i.e., units 1 through 6) is presented in

Figure 2.3. A more detailed treatment of Seq 3, and its two units pertinent to this study from core DZQ4 (i.e., units 5 and 6), is also presented below.

Unit 6. This unit extends for approximately 12 m in core DZQ4 from a total depth (TD) of 51.65 m to 39.4 m below seafloor (mbsf). Based on nearby seismic profiles, the total thickness of this unit is 16 m at the borehole. Elsewhere on the margin, this stratal package is up to 46 m thick and averages between 10 and 20 m (Figures 2.10 and 2.11). Unit 6 contains fine-grained sands with small and large cross beds that also contain terrestrial components such as pollen from land plants and wood debris. Pollen assemblages indicate a warm and humid climate that shifts to a colder and drier climate toward the top of the interval. Nannofossil assemblages (coccolithophores), however, are indicative of cold environments throughout the entire interval. This unit correlates to SF CHAO at borehole DZQ4 and extends in both strike- and dip-oriented profiles for hundreds of kilometers. Across the entire margin, SF CHAO is bound at its base by a fairly flat erosional surface previously identified as ED3 and SB3 on the inner and central margin. SF CHAO also grades laterally into basinward dipping, downlapping seismic reflections (SF DIP) on the outer margin. There, SF DIP is bound at its base by a downlap surface previously identified as the conformable portion of SB3. Based on absolute age data from OIS 5 in the overlying stratal Unit 5 and the overall sequence stratigraphic framework (i.e., overlying HST and underlying SB), Unit 6 correlates to the LST of OIS 6 (LST 6) that spanned 186 to 128 ka (Imbrie et al., 1984).

Unit 5. The lowermost 2 m of Unit 5 in core DZQ4 (39.4 to 37.4 mbsf) lies above LST 6 and below absolute ages tied to the overlying HST 5. Primarily composed of silt, there is also abundant shell debris and a sharp, basal lithologic contact that contains an abrupt deepening upward sequence. This unit correlates to the TST between LST 6 and HST 5 (i.e.,

Figure 2.10. Strike-oriented stratigraphic profile across the East China Sea continental margin. Note uplift and erosional truncation of older strata in the north and subsidence in the south, both of which are post-depositional relative to LST 6. Thus, relief observed on the LUFS SB is also post-depositional (see Figure 4), and the thinning of the LUFS (see Figure 5) is related to erosional truncation to the north.

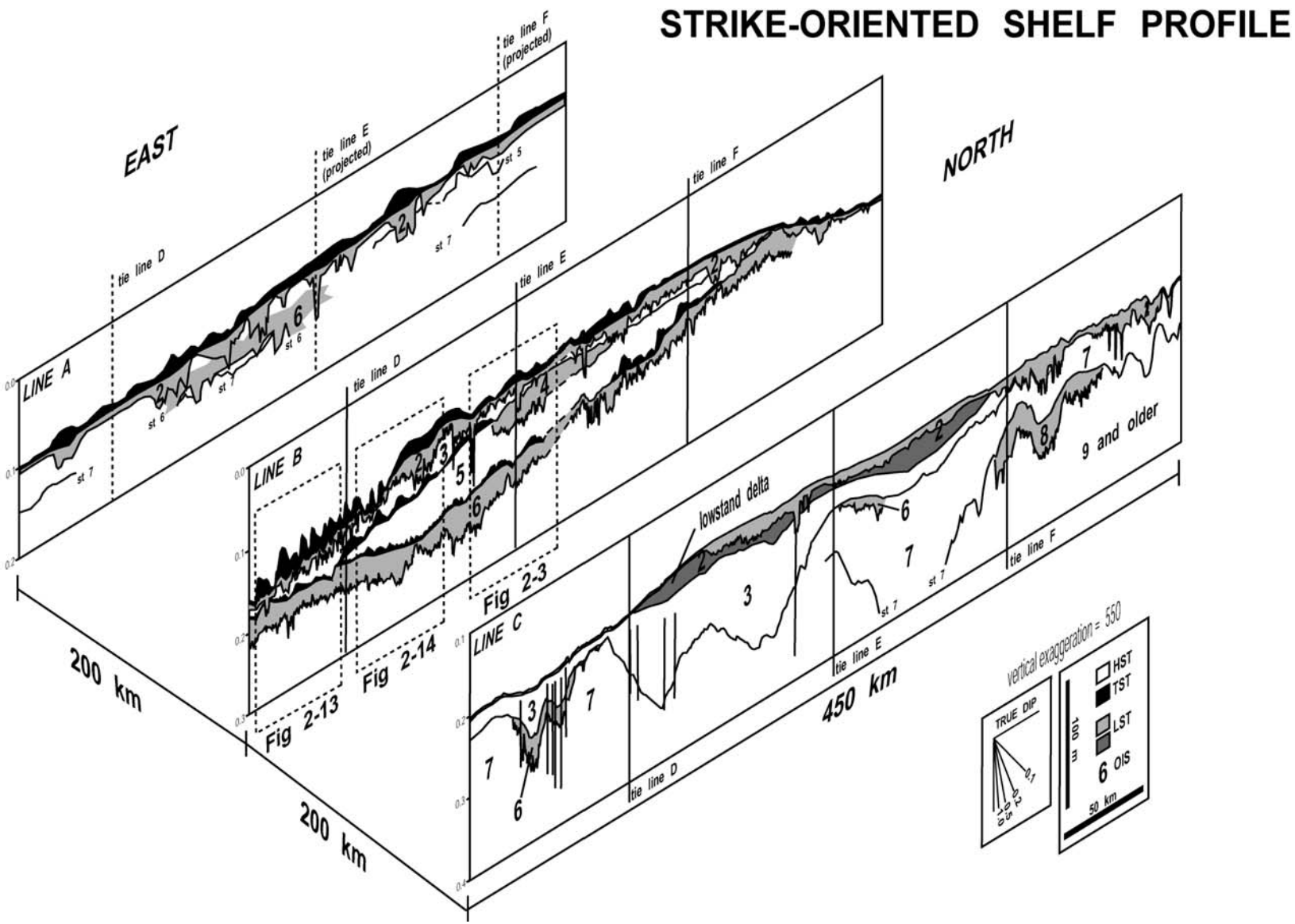
STRIKE-ORIENTED SHELF PROFILE
EAST
NORTH
LINE A
LINE B
LINE C
tie line D
tie line E
tie line F
tie line E (projected)
tie line F (projected)
st 5
st 6
st 7
lowstand delta
9 and older
Fig 2-3
Fig 2-13
Fig 2-14
200 km
200 km
450 km
vertical exaggeration = 550
TRUE DIP
HST
TST
LST
OIS
100 m
50 km

Figure 2.11. Dip-oriented stratigraphic profile across the East China Sea continental margin. Similar to Figure 1, the gradation between end-member stratal stacking patterns (i.e., prograding versus aggrading) is observed from north to south at the shelf-slope break of the ECS margin. To the north, progradation is indicative of uplift, and to the south, aggradation is indicative of subsidence.

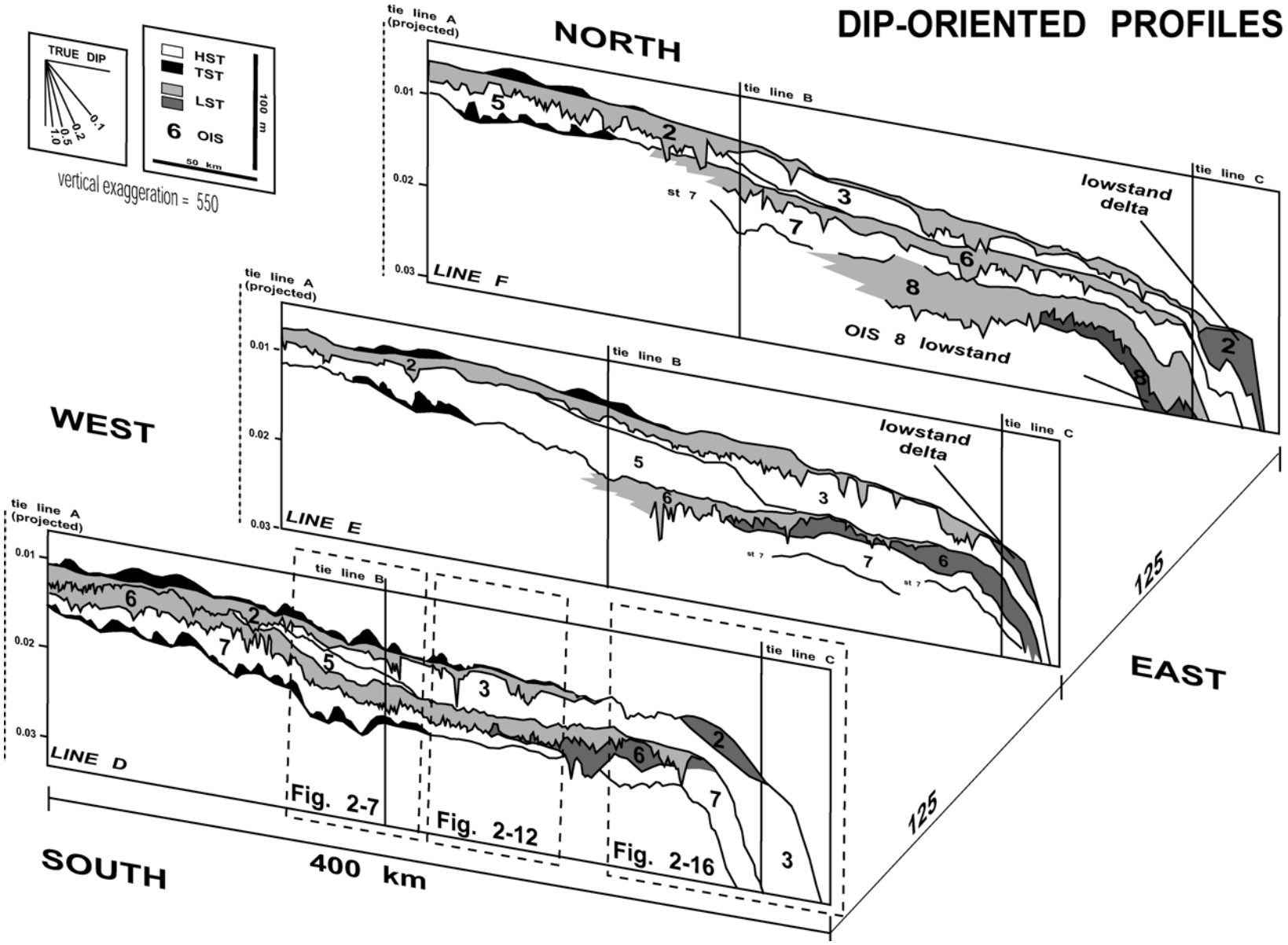
DIP-ORIENTED PROFILES
NORTH
WEST
EAST
SOUTH
TRUE DIP
0.1
0.2
0.5
1.0
HST
TST
LST
6 OIS
100 m
50 km
vertical exaggeration = 550
tie line A (projected)
tie line B
tie line C
LINE F
LINE E
LINE D
lowstand delta
OIS 8 lowstand
st 7
0.01
0.02
0.03
125
400 km
Fig. 2-7
Fig. 2-12
Fig. 2-16

TST 6/5), approximately 133 to 123 ka (Figure 2.2). At the borehole, this portion of Unit 5 is resolved in seismic profiles as a single, thick (low frequency), high-amplitude reflection and represents the TST as well as its upper and lower bounding surfaces (MFS of HST 5 and TS between LST 6 and TST 6/5, respectively). This reflection is also traceable across the entire margin and frequently thickens into the externally mounded units of SF MOUND. Thicker portions of this unit are easily resolvable in seismic profiles and are bound at the base by the high-amplitude reflection of the TS and bounded at the top by the high-amplitude MFS of HST 5. The ridges of TST 6/5 are distributed across the inner and central margin, but do not appear on the outer margin. They are on average 4 m thick with an observed maximum of 13 m, and their preservation is attributed to a high subsidence rate and subsequent burial by prodeltaic muds (Berne et al., 2002). Berne et al. report a preferred orientation of internal reflections offlapping to the SW.

The upper portion of Unit 5 in core DZQ4 (39.4 to 30.6 mbsf) contains interbedded clays, silts, and sands. The sediments are much finer than the underlying LST 6 and lack the shell hash found in the underlying TST 6/5. Fossil assemblages are indicative of warm water and middle-to-outer shelf environments (specifically the planktonic foraminifera *Globigerina ruber*). A TL date of 87,764 years (±4,388 years) collected at approximately 35 mbsf corresponds to HST 5 that spanned 128 to 71 ka (Imbrie et al., 1984). The Ehux acme biozone at 30.8 mbsf provides an additional age of approximately 73 ka (Thierstein et al., 1977), also tying this unit to the HST 5. These sediments correlate to SF FLAT at the borehole, across the inner and central margin, and laterally grade into SF DIP to the south and east. While Unit 5 is almost 9 m thick at the core location, this upper portion of the unit averages between 15 and 30 m across central portions of the margin where it reaches up to 53

m in thickness. Maps and cross-sections of this unit show a perched lobe that pinches out to the south and east on the central to outer margin and does not reach the paleo shelf-slope break (Figures 2.10 and 2.11).

2.3.5 Summary of the Physical Attributes of the Lowstand Systems Tract

Lowstand fluvial deposits in the ECS that are associated with the interval before OIS 4 (i.e., OIS 6 and older) lack major incision in both strike- and dip-oriented seismic profiles and extend laterally for more than 400 km and exceed 40 m in thickness (Figures 2.10 and 2.11). In terms of seismic facies, these strata are composed of homogenous, chaotically oriented reflections (i.e., random) with low and/or variable amplitudes and variable continuity (SF CHAO) (Figures 2.3, 2.6, 2.7, 2.12, 2.13, and 2.14). In LST 6 and LST 8, this facies grades laterally basinward into the high-amplitude, basinward-dipping reflections of SF DIP (Figures 2.5 and 2.6). The lithology of LST 6 is composed of cross-bedded, fine sands with a terrestrial influence (wood and pollen) deposited during a period when the climate was cool and dry. Overlying LST 6 is the ridge-like component (SF MOUND) of the TST or the HST of both OIS 5 (perched on central margin with no deposition on outer margin) and OIS 3 (deposited on outer margin). Underlying LST units (e.g., LST 8 and 10) contain identical seismic facies components (SF CHAO grading laterally into SF DIP) and stratal architecture (laterally extensive units lacking incision) to LST 6 and, from which similar lithologies can be inferred.

Figure 2.12. Dip-oriented seismic profile showing the lateral extent and the chaotic seismic facies of the LUFS in LST 6 and LST 8. The location of this profile, with respect to the ECS margin, is identified in Figure 2.1.

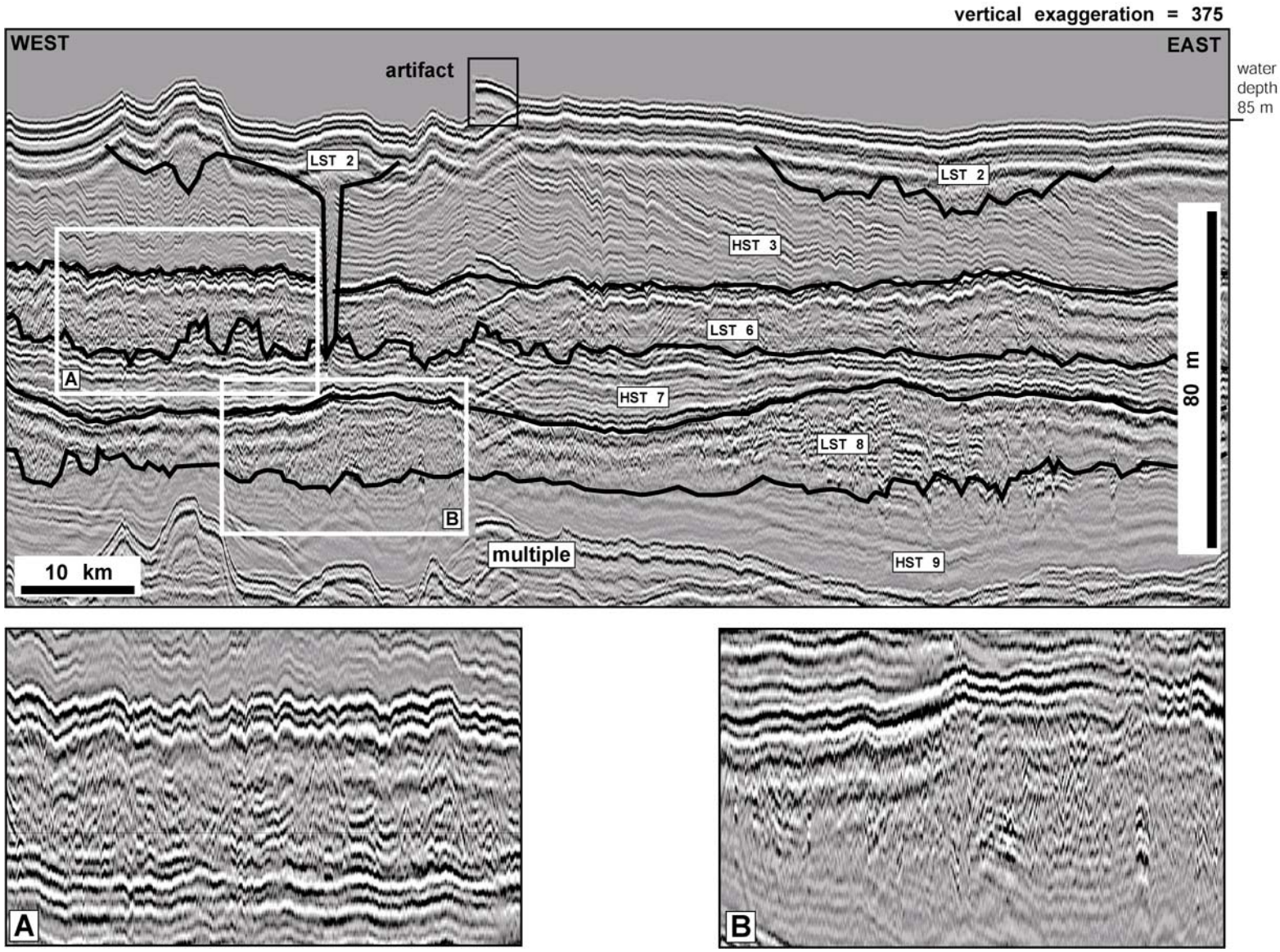
vertical exaggeration = 375
WEST
EAST
artifact
water
depth
85 m
LST 2
LST 2
HST 3
LST 6
HST 7
LST 8
HST 9
A
B
80 m
multiple
10 km
A
B

Figure 2.13. Strike-oriented seismic profile showing the lateral extent and the chaotic seismic facies of the LUFS in LST 6. The location of this profile, with respect to the ECS margin, is identified in Figure 2.1.

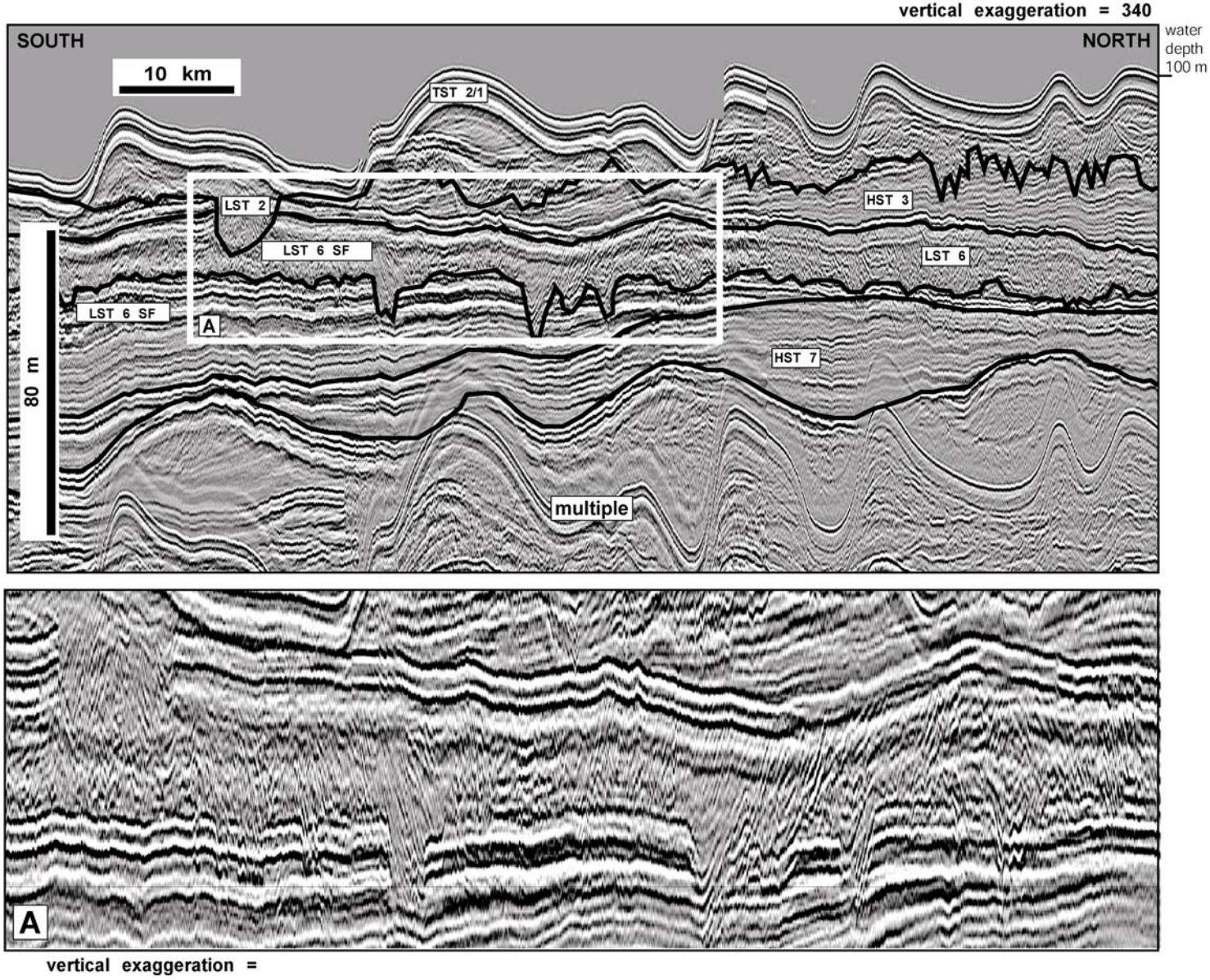
vertical exaggeration = 340
SOUTH
NORTH
water
depth
100 m
10 km
TST 2/1
LST 2
LST 6 SF
HST 3
LST 6
LST 6 SF
A
80 m
HST 7
multiple
A
vertical exaggeration =

Figure 2.14. Strike-oriented seismic profile showing the lateral extent and the chaotic seismic facies of the LUFS in LST 6. Note the incisive nature of the younger LST 2. The location of this profile, with respect to the ECS margin, is identified in Figure 2.1.

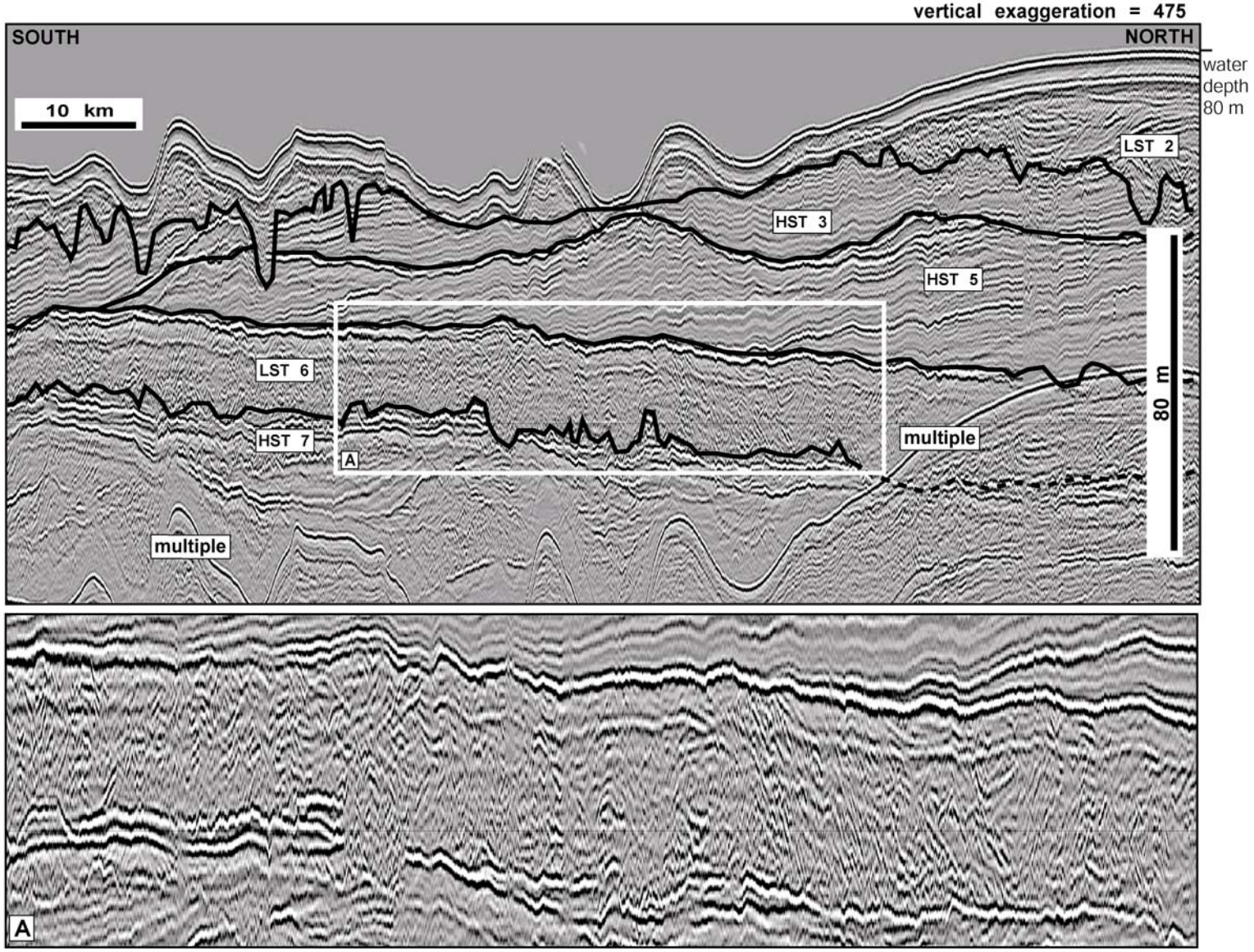
vertical exaggeration = 475
SOUTH
NORTH
water
depth
80 m
10 km
LST 2
HST 3
HST 5
LST 6
HST 7
A
multiple
80 m
multiple
A
vertical exaggeration = 1200

2.4 DISCUSSION

2.4.1 Identification of the LUFS

Based on lithofacies (cross-bedded sands with wood debris and terrestrial pollen), fossils (cold and dry environment), sequence stratigraphic and chronostratigraphic constraints (LST during OIS 6), seismic evidence (homogenous chaotic facies with laterally equivalent offlapping component, both underlain by a sequence boundary), and margin architecture (wide with a low gradient), Unit 6 (previously referred to as Seq 3) from core DZQ4 is interpreted to represent a massive, unconfined fluvial system. Other occurrences of SF CHAO deposited on the ECS margin during LST 8 and 10 are also interpreted as fluvial deposits associated with massive braid plains. Within this low energy and low sinuosity braided channel complex, sediments are expected to be coarse-grained and transported by bed load (Schumm, 1981; Schumm, 1985). Park (1987) presented a cartoon model of an exposed ECS margin during a sea level drop of approximately 120 m. The model depicts vast exposure and the extension and braided nature of the numerous fluvial systems bordering the ECS. The interpretation presented in this paper is consistent with Park's (1987) model. A modified version, based upon results of analyses of this study, is presented in Figure 2.15. The basinward stratigraphic equivalent of SF CHAO (i.e., SF DIP) is interpreted as the deltaic component of the fluvial system that progressively moved basinward during a falling sea level. On inner and middle portions of the margin, most, if not all, evidence of this deltaic element has been removed and/or truncated by subsequent exposure and erosion of the overlying fluvial system (SF CHAO). The lateral and vertical distribution of this fluvial system and its stratigraphic architecture in response to baselevel fall is presented in Figure 2.16.

Figure 2.15. Analog for fluvial system distribution across subaerially exposed East China Sea continental margin during extreme lowstands (adapted from Park, 1987).

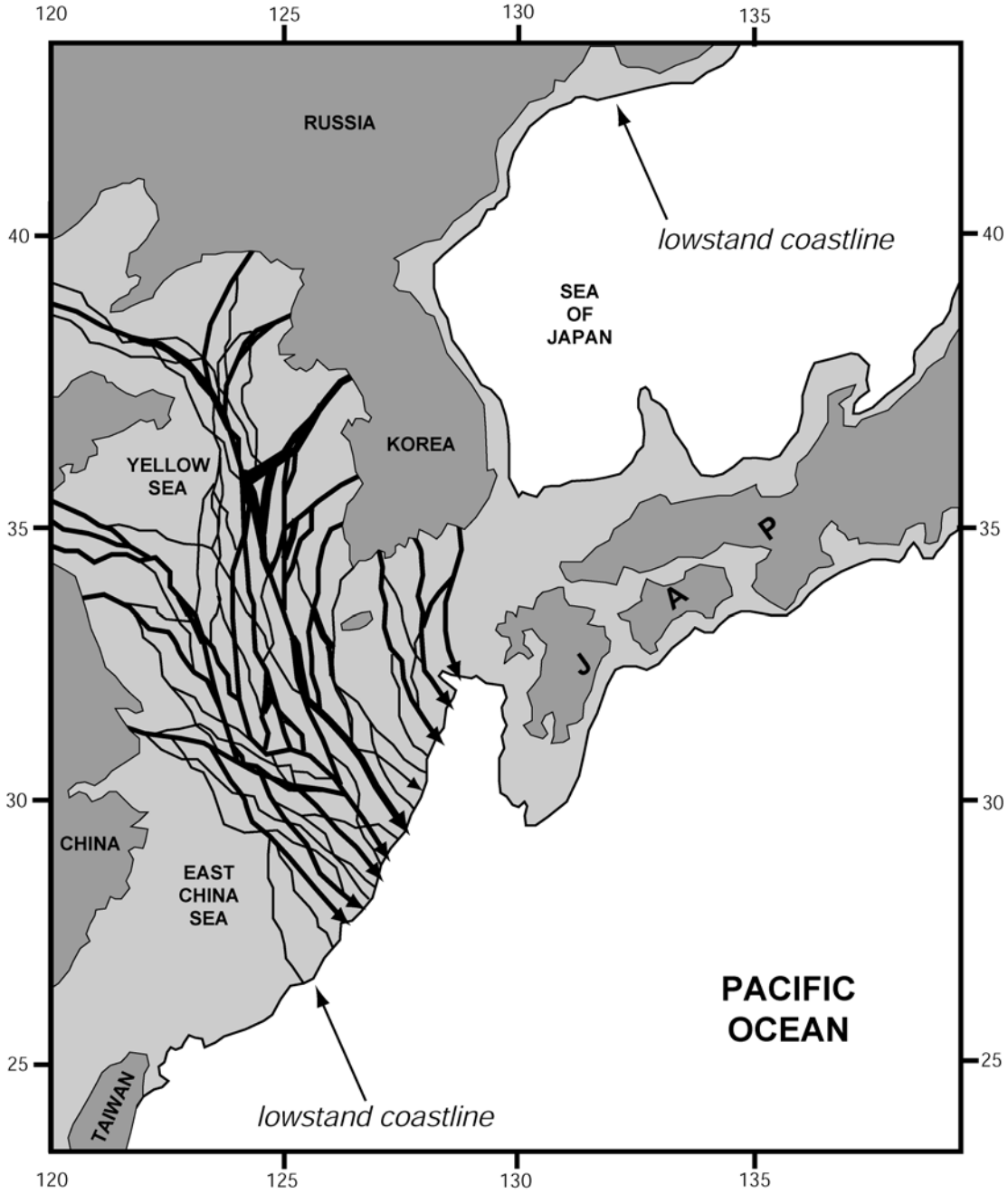
120
125
130
135
40
35
30
25
RUSSIA
lowstand coastline
SEA
OF
JAPAN
KOREA
YELLOW
SEA
P
A
J
CHINA
EAST
CHINA
SEA
PACIFIC
OCEAN
TAIWAN
lowstand coastline

Figure 2.16. Three dimensional model showing the development of the LUFS relative to RSL fall. Note the lateral transition between the chaotic, fluvial facies and the basinward dipping, deltaic facies.

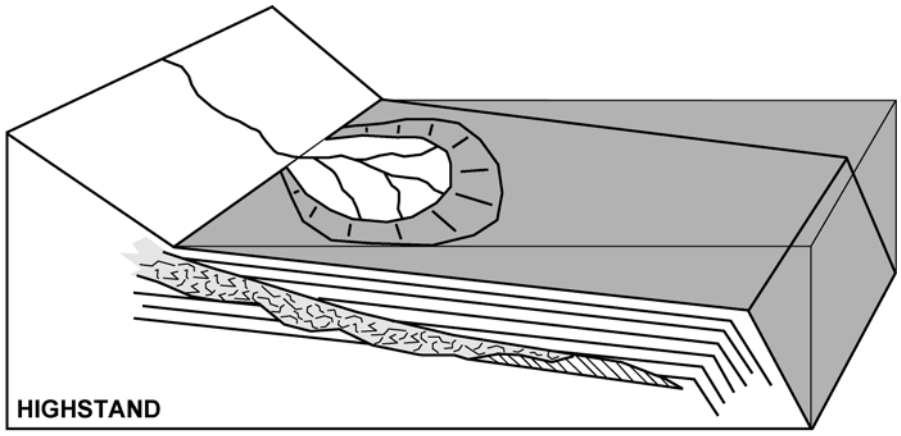

Time 3

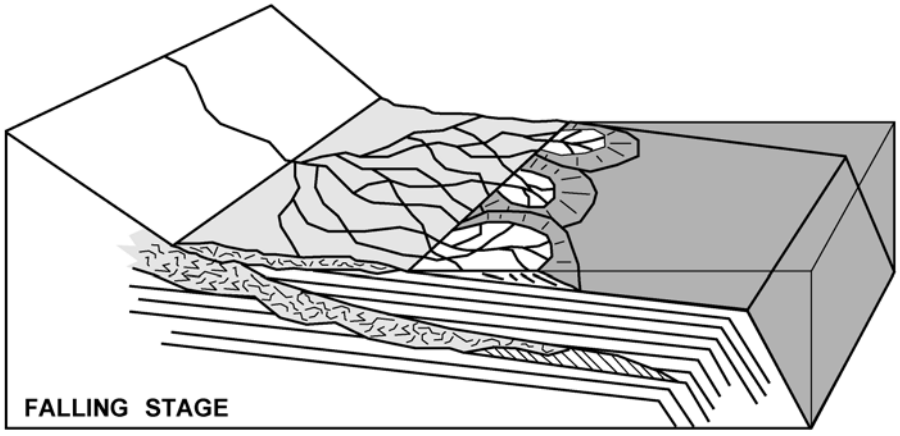

Time 2

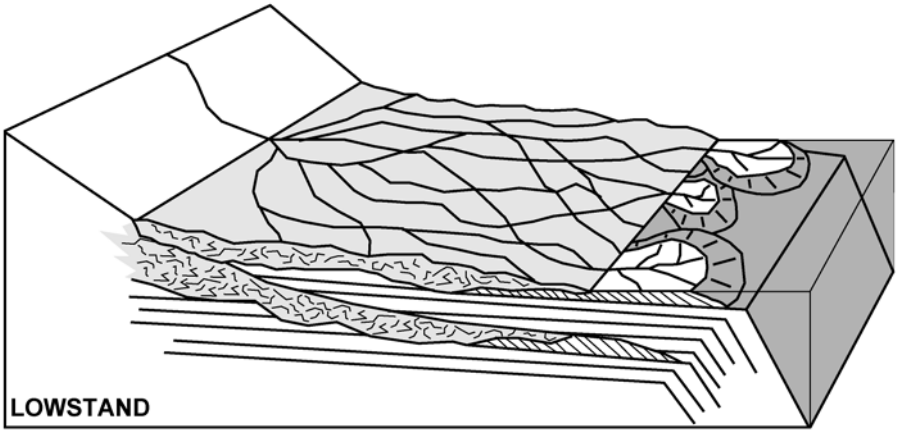

Time 1

Using preliminary results from the dataset described herein, Warren and Bartek (2002a; 2002b) and Warren et al. (2002) also considered a fluvial origin for these widespread and unconfined lowstand deposits perched on the ECS continental margin. They classified the strata, specifically LST 6, as a metastable fluvial shelf system (MFSS), and defined it as a laterally extensive, lowstand fluvial deposit that is generally unincised with little or no sedimentary bypass. They attributed the metastable conditions to high sedimentation rates and low gradient that cause the fluvial system to avulse rather than incise. Further, Warren and Bartek (2002a; 2002b) contended that the fluid dynamics of these metastable conditions are created, primarily, by the low gradient of the margin and, secondarily, by an abundant sediment supply. Over time, the channel bottom elevation becomes higher (via deposition) than the elevation of the surrounding area adjacent to the river levees and the system avulses (*sensu* Thorne, 1994). Eventually, the MFSS is expected to avulse and aggrade to form a sediment sheet similar to a braid plain. Therefore, in addition to the extremely low gradient and deep shelf-slope break of the ECS margin, the discharge and sedimentation rates of those fluvial systems must also be taken into account when considering the formation of the lowstand fluvial braidplain.

In order to create an extensive sand sheet (i.e., extensive enough to not be removed during transgressive ravinement), an abundant sediment influx is considered crucial. The majority of the ECS fluvial influx comes from the Yellow and Yangtze Rivers. At 1.56×10^9 tons/year, the combined total of these two rivers represents 10% of all sediment that is delivered to the world's oceans (Milliman et al., 1983). Many other smaller rivers along the perimeter of the ECS/YS/BS system from China and Korea contribute less than 2×10^7

tons/yr (Figure 2.1). These minor systems are negligible, representing less than 2% of the combined influx from the dominant Yangtze and Yellow rivers.

Volumes of preserved sediment, uplift and related erosion rates can be effective proxies for sedimentation rate, but an accurate assessment of paleo sedimentation rates must also take into account decreased precipitation associated with colder and drier climatic conditions throughout China during periods of glacial maxima. Estimates of paleo precipitation trends for the ECS region are derived from the terrestrial record of the Chinese Loess Plateau during the late Pliocene and Pleistocene (e.g., Liu et al., 1995; Wang, 1999; Xiao et al., 1999; An, 2000; Evans and Heller, 2001). Chinese loess is related to the cold and dry northerly winter monsoon. The development of interbedded paleosols is associated with a dominant southerly, moisture-bearing summer monsoon. During periods of glacial maxima, the winter monsoon is the dominant climate pattern, and summer monsoons dominate climate during interglacials (An, 2000). These alternating loess-paleosol successions are constrained chronologically by multiple techniques, including, thermoluminescence (e.g., Xiaomin et al., 1997; Chunchang et al., 2003), ^{14}C (e.g., Baotian et al., 2001), magnetic susceptibility (e.g., Bloemendal et al., 1995), and stable nitrogen isotopes (Tamburini et al., 2003). The silts from the Loess Plateau are distributed both regionally (e.g., Lake Biwa, Japan, Xiao et al., 1999; South China Sea, Tamburini et al., 2003) and globally (Greenland ice core, Biscaye et al., 1997), allowing worldwide correlation of these cool and dry climatic events.

Liu et al. (1995) calculated a precipitation rate of only 200 mm/yr (compared to a present rate of about 500 mm/yr for the study area; Figure 2.17A) during OIS 6 from the Xifeng section of the Loess Plateau. Evans and Heller (2001) compiled multiple datasets from the Luochuan section of the Loess Plateau that indicate somewhat higher

Figure 2.17. A) High resolution paleoprecipitation data from the Xifeng section on the Loess Plateau of China (from Liu et al. 1995). B) Low resolution paleoprecipitation from the Luochuan section of the Loess Plateau of China as compiled in Evans and Heller (2001).

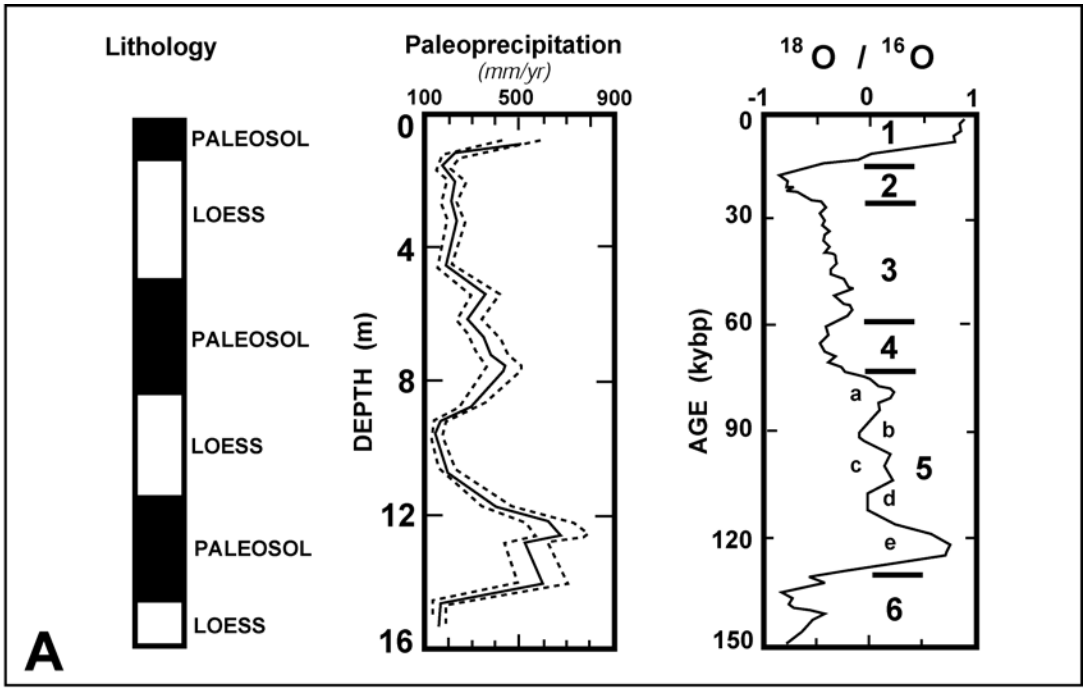
Lithology
PALEOSOL
LOESS
PALEOSOL
LOESS
PALEOSOL
LOESS
Paleoprecipitation
(mm/yr)
100
500
900
DEPTH (m)
0
4
8
12
16
18 O / 16 O
-1
0
1
AGE (kybp)
0
30
60
90
120
150
1
2
3
4
a
b
c
d
e
5
6
A

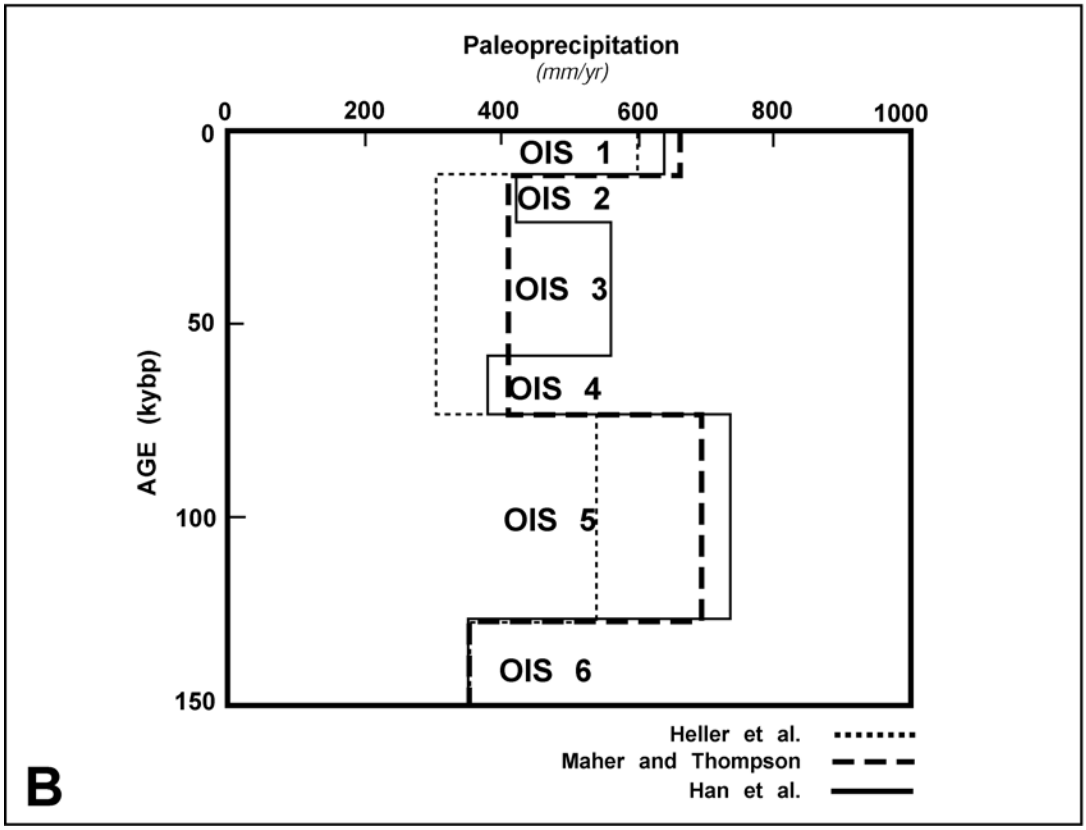
Paleoprecipitation
(mm/yr)
0
200
400
600
800
1000
AGE (kybp)
0
50
100
150
OIS 1
OIS 2
OIS 3
OIS 4
OIS 5
OIS 6
Heller et al.
Maher and Thompson
Han et al.
B

paleoprecipitation rates during OIS 6 (between 300 and 400 mm/yr), but still much less than present day for this region (i.e., 650 mm/yr; Figure 2.17B). These datasets indicate that precipitation rates in the Yangtze River valley were about half of present values. Climate models of this region are consistent with the data. In areas where present values range from 800 to 1600 mm/yr, the models produce precipitation rates during the last glacial maximum (OIS 2) that range from 600 to 800 mm/yr (Xiadong, 1997). It has been assumed in past studies of the ECS (e.g., Hori et al., 2001; Saito et al., 2001; Wellner and Bartek, 2003) that decreased precipitation during glacial maxima, and a subsequent decrease in runoff and erosion, also yielded a decrease in fluvial sedimentation rates, at least in the two major systems flowing into the ECS/YS/BS from the Asian continent (i.e., the Yellow and Yangtze rivers). Despite the reduction in precipitation, extensive LST strata were deposited on the ECS margin during OIS 2, 6, 8, and 10. Hypotheses explaining these observations include: 1) decreased precipitation rates were still adequate to carry abundant sediment load and 2) subaerial exposure of the margin during LSTs increases the drainage basins by about 1.0 x 10^6 km^2 and increases sediment erosion by an amount that compensates for the decreased precipitation in the drainage basins of the Yellow and Yangtze rivers. Even though paleo precipitation rates for this region are fairly well established, the effect of decreased precipitation on the sediment yield in fluvial systems bordering the ECS is not well documented. However, it is completely feasible that decreased precipitation and runoff rates were still capable of carrying large sediment loads (i.e., hypothesis #1). The second hypothesis is also a likely scenario based on increased sediment influx to the South China Sea during the last glacial maximum (OIS 2; Wang et al., 1995). During this time, deposition rates were twice as high as during the post-glacial times attributed, in part, to the erosion of

the subaerially exposed Sunda Shelf. Even though decreased runoff related to increased evapotranspiration across lowland regions is reported by Milliman and Syvitski (1992), lowstand exposure on the ECS margin likely caused a similar response to the South China Sea. Unfortunately, the bottommost portion of LST 6 is not observed in core DZQ4, so the extent of a finer-grained component from the cannibalization of underlying HST silts and clays cannot be assessed. While each of these hypotheses, or a combination thereof, is a viable interpretation, they only address the LUFS deposits in terms of sediment supply to the exposed margin.

Additional factors that are unrelated to sediment supply offer further insight into the large volume of LST 6 sediment perched on the margin, including the impact of exposure of the margin on fluvial gradient (hypothesis #3) and the reduction of oceanic currents in the area during lowstands (hypothesis #4). Exposure of the ECS margin during lowstand decreases fluvial gradient and leads to additional deposition, and oceanic currents that transport sediment along the Chinese coast do not exist during major lowstands of sea level, so the sediment remains in the system. Hypothesis #3 suggests that, as margin exposure occurred during LST 6, the widening coastal plain created a lower fluvial gradient, and caused fluvial systems to become overextended. Power loss, increased bed load, and deposition occured and, as a result, a greater percentage of sediment was deposited (i.e., reduced velocity leads to higher deposition rates). This idea is presented by Holbrook (1996) to explain the broad, fluvial sand sheet of the Cretaceous Mesa Rica Sandstone (Dakota Group, late Albian) of the U.S. Western Interior Basin. The Mesa Rica Sandstone, which is similar to the MFSS presented by Warren and Bartek (2002a; 2002b), experienced frequent avulsion in conjunction with a low gradient that, in turn, caused regional scouring of a flat,

planar, sequence-bounding unconformity (Holbrook and Dunbar, 1992; Holbrook, 1996). The fourth hypothesis addresses the effect of oceanic (coastal) currents on transport of fluvial sediment south and potentially out of the ECS system (e.g., Hung and Chung, 1994; Chung and Chang, 1995; Tamburini et al., 2003). Of the 4.78×10^8 tons of sediment presently transported by the Yangtze River each year, 40% (1.91×10^8 tons/year) is deposited at the river mouth and 30% (1.46×10^8 tons/year) is carried south by the Changjiang (Yangtze) Coastal Water current (Milliman et al., 1985). During lowstands, especially major events (>100 m drop), these currents are attenuated or non-existent. Without these currents, the entire sediment load of the Yangtze, Yellow, and other river systems remains in the system available for deposition on the exposed margin.

In summary, the laterally and vertically extensive fluvial sands from LST 6 seem inconsistent with a drier climate. Decreased precipitation and runoff during the glacial maximum suggests decreased sediment loads in the fluvial systems that transport sediment to the ECS margin. However, it appears that even under these conditions, the streams and rivers were still capable of transporting abundant sediment. Increased erosion of the exposed ECS margin may have also contributed to a local increase in sedimentation rates. Additional factors, unrelated to sediment supply, have the potential to increase "apparent sediment supply" through higher rates of deposition. Underpowered fluvial systems flowing across the wide, subaerially exposed margin further decrease an already low gradient and lead to greater rates of deposition. In addition, the absence of the ECS during the extreme lowstand events from LST 2, 6, 8, and 10, which traps 40% of the Yangtze sediments near the river mouth, also means the absence of the high-energy coastal current system that removes an additional 30% of the sediments from the central portion of the ECS system. It is likely that all three of

these factors (ample fluvial transport, underpowered fluvial systems, and the absence of sediment removal via oceanic currents) combined to produce the abundant, unincised fluvial deposits perched on the ECS margin during the dry climate of the LST 6, 8, and 10 glacial maxima. Of the three factors listed above associated with fluvial depositional processes, none are unique to the ECS margin, and make the observations from this investigation, specifically related to the sensitivity and interaction of these parameters to baselevel change, generally applicable.

2.4.2 Incised versus Unincised

The principle causes of incision include increases in substrate erodibility, discharge, flow velocity (i.e., through confinement), and/or gradient (i.e., fluvial gradient < coastal plain/shelf gradient). A decrease in sediment load in alluvial streams can also facilitate fluvial incision (Schumm, 1999). Factors that inhibit fluvial incision include a high degree of cohesiveness or induration of the underlying strata, a low mean water discharge, and/or a low gradient for both the coastal plain and the shelf (fluvial gradient > coastal plain/shelf gradient). Incision can also be impeded by high rates of sea level fluctuation, where the rapid change limits the time that a fluvial system has to adjust (Wolfe et al., 1998). Throughout the Quaternary, glacially driven eustasy was ubiquitous on all margins, the overwhelming majority of which underwent major incision (e.g., the Hudson River incised valley offshore New Jersey, the Ganges-Brahmaputra incised valley in the Bay on Bengal, the Indus River incised valley in the Arabian Sea). During this time, these continental margins also experienced decreased precipitation during similar climatic conditions (i.e., cool, dry glacial periods). Assuming that these incised margins experienced a fairly uniform response of fluvial systems to these conditions (in terms of sediment load and runoff) and a similar rate

of glacially driven sea level rise and fall, it can be argued that these factors (i.e., low mean water discharge, decreased sediment load, high rates of sea level fluctuation) do not effectively inhibit incision, at least during the late Pleistocene and Holocene. Therefore, rates of RSL, sedimentation, and discharge are not primary factors controlling the lack of incision in the recent and modern record on the ECS margin. Sediment studies from the ECS margin show that the underlying HST deposits are dominated by silts and clays. While lacking induration, these fine-grained sediments are still more cohesive than the overlying fluvial sands. Therefore, if incision was impeded by the underlying substrate, it was most likely a minor component (at least in the ECS), as finer grained silts and clays are not present in the sandy lithologies of the LSTs. Based on these observations (i.e., ubiquitous RSL fluctuations and decreased sedimentation, minor cohesiveness of basal sediments), the low gradient might be one of, if not the, dominant factor in preventing incision. Further support of this hypothesis is that a low gradient is the only common denominator between the ECS margin and previously documented examples of unincised fluvial systems on the margins of Australia (Woolfe et al., 1998), Java (Posamentier, 2001), and New Zealand (Browne and Naish, 2003). Even so, the gradient of the ECS margin (0.013°) is much less than northeastern Australia (0.1°), northern Java (0.03°), and southeastern New Zealand (0.3°).

With respect to gradient of the margin, fluvial systems flowing across the coastal plain/shelf, exposed during lowstand, have three potential responses to RSL fall: incision, steady state, and deposition (Posamentier et al., 1992; Posamentier and Allen, 1999). If the subaerially exposed margin profile is greater than the graded fluvial profile, incision occurs due to increased flow velocity over the positive gradient differential. This creates the oversteepened fluvial profile found in most modern coastal settings (Posamentier and Allen,

1999). If the shelf profile is equal to the fluvial profile, a steady-state system exists (no net erosion or deposition). If the shelf profile is less than the fluvial profile, aggradation and avulsions occurs. In this last scenario, velocity within the oversteepened fluvial system decreases.

The gradient relationships between fluvial systems, shelf/coastal plain, and deposition/erosion are verified empirically using flume experiments (e.g., Wood et al., 1993; Koss et al., 1994). During these investigations, Wood et al. (1993) held the coastal plain dip at a constant angle that simulated 0.4° (factoring in vertical exaggeration) and a simulated shelf gradient that fluctuated between 1.6° and 0.4°. Because the lowest shelf gradient used in the experiment matched that of the coastal plain (i.e., 0.4°), a steady-state system existed wherein deposition and incision should not have occurred. However, incision did occur in this simulation, associated with the gradient differential at the exposed shelf-slope break, and propagated landward through knickpoint migration. Koss et al. (1994) used a shallower shelf gradient simulation (0.2°) and specifically addressed incision that propagated landward from the shelf-slope break. Koss et al. (1994) noted the lack of incised valley formation until after baselevel fell below the shelf-slope break leaving it subaerially exposed. Even then, there was a delay between the onset of incision at the shelf edge and the occurrence of widespread shelf incision. The delay is associated with a slow rate of headward erosion of incised valley systems. During this time lag, unconfined fluvial systems accumulated across the simulated shelf creating a fluvial braid plain. Because the ECS shelf-slope-break remained submerged and no other incision is observed on the margin, the rate of RSL fluctuation, which shortens or lengthens this time lag, is not relevant for these observations.

The fluvial braidplains and lack of incision while the shelf-slope break remained submerged within the low-gradient system simulated by Koss et al. (1994) are analogous to the ECS margin. These results demonstrate the process-response relationship of a low-gradient and a deep shelf-slope break during the formation of an unincised fluvial system. The importance of these empirical observations, though, might not seem substantial because examples of natural systems that contain both a low gradient and a deep shelf-slope break are rare. Therefore, it is a challenge to test the control of extremely low gradients and deep shelf-slope breaks on stratigraphic successions in both modern environments and the geologic record. For example, using the digital bathymetry data from Sandwell and Smith (1997), the fifty-one passive, clastic margins assessed by O'Grady et al. (2000) have an average (and median) shelf gradient of 0.93° with a minimum of 0.043° (the Murray River, southern Australia). The next lowest gradient values (i.e., 2nd through 4th) are higher by almost an order of magnitude: 0.35° (Laurentia) and 0.38° (Fly River margin) and 0.43° (offshore New Jersey). The depths of shelf-slope breaks on these margins are 111 m (Murray), 118 m (Laurentia), 80 m (Fly), and 76 m (New Jersey). Similar physiographic data (i.e., gradient and depth of shelf-slope break) for continental margins and/or shelves throughout the Phanerozoic are rare in the literature. Because these deposits shared a similar morphology, though, the assumption is made here that margins throughout the Phanerozoic shared similar values for gradient and depth of shelf-slope break. Therefore, during lower-magnitude sea level drops (i.e., <70 m; Vail et al., 1977; Haq et al., 1988), many shelf-slope breaks, like those presented above, remained submerged and caused the exposed portion of the shelf to behave like a ramp. Talling (1998) pointed out that shelf-slope break exposure is also unexpected during non-glacial, greenhouse times, yet incision still occurs due to the

convexity of the coastal prism related to the preceding highstand shoreline. Even taking this model into account, the lower gradient that exists basinward of the coastal prism still appears favorable for LUFS formation (his Figures 1 and 2). Similar conditions of non-exposure of the shelf-slope break during moderate to minor sea level fluctuations occurred throughout the Phanerozoic (e.g., Haq et al., 1988; Hallam, 1992). The rarity of LUFS strata preserved on these margins, though, suggests that the LUFS are dependent on more than physiographic conditions alone. Based on the thick and laterally continuous fluvial sediments preserved on both the ECS margin and the Canterbury Plains (Leckie, 1994; Browne and Naish, 2003) and their association with multiple fluvial systems and a significant source area (mainland China and the Southern Alps, respectively), an abundant sediment supply is also considered to be a requisite condition of the LUFS. The thin nature (<10 m; exact thickness not reported) of Quaternary unincised fluvial systems from Java (Posamentier, 2001) and Australia (Woolfe et al., 1998) is not surprising due to the lack of association of these margins with a major fluvial source, and illustrates the effect of sediment supply on the same general physiographic conditions. Ample sediment input is critical to preservation of the LUFS. Thicker, voluminous units of sediment are less likely to be completely removed during transgressive ravinement.

2.4.3 Sequence Stratigraphic Implications of the LUFS

In the interpretation of the ECS margin LUFS that is the subject of this paper, widespread subaerial exposure occurs because the rate of eustatic fall exceeds subsidence. The high-frequency, glacio-eustatic fluctuations in the ECS (>1 cm/yr; Pillans et al., 1998; Saito et al., 1998; Figure 2.2) are often greater than basin subsidence rates (ranging from 0.3 mm/yr on outer margin to 4.4 mm/yr at the Yangtze depocenter; Stanley and Chen, 1993;

Berne et al., 2002). A minor uplift is also present in the ECS region with rates on northern and northwestern portions of the margin varying between 1.1 and 1.4 mm/yr along the east coast of the Korean peninsula (Quaternary; Kim, 1973) and 3 mm/yr in the Yellow Sea (Holocene; Wang and Wang, 1982; Kim and Kucera, 2000). Stratal stacking patterns observed in seismic profiles across the shelf-slope break verify these observations with progradation in the north and aggradation in the south (Figure 2.12).

The exposed lowstand margin is subject to modification by terrestrial (fluvial and subaerial) processes. During this time, the traditional sequence stratigraphic model predicts stream rejuvenation and incision (and associated sediment bypass) leading to cessation of widespread fluvial deposits across the exposed margin during a rapid RSL fall (i.e., RSL > subsidence) and the ensuing period of lowstand and stillstand (Posamentier et al., 1988; Van Wagoner et al., 1988). This does not appear to apply to the shallow, late Pleistocene strata on the ECS margin. Lowstand fluvial deposits in the ECS that are associated with the interval before OIS 4 (i.e., OIS 6 and older) do not contain evidence of major incision or sedimentary bypass. Widespread fluvial systems that aggrade and avulse, in lieu of incision during the LST, do not fit current stratigraphic models. Since these LUFS strata are unexpected, they may be taken out of stratigraphic context and genetically misunderstood. Posamentier (2001) noted that unincised fluvial systems are difficult to distinguish from highstand alluvial systems, such as the Canon del Tule Formation (late Cretaceous) of the Parras-La Popa foreland basin in northeastern Mexico (Halik et al., 1997) and the late Quaternary deposits from the Mississippi (Louisiana) and Colorado (Texas) rivers (Aslan and Blum, 1999). Posamentier (2001) also postulated that, since the presence of lowstand unincised fluvial deposits is unanticipated, they may also be mistaken for a large-scale

incised valley system, such as those from the late Cretaceous in the U.S. western interior (Frontier, Fall River, and Muddy formations; Stonecipher, 1996) and the Bartlesville Sandstone (middle Pennsylvanian) in northeastern Oklahoma (Ye and Kerr, 2000).

A type 2 SB, which is overlain by a type 2 sequence, was characterized by Vail (1984) as an interval of minimal erosion associated with slowdowns of RSL rise, but no period of RSL fall at the depositional shoreline break (e.g., rate of subsidence > rate of eustatic fall). A type 1 SB, which is overlain by a type 1 sequence, is associated with surfaces that formed in response to RSL fall at the depositional shoreline break (e.g., rate of subsidence < rate of eustatic fall; Vail, 1984; Posamentier and Vail, 1988). The traditional LST classification (e.g., Vail, 1987; Posamentier and Vail, 1988; Posamentier et al., 1988; Van Wagoner et al., 1990) predicts the subdivision of the LST into two separate members if the basin has a discrete margin edge (which the ECS possesses): 1) a lowstand fan and 2) a lowstand wedge. This architecture is created during incision of the shelf-slope break and bypass of sediments beyond the continental shelf onto the continental slope and rise. The lack of incision in seismic profiles along the ECS shelf-slope break suggests that the extreme depth of the present-day bathymetry was fairly consistent throughout the late Pleistocene. The ECS margin is intriguing because it possesses a shelf-break morphology, yet during lowstand there is a lack of deep incision of the outer margin and sediment bypass. Sediment remained perched on the ECS margin during the LST, and it behaved more like a ramp (i.e., no discrete shelf edge). For ramp margins, the sequence stratigraphic model predicts that LSTs (both type 1 and type 2) are deposited on the shelf and do not contain basin floor fans (Van Wagoner et al., 1990). The LUFS of the ECS LST shares these similarities, but it does not fit the definition of the shelf-margin systems tract (SMST). The SMST is defined by Vail

(1987) as a prograding wedge that overlies a type 2 SB (and is, therefore, a type 2 sequence) and laps out on the shelf landward of the previous shoreline break. The SB of the LUFS has a significant shift of landward facies above the SB, that then overlies marine facies, which is inconsistent with a type 2 SB. Therefore, even the ramp margin SMST is an inaccurate classification. Posamentier and Allen (1999) suggested the elimination of the "type 1" and "type 2" terminology due to widespread misuse and confusion. The conflict between the ECS strata and this sequence stratigraphic terminology illustrates the limitations associated with of these "typed" classifications and provide further evidence to abandon this terminology. Moss (2002) observed the same inconsistencies in Yellow Sea strata of the same age. Regardless of the terminology, though, the processes that control the formation of the LST and SB associated with OIS 6 (previously referred to as ED3 and SB3) remain the same (i.e., eustasy > subsidence).

As discussed above, the hybrid nature of the ECS lowstand strata is partially dependent on a consistently submerged shelf-slope break that allows the margin to behave like a ramp. However, the wide, low-gradient nature of the margin and an abundant sediment influx are also responsible for controlling the unique stratal architecture of the LUFS. This collection of depositional end members, while unique in modern systems, exists throughout the geologic record. For example, most foreland basin systems possess a low-gradient, wide shelf with minimal incision, and ample sediment influx. Upon review of many of these ancient foreland basins throughout the Phanerozoic, stratigraphy similar to the ECS is observed and suggests formation by depositional processes analogous to those observed on the ECS continental margin.

During the Paleozoic, sheet sands from the foreland Bowen Basin in eastern Queensland Australia (Permian) are attributed to low-sinuosity braided stream during times of abundant sand influx (oversupply) to the basin (Fielding et al., 1993). These deposits are >40 m thick and at least 2.2 km wide and include an erosive base, sharp tops, cross-bedded coarse sands, and vertical aggradation. The Cutler Formation (Pennsylvanian-Permian) from north-central New Mexico is preserved within a foreland basin related to the San Luis-Uncompahgre Uplift (Eberth and Miall, 1991). Thick sequences (up to 20 m) of multi-storied coarse-grained sand sheets attributed to poorly confined shallow, braided flow were deposited during periods of increased aridity. These deposits were considered by Everth and Miall (1991) to be laterally extensive, although the true extent is unknown due to limited access and exposure. The Cenozoic also contains geologic examples with many similarities to the LUFS on the ECS margin. The Rio Vero and Escanilla formations (Miocene and Eocene, respectively) from the Ebro Foreland Basin adjacent to the Spanish Pyrenees are two such analogs. The Rio Vero Formation forms well developed cliff sections that contain broad, low-sinuosity, moderate-energy streams that formed sandy braided rivers approximately 10 m thick (Jones et al., 2001). The Escanilla Formation is also composed of low sinuosity, braided sands that formed a sand-dominated channel-fill facies that are about 10 m thick (Bentham et al., 1993).

Two of the best, and probably the most well known, examples of extensive, unincised fluvial deposits are preserved in the Mesozoic foreland basins of the U.S. western interior. The Castlegate Formation (late Campanian; eastern Utah) exhibits extensive, continuous cliff face exposures that are attributed to lowstand and transgressive non-marine fluvial deposits formed by vigorous braided river systems on a foreland basin ramp over a period of 5 million

years (Yoshida et al., 1996; Miall and Arush, 2001). Exposures along the Book Cliffs, Utah extend for more than 220 km with an average thickness of 30 m and a maximum thickness exceeding 60 m (Yoshida et al., 1996; McLaurin and Steel, 2000). The SB at the base of the Castlegate has minimal relief (10 m over 50 km, or 0.01°; Yoshida, 2000). Van Wagoner (1995) suggests a depositional environment wherein a fluvial complex formed a mega fan complex that did not connect to the sea, but died out in a broad, swampy complex of shallow lakes. The Mesa Rica Sandstone (Dakota Group, Albian; northeastern New Mexico) is a broad sandstone sheet (>87 km wide and 100 km long) of similar thickness (average = 12 m, maximum = 30 m; Holbrook and Dunbar, 1992) deposited across the alluvial and/or coastal plain during the maximum Kiowa-Skull Creek regression during the late Albian. During this time, the Dalhart Basin maintained a low offshore gradient (angle not reported; Holbrook, 1996). Gradient reduction in the adjacent coastal plain from delta progradation is hypothesized to have forced both stream straightening and the storage of coarser (non-transportable) sediments in channels. The stable baselevel conditions (i.e., minimal RSL drop; Holbrook, 1996) only allowed minimal channel aggradation, frequent avulsion, caused regional scouring of a sequence-bounding unconformity (Holbrook and Dunbar, 1992; Holbrook, 1996). This unconformity is relatively smooth, expressing relief typically less than 0.01° on a regional scale (i.e., 15 m across 87 km length of cross section; Holbrook, 1996).

Braided fluvial systems are non-unique responses to numerous depositional conditions. The geologic examples mentioned above, when compared to the ECS LUFS from LST 6, indicate many similarities in braided fluvial morphology. Primarily, these are analogous deposits based on abundant sediment influx and the fairly low gradient associated with

foreland basins in general. Insights gained from the investigation of the ECS provide opportunities to better understand the process-response relationships between sediment supply and gradient in ancient systems with shared characteristics. Comparison with the examples above, though, also indicate differences based primarily on tectonic activity and lateral extent. As is the case in Spanish Pyrenees, rapid subsidence limits lateral avulsions through vertical aggradation, a component most likely present to some degree in the other examples as well. However, even these differences in tectonic setting (i.e., active basin subsidence and source uplift in foreland basins versus the passive ECS margin) illustrate the importance of sediment supply and a low gradient for the creation of low-energy, low-sinuosity braided fluvial systems.

2.4.4 Alternative Hypotheses to the Lowstand Unincised Fluvial System

Previous investigations discussed a fluvial element of LST 6 preserved in core DZQ4 (e.g., Liu et al., 2000; Berne et al., 2002), but considered it a minor component unrelated to the massive, braided fluvial complex presented in this paper. Liu et al. (2000) offered only brief interpretations relating to the lowstand units. The focus of their investigation was the transgressive tidal ridges (SF MOUND). They considered the chaotic nature of seismic reflections in the lowstand units as being representative of the lateral migration of numerous small channels. Based on correlation to core DZQ4, Liu et al. (1998) linked the chaotic facies to fluvial, swamp, and lacustrine sediments, and specifically identify LST 6 as a product of depositional environments ranging from river mouth, river, and shallow sea (their unit U7; their Table 1). However, the fluvial system identified in the Liu et al. (1998) was presented as an anastamosing system across a delta plain rather than a braided complex presented in this study. While an anastamosing system generally has a low gradient and low

stream power, lateral channel migration is considered minimal with channels bound in place by floodplain deposits (Miall, 1996). Stratigraphic evidence for distinct channels, floodplain deposits, crevasse splays, ribbon sands, or the infilling of channels by accretion (i.e., parallel to the channel floor) are not observed within seismic profiles. There is also no evidence within the cored portion of LST 6 (> 10 m) for a traditional floodplain facies (fine laminae, clays and muds, concentrated organic material). The data gathered during the course of this investigation do not support the anastomosing system of Liu et al. (1998) as a viable hypothesis.

Similar to Liu et al. (1998), the focus of the Berne et al. (2002) investigation was the transgressive tidal ridges (SF MOUND), and interpretations related to the LST deposits preserved on the ECS margin were limited and concise. Based on the lithology and biostratigraphy, Berne et al. (2002) identified fluvial components at the bottom and top of Unit 6 in core DZQ4 (i.e., LST 6). They also correlated this unit to a chaotic seismic facies that, as presented in this paper, was observed to thin on the outer margin and grade laterally into low-angle clinoforms. However, Berne et al. attributed the majority of the stratal package in LST 6 to a deltaic/estuarine environment (their unit U110; their Figure 8). The Berne et al. (2002) estuary model considered this to be a forced regressive deposit (*sensu* Posamentier et al., 1992). Analyses in this investigation are consistent with the Berne et al. (2002) association of LST 6 with a forced regression. However, in the estuary scenario of Berne et al. (2002), the laterally extensive, basal unconformity (their surface D110, our ED3) is not attributed to fluvial processes and subaerial erosion. Rather, it is considered to be a regressive surface of marine erosion formed during RSL fall (forced regressive systems tract of Hunt and Tucker, 1995; falling stage systems tract of Plint and Nummedal, 2000).

Therefore, Berne et al. (2002) place the fluvially incised SB near the top of the unit's SF CHAO. They stated that the SBs "are difficult to detect because they separate similar (from a seismic point of view) facies (estuarine/deltaic and continental)" and do not identify the SB in seismic profiles (Berne et al., 2002; p. 311). The SB and the stratigraphic context of their model is presented in an idealized cartoon (their Figure 13). In this scenario, Berne et al. (2002; p. 311) place the fluvial facies at the top of LST 6 (over the estuarine sediments) and not at the bottom. However, their core description of this unit presented a transition from fluvial (bottom) to prodeltaic then back to fluvial/estuarine (top) environments (Berne et al., 2002; p. 303). Liu et al. (2000) observed these sediments at both the bottom and top of this unit and attributed them to fluvial deposition. These descriptive inconsistencies reported by Berne et al. (2002) raise concern about the accuracy of the application of the estuarine/deltaic model.

The estuarine model is also challenged by the lack of incised embayments during LST 6. As defined by Pritchard (1967), an estuary is a semi-enclosed coastal body of water with a free connection to the open sea. Within the estuary, seawater is measurably diluted with freshwater derived from the land. Dalrymple et al. (1992) modified this definition by classifying an estuary as the seaward portion of a drowned valley system which receives sediment from both fluvial and marine sources and which contains facies influenced by tide, wave, and fluvial processes. Berne et al. (2002) hypothesized that submarine tidal scouring, and not subaerial fluvial erosion, was a possible mechanism for incision deeper than the lowest sea level (-120 m). However, evidence for incision at the base of LST 6 SF CHAO is not observed within the regional dataset used in this investigation (Figure 2.5). This lack of

incision indicates that the embayments needed for estuarine development did not exist and that estuary formation was limited, if not impossible.

2.5 CONCLUSIONS

The traditional sequence stratigraphic model predicts incision and sedimentary bypass across the continental margin during RSL lowstands. This trend is not observed in the shallow, late Pleistocene strata on the ECS continental margin. There, lowstand fluvial deposits prior to OIS 4 (i.e., OIS 6 and older) do not experience major incision or sedimentary bypass. Instead, strata associated with lowstand unincised fluvial systems are deposited across the ECS margin. They are present in both strike- and dip-oriented seismic profiles, extending laterally along depositional strike for more 400 km, and are greater than 40 m thick. Results from earlier studies of the ECS continental margin (e.g., Bartek and Wellner, 1995; Tang, 1996; Liu et al., 1998; Saito et al., 2000; Berne et al., 2002; Yoo et al., 2002; Wellner and Bartek, 2003) do not identify these units as unincised fluvial systems. The regional extent of the large seismic dataset used herein provides a unique set of observations unavailable to previous investigations, particularly the lack of incision of the LST 6 SB and the margin-wide distribution of a thick fluvial unit consisting of chaotic seismic facies that grade into dipping reflections that offlap basinward.

The critical factors for deposition of the LUFS in the ECS are related to basin physiography (extremely low gradient and deep shelf-slope break) and an abundant sediment influx. The extreme depth of the shelf-slope break caused it to remain submerged during even the lowest lowstands and did not allow incision and knickpoint migration. The wide margin, in addition to subsidence (Figure 2.10), provided abundant subaerial accommodation and allowed most, if not all, of the LUFS to remain perched and not bypass the margin. During the decreased precipitation of glacial maxima, the low gradient and large width of the exposed margin compensated for a possible decrease in sediment supply by forming an

extensive bed-load-dominated fluvial system. Other factors such as decreased low mean water discharge, cohesiveness of substrate, and rate of sea level fluctuations are considered to have minimal, if any, effect.

The formation of a fluvial element that aggrades instead of incising the exposed shelf during lowstand is shown empirically by Wood et al. (1993) and Koss et al. (1994). Observations of natural systems that exhibit these conditions (i.e., low-gradient margins with higher gradient, and therefore unincised, fluvial systems), while rare in the geologic literature, do exist, even though they are not predicted by the traditional sequence stratigraphic model. Aside from the ECS, the only evidence of similar physiography is found in Quaternary deposits in Australia (Woolfe et al., 1998), offshore Java (Posamentier, 2001), and New Zealand (Browne and Naish, 2003). Of these examples, only the Canterbury Plains of New Zealand is associated with fluvial systems that provide an abundant sediment influx to the exposed margin. Therefore, in addition to the ECS margin, only the Canterbury Plains exhibit the same thick and laterally continuous, unincised fluvial braidplain deposits across the margin. More examples of the LUFS may exist, but are identified incorrectly as highstand alluvial system or extensive incised valley deposit (*sensu* Posamentier, 2001). The results from this investigation will hopefully challenge the geologic community to re-evaluate margins with similar depositional boundary conditions to determine the true spatial and temporal distribution of the LUFS.

It is hypothesized that the rarity of the LUFS-forming conditions, both physiographic and depositional, is responsible for the lack of LUFS formation on passive continental margins throughout the geologic record. Foreland basins, on the other hand, have a ramp morphology, exhibit a low-gradient, and are associated with an ample sediment influx.

Lowstand fluvial architecture similar to the LUFS presented in this paper is preserved in foreland basins throughout the geologic record. Examples of these strata are found in the Bowen Basin in eastern Queensland, Australia (Permain; Fiedling et al., 1993), the Devonian Catskill Delta, U.S. Appalachian Basin (Devonian; Ettensohn, 1985; Woodrow, 1985); the Mesa Rica Sandstone (Holbrook and Dunbar, 1992; Holbrook, 1996) and the Castlegate Formation (Van Wagoner et al., 1990; Van Wagoner and Bertram, 1995; Miall and Arush, 2001) from the Cretaceous U.S. western interior; the Alaska Range (Miocene; Lesh et al., 2001), the Pakistani foreland (Miocene; Pivnik and Johnson, 1995), the Ganga Megafan, India (Miocene; Shukla et al., 2001), and the Spanish Pyrenees foreland basin (Eocene; Bentham et al., 1993; Miocene; Jones et al., 2001). Due to the similar conditions and similar stratal architecture, it is hypothesized that the fluvial foreland basin deposits are formed under depositional conditions analogous to those observed on the ECS continental margin.

The data presented in this paper support the hypothesis that ECS margin physiography throughout the late Pleistocene and Holocene was similar to present (i.e., gradient, width, depth of shelf-slope break). The high-resolution core and seismic data utilized in this investigation also correlate with regional (e.g., Yangtze River coastal plain and the Loess Plateau; Xiaodong et al., 1997 and An, 2000, respectively) and global (e.g., Greenland ice core; Biscaye et al., 1997) high-resolution, paleoclimate data (e.g., precipitation, temperature, water salinity) that record glacial climatic conditions that were vastly different from present conditions on the ECS margin. Even though present conditions do not reflect those active during glacial intervals, an extensive understanding of the last glacial maximum in and around the ECS, in conjunction with the high-resolution core data and seismic profiles used in this investigation, places constraints on those depositional processes as well (e.g.,

paleoprecipitation rates, paleotemperatures, sediment supply). A better understanding of the interaction between depositional processes and associated stratigraphic response on the ECS margin has implications for understanding the origin of strata preserved in foreland basins throughout the geologic record. A thorough understanding of the depositional conditions under which these rocks were formed will allow a more complete interpretation of basin history. This is particularly challenging when many ancient basins lack extensive outcrop, have limited core and well data, and/or are constrained by low-resolution dating techniques (e.g., K-Ar and biostratigraphy) and low-resolution seismic techniques.

2.6 REFERENCES CITED

Adams, J., 1980, Contemporary uplift and erosion of the Southern Alps, New Zealand. Geological Society of America Bulletin, part II, v. 91, p. 1-114.

An, Z., 2000, The history and variability of the East Asian paleomonsoon climate. Quaternary Science Reviews, v. 19, p. 171-187.

Aslan, A. and Blum, M., 1999, The significance of avulsion during valley filling (transgressive and highstand systems tracts), Louisiana and Texas coast. Annual Meeting Expanded Abstratcs, American Association of Petroleum Geologists, v. 1999, p. A7.

Baotian, P., Guangjian, W., Yixiang, W., Zhigang, L., Qingyu, G., 2001, Age and genesis of the Shagou River terraces in eastern Qilian Mountains. Chinese Science Bulletin, v. 46, p. 509-513.

Bark, L.S., Ganson, P.P., and Meister, N.A., 1964, Tables of the Velocity of Sound in Sea Water: Pergamon Press, Oxford, England, 182 p.

Bartek, L.R., and Wellner, R.W., 1995, Do equilibrium conditions exist during sediment transport studies on continental margins? An example from the East China Sea. Geo-Marine Letters, v. 15, p. 23-29.

Bartek, L.R. and Warren, J.D., 2002, Concurrent incised and unincised valley systems and their geomorphic control during Quaternary lowstands on the East China Sea continental margin. SEPM Research Conference: Incised Valleys: Images and Processes, August 18-23, 2002, Casper and Newcastle, WY.

Bartek, L.R., Anderson, J.L.R., Oneacre, T.A., 1997, Substrate control on distribution of subglacial and glaciomarine seismic facies based on stochastic models of glacial seismic facies deposition on the Ross Sea continental margin, Antarctica. Marine Geology, v. 143, p. 223-262.

Bentham, P.A., Talling, P.J., Burbank, D.W., 1993, Braided stream and flood-plain deposition in a rapidly aggrading basin: the Escanilla Formation, Spanish Pyrenees. In Best, J.L. ad Bristow, C.S. (eds.), Braided Rivers, Geological Society Special Publications, v. 75, Geological Society of London, p. 177-194.

Berne, S., Vagner, P., Guichard, F., Lericolais, G., Liu, Z., Trentesaux, A., Yin, P., and Yi, H.I., 2002, Pleistocene forced regressions and tidal sand ridges in the East China Sea: Marine Geology, v. 188, p. 293-315.

Biscaye, P.E., Grousset, F.E., Revel, M., Van der Gasst, S., Zielinski, G.A., Vaars, A., 1997, Asian provenances of Last Glacial Maximum dust in GISP2 ice core, Summit, Greenland. Journal of Geophysical Research, v. 102, p. 26,765-26,781

Bloemendal, J., Liu, X.M., Rolph, T.C., 1995, Correlation of the magnetic susceptibility stratigraphy of Chinese loess and the marine oxygen isotope ercord: chronological and paleoclimatic implications. Earth and Planetray Science Letters, v. 131, p. 371-380.

Browne, G.H. and Naish, T.R., 2003, Facies development and sequence architecture of a late Quaternary fluvial-marine transition, Canterbury Plains and shelf, New Zealand: implications for forced regressive deposits. Sedimentary Geology, v. 158, p. 57-86.

Chough, S.K. and Kim, D.C., 1981, Dispersal of fine-grained sediments in the southeastern Yellow Sea: A steady-state model: Journal of Sedimentary Petrology, v. 51, no. 3, p. 721-728.

Chunchang, H., Jiangli, P., Shu'e, C., Zhanping, Z., 2003, Holocene dust accumulation and the formation of polycyclic cinnamon soils (luvisols) in the Chinese Loess Plateau. Easrth Surface Processes and Landforms, v. 28, p. 1259-1270.

Chung, Y. and Chang, W.C., 1995, Pb-210 fluxes and sedimentation rates on the lower continental slope between Taiwan and the South Okinawa Trough. Continental Shelf Research, v. 15, p. 149-164.

Congxian, L., Gang, C., Ming, Y., Ping, W., 1991, The influences of suspended load on the sedimentation in the coastal zones and continental shelves of China. Marine Geology, v. 96, p. 341-352.

Dalrymple, R.W., Zaitlin, B.A., Boyd, R., 1992, Estuarine models: conceptual basis and stratigraphic implications. Journal of Sedimentary Petrology, v. 62, p. 1130-1146.

Evans, M.E. and Heller, F., 2001, Magnetism of loess/paleosol sequences: recent developments. Earth-Science Reviews, v. 54, p. 129-144.

Fielding, C.R., Falkner, A.J., Scott, S.G., 1993, Fluvial response to foreland basin overfilling: the late Permian Rangal Coal Measures in the Bowen Basin, Queensland, Australia. Sedimentary Geology, v. 85, p. 475-497.

Forman, S.L., Pierson, J., Lepper, K., 2000, Luminescence geochronology. In: Noller, J.S., Sowers, J.M., Lettis, W.R. (eds.), Quaternary Geochronology, Methods and Applications. American Geophysical Union, Washington, DC, p. 157-176.

Halik, N., Soegaard, K., Ye, H., Daniels, A., 1997, Sequence stratigraphy of Canon del Tule Formation, Parras-La Popa foreland basin, Northeast Mexico. Annual Meeting Abstracts, American Association of Petroleum Geologists and Society of Economic Paleontologists and Mineralogists, v. 6, p. 45-46.

Hallam, A., 1992, Phanerozoic Sea-Level Changes. Columbia University Press, New York, 266 p.

Han, J.M., Lu, H.Y., Wu, N.Q., Guo, Z.T., 1996, The magnetic susceptibility of moern soils in China and its use for paleclimate reconstruction. Stduies in Geophysics and Geodesy, v. 40, p. 262-275.

Haq, B.U., Hardenbol, J., Vail, P.R., 1988, Mesozoic and Cenozoic chronostratigraphy and eustatic cycles. In Wilgus, C.K., Hastings, B.S., Kendall, C.G.St.C., Posamentier, H.W., Ross, C.A., Van Wagoner, J.C. (eds.), Sea-Level Changes: An Integrated Approach. SEPM Special Publication 42, Society of Exonomic Paleontologists and Mineralogists, Tulsa, p. 71-109.

Heezen, B., Tharp, M., and Ewing, M., 1959, The floors of the oceans: I. The North Atlantic. Geological Society of America Special Paper 65, 122 p.

Heller, F., Shen, C.D., Beer, J., Liu, X.M., Liu, T.S., Bronger, A., Suter, M., Bonani, G., 1993, Quantitative estimates and paleoclimatic implications of pedogenic ferromagnetic mineral formation in Chinese loess. Earth and Planetary Science Letters, v. 114, p. 385-390.

Holbrook, J., 1996, Complex fluvial response to low gradients at maximum regression: a genetic link between smooth sequence-boundary morphology and architecture of overlying sheet sandstone. Journal of Sedimentary Research, v. 66, p. 713-722.

Holbrook, J.M. and Dunbar, R.W., 1992, Depositional history of Lower Cretaceous strata in northeastern New Mexico; implications for regional tectonics and depositional sequences. Geological Society of America Bulletin, v. 104, p. 802-813.

Hori, K., Saito, Y., Zhao, Q., Cheng, X., Wang, P., Sato, Y., Li, C., 2001, Sedimentary facies and Holocene progradation rates of the Chanjiang (Yangtze) delta, China. Geomorphology, v. 41, p. 233-248.

Hori, K., Saito, Y., Zhao, Q., Wang, P., 2002, Evolution of the coastal depositional systems of the Changjiang (Yangtze) River in response to Late Pleistocene-Holocene sea-level changes. Journal of Sedimentary Research, v. 72, p. 884-897.

Hung, G.W. and Chung, Y.C., 1994, Sedimentation rates on the continental slope off eastern Taiwan: Marine Geology, v. 119, p. 99-109.

Hunt, D. and Tucker, M.E., 1995, Stranded parasequences and the forced regressive wedge systems tract: deposition during baselevel fall – reply. Sedimentary Geology, v. 96, p. 147-160.

Imbrie, J., Hays, J.D., Martinson, D.G., McIntyre, A., Mix, A.C., Morley, J.J., Pisias, N.G., Prell, W.L. and Shackleton, N.J., 1984, The orbital theory of Pleistocene climate: support from a revised chronology of the marine $\partial^{18}O$ record. In, Berger A.L., Imbrie, J., Hays, J., Kukla, G., and Saltzman, B. (eds.), Milankovitch and Climate: Understanding the Response to Astronomical Forcing, Part I. NATO ASI Series, series C, mathematical and physical sciences, v. 126, D. Reidel Publishing Company, Dordrecht, Holland, p. 269-305.

Jones, S.J., Frostick, L.E., Astin, T.R., 2001, Braided stream flood plain architecture: the Rio Verde Formation, Spanish Pyrenees. Sedimentary Geology, v. 139, p. 229-260.

Kim, S.W., 1973, A study on the terraces along the southeastern coast (Bang-eojin-Pohang) of the Korean Peninsula. The Journal of Geological Society of Korea, v. 9, no. 2, p. 89-121.

Kim, J.-M. and Kucera, M., 2000, Benthic foraminifer record of environmental changes in the Yellow Sea (Hwanghae) during the last 15,000 years. Quaternary Science Reviews, v. 19, p. 1067-1085.

Kong, F., 1998, Continental margin deformation analysis and reconstruction – evolution of the East China Sea Basin and adjacent plate interaction: PhD dissertation, University of Texas at Austin, 263 p.

Koss, J.E., Ethridge, F.G., and Schumm, S.A., 1994, An experimental study of the effects of baselevel change on fluvial, coastal plain and shelf systems. Journal of Sedimentary Research, v. B64, p. 90-98.

Leckie, D.A., 1994, Canterbury Plains, New Zealand – implications for sequence stratigraphic models. American Association of Petroleum Geologists Bulletin, v. 78, p. 1240-1256.

Lee, H.J. and Chough, S.K., 1989, Sediment distribution, dispersal and budget in the Yellow Sea. Marine Geology, v. 87, p. 195-205.

Li, C.-X., Zhang, J.Q., Fan, D.D., Deng, B., 2001, Holocene regression and the tidal radial sand ridge system formation in the Jiangsu coastal zone, east China. Marine Geology, v. 173, p. 97-120.

Liu, X., Rolph, T., Bloemendal, J., Shaw, J., Liu, T., 1995, Quantitative estimates of paleoprecipitation at Xifeng, in the Loess plateau of China. Palaeogeography, Palaeoclimatology, Palaeoecology, v. 113, p. 243-248.

Liu, Z.X., Berne, S., Saito, Y., Lericolais, G., Marsset, T., 2000, Quaternary seismic stratigraphy and paleoenvironments on the continental shelf of the East China Sea: Journal of Asian Earth Sciences, v. 18, p. 441-452.

Maher, B.A., Thompson, R., 1995, Paleorainfall reconstructions from pedogenic magnetic susceptibility variations in the Chinese loess and paleosols. Quaternary Research, v. 44, p. 383-391.

McLauren, B.T. and Steel, R.J., 2000, Fourth-order nonmarine to marine sequences, middle Castlegate Formation, Book Cliffs, Utah. Geology, v. 28, p. 359-362.

Miall, A.D., 1996, The Geology of Fluvial Deposits: Sedimentary Facies Analysis, Basin Analysis, and Petroleum Geology. Springer-Verlag, Berlin, 582 p.

Miall, A.D. and Arush, M., 2001, The Castlegate Sandstone of the Book Cliffs, Utah: sequence stratigraphy, paleogeography, and tectonic controls. Journal of Sedimentary Research, v. 71, p. 537-548.

Milliman, J.D. and Meade, R.H., 1983, World-wide delivery of river sediments to the oceans: Journal of Geology, V. 91, no. 1, p. 1-21.

Milliman, J.D. and Syvitski, J.P.M., 1992, Geomoprhic/tectonic control of sediment discharge to the ocean: The importance of small mountainous rivers: Journal of Geology, v. 100, p. 525-544.

Milliman, J.D., Beardsley, R.C., Yang, Z.-S., Limeburner, R., 1985, Modern Huanghe-derived muds on the outer shelf of the East China Sea: identification and potential transport mechanisms. Continental Shelf Research, v. 4, p. 175-188.

Mitchum, R.M., Vail, P.R., Sangree, J.B., 1977, Seismic stratigraphy and global changes of sea level, part 6: stratigraphic interpretation of seismic reflection patterns in depositional sequences. In Payton, C.E. (ed.), Seismic Stratigraphy – applications to hydrocarbon exploration, AAPG Memoir 26, American Association of Petroleum Geologists, Tulsa, p. 117-133.

Moss, C.C., 2002, Three-dimensional relationship and distribution of Holocene and Late Pleistocene seismic facies beneath the Yellow Sea. Unpublished Doctoral Dissertation, University of North Carolina at Chapel Hill, 205 p.

O'Grady, D.B., Syvitski, J.P.M., Pratson, L.F., Sarg, J.F., 2000, Categorizing the morphologic variability of siliciclastic passive margins. Geology, v. 28, p. 207-210.

Park, Y.A., 1987, Continental shelf sedimentation (chapter 25). In, Lee, D. (ed.), Geology of Korea, Kyohak-sa Publishing Company, Geological Society of Korea, Seoul, p. 406-426.

Park, S.-C., Han, H.-S., Yoo, D.-G., 2003, Transgressive sand ridges on the mid-shelf of the souther sea of Korea (Korea Strait): formation and development in high-energy environments. Marine Geology, v. 193, p. 1-18.

Pillans, B., Chappell, J., Naish, T.R., 1998, A review of the Milankovitch climatic beat: template for Plio-Pleistocene sea-level changes and sequence stratigraphy. Sedimentary Geology, v. 122, p. 5-21.

Plint, A.G., and Nummedal, D., 2000, The falling stage systems tract: Recognition and importance in sequence stratigraphy. In: Hunt, D., Gawthorpe, R.L. (eds.), Sedimentary Responses to Forced regressions. Geolgoical Society, London, p. 1-17.

Posamentier, H.W., 2001, Lowstand alluvial bypass systems: Incised vs. unincised. American Association of Petroleum Geologists Bulletin, v. 85, p. 1771-1793.

Posamentier, H.W. and Vail, P.R., 1988, Eustatic controls on clastic deposition II – sequence and systems tracts models. In Wilgus, C.K., Hastings, B.S., Kendall, C.G.St.C., Posamentier, H.W., Ross, C.A., Van Wagoner, J.C. (eds.), Sea-Level Changes: An Integrated Approach. SEPM Special Publication 42, Society of Exonomic Paleontologists and Mineralogists, Tulsa, p. 125-154.

Posamentier, H.W. and Allen, G.P., 1999, Siliciclastic Sequence Stratigraphy – Concepts and Applications. SEPM Concepts in Sedimentology and Paleontology #7, Tulsa, 210 p.

Posamentier, H.W., Jervey, M.T., Vail, P.R., 1988, Eustatic controls on clastic deposition I – conceptual framework. In Wilgus, C.K., Hastings, B.S., Kendall, C.G.St.C., Posamentier, H.W., Ross, C.A., Van Wagoner, J.C. (eds.), Sea-Level Changes: An Integrated Approach. SEPM Special Publication 42, Society of Exonomic Paleontologists and Mineralogists, Tulsa, p. 109-124.

Posamentier, H.W., Allen, G.P., James, D.P., Tessno, M., 1992, Forced regressions in a s equence stratigraphic framewrok: concepts, examples and exploration significance. AAPG Bulletin, v. 76, p. 1687-1709.

Pritchard, D.W., 1967, Observations of circulation in coastal plain estuaries. In: Lauff, G.H. (ed.), Estuaries, American Association for the Advancement of Science, Publication 83, Washington, D.C., p. 3-5.

Quanxing, L. (ed.), 1990, Marine Atlas of Bohai Sea, Yellow Sea, East China Sea: Geology and Geophysics. China Ocean Press, Beijing, 99 p.

Qian, N. and Dai, D.-Z., 1980, Problems of river sedimentation and the present status of its research in China: Chinese Society Hydraulic Engineers, Proceedings of the International Symposium on River Sedimentation, v. 1, p. 1-39.

Saito, Y., Katayama, H., Ikehara, K., Kato, Y., Matsumoto, E., Oguri, K., Oda, M., Yumoto, M., 1998, Transgressive and highstand systems tracts and post-glacial transgression, the East China Sea: Sedimentary Geology, v. 122, p. 217-232.

Saito, Y., Yang, Z., Hori, K., 2001, The Hunaghe (Yellow River) and Changjiang (Yangtze River) deltas: a review on their characteristics, evolution and sediment duscharge during the Holocene. Geomorphology, v. 41, p. 219-231.

Sandwell, D.T. and Smith, W.H.F., 1997, Global sea floor topography from satellite altimetry and ship depth soundings. Science, v. 277, p. 1956-1962.

Schumm, S.A., 1981, Evolution and response of the fluvial system, sedimentological implications. In Ethridge, F.G., Flores, R.M. (eds.), Recent and Ancient Nonmarine Depositional Environments: Models for Exploration. SEPM Special Publication 31, Society for Economic Palentologists and Mineralogists, Tulsa, Oklahoma, p. 19-29.

Schumm, S.A., 1985, Patterns of alluvial rivers. Annual Review of Earth and Planetary Science, v. 13, p. 5-27.

Schumm, S.A., 1999, Causes and controls of incision. In, Darby, S.E. and Andrew, S. (eds.), Incised River Channels: Processes, Forms, Engineering and Management, John Wiley & Sons, Chichester, United Kingdom, p. 19-33.

Schumm, S.A., Harvey, M.D., Watson, C.C., 1984, Incised channel morphology, dynamics and control. Water Resource Publications, Littleton, Colorado, 200 p.

Shackleton, N.J., 1987, Oxygen isotopes, ice volume and sea level. Quaternary Science reviews, v. 6, p. 183-190.

Stanley, D.J. and Chen, Z., 1993, Yangtze delta, eastern China: 1. Geometry and subsidence of Holocene depocenter. Marine Geology, v. 112, p. 1-11.

Stonecipher, S.A., 1996, Diagenetic signatures of incised valley fills: differentiation of sequence boundaries from diastems and implications for potential reservoir quality. Annual Meeting Abstracts, American Association of Petroleum Geologists and Society of Economic Paleontologists, v. 5, p. 134-135.

Talling, P.J., 1998, How and where do incised valleys form if sea level remains above the shelf edge? Geology, v. 26, p. 87-90.

Tamburini, F., Adatte, T., Föllmi, Bernasconi, S.M., Steinmann, P., 2003, Investigating the history of East Asian monsoon and climate during the last glacial-interglacial period (0-140,000 years): mineralogy and geochemistry of ODP Sites 1143 and 1144, South China Sea. Marine Geology, v. 201, p. 147-168.

Tang, B.G., 1996, Quaternary stratigraphy in the shelf of the East China Sea in Yang, Z.G. and Lin, H.M. (eds.), Quaternary Stratigraphy in China and its International Correlation: Geology Press, Beijing, China, p. 56-75 (in Chinese).

Thierstein, H.R., Geitzenauer, K.R., Molfino, B., Shackleton, N.J., 1977, Global synchroneity of late Quaternary coccolith datum levels: Validation by oxygen isotopes: Geology, v. 5, p. 400-404.

Thorne, J., 1994, Constraints on riverine valley incision and the response to sea-level change based on fluid mechanics. In: Dalrymple, R.W., Boyd, R., Zaitlin, B.A. (eds.), Incised-Valley Systems: Origin and Sedimentary Sequences, SEPM Special Publication no. 51, Society for Sedimentary Geology, Tulsa, p. 29-43.

Vail, P.R., 1987, Seismic stratigraphic interpretation procedure. In: Bally, A.W., (ed.), Atlas of Seismic Stratigraphy: AAPG Studies in Geology no. 27, p. 1-10.

Vail, P.R., Mitchum, R.M., Jr., Thompson, S., III, 1977, Seismic stratigraphy and global changes of sea level, part 4: global cycles of relative changes of sea level. In Payton, C.E. (ed.) 1977, Seismic Stratigraphy – applications to hydrocarbon exploration, AAPG Memoir 26, American Association of Petroleum Geologists, Tulsa, p. 83-97.

Van Wagoner, J.C., 1995, Sequence stratigraphy and marine to nonmarine facies architecture of foreland basin strata, Book Cliffs, Utah, U.S.A. In Van Wagoner, J.C. and Bertram, G.T. (eds.), Sequence Stratigraphy of Foreland Basin Deposits: Outcrop and Subsurface Examples from the Cretaceous of North America. AAPG Memoir 64, American Association of Petroleum Geologists, Tulsa, p. 137-223.

Van Wagoner, J.C., Posamentier, H.W., Mitchum, R.M., Vail, P.R., Sarg, J.F., Loutit, T.S., and Hardenbol, J., 1988, An overview of the fundamentals of sequence stratigraphy and key definitions. In: Wilgus, C.K., Hastings, B.S., Kendall, C.G.S.C., Posamentier, H.W., Ross, C.A., Van Wagoner, J.C. (eds.), Sea-Level Changes: An Integrated Approach, SEPM Special Publication no. 42, Tulsa, p. 39-46.

Van Wagoner, J.C., Mitchum, R.M., Campion, K.M., Rahmanian, V.D. (eds.), 1990, Siliciclastic Sequence Stratigraphy in Well Logs, Cores, and Outcrops: Concepts for High-Resolution Correlation of Time and Facies. AAPG Methods in Exploration Series #7, American Association of Petroleum Geologists, Tulsa, 55 p.

Wageman, J.M., Hilde, T.W.C., Emery, K.O., 1970, Structural framework of the East China Sea and Yellow Sea: AAPG Bulletin, v. 54, no. 9, p. 1611-1643.

Wagner, G.A., 1998, Age Determination of Young Rocks and Artifacts: Physical and Cemical Clocks in Quaternary Geology and Archaeology. Springer-Verlag, Berlin, 466 p.

Wang, P., 1999, Response of Western Pacific marginal seas to glacial cycles: paleoceanographic and sedimentological features. Marine Geology, v. 156, p. 5-39.

Wang, J. and Wang, P., 1982, Relationship between sea-level changes and climatic fluctuations in East China since last Pleistocene. The Quaternary Research, v. 21, p. 101-114 (in Japanese).

Wang, Y. and Aubrey, D.G., 1987, The characteristics of the China coastline: Continental Shelf Research, v. 7, no. 4, p. 329-349.

Wang, P., Wang, L., Bian, Y., Jian, Z., 1995, Late Quaternary paleoceanography of the South China Sea: surface circulation and carbonate cycles. Marine Geology, v. 127, p. 145-165.

Warren, J.D. and Bartek, L.R., 2002a, The Metastable Fluvial Shelf System (MFSS): An alternative hypothesis to lowstand unincised fluvial bypass on the East China Sea continental margin. SEPM Research Conference: Incised Valleys: Images and Processes, August 18-23, 2002, Casper and Newcastle, WY.

Warren, J.D. and Bartek, L.R., 2002b, The Sequence Stratigraphy of the East China Sea: Where are the incised valleys? GCSSEPM Foundation Bob F. Perkins Research Conference: Sequence Stratigraphic Models for Exploration and Production: Evolving Methodology, Emerging Models and Applications History, December 8-11, Houston, TX, p. 729-738.

Warren, J.D., Bartek, L.R., and Miller, K.L., 2002, Stratigraphic architecture of the East China Sea continental margin: a case study of eustacy and sediment supply: AAPG Annual Meeting Program, March 10-14, Houston, TX, p. A185.

Wellman, H.W., 1979, An uplift map for the South Island of New Zealand, and a model for uplift of the Southern Alps. In Walcott, R.I. and Cresswell, M.M. (eds.), The origin of the Southern Alps, Royal Society of New Zealand Bulletin, v. 18, p. 13-20.

Wellner, R.W. and Bartek, L.R., 2003, The effect of sea level, climate, and shelf physiography on the development of incised valley complexes: a modern example from the East China Sea. Journal of Sedimentary Research, v. 73, p. 926-940.

Wong, G.T.F., Chao, S.-Y., Li, Y.-H., Shiah, F.-K., 2000, The Kuroshio edge exchange processes (KEEP) study – an introduction to hypotheses and highlights. Continental Shelf Research, v. 20, p. 335-347.

Wood, L.J., Ethridge, F.G., Schumm, S.A., 1993, An experimental study of the influence of subaqueous shelf angles on coastal plain and shelf deposits. In Weimer, P. and Posamentier, H. (eds.), Siliciclastic Sequence Stratigraphy: Recent Developments and Applications, AAPG Memoir 58. American Association of Petroleum Geologists, Tulsa, Oklahoma, p. 381-391.

Woolfe, K.J., Larcombe, P., Naish, T., Purdon, R.G., 1998, Lostand rivers need not incise the shelf: An example from the Great Barrier Reef, Australia, with implications for sequence stratigraphic models. Geology, v. 26, p. 75-78.

Xiao, J.L., An, Z.S., Liu, T.S., Inouchi, Y., Kumai, H., Yoshikawa, S., Kondo, Y., 1999, East Asian monsoon variation during the last 130,000 years: evidence from the Loess Plateau of central China Lake Biwa of Japan. Quaternary Science Reviews, v. 18, p. 147-157.

Xiaodong, L., Zhisheng, A., Xihao, W., Valdes, P.J., Dong, B., 1997, East Asian paleoclimates of the Last Glacial Maximum in an atmospheric general circulation model from geological records. In Zhisheng, A. and Weijian, Z. (eds.), Proceedings of the 30th International Geological Congress, volume 21, Quaternary Geology, Beijing, China, August 4-14, 1996, VSP, Utrecht, p. 156-171.

Xiaomin, F., Jijun, L., Van der Voo, R., Conall, M.N., Xuerong, D., Kemp, R.A., Derbyshire, E., Jixiu, C., Jianming, W., Guo, W., 1997, A record of the Blake Event during the last interglacial paleosol in the western Loess Plateau of China. Earth and Planetary Science Letters, v. 146, p. 73-82.

Yanagi, T., Takahashi, S., Hoshika, A., and Tanimoto, T., 1996, Seasonal variation in the transport of suspended matter in the East China Sea: Journal of Oceanography, v. 52, p. 539-552.

Yang, C.S., 1989, Active, moribund and buried tidal sand ridges in the East China Sea and the southern Yellow Sea: Marine Geology, v. 88, p. 97-116.

Yang, C.S. and Sun, J.S., 1988, Tidal sand ridges on the East China Sea shelf. In: de Boer, P.L., van Gelder, A., Nio, S.D. (eds.), Tide-influenced Sedimentary Environments and Facies. Sedimentology and Petroleum Geology, Reidel, Dordrecht, p. 23-38.

Ye, L. and Kerr, D., 2000, Sequence stratigraphy of the Middle Pennsylvanian Bartlesville Sandstone, northeastern Oklahoma: a case study of an underfilled incised valley. American Association of Petroleum Geologists Bulletin, v. 84, p. 1185-1204.

Yoo, D.G., Lee, C.W., Kim, S.P., Jin, J.H., Kim, J.K., Han, H.C., 2002, Late Quaternary transgressive and highstand systems tract in the northern East China Sea mid-shelf. Marine Geology, v. 187, p. 313-328.

Yoshida, S., 2000, Sequence and facies architecture of the upper Blackhawk Formation and the Lower Castlegate Sandstone (Upper Cretaceous), Book Cliffs, Utah. Sedimentary Geology, v. 136, p. 239-276.

Yoshida, S., Willis, A., Miall, A.D., 1996, Tectonic control of nested sequence architecture in the Castlegate Sandstone (Upper Cretaceous), Book Cliffs, Utah. Journal of Sedimentary research, v. 66, p. 737-748.

Zhang, G. and Li, C., 1996, The fills and stratigraphic sequences in the Qiantangjiang incised paleovalley, China. Journal of Sedimentary Research, v. 66, p. 406-414.

Zhu, Y. and Chen, Q., 2005, On the origin of the radial sand ridges in the southern Yellow Sea: Results from the modeling of the paleoradial tidal current fields off the paleo-Yangtze River estuary and northern Jiangsu Coast. Journal of Coastal Research, v. 21, p. 1245-1256.

CHAPTER 3

STRATIGRAPHIC MODELING OF LOW-GRADIENT MARGINS USING FUZZY LOGIC: A CASE STUDY FROM THE EAST CHINA SEA CONTINENTAL MARGIN (LATE PLEISTOCENE TO PRESENT)

3.0 INTRODUCTION

Studies of the stratigraphic response of low-gradient margins with deep shelf-slope breaks are rare. These margins still exhibit the shelf-slope-rise morphology typical of most passive continental margins (Heezen et al., 1959), however, major incision does not occur at the margin's edge during sea level lowstands. This geologic response is contrary to the traditional sequence stratigraphic model, which predicts incision and sedimentary bypass across a continental margin during sea level lowstand. Numerous quantitative models have simulated this stratigraphic response and been validated with examples that span the geologic record (a thorough review of many of these models is presented in Kendall et al., 1991a; Kendall et al., 1991b; Bowman and Vail, 1999; Watney et al., 1999). The typical gradient of a passive continental margin is <0.5° (Van Wagoner et al., 1990) but generally >0.05° (Posmanetier and Allen, 1999). Low-gradient margins (<0.02°) margins, on the other hand, have received minimal attention by the modeling community. The response of an unconfined fluvial system across a low gradient (especially one that is lower than the fluvial gradient) is deposition and avulsion throughout the basin with little sedimentary bypass beyond the shelf-slope break. Margins with these characteristics do not conform to the sequence stratigraphic model. Recent examples from the Quaternary, all of which are attributed to low-gradient

margins, are limited to the passive margins of Australia (Woolfe et al., 1998), Java (Posamentier, 2001), New Zealand (Browne and Naish, 2003) and the East China Sea (Bartek et al., 2001, Bartek and Warren, 2002; Warren and Bartek, 2002a; 2002b; Warren et al., 2002a). Ancient examples of foreland basin deposits have a similar fluvial architecture that is analogous to low-gradient continental margins. Examples include the Cenozoic Ebro basin (Spanish Pyrenees; e.g., Bentham et al., 1993; Jones et al., 2001), the Mesozoic U.S. western interior (e.g., Holbrook and Dunbar, 1992; Van Wagoner, 1995; Holbrook, 1996; Yoshida, 2000; Miall and Arush, 2001), and the Paleozoic Bowen basin (Queensland, Australia; e.g., Fielding et al., 1993). Quantitative models have been developed to better understand the depositional processes within foreland basins (e.g., Flemings and Jordan, 1989; Garcia-Castellanos et al., 2002; du Fornel et al., 2003; Zhou et al., 2003). Furthermore, the fluvial response to a low-gradient has been discussed theoretically (Posamentier and Allen, 1999) and the fluvial response (laterally extensive, unincised, braided sand sheets) has been verified empirically using flume experiments (e.g., Wood et al., 1993; Koss et al., 1994). However, computational simulations of the stratigraphic evolution of low-gradient continental margins remain undeveloped.

In order to better understand the depositional processes and stratigraphic response of low-gradient systems, a broader investigation of the East China Sea (ECS) continental margin acquired a high-resolution seismic dataset (14,000 km over a 300,000 km^2 area) on the ECS continental margin to investigate the stratal architecture on a low-gradient margin with a deep shelf-slope break. These data, combined with other related studies, provide an understanding of the geologic conditions that affected relative sea level, eustasy, tectonic subsidence, sediment influx, and margin physiography during the late Quaternary. The

extensive nature of the ECS data, and the general knowledge gained from it, provide the opportunity to develop a method for quantitative simulation of stratigraphic development in a low-gradient system. Constraining simulations with these data not only aid in model validation, but also provide the opportunity to explore different scenarios of stratigraphic sensitivity under numerous scenarios of sea level, tectonic subsidence, sediment influx, and margin physiography.

The model developed for these stratigraphic simulations is based on fuzzy logic for three reasons. First, the lack of detailed investigations of low-gradient continental margins creates a knowledge gap for common variables needed for the complicated differential equations used in traditional depositional models. For example, the delta progradation and basin filling model DELTA2 of Syvitski and Daughney (1992) requires input of values of seasonal concentrations of suspended sediment, removal-rate constants, bulk densities of sediments, seasonal velocity of river at river mouth, seasonal dimension of the river mouth (width and depth), and maximum depth of river plume. Li and Amos (2001) considered over 100 variables for the sediment transport model SEDTRANS96. SedFlux (Syvitski et al., 1999) was designed to simulate and predict the geomorphic evolution of a continental margin. It used a suite of nine separate models to address sediment discharge, deltaic plain sedimentation and erosion, bedload dumping on a tidal flat, fallout from river mouth plumes, storm re-suspension and transport, sediment stability and failure, erosion and deposition by turbidity currents, sedimentation from debris flows, flexural subsidence, tectonic motion ad faulting, sediment compaction, and sea level fluctuations. On the other hand, a fuzzy logic inference system can be assembled with general concepts and expert knowledge about a geologic system without relying on hundreds of variables, non-linear relationships, and

complicated differential equations. It is not suggested that fuzzy logic modeling can, or should, replace traditional techniques. However, fuzzy applications can certainly complement existing analytical tools. For example, fuzzy logic has the ability to handle complicated, nonlinear variables that cannot be, or have not yet been, defined mathematically. Fuzzy logic may also narrow potential values needed for traditional model input to a field of few. Mathematical models may still be used, but the computational efficiency and ease of fuzzy logic modification has the potential to significantly speed up the process of variable selection by discarding values that are inaccurate or not important. Finally, because fuzzy logic applications require no special knowledge apart from basic mathematical logic, it can be understood and widely applied by the geologic community *en toto* rather than being limited to modeling specialists. For the time being, though, the use of fuzzy logic within the geological sciences is not widespread, although fuzzy techniques have proven successful in the simulation of stratigraphic development (Nordlund and Slivfersparre, 1994; Nordlund, 1996; 1999a; 1999b; Parcell, 2000; Demicco and Klir, 2001; Parcell, 2003a; 2003b; Demicco, 2004). The fuzzy logic simulation described in this paper builds on these concepts, but uses the ECS dataset described in this paper to constrain the "expert knowledge" required to develop the model and validate its output. The chronologically constrained seismic data are able to provide spatial and temporal constraints unavailable to previous fuzzy stratigraphic models. Prior to this investigation, the largest area of a fuzzy logic stratigraphic simulation was 45,000 km^2 (150 x 300) and spanning only 10 ky (Demicco and Klir, 2004). The longest duration of a stratigraphic model using fuzzy logic was 1 My; however, time steps were coarsely spaced at 100 ky intervals and the simulation only covered an area of 25 km^2 (5 x 5 km) (Parcell 2000; 2003a; 2003b). The

ECS dataset covers an area of 300,000 km^2 to constrain a 600 x 600 km margin simulation. Simulations presented herein span almost 200 ky with 500-year time steps.

Watney et al. (1999) defined an effective geologic model as one that expands on descriptions by logical or mathematical relations to synthesize and/or predict a geologic system. The goal of this investigation is to determine whether a set of general, non-mathematical rules could be developed to simulate the generic stratigraphic response of a continental margin (with any gradient) to changes in eustasy, tectonics, sediment influx and margin physiography. The fuzzy sets and linguistic rules of fuzzy logic provide the framework to test this approach. The fuzzy simulation is able to run numerous permutations of sea level, tectonic subsidence, and sediment influx (although users can also change margin geometry as well as simulate the response to various margin physiographies by merely changing sea level magnitude and periodicity).

The simulation of conditions on the low-gradient ECS margin during the last 195 ky are constrained by those established through a combination of previous studies (e.g., Saito et al., 1998; Liu et al., 2000; Saito et al., 2001; Hori et al., 2001; 2002a; 2002b; 2002c; Berne et al., 2002) and the seismic dataset presented in this paper. A better understanding of the interaction between depositional processes and associated stratigraphic response on the ECS margin will assist continued model development and lead to more accurate simulations. Such a suite of quantitative tools, fuzzy or otherwise, has implications for understanding the origin of strata preserved on other low-gradient margins and basins with similar depositional conditions throughout the geologic record. Foreland basins are analogous to the ECS and other low-gradient margins by exhibiting low-gradient ramp morphology, ample sediment influx, and unconfined fluvial deposits with minimal incision. A thorough understanding of

the depositional conditions under which these rocks were formed will allow a more complete interpretation of basin history. This is particularly challenging when many ancient basins lack extensive outcrop, have limited core and well data, and/or are constrained by low-resolution dating techniques (e.g., K-Ar and biostratigraphy) and low-resolution seismic techniques.

3.1 FUZZY LOGIC

3.1.1 Fuzzy Logic and Fuzzy Sets

Fuzzy logic is a system of concepts, principles and methods for dealing with modes of reasoning that are approximate rather than exact (Novak and Perfilieva, 2000). Fuzzy logic is based on the theory of fuzzy sets (Zadeh, 1965; Zadeh, 1975) and utilizes fuzzy sets to formulate various forms of logical, approximate reasoning in natural language (Klir, 2004). A fuzzy set has imprecise boundaries that allow objects to have fractional membership in one or more sets. This multi-valued logic approach is different than the classical logic of Aristotle and Boole (e.g., Boole, 1951; Lukasiewicz, 1957) where sets are defined by distinct, crisp boundaries – an object is either a member of a specific set or it is not a member (e.g., black or white, yes or no, on or off, hot or cold). Therefore, membership in a traditional crisp set is either one (full membership) or zero (no membership) and no fractional values are allowed. Fuzzy sets, on the other hand, not only have the ability to assign a Membership Function (MF) of zero or one, but also any value between zero and one. Zadeh (1965) recognized that classes of objects in the real world often lack precisely defined criteria and suggested that fuzzy sets could exploit the imprecision related to the absence of these sharply defined boundaries.

A fuzzy set is represented by a function. This line, the MF, is plotted on a standard Cartesian axis. The domain value (x axis) is specific to the elements of the set being classified. A fuzzy set classifying stratal thickness will have a domain variable of appropriate units (such as meters or feet) spanning the appropriate values needed to classify set members. The degree of membership (y axis) falls between zero and one (zero = no membership and one = full membership). Therefore, at any given point along the domain, an

appropriate value of membership to a particular fuzzy set (or sets) is established. For example, Figure 3.1 presents the a crisp set and fuzzy sets defining grain size. In these sets, grain size diameter (Φ) is the domain variable. Sediments with a grain size diameter of 2 Φ have full membership (MF=1) in the fuzzy set "sand." Sediments with a grain size diameter of –1 Φ have partial membership in two fuzzy sets – sand (MF=0.5) and "gravel" (MF=0.5). Partial membership in multiple fuzzy sets is also applied to sediments with a grain size diameter of 3.5 Φ (i.e., MF in "sand" = 0.75 and MF in "silt" = 0.25). Using the same values along the x-axis (i.e., the domain variables), additional fuzzy sets could be added between "sand" and "silt" to classify terms such as "silty sand", "very sandy", or "extremely clay rich." These are qualitative, subjective descriptors (i.e., "soft" data), but data nonetheless, and they are easily adapted into fuzzy sets. Using this approach, the uncertainty of vague, linguistic descriptions is captured and quantified.

When designing a MF, multiple widths and shapes should be considered as potential candidates to capture the intended meaning of a variable in the context of a particular process, system or application. The MF defines the boundary of each fuzzy set and initially can be created using specific data or general knowledge (or a combination of both) and then "tuned" through testing the sensitivity of the fuzzy system through multiple iterations. MFs are easily modified and subtle changes in function shape or function boundaries (along the domain, or x, axis) may or may not affect the accuracy of describing complicated relationships (see examples in Figure 3.1B-D). The shape of MFs is discussed in more detail later in this paper (see *Fuzzy Variables, Fuzzy Sets, Fuzzy Inference Systems*).

Linking fuzzy sets together with standard logic operators (AND, OR, NOT) to form a premise and a conclusion is the basis of fuzzy logic (Zadeh, 1985). Assembling such a series

Figure 3.1. Sediment grain size classification sets. A) Traditional classification scheme (crisp logic) of Wentworth (1922). Fuzzy classifications of B) Nordlund (1996; 1996), C) Saggaf and Nebrija (2003), and D) Demicco and Klir (2001) and Demicco (2004a).

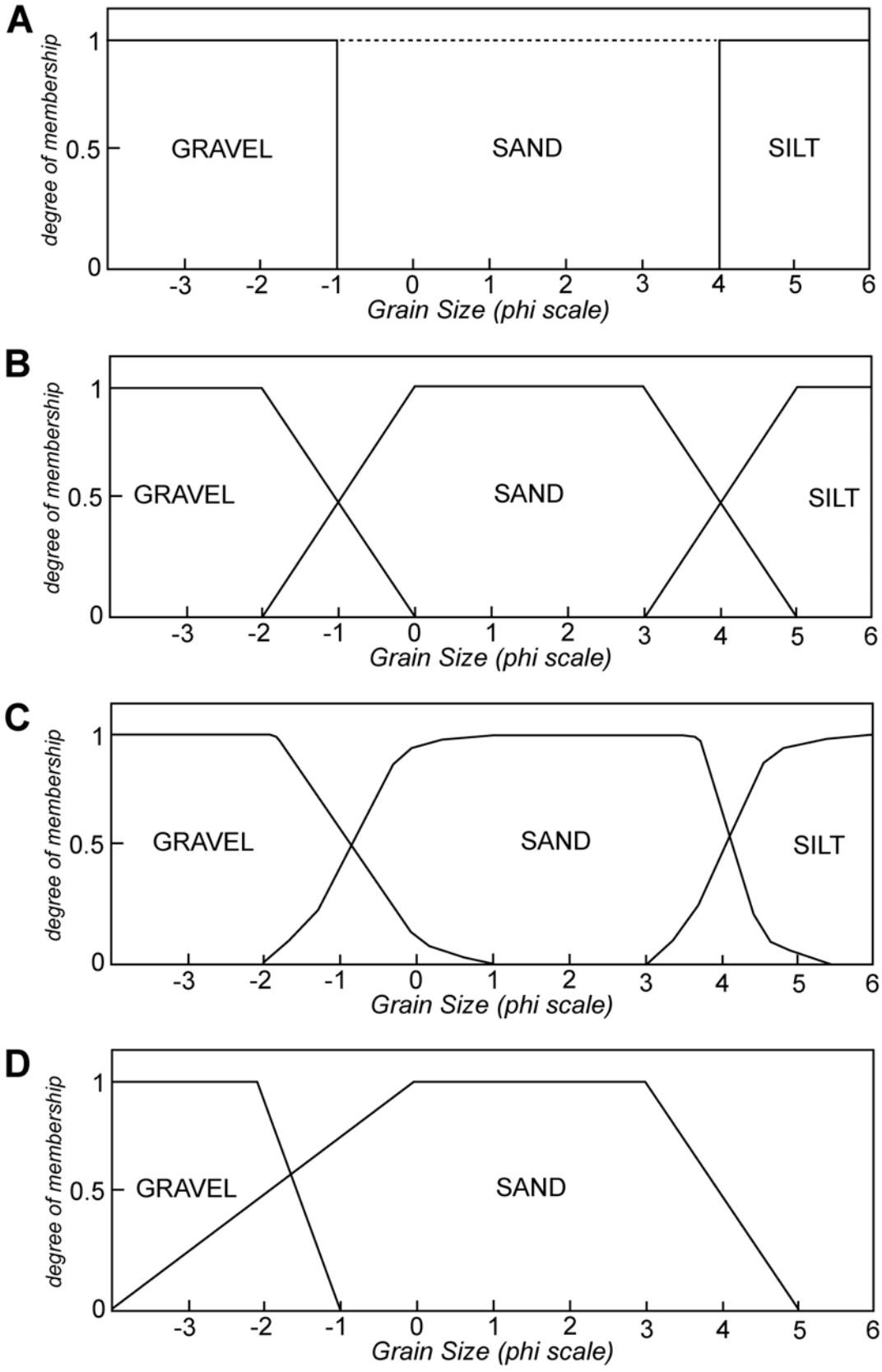
A
degree of membership
1
0.5
0
GRAVEL
SAND
SILT
-3 -2 -1 0 1 2 3 4 5 6
Grain Size (phi scale)
B
degree of membership
1
0.5
0
GRAVEL
SAND
SILT
-3 -2 -1 0 1 2 3 4 5 6
Grain Size (phi scale)
C
degree of membership
1
0.5
0
GRAVEL
SAND
SILT
-3 -2 -1 0 1 2 3 4 5 6
Grain Size (phi scale)
D
degree of membership
1
0.5
0
GRAVEL
SAND
-3 -2 -1 0 1 2 3 4 5 6
Grain Size (phi scale)

of linguistic-based rules to define a natural system provides a logical method for computing with words rather than numbers (e.g., Zadeh, 1995; Wang, 2001). Several rules used together describe a system or solve a specific problem and can be considered a fuzzy system. Each rule represents a fragment of knowledge about the problem in question or the system being described (Nordlund, 1999a). The rules defining the system, the fuzzy sets supporting the rules and the membership functions defining each set are based on general knowledge about the system (i.e., an "expert system"; Fang, 1987), data, or a combination of both. In a process similar to human reasoning and decision-making, each rule in a fuzzy system is evaluated separately and each modifies the respective conclusion based on the degree of truth (degree of membership or MF) derived from the premise (rule) (Nordlund, 1999a).

Despite its power, fuzzy logic is simple. No special knowledge apart from basic mathematical logic is required for its application (Nordlund, 1999b). Fuzzy logic provides the ability to quantify subjectivity by capturing the vagueness of linguistic terms, thus making it flexible and tolerant of imprecise data (Demicco and Klir, 2004b). General concepts and expert knowledge can assemble, in a relatively short amount of time, a robust fuzzy logic inference system that can describe complicated, nonlinear relationships. Fuzzy sets retain the ability to represent crisp data using a MF equal to either one or zero, but crisp sets do not have the ability to represent partial membership between zero and one. In this way, crisp data and traditional logic is a subset of fuzzy logic. Therefore, fuzzy data have the potential to possess greater capabilities than their classical counterparts.

3.1.2 Geological Examples of Fuzzy Variables

Fuzzy logic is well suited for a broad array of geological concepts and data. The inherent complexity of geological systems and the knowledge of their processes are many

times too incomplete for quantitative modeling with mathematical equations (Fang, 1987). Fuzzy logic is able to exploit the highly descriptive nature of geological phenomena and the subjective nature of the majority of geological data (Nordlund, 1996; Nordlund, 1999). Many geological phenomena are described or classified using rigid boundaries that do not correspond to the conceptual notion of gradational transitions along a continuum. In the examples presented below, this type of "pigeon holing" (*sensu* Demicco and Klir, 2001) is eliminated with fuzzy sets.

Sediment Classification. Sediment grain size classification is a common geologic example commonly used to illustrate the difference between crisp and fuzzy sets (e.g., Nordlund, 1996; Nordlund, 1999; Demicco and Klir, 2001; Saggaf and Nebrija, 2003; Demicco, 2004a). Using the traditional Udden-Wentworth classification scheme (Wentworth, 1922), a grain diameter of 1.999 mm is classified as coarse sand and a grain diameter of 2.001 is classified as gravel. Nordlund (1996) pointed out that such a rigid classification does not correspond to the conceptual notion of a continuum between arbitrarily defined grain-sized classes (Figure 3.1A). A fuzzy set reflects the similarity in grain diameters of 1.999 and 2.001 mm by assigning similar if not identical degrees of membership in both sand and gravel (i.e., both diameters express the same degree of "sand-ness" and "gravel-ness"). Subtle differences of the interpretation of grain size classification are observable in Figure 3.1B-C. Even so, these variations do not detract from the overall ability of fuzzy sets to provide greater accuracy than traditional logic. Categorizing similar grain size concepts that also deal with sediment texture (e.g., sorting, roundness, shape) is arguably achieved with greater accuracy using fractional membership along a continuum.

Fluvial Classification. Fluvial systems classically are subdivided into three general channel patterns (i.e., straight, meander and braided; Leopold and Wolman, 1957). The anastamosing channel later became a fourth classification (e.g., Schumm 1968; Rust, 1978; Smith, 1983; Brice, 1985), but does not fit very well into the existing single channel classification scheme as it refers to multi-channel systems that split and rejoin on length scales larger than the channel width itself (van den Berg, 1995). The axes of Figure 3.2 illustrate the relative relationship (and linguistic descriptors) between straight, meandering and braided channel morphologies and many of the controlling morphological variables, including sediment load (suspended, mixed, bed), sediment size (small versus large), flow velocity (low versus high), and stream power (low versus high). In the absence of exact units, information is still conveyed in linguistic terms such as "high" and "low."

In addition to the ability to delineate each of these three channel classifications, fuzzy sets and fuzzy logic can also be used to describe the relationship between each major morphological category. Early research suggested that abrupt thresholds exist between the three classical patterns of fluvial systems: 1) straight, 2) meander and 3) braided (e.g., Ackers and Charlton, 1970; Schumm and Kahn, 1972; Schumm, 1981). Recent studies have suggested that changes between fluvial patterns (e.g., straight to meandering, meandering to braided) are gradual (e.g., Ferguson, 1981; Knighton and Nanson, 1993; van den Berg, 1995; Woolfe and Balzary, 1996; Heritage et al., 2001). Fuzzy sets defining the three classical fluvial patterns and their relationship sediment size, sediment load, flow velocity, and stream power are presented in Figure 3.3. Minor modifications in the shape and slope of MFs for each of the three fuzzy sets (i.e., "straight", "meandering", and "braided") can accommodate either the gradual transition of fluvial morphology (Figure 3.3A) or the abrupt transition of

Figure 3.2. Channel classification based on pattern and type of sediment load, showing types of channels, their relative stability, and some associated variables (after Schumm, 1981).

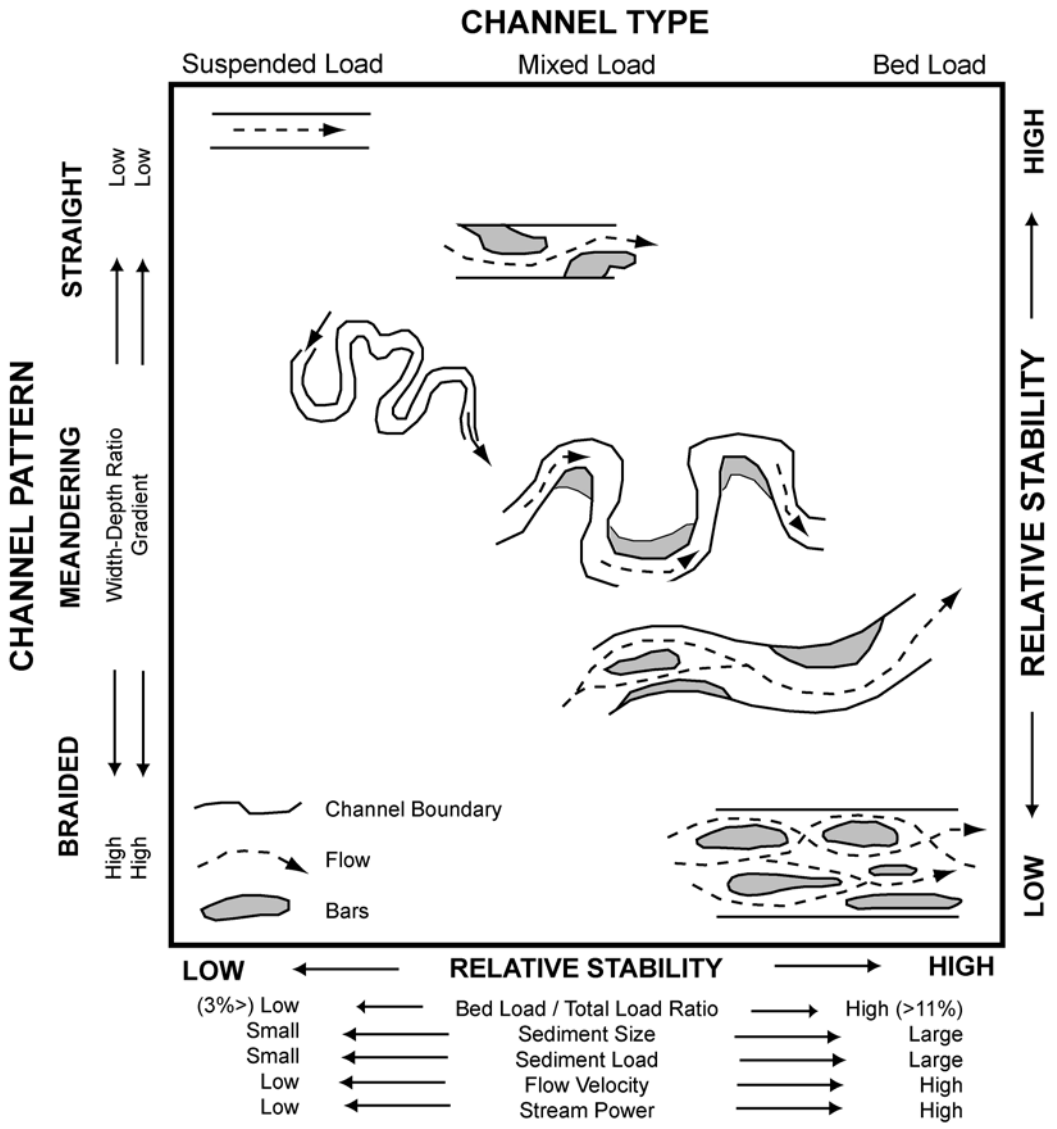
CHANNEL TYPE
Suspended Load
Mixed Load
Bed Load
CHANNEL PATTERN
STRAIGHT
MEANDERING
BRAIDED
Low
Low
Width-Depth Ratio
Gradient
High
High
RELATIVE STABILITY
HIGH
LOW
Channel Boundary
Flow
Bars
LOW
RELATIVE STABILITY
HIGH
(3%>) Low
Bed Load / Total Load Ratio
High (>11%)
Small
Sediment Size
Large
Small
Sediment Load
Large
Low
Flow Velocity
High
Low
Stream Power
High

Figure 3.3. Fuzzy sets used to classify three major fluvial channel morphologies (see Figure 3.2) based on A) a gradual transition and a B) more abrupt transition.

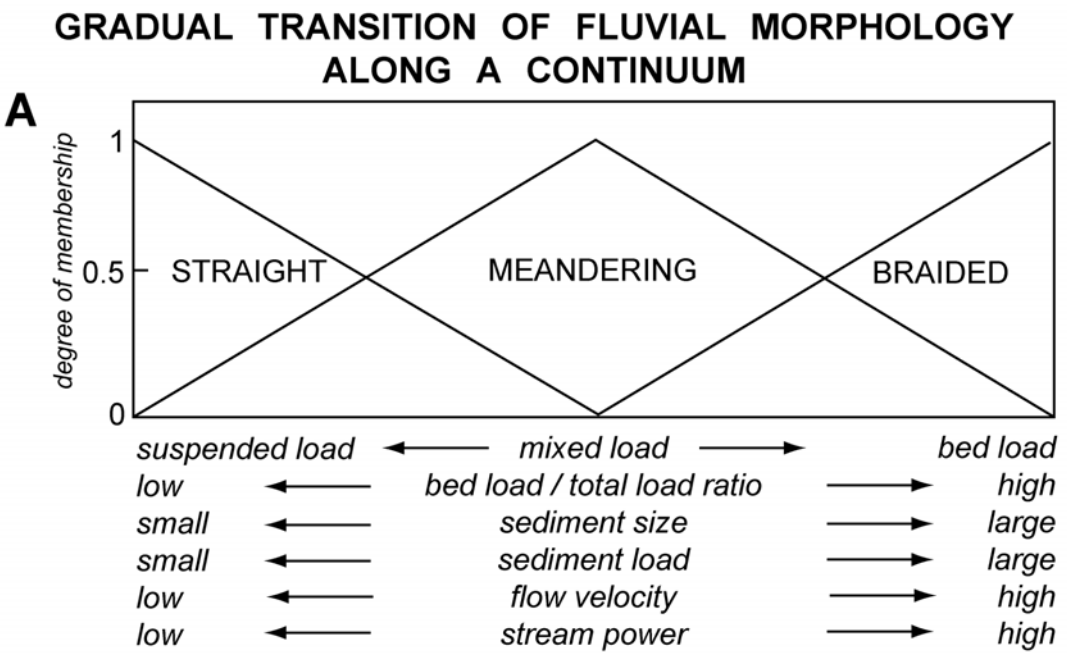
GRADUAL TRANSITION OF FLUVIAL MORPHOLOGY
ALONG A CONTINUUM
A
degree of membership
1
0.5
0
STRAIGHT
MEANDERING
BRAIDED
suspended load
mixed load
bed load
low
bed load / total load ratio
high
small
sediment size
large
small
sediment load
large
low
flow velocity
high
low
stream power
high

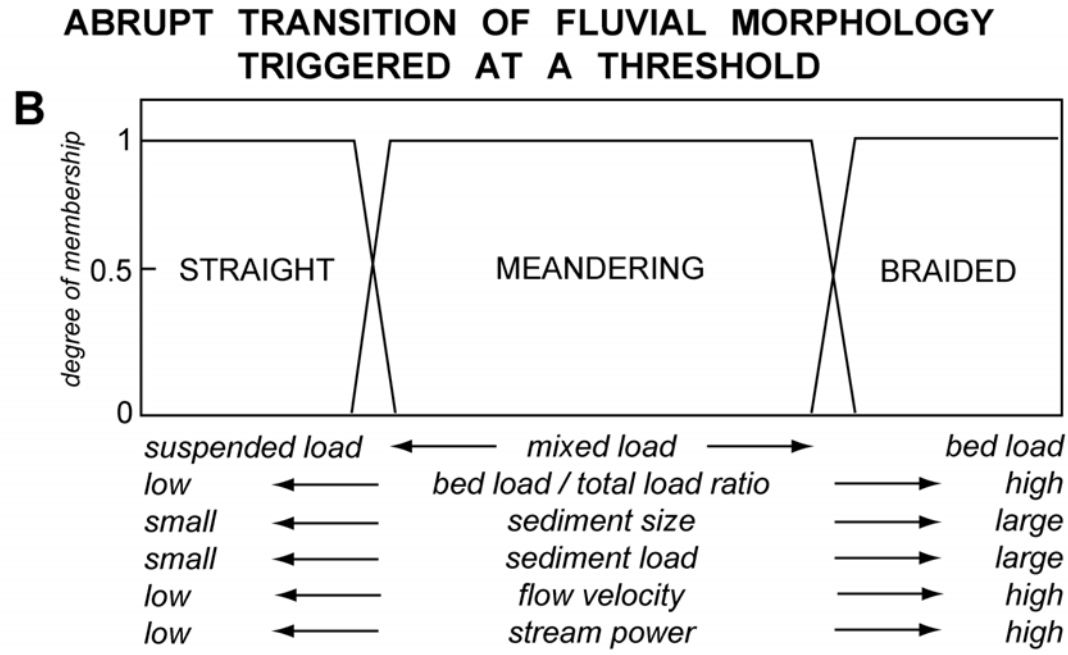
ABRUPT TRANSITION OF FLUVIAL MORPHOLOGY
TRIGGERED AT A THRESHOLD
B
degree of membership
1
0.5
0
STRAIGHT
MEANDERING
BRAIDED
suspended load
mixed load
bed load
low
bed load / total load ratio
high
small
sediment size
large
small
sediment load
large
low
flow velocity
high
low
stream power
high

fluvial morphology (Figure 3.3B). More important than understanding whether the transition between channel morphologies is abrupt or gradual is the derivation of relationships between channel morphology and the processes of deposition and erosion that control it. Schumm (1972; his Table 1) and Orton and Reading (1993; Their Table 2) presented some general links between fluvial variables (e.g., slope, discharge, sediment load, velocity, etc.) and channel morphology. Creating fuzzy inference systems (FISs) based on these investigations is not difficult. The variables controlling channel morphology are easily defined by fuzzy sets. The manner in which the variables identified by Schumm (1972) and Orton and Reading (1993) interact is the basis for the general rules that describe the system and, hence, drive the FIS.

Some classifications in the literature do not even need modification into fuzzy sets, because they are already in a fuzzy format (although the investigation had nothing to do with fuzzy logic). For example, a figure presented in Dalrymple et al. (1992) describes the relative nature of active processes defining an estuary (Figure 3.4). The transition between marine and river systems is more accurately described with fuzzy sets rather than crisply defined boundaries. The nature of the curves in this diagram is analogous to a MF. The values on the y-axis are along a continuum between 0 and 100% (representing none and all, respectively). The domain is a relative, unit-less axis that defines the transitional environment between fluvial and marine processes that define an estuary. Two MFs define the river-dominated processes and marine-dominated processes, and an estuary is defined as a combination of the two, overlapping processes (and two, overlapping fuzzy sets).

Deltaic Classification. The ternary, process-based, delta classification of Galloway (1975) was based on three end-member variables (sediment input, wave energy flux, tidal

Figure 3.4. The schematic distribution of the physical processes operating within estuaries, and the resulting zonation of Dalrymple et al. (1992), is similar in function and form to fuzzy sets.

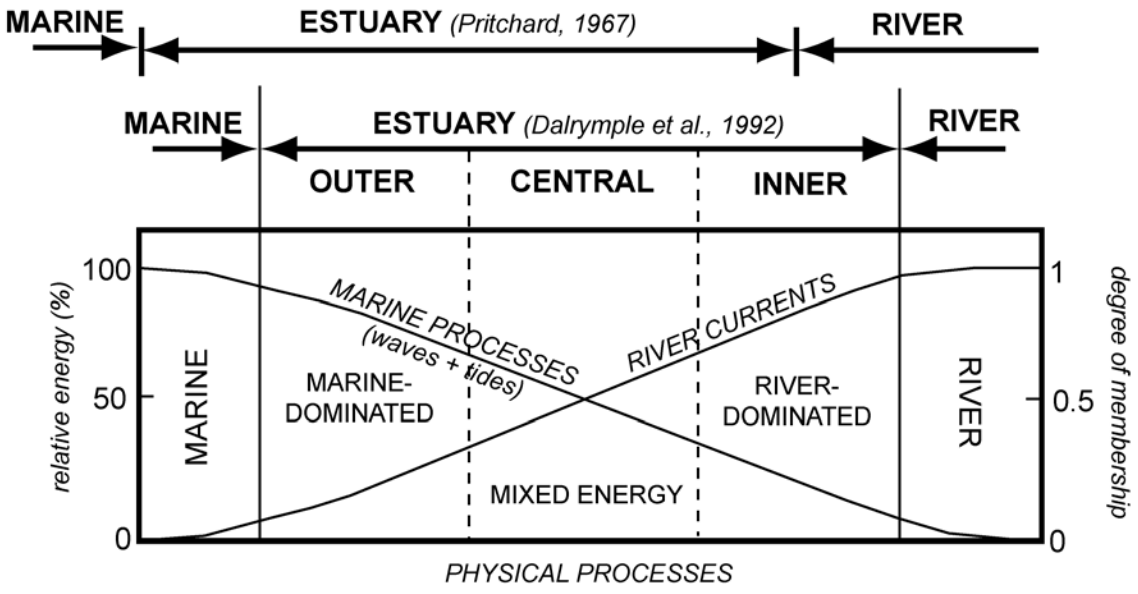
MARINE
ESTUARY (Pritchard, 1967)
RIVER
MARINE
ESTUARY (Dalrymple et al., 1992)
RIVER
OUTER
CENTRAL
INNER
100
50
0
relative energy (%)
MARINE PROCESSES
(waves + tides)
RIVER CURRENTS
MARINE
MARINE-
DOMINATED
MIXED ENERGY
RIVER-
DOMINATED
RIVER
1
0.5
0
degree of membership
PHYSICAL PROCESSES

energy flux). Traditional interpretation associated elongate and lobate delta morphologies with fluvial-dominated systems, even though "lobate" occurred near the crisp boundary between fluvial- and wave-dominated systems. In fuzzy terms, the modern lobe of the Mississippi River would have full membership in the fuzzy set "fluvial dominated", the Brazos River would have full membership in the fuzzy set "wave dominated" and the Ebro delta would have equal membership in both fuzzy sets (see Figure 3.5). Orton and Reading (1993) adapted this classification to include grain size (Figure 3.6). The categories "mixed mud and silt", "fine sand" and "gravelly sand" illustrate the fuzzy nature of gradual transitions between grain-size categories defined linguistically, based on relative, rather than absolute, values. Dalrymple et al. (1992, their Figures 2 and 3) used a similar ternary classification scheme to place not only deltas, but coastal systems in general, into the framework of a continuum. Dalrymple et al. (1992) also described these delta classifications linguistically (e.g., low, moderate, high, as well as low to moderate and extremely high) based on tidal, wave and fluvial influenced processes (their Table 1). Similarly, the linguistic descriptors of deltas and related depositional systems (e.g., drainage basin, fluvial parameters, shoreline and marine processes) presented by Orton and Reading (1993; their Table 2) were not intended as a fuzzy inference system, but created the general rules to define such a system.

3.1.3 Stratigraphic Modeling using Fuzzy Logic

Application of fuzzy logic to the geological sciences has dramatically increased during the past few decades. For example, one paper (the first; Chappaz, 1977) was published during the 1970s, 151 in the 1980s, and 640 in the 1990s. Complete journal volumes (Journal of Petroleum Geology, 2001) and books (Wong et al., 2002; Nikravesh et al., 2003;

Figure 3.5. Schematic diagrams of A) Galloway (1975) and B) Piggot (1995) illustrating the threefold division of deltas into fluvial-dominate, wave-dominated, and tide-dominated types. The continuum between each end member (the apices of the ternary diagram) is well suited for classification using fuzzy logic.

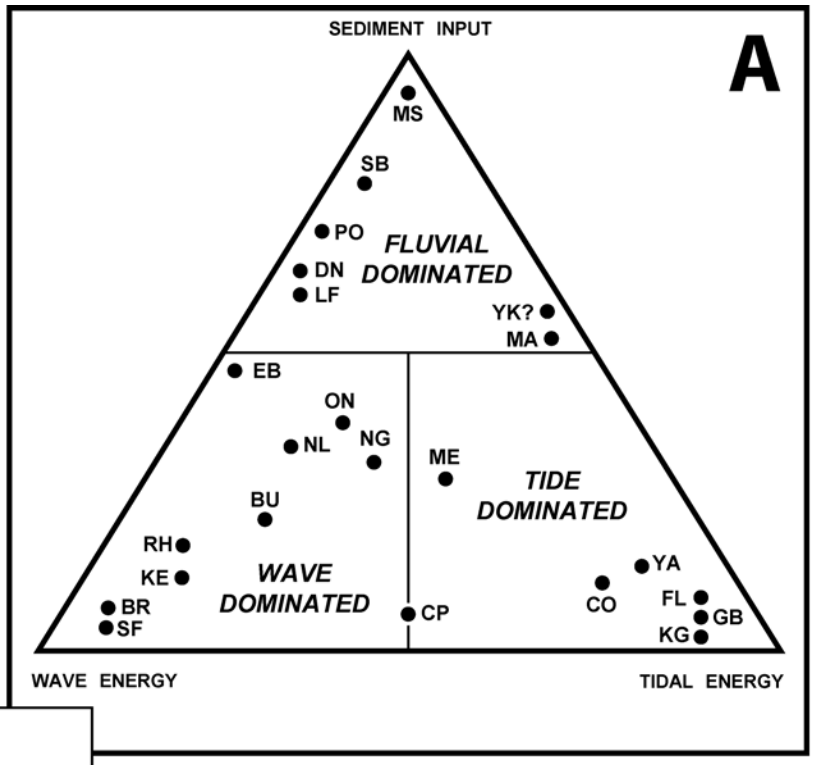

BR	Brazos
BU	Burdekin
CO	Colorado
CP	Copper
DN	Danube
EB	Ebro
FL	Fly
GB	Ganges-Brahmaputra
KG	Klang-Langat
KE	Kelanton
LF	Lafourche Lobe (MS River)
MA	Mahakam
ME	Mekong
MS	Mississippi (modern lobe)
NG	Niger
NL	Nile
OR	Orinoco
PO	Po
RH	Rhone
SB	St. Bernard Lobe (MS River)
SF	Sao Francisco
YA	Yalu
YK	Yukon

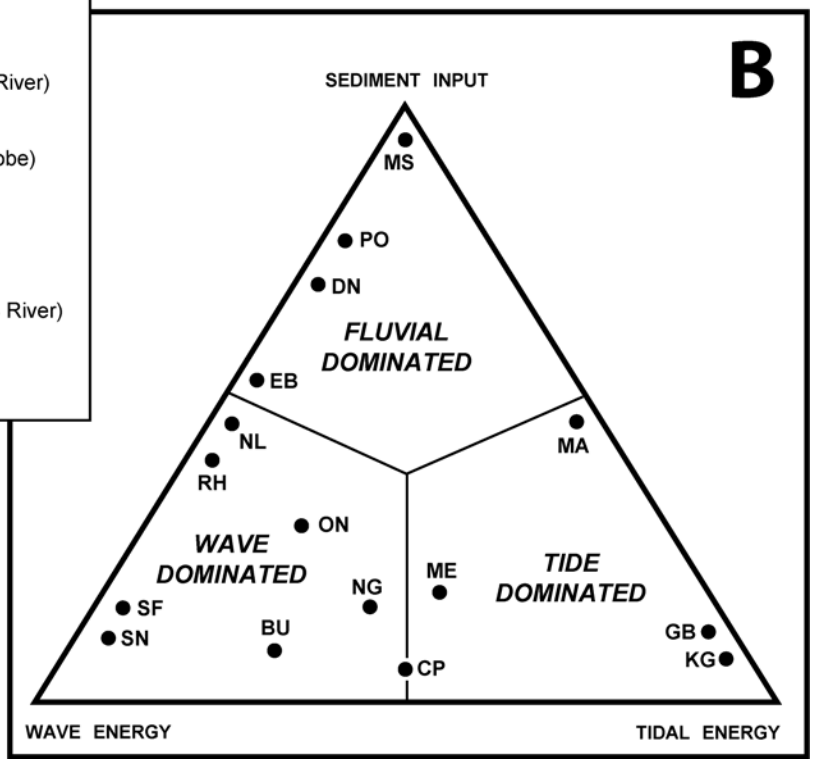

Figure 3.6. Deltaic classification of Orton and Reading (1993) based, in part, on Galloway (1975). The continuums between the apices on each ternary diagram as well as between each individual ternary diagram are well suited for fuzzy logic classifications.

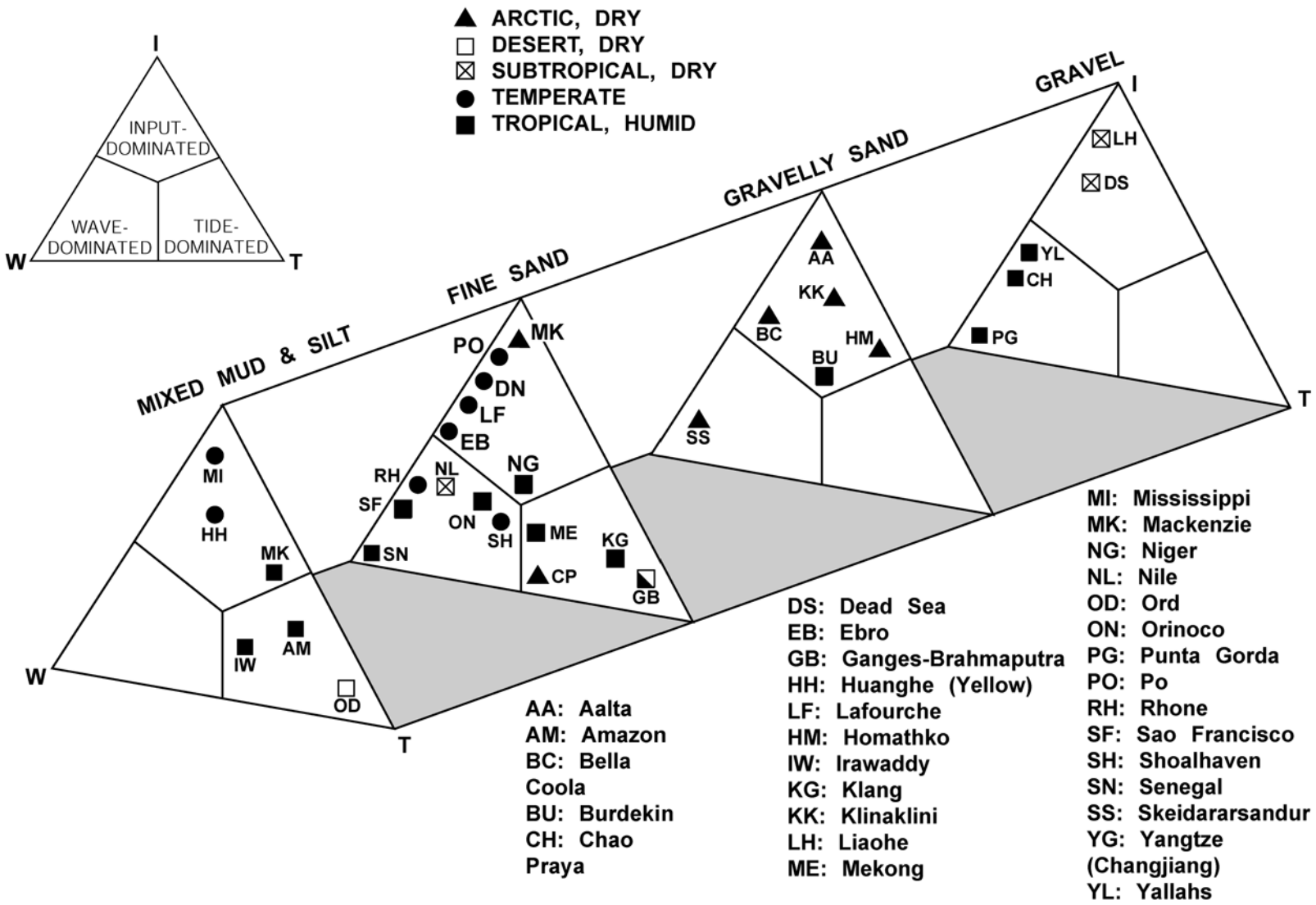
ARCTIC, DRY
DESERT, DRY
SUBTROPICAL, DRY
TEMPERATE
TROPICAL, HUMID
I
INPUT-DOMINATED
WAVE-DOMINATED
TIDE-DOMINATED
W
T
MIXED MUD & SILT
FINE SAND
GRAVELLY SAND
GRAVEL
MI
HH
MK
IW
AM
OD
SN
RH
NL
SF
ON
SH
PO
MK
DN
LF
EB
NG
ME
CP
KG
GB
SS
AA
KK
BC
BU
HM
LH
DS
YL
CH
PG
AA: Aalta
AM: Amazon
BC: Bella Coola
BU: Burdekin
CH: Chao Praya
DS: Dead Sea
EB: Ebro
GB: Ganges-Brahmaputra
HH: Huanghe (Yellow)
LF: Lafourche
HM: Homathko
IW: Irawaddy
KG: Klang
KK: Klinaklini
LH: Liaohe
ME: Mekong
MI: Mississippi
MK: Mackenzie
NG: Niger
NL: Nile
OD: Ord
ON: Orinoco
PG: Punta Gorda
PO: Po
RH: Rhone
SF: Sao Francisco
SH: Shoalhaven
SN: Senegal
SS: Skeidararsandur
YG: Yangtze (Changjiang)
YL: Yallahs

Sandham and Leggett, 2003; Demicco and Klir, 2004) focusing on specific geological applications of fuzzy logic were published only recently. A comprehensive literature review of many of these specific studies was presented by Demicco (2004c), and the general applicability of fuzzy techniques to the field of geological science is addressed by Demicco (2004a; 2004c), Fang (1987; 1997) and Nordlund (1996; 1999a). These reviews indicate that few fuzzy applications had developed up until that time to model sediment deposition and stratigraphic evolution. In fact, there are only three in the literature as of 2006. Each of these three stratigraphic simulations is summarized in this paper to offer an overview of fuzzy stratigraphic modeling and provide evidence that a "fuzzy" approach offers an alternative, yet complementary, method to traditional mathematical models. In addition, these models, especially FUZZIM and the work of Demicco (2004) and Demicco and Klir (2001) as well as Warren et al. (2002b; 2003), contributed to the development of *fuzzy*PEACH, which will be described next.

The first stratigraphic simulator to be developed was FUZZIM, a Macintosh-based program developed in C/C++ by Nordlund (1996; 1999a; 1999b) and Nordlund and Silfversparre (1994). FUZZIM simulated sedimentation rates (thickness), grain size and erosion rates across idealized ramp margins (no antecedent topography) and was able to consider both clastic and carbonate systems. Nordlund (1996) identified the following conditions used in the simulation: 1) a set of 10 fuzzy rules, 2) a 25 km x 25 km model grid (10 km shelf with no antecedent topography/bathymetry, shelf-slope break <50 m below sea level at final time step), 3) a run time of 70 ky and 4) a sinusoidal sea level curve with an amplitude of 30 m and a frequency of 20 ky. Tectonic subsidence was implemented at a rate of 1 mm/yr (maximum rate located at distal margin with a linear decrease to zero at a

landward hinge point located 10 km outside the modeled universe). Nordlund (1999a) simulated the Miocene carbonate platform of Mallorca, Spain with the following conditions: 1) a set of 12 fuzzy rules that controlled deposition (grain size and distribution), erosion and carbonate production, 2) a model grid <10 km square, 3) a run time of 130 ky and 4) a sea level curve inferred from outcrop observations (max amplitude of 100 m below present with a frequency of 100 ky). Subsidence and compaction variables were not reported for this model. Nordlund (1999b) provided a general tutorial of FUZZIM with the following conditions: 1) a set of 5 fuzzy rules, 2) a model grid of 40 km x 80 km, 3) a run time of 100 ky (5 ky time steps), and 4) a sinusoidal sea level curve with an amplitude of 50 m and a frequency of 100 ky. Regional tectonic subsidence was defined using a model of a titled plane defined by three separate subsidence curves (one for each of three geographically defined reference points). Compaction and load-driven subsidence (simple Airy isostasy) are included using separate fuzzy systems. All three of the models experienced subaerial erosion and deposition. Submerged portions of all three models experienced deposition. The only erosion to occur in submerged portions of the model was in FUZZIM and was limited to simulated gravity deposits affecting strata exceeding a slope of 10° (Nordlund 1999a; 1999b). Visualization of output for each version included sediment distribution maps for each time step and dip-oriented cross-sections.

A set of models developed by Demicco (2004) and Demicco and Klir (2001), using MATLAB and its associated Fuzzy Logic Toolbox, simulated in three dimensions, clastic, carbonate and evaporitic depositional systems. Visualization of output for all three models included sediment type superimposed on the topography that was generated for each time step, synthetic cross-sections (strike and dip) through the final thickness of the deposits and

synthetic stratigraphic columns for predetermined locations in the simulation. The first model used four rules to govern depositional environments in Death Valley, CA (freshwater lake, playa mud flat, salt pan, saline lake) with respect to precipitation and temperature. Conditions of the model included: 1) a 15 km x 65 km basin, 2) a run time of 191 ky, 3) initial basin floor based on present topography and 4) a subsidence component varied between 0.2 and 1 mm/yr. The fuzzy systems governing basin floor sediments were calibrated with core data. Erosion, compaction and isostatic flexure were not incorporated into this model.

Demicco and Klir (2001) also used the same general modeling approach to apply a total of 19 rules to determine carbonate production, erosion, and lithology to simulate the past 10,000 years of tidal flat deposition on Western Andros Island (western side of the Great Bahama Bank). Conditions of the model included: 1) a 150 km x 300 km ramp margin, 2) a run time of 101 ky (100-yr time steps), 3) a data-based sea level curve and a 4) bathymetry/topography simplified from the literature. The fuzzy logic systems were calibrated with cores and maps. Tectonic subsidence, compaction and isostatic flexure were not incorporated into this model. Both of these models were tuned to reproduce the deposition conditions observed in data from Death Valley and Western Andros Island.

Demicco and Klir (2001) also adapted the general model to simulate a simplified, hypothetical delta and floodplain system. The river system, adjacent levee and crevasse-splay systems, as well as the simple deltaic dispersive cone were modeled by fuzzy logic systems based on the rules of Nordlund (1996). Simulation conditions included: 1) a 125 km x 125 km ramp margin approximately 60 km wide, 2) a run time of 50 ky (200-yr time steps), 3) a simple sinusoidal sea level oscillation (amplitude of 10 m and a frequency of 20 ky), and

4) random upstream avulsions of the river system. Tectonic (thermal) subsidence (maximum subsidence of approximately 3 mm/yr in center of model, decreasing to zero towards the edges of the modeled universe) remained constant for the duration of the simulation. Erosion, compaction and isostatic flexure were not incorporated into this model. This deltaic model was later adapted by Demicco (2004b) to include 17 rules (their Table 5.1) and applied to the Southwest Pass of the Mississippi River Delta complex. Revisions included additional fuzzy rules to simulate bedload transport, suspended sediment plumes, variable wave regimes, and long-shore drift at the river mouth. Isostatic compensation (subsidence due to sediment loading) was incorporated into this model, but erosion and compaction were not.

The third and final approach to stratigraphic simulation, FUZZYREEF, was developed by Parcel (2000; 2003a; 2003b) as a Windows-based program developed in C/C++. FUZZYREEF modeled depositional facies distribution and productivity rates on a carbonate platform using an example of microbial reef development on a Jurassic carbonate ramp from the US Gulf coast (Smackover Formation). Simulated conditions included: 1) an area less than 5 km x 5 km of a ramp margin (initial topography determined from 3D seismic), 2) a run time of 4 million years (100 ky time steps) and 3) eustatic curves with variable amplitudes between 0 and 200 m. Carbonate productivity and facies distribution were determined by fuzzy rules based on climate (arid, temperate, humid), latitude (low, mid, high), water energy (low, mid, high), slope (low, mid, high), and hardground location (soft, firm, hard). Although three fuzzy inference systems were identified, the individual rules were not reported. Subsidence parameters (thermal, loading and compaction) were included

in the simulation, but were implemented using traditional mathematical equations rather than fuzzy logic.

While there are only minor differences to the overall mechanics of how these three models operate as compared to the simulation presented in this paper, there is a significant difference in the amount of data used to constrain and interpret modeling output. Simulations presented in this paper extend over a time interval that is twice as long and cover and area twice as large as the other fuzzy logic models reviewed in this paper. The majority of the depositional conditions simulated during the investigation presented in this paper were established using approximately 14,000 km of high-resolution, two-dimensional seismic profiles that are chronologically constrained by multiple cores and covers a study area of 300,000 km^2. From these and other published data, the variables affecting relative sea level on the ECS margin during the past 195 ka (i.e., eustasy, tectonics, sediment supply as well as the morphology of the margin itself) are known with a high degree of certainty. The regional extent of the seismic profiles provided many of the constraints driving these simulations (e.g., tectonic subsidence rate, margin geometry). However, more importantly, stratal architecture defined by these seismic profiles provide a comparison to model output to assess whether the simulations accurately represent geologic conditions found not only on the ECS margin, but on continental margins in general.

3.2 HOW THE *fuzzy*PEACH WORKS

A three-dimensional computer simulation was developed to examine the sensitivity of stratigraphic evolution on a passive continental margin with respect to sea level, sediment supply and subsidence. The model uses the MATLAB programming language and the software's Fuzzy Logic Toolbox and is referred to as *fuzzy*PEACH (Predictive Earth Analysis Constrained by Heuristics). Here, the term "heuristics" represent general rules that simply describe complicated processes within geologic systems. The heuristics driving this particular simulation were controlled by a series of 21 rules contained within five fuzzy inference systems (FISs). Sediment distribution within the fluvial system (i.e., grain size and sediment volume) is governed by three rules contained within a single FIS. Deltaic deposition is controlled with three similar rules and one FIS. Three additional FISs govern avulsion, sediment compaction and isostatic flexure (sediment loading). A more detailed explanation of how fuzzy logic is integrated into the *fuzzy*PEACH model is presented below (see *Fuzzy Sets, Fuzzy Logic and Fuzzy Variables*).

In addition to compaction and isostatic compensation, tectonic subsidence is also included in the simulation as a user-defined variable not controlled with fuzzy logic. Other user-defined variables include model duration, duration of individual time steps, margin physiography (width, depth of shelf-slope break), sedimentation rate and sea level (frequency, amplitude and overall shape of curve). The general assumptions of the overall simulation are those of the sequence stratigraphic model (*sensu* Posamentier et al., 1988): 1) a passive margin, 2) constant rate of tectonic subsidence at any given location on the margin each time step, 3) a basinward increase in subsidence, 4) a sediment supply that remained

constant during each time step and 5) curvilinear sea level trends. The general processes of the model are presented as a flow chart in Figure 3.7.

*Fuzzy*PEACH uses a combination of triangular and trapezoidal MFs in each of its five FISs. These simple function shapes were chosen because of their successful application in previous stratigraphic models (Nordlund and Silfversparre, 1994; Nordlund, 1996, 1999a, 1999b; Parcell, 2000, 2003; Demicco and Klir, 2001; Demicco, 2004). The shape of a MF can vary, and the process of choosing a MF has been addressed by multiple authors (e.g., Lotfi and Tsoi, 1994; Rondeau et al., 1996; Sancho-Royo and Verdegay, 1999; Klir, 2004). For example, Lotfi and Tsoi (1994) suggested bell-shaped MFs (Gaussian or Cauchy curves) as better choices than triangular MFs when designing a fuzzy system. To test this hypothesis, sensitivity tests of *fuzzy*PEACH FIS output were conducted. The triangular MFs of the fuzzy sets defining deltaic sediment volume (Figure HMW7c) were replaced with trapezoidal and bell-shaped MFs. All other values within the FIS remained fixed. Output variations were negligible. For example, the deltaic deposition FIS consistently returned results with a difference of less than 10% (average <5%) when bell-shaped MFs replaced triangular MFs. Trapezoidal MFs returned results with a difference no higher than 5% (average <2%) than those generated with triangular MFs. Many times, there was no difference in output regardless of MF shape. The affect of MF shape on fuzzy logic simulations of depositional processes and stratigraphic response has not been addressed in a large-scale investigation, and further research seems warranted.

3.2.1 Defining Geological Variables

Model Duration. For the purpose of this investigation, *fuzzy*PEACH was designed to simulate conditions on a low-gradient continental margin (0.017°) over a period of

Figure 3.7. Flow chart identifying the major processes, and general operation, of the *fuzzy*PEACH stratigraphic simulator.

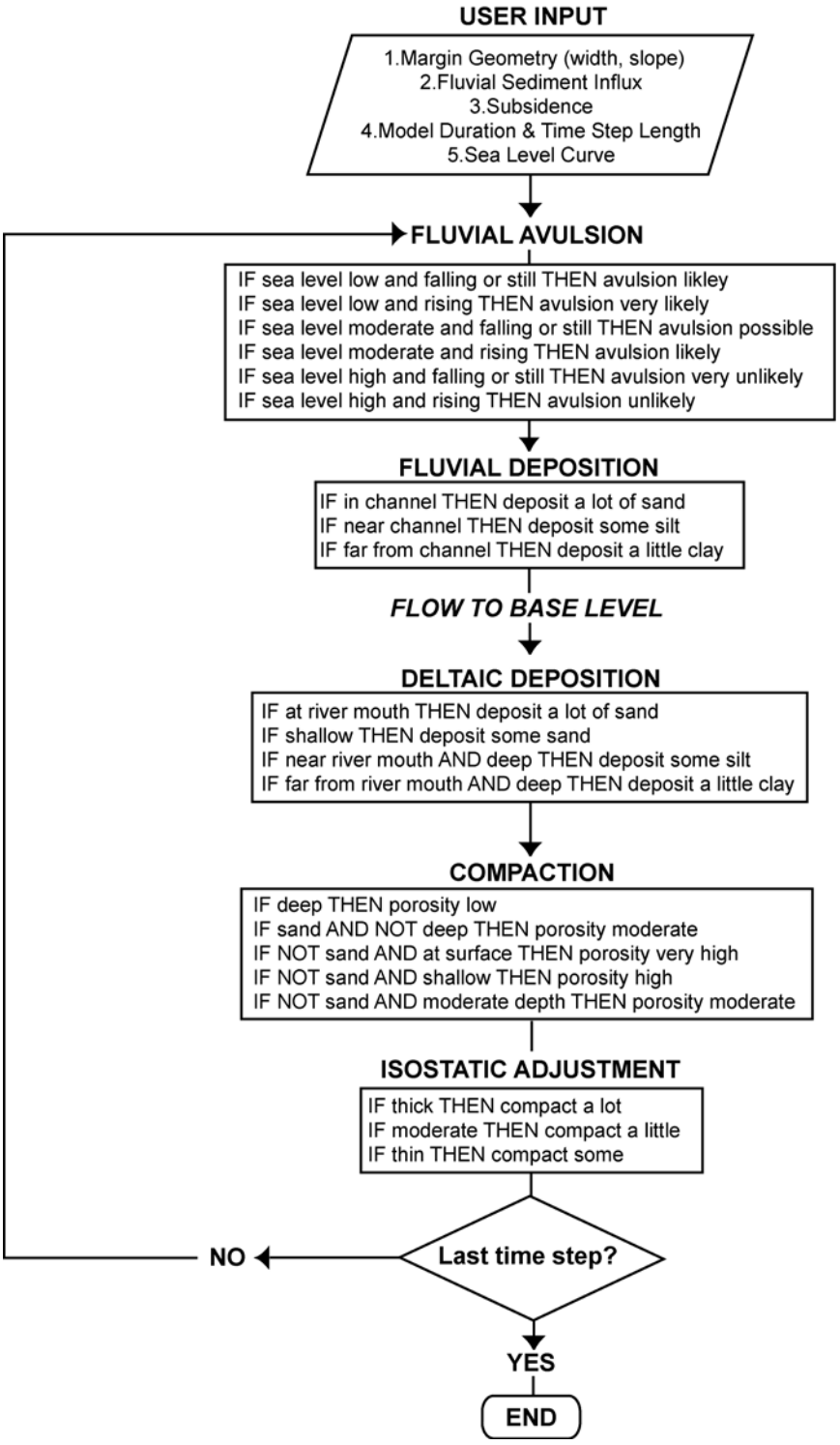
USER INPUT
1.Margin Geometry (width, slope)
2.Fluvial Sediment Influx
3.Subsidence
4.Model Duration & Time Step Length
5.Sea Level Curve
FLUVIAL AVULSION
IF sea level low and falling or still THEN avulsion likley
IF sea level low and rising THEN avulsion very likely
IF sea level moderate and falling or still THEN avulsion possible
IF sea level moderate and rising THEN avulsion likely
IF sea level high and falling or still THEN avulsion very unlikely
IF sea level high and rising THEN avulsion unlikely
FLUVIAL DEPOSITION
IF in channel THEN deposit a lot of sand
IF near channel THEN deposit some silt
IF far from channel THEN deposit a little clay
FLOW TO BASE LEVEL
DELTAIC DEPOSITION
IF at river mouth THEN deposit a lot of sand
IF shallow THEN deposit some sand
IF near river mouth AND deep THEN deposit some silt
IF far from river mouth AND deep THEN deposit a little clay
COMPACTION
IF deep THEN porosity low
IF sand AND NOT deep THEN porosity moderate
IF NOT sand AND at surface THEN porosity very high
IF NOT sand AND shallow THEN porosity high
IF NOT sand AND moderate depth THEN porosity moderate
ISOSTATIC ADJUSTMENT
IF thick THEN compact a lot
IF moderate THEN compact a little
IF thin THEN compact some
Last time step?
NO
YES
END

approximately 200 ky (although model duration is a user-defined variable). This time period was quantized into 500-year time steps, an increment that resolves the avulsion frequency of highly avulsive river systems (e.g., Yellow, Mississippi, Po) tabulated by Stouthamer and Berendsen (2001). The simulation of fluvial avulsions is discussed in greater detail below (see *Fuzzy Variables, Fuzzy Sets, Fuzzy Inference Systems*).

Margin Physiography. The simulated margin geometry at the first time step includes a flat margin lacking antecedent topography with a length (shore parallel) of 600 km and a shelf width (shore normal) of 500 km. The shelf-slope break is shore parallel at 150 m below modern sea level and creates a shelf gradient of 0.017° (Figure 3.8). The synthetic margin is spatially referenced to a 600 km x 600 km horizontal grid of 1-km^2 cells (i.e., 360,000 cells). This idealized margin physiography was established based on the geometry of margins sharing similar unincised fluvial architecture. Widths of these margins are 500 km (northwestern Australia; Woolfe et al., 1998), 100 km (southeastern New Zealand; Browne and Naish, 2003), and 500 km (ECS; Warren and Bartek, 2002a; 2002b). Depths of shelf-slope breaks are 113 m (northwestern Australia), 150 m (southeastern New Zealand), and 150 m (ECS). Offshore northern Java is a ramp margin (gradient = 0.03°) without a defined shelf-slope break. The gradient of the other margins is 0.1° (northwestern Australia), 0.1° (southeaster New Zealand), and 0.013° (ECS). Similar physiographic data (i.e., gradient and depth of shelf-slope break) for other margins and basins throughout the Phanerozoic are rare in the literature.

Subsidence. Tectonic subsidence within *fuzzy*PEACH is user-defined (with the assumed relationship to thermal contraction; e.g., Watts et al., 1982). For the simulations presented here, rates varied between 0 and greater than 4 mm/yr based on values associated with

Figure 3.8. Idealized continental margin from *fuzzy*PEACH simulation of low-gradient conditions similar to those on the ECS margin. The shelf gradient is 0.017° and the shelf-slope break is at 150 m below present day sea level (elevation of 0 meters at the left edge of the margin).

meters
200
0
-200
-400
-600
-800
-1000
0
100
200
300
400
500
600
kilometers
0
100
200
300
400
500
600
kilometers

modern margins. Rates of subsidence are well established for numerous continental margins, including the northern Gulf of Mexico from south Texas to western Louisiana (up to 5 mm/yr; Anderson et al., 2004), the northern Gulf of Mexico at the mouth of the Mississippi River (up to 8 mm/yr; Wells, 1996), the Ganges River delta plain in the Bengal Basin (up to 5.5 mm/yr; Alam, 1996), the Canterbury Plains in New Zealand (up to 2 mm/yr; Wellman, 1979), and the ECS near the mouth of the Yangtze River (up to 4.4 mm/yr; Stanley and Chen, 1993). However, these rates reflect total subsidence and do not separate tectonics from compaction and isostatic flexure. Because compaction and flexural isostasy associated with sediment loading have considerable effect on sequence architecture (e.g., Reynolds et al., 1991; Steckler et al., 1993), an attempt was made in this investigation to de-couple these two components from tectonic subsidence. Tectonic (thermal) subsidence is held constant for every time step and compaction and isostatic compensation from sediment loading are controlled separately by fuzzy logic (discussed below in *Fuzzy Variables, Fuzzy Sets, Fuzzy Inference Systems*).

Sediment Influx. *Fuzzy*PEACH uses a single fluvial system to deliver sediment to the simulated margin. The rate is a user-defined variable held constant for each time step. Rates varied in this investigation from between 1 x 10^8 and 5 x 10^8 tons/yr and were based on values expected from modern fluvial systems (Figure 3.9). The average of the world's top 25 rivers is about 2.43 x 10^8 tons/yr (Milliman and Meade, 1983; Milliman and Syvitski, 1992). Fluvial sedimentation is tied to a mass balance algorithm embedded within *fuzzy*PEACH to ensure the depositional volume of sediment deposited in both the fluvial and deltaic systems is equal to the sediment influx for each time step. This is accomplished by using a mass-to-volume conversion algorithm that assumes a clastic-dominated, silica-rich sediment load

Figure 3.9. Sediment discharge, in terms of tons per year, of the world's top 25 rivers (compiled from Milliman and Meade, 1983; Milliman and Syvitski, 1992).

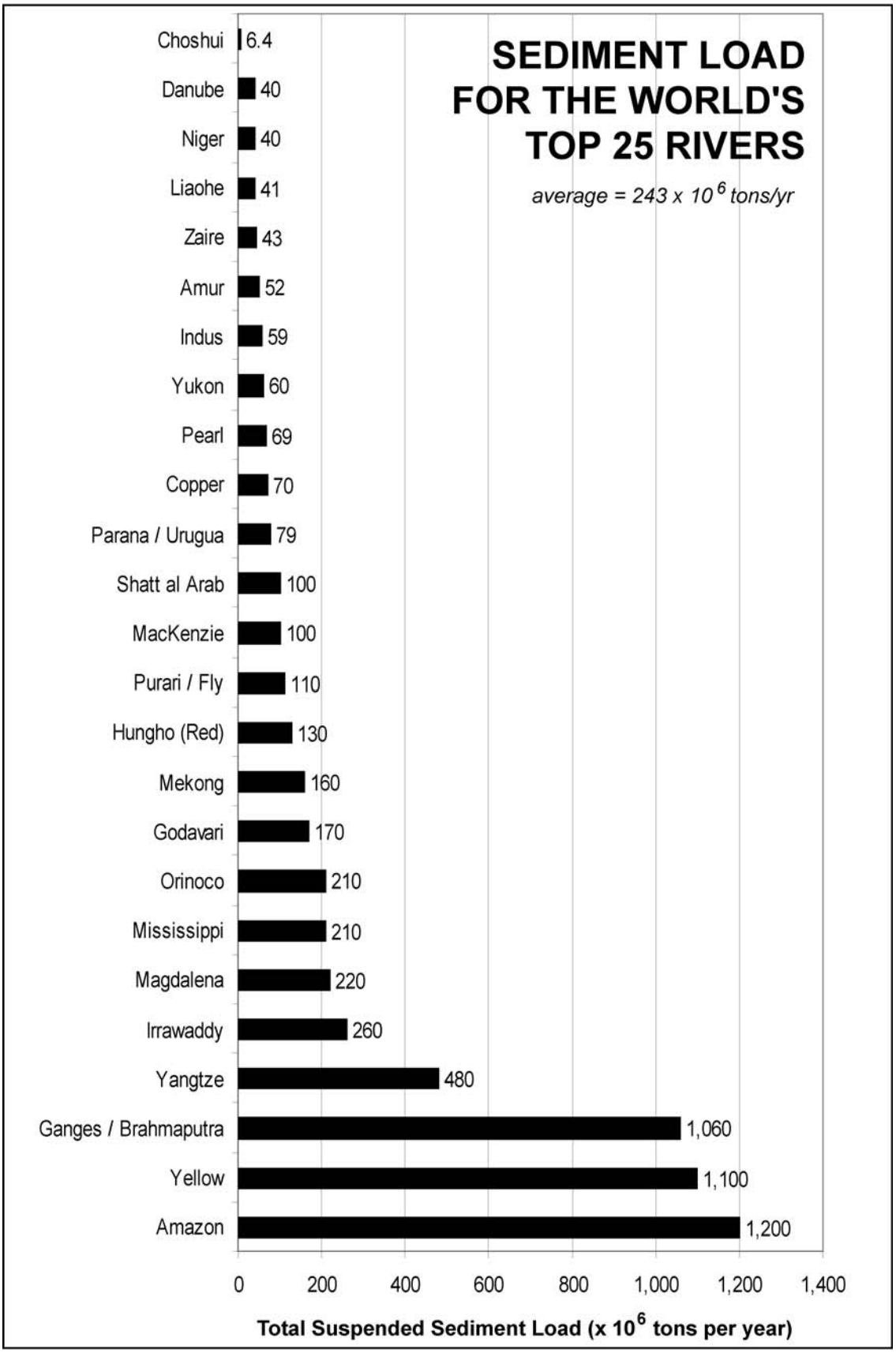
SEDIMENT LOAD FOR THE WORLD'S TOP 25 RIVERS
average = 243 x 10^6 tons/yr
Choshui 6.4
Danube 40
Niger 40
Liaohe 41
Zaire 43
Amur 52
Indus 59
Yukon 60
Pearl 69
Copper 70
Parana / Urugua 79
Shatt al Arab 100
MacKenzie 100
Purari / Fly 110
Hungho (Red) 130
Mekong 160
Godavari 170
Orinoco 210
Mississippi 210
Magdalena 220
Irrawaddy 260
Yangtze 480
Ganges / Brahmaputra 1,060
Yellow 1,100
Amazon 1,200
0 200 400 600 800 1,000 1,200 1,400
Total Suspended Sediment Load (x 10^6 tons per year)

(density of quartz = ρ_{qtz} = 2643 kg/m^3) and an average porosity (Φ) of 50% (although ρ and Φ can be user-defined variables with *fuzzy*PEACH). The average porosity was chosen as a moderate value between unconsolidated sands and sandstones that can range in porosity from 28% to 46% (Beryl and Weyl, 1973; Domenico, 1977; Giles et al., 1998; Curry et al., 2004) and silts and clays that commonly have Φ values between 60% and 70% (Rieke and Chilangarian, 1974; Baldwin and Butler, 1985; Giles et al., 1998).

Eustatic Sea Level. *Fuzzy*PEACH relies upon prescribed eustatic curves to drive simulations. During this investigation, idealized sinusoid curves of multiple periodicities (100 ky, 40 ky, 20 ky) were used to simulate Milankovitch-band frequencies observed throughout the Quaternary (e.g., Imbrie et al., 1984; Weedon, 1991). Functions of different frequencies and magnitudes were convolved to simulate more complex eustatic change (e.g., parasequences). In addition to sea level curves that were either theoretical and/or idealized (Figure 3.10), actual sea level conditions were based on SPECMAP data presented by Winograd et al. (1988, 1992) (Figure 3.11).

3.2.2 Fuzzy Variables, Fuzzy Sets, Fuzzy Inference Systems

During each time step, the simulation of sediment distribution and deposition throughout the fluvial system, flood plain, delta and continental shelf is controlled by rules, or heuristics, based on basic geologic principles. Five distinct Takagai-Sugeno type FISs apply 21 rules and their logic operators (AND, OR, NOT) to a collection of fuzzy sets. (Each FIS is outlined in Figure 3.12). Two types of FISs are commonly used: Mamdani (Mamdani, 1975) and Takagi-Sugeno (Takagi and Sugeno, 1985). The output of each FIS is an aggregate of the appropriate MFs to create a single "defuzzified" variable. The difference between the Mamdani and Takagi-Sugeno FIS is the averaging process that calculates this variable.

Figure 3.10. Eighteen variations of sea level functions used for sensitivity testing of *fuzzy*PEACH simulations.

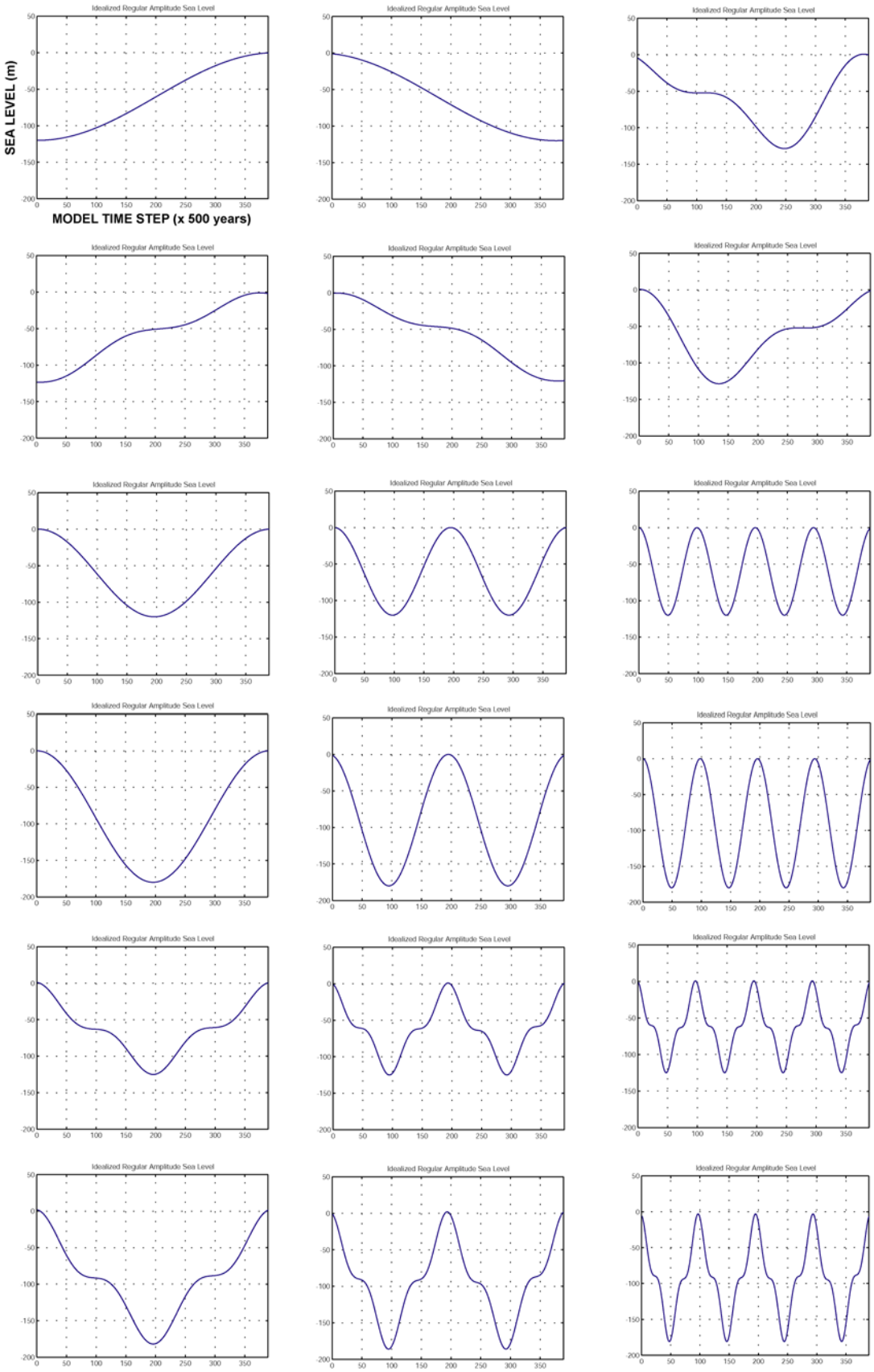
Idealized Regular Amplitude Sea Level
SEA LEVEL (m)
MODEL TIME STEP (x 500 years)

Figure 3.11. A) Sea level curve based on SPECMAP data from Winograd et al. (1988, 1992). B) Sea level curve from the South Pacific from Pillans et al. (1998). C) Relative sea level curve from the ECS from Saito et al. (2001).

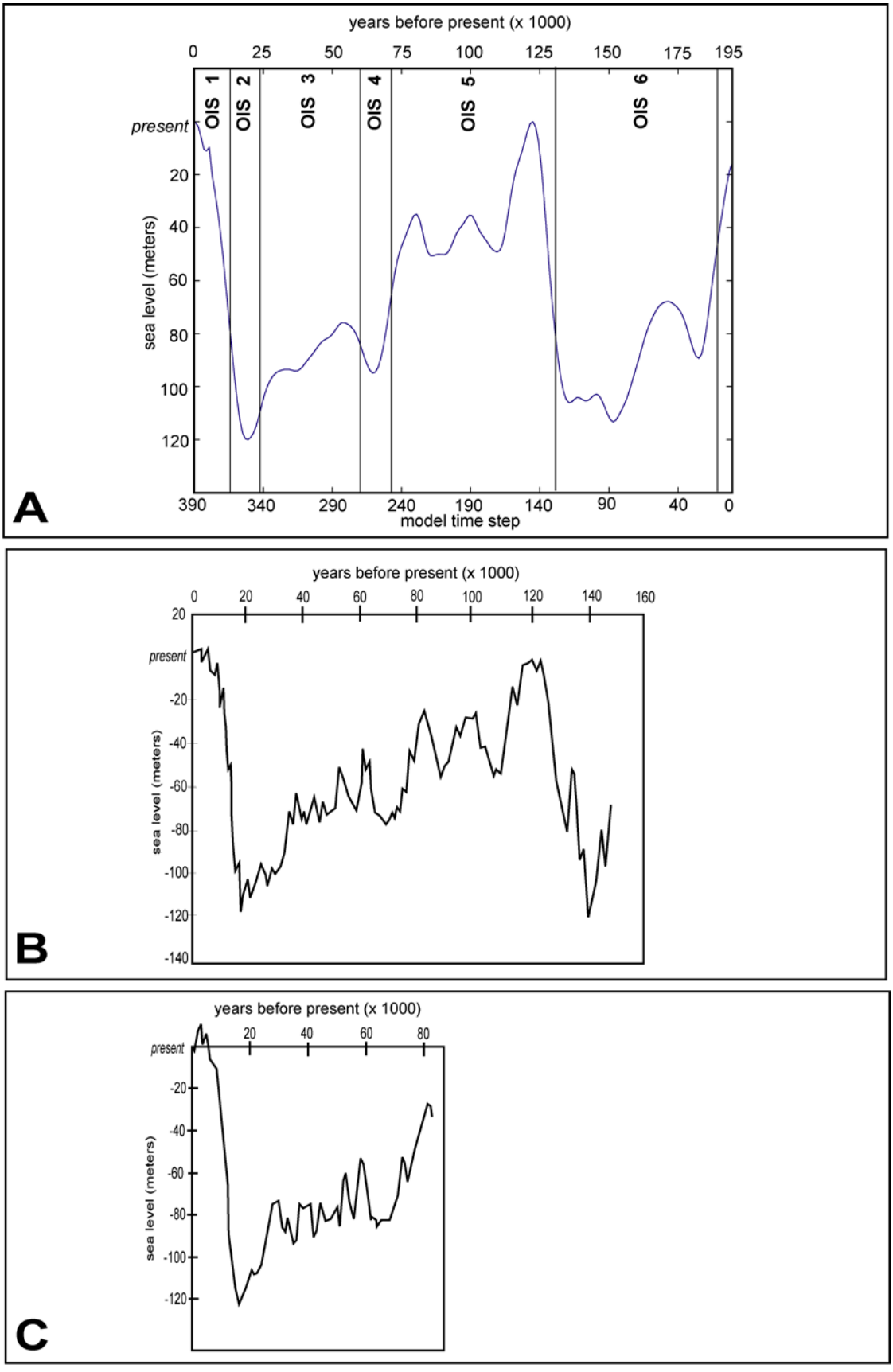
years before present (x 1000)
0 25 50 75 100 125 150 175 195
OIS 1
OIS 2
OIS 3
OIS 4
OIS 5
OIS 6
present
20 40 60 80 100 120
sea level (meters)
390 340 290 240 190 140 90 40 0
model time step
A
years before present (x 1000)
0 20 40 60 80 100 120 140 160
20
present
-20 -40 -60 -80 -100 -120 -140
sea level (meters)
B
years before present (x 1000)
20 40 60 80
present
-20 -40 -60 -80 -100 -120
sea level (meters)
C

Figure 3.12. The five fuzzy inference systems included in *fuzzy*PEACH stratigrahpic simulations: A) fluvial deposition, B) fluvial avulsion, C) deltaic deposition, D) compaction, and E) isostatic flexure.

A

FLUVIAL DEPOSITION

Grain Size and Sediment Volume

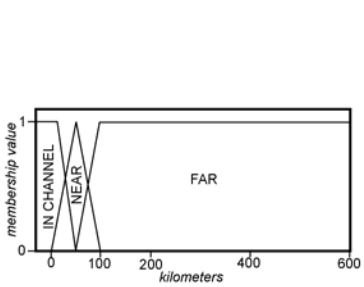

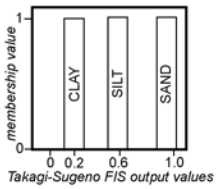

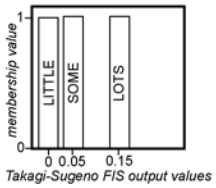

RULES

IF in channel THEN deposit sand
IF near channel THEN deposit silt
IF far from channel THEN deposit clay

IF in channel THEN deposit a lot
IF near channel THEN deposit some
IF far from channel THEN deposit little

Six rules are presented here to illustrate the mechanics of how the logically defines grain size and sediment thickness, however, the variables have been comdbined and presented as three rules in the paper.

B

FLUVIAL AVULSION

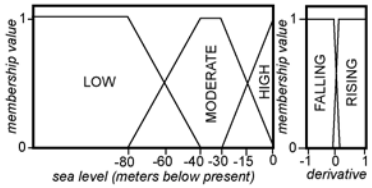

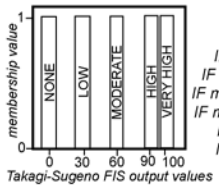

RULES

IF low AND falling THEN high avulsion
IF low and rising THEN very high avulsion
IF moderate AND falling THEN mod avulsion
IF moderate AND rising THEN high avulsion
IF high AND falling THEN no avulsion
IF high AND rising THEN low avulsion

C

DELTAIC DEPOSITION

Grain Size and Sediment Volume

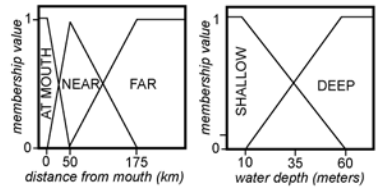

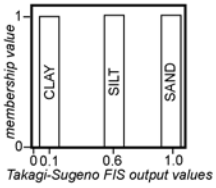

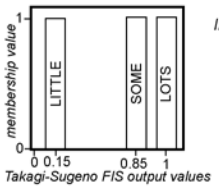

RULES

IF at river mouth THEN deposit sand
IF shallow THEN deposit sand
IF deep AND near THEN deposit silt
IF deep AND far THEN deposit clay

IF at river mouth THEN deposit a lot
IF shallowTHEN deposit some
IF deep AND near THEN deposit some
IF deep AND far THEN deposit little

Eight rules are presented here to illustrate the mechanics of how the logically defines grain size and sediment thickness, however, the variables have been combined and presented as four rules in the paper.

D

COMPACTION

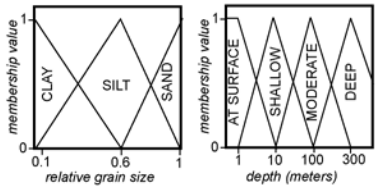

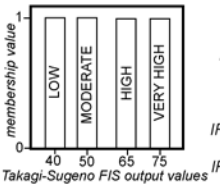

RULES

IF deep THEN porosity low
IF sand AND NOT deep THEN porosity moderate
IF NOT sand AND at surface THEN porosity very high
IF NOT sand AND shallow THEN porosity high
IF NOT sand AND moderate depth THEN porosity moderate

E

ISOSTATIC FLEXURE

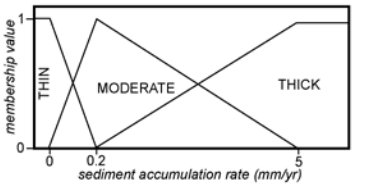

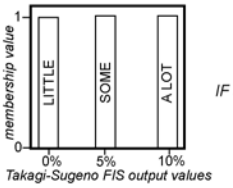

RULES

IF strata thin THEN subside little
IF strata moderate THEN subside some
IF strata thick THEN subside a lot

Summarily, the Mamdani FIS integates across the entire domain of the final output fuzzy set, and the Takagi-Sugeno FIS employs only the weighted average of a few points to create a single spike. The computational efficiency of the Takagi-Sugeno process is well suited for the more than 280 million data points generated during each *fuzzy*PEACH stratigraphic simulation. A more detailed discussion of the Takagi-Sugeno and Mamdani FIS is illustrated by Demicco (2004a, 2004b) by using mutliple geologic examples, including the determination of carbonate production, carbonate exposure indices, and the determination of paleoclimates.

Five individual FISs accomplish the following tasks: 1) determine relative grain size of fluvial sediment (coarse to fine) and distribution (thickness and lateral extent), 2) control fluvial avulsion, 3) determine relative grain size of deltaic sediment (coarse to fine) and distribute deltaic sediment (thickness and lateral extent), 4) control compaction based on porosity and depth, and 5) control subsidence via stratigraphic thickness and isostatic compensation. Together, the five FISs and their components (e.g., rules, MFs, domain values of fuzzy sets, etc.) are the engine that drives the fuzzy portion of the model and, therefore, remained constant throughout the entire investigation. The user-defined variables (i.e., margin geometry, sediment influx, sea level, tectonic subsidence) interact with the logic rules and fuzzy sets within each FIS at each time step and determine sediment type and thickness for each time step at each of the 360,000 1-km-square cells that define the idealized continental margin (i.e., 2 variables x 360,000 cells x 390 time steps).

Previous simulations of fluvio-deltaic deposition using fuzzy sets and fuzzy logic were critical to this investigation (Nordlund and Silvfersparre, 1994; Nordlund 1996, 1999a, 1999b; Demicco and Klir, 2001; Demicco, 2004b). The geological engine driving these

models, as well as *fuzzy*PEACH, is based on a set of general rules governing deposition (grain size and volume) within in any given fluvio-deltaic system. The actual rules are presented below (see *Fluvial Deposition*), but can be summarized as follows: 1) the coarsest sediment is deposited proximal to both the fluvial channel and the mouth of the river at the delta, 2) the highest sediment volume is also deposited proximal to the fluvial channel and river mouth, 3) sediment becomes more fine-grained, and 4) the sediment volume decreases as distance from the channel axis and river mouth increase. Therefore, in relative terms, the coarsest and thickest sediments are deposited in the channel and at the head of the delta, while the finest-grained and thinnest sediments are deposited the farthest from the channel on the floodplain or farthest from the delta on the shelf. Variation of sediment grain size and stratal thickness, between end-member locations (i.e., proximal versus distal relative to the channel or delta head), are calculated along a continuum defined by fuzzy sets. The values and justifications for these variables, fuzzy sets, and linguistic rules associated with each FIS are discussed in detail below. Variables were tuned during sensitivity testing in order to ensure that reasonable stratal architectures were produced. Selected examples of these tests are presented later in this paper (see *Results* and *Discussion*).

Fluvial Deposition. At the beginning of each simulation, a single river flows from the upstream end of the model toward adjacent cells with the lowest elevation. During rising sea level, the river mouth backtracks up the river course. During falling sea level or stillstands, the river seeks out the lowest adjacent cell in front of it until reaching zero elevation (base level). Fluvial deposition is simulated during every time step for every cell above base level, and a single FIS (Figure 3.12A) uses three rules to determine grain size and sediment volume relative to the location of the channel.

IF in channel THEN a lot of sand
IF near channel THEN some silt
IF far from channel THEN little clay

The left-hand side of the rule (the premise) defines the distance from the channel. The right-hand side of the rule (the conclusion) determines the amount and type of sediment deposited per time step at each grid cell. The three variables in these rules (i.e., distance from source, sediment volume, grain size) contain multiple fuzzy sets, and the boundary of each set is determined by a MF. The geological data and/or justification(s) for these sets (domain variables and set boundaries) are discussed below.

The simulated channel in *fuzzy*PEACH is idealized and does not distinguish between the end-members of fluvial morphology (i.e., straight and braided; Figure 3.2). Therefore, the widths of the channel axis are based on both modern and recent fluvial systems. The average widths of individual channels and channel braids are used to define the simulated channel width. The distance from the channel axis under the influence of the channel is based on floodplain widths. The distance relative to the channel is defined (in kilometers) by three fuzzy sets: 1) "in channel", 2) "near channel", and 3) "far from channel." The minimum channel width is set at 2 km ("in channel"). The main channel of the Mississippi River is between 1 and 2 km wide (Wells, 1996). Paleo channels of similar widths of are preserved in the shallow strata offshore Java and are approximately the same width (2 km; Posamentier, 2001). The Yangtze River is also about 5 km wide just upstream from its estuary (Hori et al., 2001). Individual channels within braided complexes are not as wide, but braids associated with these channels have similar widths. The entire braid is considered a site of active deposition during the 500-year resolution of time steps during the simulation. The braided Rangitata River on the Canterbury Plains (New Zealand) has an overall width between 2 and

5 km wide (Carson, 1984). The bankfull widths of the braided Tana (Kenya) and Slims (Canada) rivers are 0.6 to 2 km and 0.3 to 1.8 km, respectively (Miall, 1977). The fuzzy set "in channel" is defined as less than, or equal to, 5 km (Figure 3.12A). This is a reasonable value based on the width of fluvial channels and channel complexes presented above.

The fuzzy set "near" encompasses the floodplain, the width of which is based on fluvial observations from various geologic settings. The floodplain associated with the modern Mississippi River averages 100 km wide from the Gulf of Mexico up into Missouri. This width has remained fairly constant throughout the Holocene (Saucier, 1994). Core data from the Yangtze coastal plain identify a floodplain width of at least 100 km throughout the Quaternary (Baeteman et al., 1992). The floodplain from Cooper Creek (Australia) has a smaller, but still substantial, floodplain of 50 km (Fagan and Nanson, 2004). The fuzzy set "near channel" is defined as less than, or equal to, 50 km. This is measured in both directions from the axis of the channel (i.e., a total width of 100 km). This is a reasonable value based on the floodplain data above. The fuzzy set "far" includes distances greater than 100 km from the channel axis (Figure 3.12A). Deposition in *fuzzy*PEACH does not occur farther than 100 km from the channel.

Justified by the widths above, complete membership (MF=1) in each of the fuzzy sets that define distance from channel occurs at ≤5 km ("in channel"), 50 km ("near channel") and ≥100 km ("far from channel"). Partial membership (overlap in adjacent sets where MF<1) is defined along the continuum of values between 0 and 50 km (partial membership in both "in channel" and "near channel") as well as 50 km and 100 km (partial membership in both "near channel" and "far from channel"). Distances from the channel axis greater than 100 km are classified solely as "far" (Figure 3.12A).

Two outputs, volume of sediment and grain size, also subdivide into multiple fuzzy sets. Volume is defined by three fuzzy sets ("little", "some", "a lot") whereas grain size categories correspond to the three basic grain-size fractions ("sand", "silt", "clay"). The values for both output variables (volume and grain size) are presented in Figure 3.12A. Volume of sediment deposited (stratal thickness in a 1-km-square grid) defines full membership (MF=1) at 0.15 ("a lot"), 0.05 ("some"), and 0 ("little"). Partial membership (overlap in adjacent sets where MF<1) is defined along the continuum of values between 0.15 and 0.05 (partial membership in both "a lot" and "some"), as well as 0.05 and 0 (partial membership in both "some" and "little"). The values are unit-less as well as dimensionless (i.e., they are scalable based on total sediment influx). In conjunction with the mass balance algorithm described above (see *Defining Geologic Variables*), the output defines the depositional volume (stratal thickness) to each grid cell above base level at that particular time step. This mass balance calculation ensures that the volume of sediment influx deposited on the entire margin (throughout the entire fluvio-deltaic system) equals the sediment influx at every time step. Sediment volumes are determined relative to the output ratios described above (e.g., 0.15 being the maximum thickness and 0 being the minimum and determining areas without deposition). Due to the unit-less nature of this FIS, sediment accumulation rates were calculated during sensitivity testing to ensure reasonable deposition was occurring. Sediment influx primarily affected the deltaic system, therefore, sediment accumulation in the fluvial system averaged about 1 mm/yr during high rates of sediment influx (>2 x 10^8 tons/yr). Simulated, in-channel sediment accumulation rates averaged 1.3 mm/yr. Similar fluvial accumulation is calculated from the Canterbury Plains (New Zealand) between 0.7 mm/yr (OIS 6, 8, 10) and 1.7 mm/yr (OIS 4 and 2) (Browne and Naish, 2003). An average accumulation rate of 0.5 mm/yr is

calculated from fluvial deposits deposited on the ECS margin during OIS 6 (Warren and Bartek, 2002b). Floodplain accumulation rates from *fuzzy*PEACH simulations averaged 0.2 mm/yr. Rates similar to those in the model are observed in the floodplains of the Indus River (0.2 mm/yr; Kukal, 1971), the Tigris and Euphrates (0.2 mm/yr; Bridge and Leeder, 1979), the Delaware River (as low as 0.1 mm/yr; Schindel, 1980), and the Wisconsin valley (0.35 mm/yr; Bridge and Leeder, 1979).

Grain size is also determined along a unit-less, relative continuum spanning coarse and fine grain sizes (Figure 3.12A). The relative nature of these fuzzy grain size sets is dimensionless and scalable. Therefore, identical results could be achieved with grain size defined in relative terms as "coarse", "medium", and "fine." Full membership (MF=1) at each fuzzy singleton occurs at 1.0 (sand), 0.6 (silt), and 0.2 (clay). Partial membership (overlap in adjacent sets where MF<1) is defined along the continuum of values between 1.0 and 0.6 (partial membership in both "sand" and "silt") as well as 0.6 and 0.2 (partial membership in both "silt" and "clay").

Fluvial Avulsions. Fluvial avulsion is the relatively sudden shift to a new course on a floodplain or deltaic plain (Törnqvist and Bridge, 2002). At the beginning of each 500-year time step, the fluvial system has the potential to avulse. The point of avulsion along the longitudinal axis of the river, as well as the direction of movement (right or left of the existing river), is programmed to be random. The new fluvial pathway establishes along the lowest topographic profile between the point of avulsion and sea level. Avulsions, when they do occur, are instantaneous and resolve to the model's 500-year time steps. This time window is similar to that of Törnqvist (1994) who defined instantaneous avulsion as one that occurs within a period of 200 years (^{14}C dates limit resolution to ±200 years). Avulsion data

tabulated by Stouthamer and Berendsen (2001) also validate the resolution of avulsion within 500-year time steps. For example, the lower Mississippi River and its delta complexes have avulsion frequencies that average 1380 and 1400 years, respectively. Other rivers experiencing frequent avulsion include the Rhine and Meuse rivers (945 years), the Saskatchewan River (675 years), the Yellow River (600 years), and the Po River (490 years).

The mechanics of fluvial avulsion, while relatively easy to describe in general terms, are complicated, and a governing set of mathematical equations does not exist. However, general trends have been observed, are established, and are described (e.g., Schumm, 1993; Koss et al., 1994; Thorne, 1994; Törnqvist, 1994; van Gelder et al., 1994; Bryant et al., 1995; Holbrook, 1996; Morozova and Smith, 1999; Stouthamer and Berendsen, 2001; Törnqvist and Bridge, 2002; Ashworth et al., 2004). It is these general trends that form the foundation for the six linguistic rules controlling avulsion during each time step (Figure 3.12B).

IF sea level low AND falling THEN high chance of avulsion
IF sea level low AND rising OR still THEN very high chance of avulsion
IF sea level moderate AND falling THEN moderate chance of avulsion
IF sea level moderate AND rising OR still THEN high chance of avulsion
IF sea level high AND falling THEN no chance of avulsion
IF sea level high AND rising OR still THEN low chance of avulsion

The premise of the rule (left side) defines the position of sea level relative to present (i.e., modern sea level is considered high) and its direction of movement (rise or fall). The conclusion of the rule (right side) determines the likelihood the river will avulse during any given time step. The three variables of each rule (i.e., sea level, direction of sea level movement, chance of avulsion) contain multiple fuzzy sets. The boundary of each set is determined by a MF. The geological data and/or justification(s) for these sets (domain variables and set boundaries) are discussed below.

The elevation of sea level determines the degree of subaerial exposure of the margin that, in turn, determines the distance over which a river must flow to reach sea level. As fluvial systems become overextended, avulsion potential increases (van Gelder et al., 1994; Holbrook, 1996) because an increasing length decreases fluvial gradient and results in an overall loss of power (i.e., the ability for the system to carry sediment). The Yellow River illustrates the effect of overextension and power loss, although it is occurring at present during a period of slow sea level rise. It is the river's abundant sediment load (1.08×10^9 tons/yr; Milliman and Meade, 1983), and not sea level lowstand, that is responsible for delta progradation rates as high as 2 km/yr (van Gelder et al., 1994). However, the result is the same: a lowered fluvial gradient (from either 1) a shelf or exposed margin with a gradient equal to or lower than the fluvial system, or 2) rapid progradation of the delta) leads to overextension and power loss. As these individual delta lobes rapidly build seaward, stream gradients substantially lower and lead to an overall straightening and overextension of the fluvial system (Holbrook, 1996). The resulting power loss causes channels to aggrade above the surrounding floodplain, and an eventual levee breach shifts the channel to a shorter, higher-gradient course to base level. To illustrate this point, nine avulsions of the Yellow River (nodal points 20-50 km updip from delta lobes) since 1855 are attributed to this cycle of overextension, aggradation, and avulsion (van Gelder et al., 1994). An ancient example of fluvial overextension and high-frequency avulsion is the laterally extensive Mesa Rica Sandstone (Lower Cretaceous, New Mexico; Holbrook, 1996). The Mesa Rica has been presented as an analog to the ECS margin during OIS 6 (Bartek et al., 2001; Bartek and Warren, 2002; Warren and Bartek, 2002a; 2002b).

The unconfined fluvial systems on the margins of Australia (Woolfe et al., 1998), New Zealand (Browne and Naish, 2003), Java (Posamentier, 2001) and eastern China (Bartek et al., 2001, Bartek and Warren, 2002; Warren and Bartek, 2002a; 2002b) were deposited during subaerial exposure of the low-gradient margin during recent glacial maxima (OIS 2 and OIS 6). The 100 ky periodicity of these extreme lowstands correlates to the eccentricity Milankovitch band (e.g., Imbrie et al., 1984). The inferred eustatic signal during those times was less than 80 m below present (Figure 3.11). Since sea level is used as an input variable for the six rules in the avulsion FIS, the fuzzy classification considers sea level "low" for elevations greater than 80 m below present. The remaining sea level values are defined by two additional sets: "moderate" and "high." Complete membership (MF=1) in each of these three fuzzy sets occurs at 0 m (modern sea level = "high"), 40 m below present ("moderate"), and ≥80 m below present ("low"). Partial membership (overlap in adjacent sets where MF<1) is defined along the continuum of values between 0 and –40 m (partial membership in both "high" and "moderate") as well as –40 and –80 m (partial membership in both "moderate" and "low"). The collection of fuzzy sets defining sea level elevation for this FIS is presented in Figure 3.12B.

Two general trends, relative to avulsion, are defined by the direction of sea level movement. First, avulsion rates increase during rising sea level (and continue to increase as rate and magnitude of sea level rise increases) as a river aggrades to positively adjust its equilibrium profile (Schumm, 1993; Koss et al., 1994). Second, avulsion rates decrease (and continue to decrease as rate and magnitude of sea level rise decreases) during falling sea level as fluvial sedimentation tries to keep pace and negatively adjust its equilibrium profile (Schumm, 1993; Koss et al., 1994; Stouthamer and Berendsen, 2001). Two fuzzy sets define

sea level movement: 1) falling and 2) rising. The derivative of the sea level curve for each time step determines slope. Complete membership (MF=1) in each fuzzy set occurs for slopes ≤-0.1 ("falling") and ≥0.1 ("rising"). Partial membership (overlap in adjacent sets where MF<1) is defined along the continuum of values between –0.1 and 0.1 where sea level change rates are negligible (essentially stillstand). The two fuzzy sets defining direction of sea level are presented in Figure 3.12B.

In addition to sea level elevation, the direction of elevation change affects the stability of a fluvial system and also contributes to the rate of avulsion (Koss et al., 1994). Rate of change also is important. Higher rates of sea level change make it more difficult for fluvial systems to keep an equilibrium profile. Faster rates of change during sea level rise increase the chance for avulsion (the fluvial system cannot reach equilibrium), and slower rates of change during falling sea level increase the chance for avulsion (sediments prograde and lower the fluvial gradient). During the past 195 ky, rates of sea level change were consistently high (up to 7 mm/yr; Figure 3.11). Therefore, rate was not included in the *fuzzy*PEACH simulations presented in this paper, but will be considered during future upgrades of the model.

The output of the avulsion FIS determines whether fluvial avulsions will occur during any given time step. This possibility for avulsion is defined by five fuzzy sets: 1) "none", 2) "low", 3) "moderate", 4) "high", and 5) "very high." Full membership (MF=1) occurs at 0% ("none"), 30% ("low"), 60% ("moderate"), 90% ("high"), and 100% ("very high") (Figure 3.12B). Partial membership (overlap in adjacent sets where MF<1) is defined along the continuum of values between 0 and 30% (membership in both "none" and "low"), 30 and 60% (membership in both "low" and "moderate"), 60 and 90% (membership in "moderate"

and “high”) as well as 90 and 100% (membership in “high” and “very high”). Based on this fuzzy approximation of probability, avulsions frequencies can be established at 500 years (100% chance at each time step), 1,000 years (50% chance), 4,000 years (25% chance), 8,000 years (12.5% chance), etc.

*Fuzzy*PEACH uses output values as a proxy for avulsion probability because, even though membership functions are similar to probability density functions in form and function (Nordlund, 1996), fuzzy sets address imprecision from the absence of sharply defined criteria rather than the presence of random variables (Zadeh, 1965). Fuzzy logic addresses the degree to which something is believed to be possible rather than the likelihood of an event to occur (Wolkenhauer, 1998). Dealing with these two forms of uncertainty (i.e., probability and possibility) has been widely discussed and is somewhat controversial (e.g., Laviolette et al., 1995; Kandel et al., 1995; Zadeh, 1995). For the purpose of *fuzzy*PEACH simulations, fluvial avulsion either occurs or it does not occur (traditional logic). However, the FIS bases the possibility of avulsion on geologically reasonable conditions easily defined and governed by linguistic terms. The domain variables (i.e., the values along the x-axis that represented percent chance of avulsion between 1 and 100) defining the fuzzy set boundaries were chosen arbitrarily between 1 and 100% to represent a logical subdivision of avulsion potential. After setting the boundaries to these fuzzy sets, numerous sensitivity tests during model development produced avulsion rates similar to natural systems (e.g., Rhine and Meuse, Saskatchewan, Yellow and Po rivers; Stouthamer and Berendsen; 2001). Future versions of *fuzzy*PEACH will record a detailed avulsion history of each simulation, including the number of fluvial avulsions and when they occurred (time step, eustatic elevation, direction of sea level movement) to facilitate a more quantitative review.

Deltaic Deposition. Simulated deltaic deposition propagates seaward at the intersection of the river and the shoreline (base level). The delta FIS controls deposition for every grid cell below base level for any given time step with a single FIS (Figure 3.12C). Four rules within this FIS determine grain size and sediment volume relative to the location of the river mouth and water depth. The second rule (below) simulates shoreface deposition by spreading a thin veneer of sand along the entire shoreline.

IF at river mouth THEN deposit a lot of sand
IF shallow THEN deposit some sand
IF near river mouth AND deep THEN deposit some silt
IF far from river mouth AND deep THEN deposit a little clay

The left-hand side of the rule (premise) defines the distance from the river mouth and the water depth. The right-hand side of the rule (the conclusion) determines the amount and type of sediment deposited per time step at each grid cell. The four variables of the rules (i.e., distance from source, depth of water, sediment volume, grain size) contain multiple fuzzy sets, the boundary of each set being determined by a MF. The geological data and/or justification(s) for these sets (domain variables and set boundaries) are discussed below.

The distance from the river mouth is defined (in kilometers) by three fuzzy sets: 1) "at river mouth", 2) "near river mouth", and 3) "far from river mouth" (Figure 3.12C). These sets only deal with distance; the physical processes in the water column affecting deltaic deposition are addressed below. The 1-km grid spacing of the model, by default, sets "at river mouth" at 1 km. However, domain variables defining distance for the fuzzy sets "near river mouth" and "far from river mouth" are based on actual distances of the 30 largest modern deltas in the world (in terms of area of delta plain; Wells and Coleman, 1984; their Figure 3). This group of 30 deltas was broken up into two tiers (the top 15 = Tier I and the bottom 15 = Tier II). The average area of Tier II is about 4,500 km^2 (Coleman, 1981; Wells

and Coleman, 1984; Orton and Reading, 1993). The radius of a delta with this area, assuming a semi-circular delta where area=[(πR^2)/2], the radius is just over 50 m. The average area of the deltas from Tier II is about 48,000 km^2 (Coleman, 1981; Wells and Coleman, 1984; Orton and Reading, 1993), and the radius is 175 km. An assumption is made here that the deltaic radii from these two groups are a good representation of average boundaries expected between major deltas in the modern record. All deltas, on average, are expected to have a radius of at least 50 km and a maximum width no more than 175 km. These two values define the fuzzy sets "near river mouth" and "far from river mouth", where complete membership (MF=1) 50 and 175 km, respectively. Therefore, complete membership (MF=1) in the fuzzy set "far from river mouth" is set at 175 km. Values equal to, or greater than, 175 km were classified solely as "far from river mouth." Partial membership (overlap in adjacent sets where MF<1) is defined along the continuum of values between 0 and 50 km (membership in both "at river mouth" and "near river mouth") as well as 50 and 175 km (membership in both "near river mouth" and "far from river mouth") (Figure 3.12C).

The second input variable, water depth, is defined (in meters) by two fuzzy sets: 1) "shallow" and 2) "deep." Water depth is determined by the general depth at which the physical processes affecting depositional processes are no longer affected by surface waves. The depth of fair-weather wave base has been reported as deep as 60 m for specific locations (Ebro Delta; Puig et al., 2001) to as shallow as 10 m for modern, high-energy coasts in general (Clifton, 2000). Wells and Coleman (1984) correlated offshore delta slope with wave power at the shoreline for 18 major deltas of the world (their Figure 13). The average wave energy of these deltas was approximately 2 x 10^7 Ergs/sec.

The amount of wave energy at the shoreline depends mainly on the subaqueous profile of the delta (i.e., the flatter the slope, the greater the attenuation of deep water wave energy). The major effect of incoming wave energy impacts sediment distribution (Wells and Coleman, 1984). Therefore, defining an average value of slope from the dataset of Wells and Coleman (1984) is helpful in defining the boundaries of fuzzy sets that define water depth (which, in part, establishes the sediment distribution during *fuzzy*PEACH simulations). Transposing the average wave energy discussed above (2 x 10^7 Ergs/sec) from the vertical axis onto a best-fit line through the plot of Wells and Coleman (1984; their Figure 13) results in a slope value along the horizontal axis of 0.04°. Application of this slope to the distance defining "near river mouth" above (i.e., 50 km) produces a water depth of 35 m, a value that falls halfway between 10 and 60 m (the depths of wave base above). Therefore, full membership (MF=1) in the fuzzy set "shallow" occurs from 0 to –10 m and is the area of the delta dominated by fluvial and other coastal processes. Full membership (MF=1) in the fuzzy set "deep" occurs in depths greater than 60 m. Partial membership (overlap in adjacent sets where MF<1) is defined along the continuum of values between 10 and 60 m (membership in both "shallow" and "deep") where wave processes still affect deposition, but to a lesser degree at increasing depths. Hence, the environment is a combination of fluvial, coastal and marine processes. The crossing point of the two MFs occurs at 35 m (membership in both "shallow" and "deep" is 0.5) (Figure 3.12C).

Similar to the FIS controlling fluvial deposition, two outputs (volume of sediment and grain size) subdivide linguistically into multiple fuzzy sets. Volume is defined by three fuzzy sets ("little", "some", "a lot") whereas grain size categories correspond to the three basic grain-size fractions ("sand", "silt", "clay"). Full membership (MF=1) occurs at 1 ("a

lot"), 0.85 ("some"), and 0.15 ("little"). Partial membership (overlap in adjacent sets where MF<1) is defined along the continuum of values between 1 and 0.85 (partial membership in both "a lot" and "some") as well as 0.85 and 0.5 (partial membership in both "some" and "little"). The values are unit-less as well as dimensionless (i.e., they are scalable based on total sediment influx). In conjunction with the mass balance algorithm described above (see *Defining Geologic Variables*), the output defines the depositional volume (stratal thickness) to each grid cell below base level at that particular time step. This mass balance calculation ensures the volume of sediment influx deposited on the entire margin (throughout the entire fluvio-deltaic system) equals the sediment influx at every time step. The depositional volume is relative to the output ratios described above (e.g., 1 being the maximum thickness and 0.15 being the minimum and determining areas with minimal thickness). Due to the unit-less nature of this FIS, sediment accumulation rates were calculated during model development to ensure reasonable deposition was occurring. Sediment influx primarily affected the deltaic system (higher sedimentation rates correspond to higher discharge at the river mouth and higher deposition at the delta and surrounding continental margin. Using a sedimentation rate of 5×10^8 tons/yr to illustrate (the average of the world's top 10 rivers; Milliman and Meade, 1983; Milliman and Syvitski, 1992), the sediment accumulation rate at the delta mouth was about 10 mm/yr. For comparison, the Nile River delta has a sediment accumulation rate of 10 mm/yr (Kukal, 1971) and an annual sediment load of 1×10^8 tons/yr (Orton and Reading, 1993). The Orinoco River has an average annual sedimentation rate of 2×10^8 tons/yr (Milliman and Meade, 1983; Milliman and Syvitski, 1992) and a sediment accumulation rate associated with its delta of 5 to 6 mm/yr (Lisitzin, 1972) and. The Yangtze River has a sediment accumulation rate at its mouth between 10 and 54 mm/yr (DeMaster et

al., 1985) and an annual sedimentation rate of 5 x 10^8 tons/yr. Sediment accumulation rates at the toe of the delta in *fuzzy*PEACH were also reviewed to ensure a reasonable value. Using a sediment influx of 5 x 10^8 tons/yr, simulations had accumulation rates between 1.5 and 2 mm/yr. Modern systems, such as the Rhone River, accumulates 6 mm/yr of sediment 45 km offshore (the radius of the delta; Orton and Reading, 1993) from the river mouth (Lisitzin, 1972). The Nile River delta toe has an approximate sediment accumulation rate of 0.7 mm/yr (Schindel, 1980). Finally, sediment accumulation on the outer shelf was also calculated from from *fuzzy*PEACH model results (also using a sedimentation rate of 5 x 10^8 tons/yr) at a rate of 0.1 mm/yr. Sedimentation accumulation at the Bengal cone (Ganges prodelta) is 0.06 mm/yr (Moore et al., 1974). The sediment load of the Ganges-Brahmaputra River is 1.7 x 10^9 tons/yr, the largest in the world; Milliman and Meade, 1983; Milliman and Syvitski, 1992). Sediment accumulation on the open shelf, 30 km basinward of the Rhone River delta toe, is 1 mm/yr (Lisitzin, 1972). The Yangtze River has an accumulation rate on the outer margin, about 300 km from the Yangtze mouth, of 0.3 mm/yr (Berne et al., 2002). The sedimentation rates in the Atlantic and Pacific basins (abyssal) are, on average, 0.01 mm/yr (Dymond and Lyle, 1994).

Grain size is also determined along a unit-less, relative continuum spanning coarse and fine grain sizes (Figure 3.12A). The relative nature of these fuzzy grain size sets is dimensionless and scalable. Therefore, identical results could be achieved with grain size defined in relative terms as “coarse”, “medium”, and “fine.” Full membership (MF=1) at each fuzzy singleton occurs at 1.0 (sand), 0.6 (silt), and 0.2 (clay). Partial membership (overlap in adjacent sets where MF<1) is defined along the continuum of values between 1.0 and 0.6 (partial membership in both “sand” and “silt”) as well as 0.6 and 0.2 (partial

membership in both “silt” and “clay”). Values in the output set were unit-less and relative to each other (rather than absolute) where coarsest grain size was 1 and the finest grain size was 0.1. The value for “clay” deposited on the subaerial coastal plain is “clay” (0.2). This fractional difference is visible in synthetic cross-sections and is assigned a different color and allows floodplain deposits to be distinguished from finer-grained pelagic muds on the shelf.

Compaction. In addition to a user-defined variable for tectonic subsidence (see *Defining Geologic Variables*), *fuzzy*PEACH also simulates sediment compaction. This calculation occurs at the end of every time step for the entire vertical sediment succession. Demicco (2004a; his Figure 3.4) effectively used a similar technique using fuzzy logic to simulate the burial and compaction of carbonate mud. Five rules within a single FIS (Figure 3.12D) determine the amount of compaction based on porosity and depth.

IF deep THEN porosity low
IF sand AND NOT deep THEN porosity moderate
IF NOT sand AND at surface THEN porosity very high
IF NOT sand AND shallow THEN porosity high
IF NOT sand AND moderate depth THEN porosity moderate

The premise of the rules (left side) defines the vertical extent (height) of the sediment column and grain size. The conclusion (right side) determines the amount of porosity expected after compaction, and the three variables of the rules (i.e., depth, grain size, porosity) contain multiple fuzzy sets. The boundary of each set is determined by a MF. The geological data and/or justification(s) for these sets (domain variables and set boundaries) are discussed below.

Both grain size and sediment volume classifications are assigned to each grid cell at every time step by the two FISs controlling fluvial and deltaic deposition (i.e., output from the fluvial FIS and delta FIS become input for the compaction FIS). Therefore, fuzzy grain

size values correspond to the relative, unit-less categories described above: “sand”, “silt”, and “clay.” Full membership (MF=1) occurs at 1.0 (“sand”), 0.6 (“silt”), and 0.1 (“clay”). This FIS is shown in Figure 3.12D. Partial membership (overlap in adjacent sets where MF<1) is defined along the continuum of values between 0.1 and 0.6 (partial membership in both “clay” and “silt”) as well as between 0.6 and 1 (partial membership in both “silt” and “sand”). In addition to grain size, the depth of sediment is also used to simulate compaction based on the application of expected porosity trends (see Figure 3.13). Depth is calculated for the entire stratigraphic column that was deposited at the end of each time for every grid cell. This is a cumulative process. For example, at the end of the first time, sediment depth (and its respective grain size value) is merely the height (in meters) of the sediment deposited during only that time step. Subsequently, at the end of the last time step (time step 390), the model analyzes the matrix of values (grain size and height of sediment column) deposited at each grid cell during each subsequent time step (in this case, 390 time steps). *Fuzzy*PEACH then simulates compaction by assigning a porosity value to each cell for each of the 390 time steps. Using this approach, the porosity matrix is re-calculated at each time step and the model will not continue to decrease porosity and over-compact sediments.

Depth is divided (in meters) into four fuzzy sets: 1) “at surface”, 2) “shallow”, 3) “moderate”, and 4) “deep.” These values are based upon the suite of compaction curves presented by Baldwin and Butler (1985; their Figure 3), although multiple investigations of porosity and volume loss during compaction were reviewed for both sand (Athy, 1930; Holbrook, 2002; Karner et al., 2003; Karner et al., 2005) and argillaceous sediment (Rieke and Chilingarian, 1974; Baldwin and Butler, 1985; Holbrook, 2002). The logarithmic scale of depth (meters) of the Baldwin and Butler (1985) curves establishes the domain of four

Figure 3.13. Compaction curves compiled by Baldwin and Butler (1985).

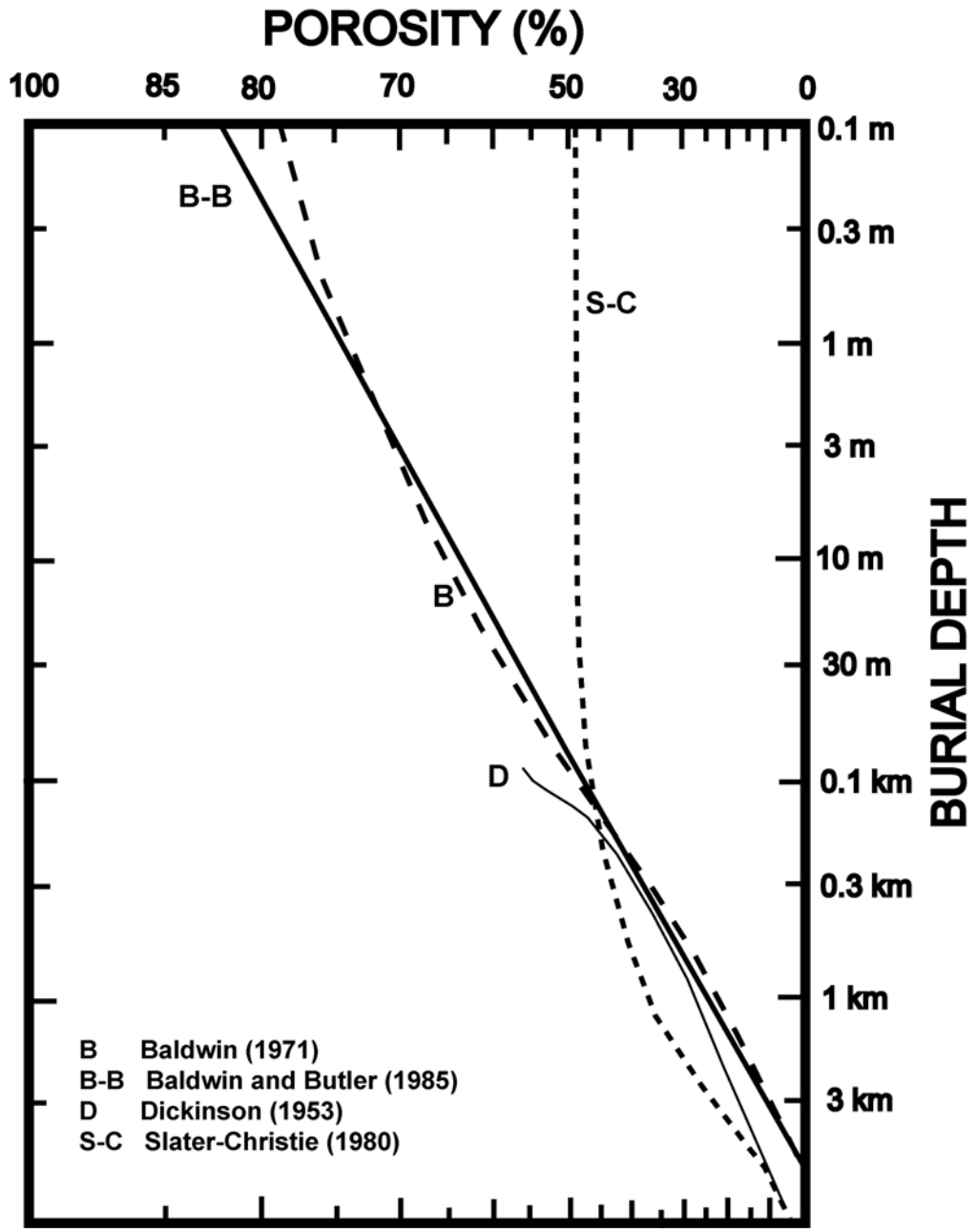
POROSITY (%)
100
85
80
70
50
30
0
0.1 m
0.3 m
1 m
3 m
10 m
30 m
0.1 km
0.3 km
1 km
3 km
BURIAL DEPTH
B-B
S-C
B
D
B Baldwin (1971)
B-B Baldwin and Butler (1985)
D Dickinson (1953)
S-C Slater-Christie (1980)

fuzzy sets: 1) “at surface”, 2) “shallow”, 3) “moderate”, and 4) “deep” (Figure 3.13). Complete membership in each of these sets (MF=1) occurs at ≤1 m (“at surface”), 10 m (“shallow”), 100 m (“moderate”), and 300 m (“deep”). Partial membership (overlap in adjacent sets where MF<1) is defined along the continuum of values between 1 and 10 m (membership in both “at surface” and “shallow”), 10 and 100 m (membership in both “shallow” and “moderate”), and 100 and 300 m (membership in both “moderate” and “deep”) (Figure 3.12D). During *fuzzy*PEACH simulations specific to this study, it was not necessary to continue the logarithmic trend for the fuzzy set “deep” (e.g., depth = 1,000 km). Model results were validated using the shallow stratigraphy of the last 195 ky on the ECS margin and the average thickness of these strata is 100 m. However, a simple modification to *fuzzy*PEACH could either modify the boundaries of the fuzzy set “deep” or add an additional fuzzy set “very deep” to handle depths ≥1 km. For the purpose of this investigation, all depths greater than 300 m were considered to have full membership (MF=1) in the fuzzy set “deep.”

The output of the compaction FIS (i.e., percent porosity) is defined based on the grain size and depth of sediment deposited during each discrete time step. Based on the compaction curves presented by Baldwin and Butler (1985; their Figure 3), the values defining the fuzzy sets for porosity corresponded the fuzzy set boundaries used for depth. Following the compaction curves for finer-grained sediments (see Figure 3.13), the porosity is defined as 75% at 1 m, 65% at 10 m, and 50% at 100 m. The volume loss for coarser material on these compaction curves is 50%. This is based on sandstone data (Sclater and Christie, 1980) rather than unconcsolidated material. Unpacked, sand-sized sediments typically have porosity values between 30 and 40% (Domenico, 1977; Karner et al., 2003;

Karner et al., 2005) although values have been reported as high as 45 to 50% (Beard and Weyl, 1973; Curry et al., 2004). *Fuzzy*PEACH makes the assumption that, regardless of the coarse-grained porosities, there is no compaction of sand-sized material until depths of 100 km are reached (i.e., following the trend shown in Figure 3.13). Based on the empirical data on compaction of St. Peter quartz sand (St. Peter Formation, Minnesota, Ordovician; Karner et al., 2003; Borg et al., 1960), which show a porosity change of less than 2% at 10 MPa (1450 psi = 500 km in depth; Maxwell, 1960), this is a reasonable assumption. From 100 to 300 m, all sediments along the compaction curves lose an additional 10% of porosity. Based on these trends, porosity is defined by four fuzzy sets ("low", "moderate", "high", and "very high"). Full membership (MF=1) at each of these porosity values occurs at 40% ("low"), 50% ("moderate"), 65% ("high"), and 75% ("very high"). Partial membership (MF<1) is defined along the continuum of values between 40 and 50% (membership in both "low" and "moderate"), 50 and 65% (membership in "moderate" and "high"), and 65 and 75% (membership in both "high" and "very high"). Values equal to or greater than 75% are classified solely as "very high" (Figure 3.12D). The model can easily be adapted to include additional fuzzy sets for porosities less than 30% (e.g., "very low").

Isostatic Flexure. It is difficult to separate compaction from isostatic loading (a point that is underscored by the paucity of such data in the literature) when measuring subsidence. The effect of isostatic compensation is best observed at rivers with abundant sediment influx. A regional comparison of the coastline flanking the river makes the point that, while compaction is certainly occurring at the site of deposition, isostatic compensation is also occurring at, but not away from, the depocenter. For example, the Mississippi River delivers 2×10^8 tons/yr of sediment to the Gulf of Mexico (Milliman and Meade, 1983; Milliman and

Syvitski, 1992). While numerous, independent analyses of eustatic rise show similar rates of change between 1 and 1.5 mm/yr (Gutenberg, 1941; Fairbridge and Krebs, 1962; Hicks, 1978; Gornitz et al., 1982), the average rate of subsidence for the Mississippi delta region is 9.4 mm/yr (Wells, 1996), or about 8 mm/yr corrected for eustasy. Subsidence drops, moving laterally away from Louisiana and away from high sediment influx, to about 0.5 mm/yr (Florida-Alabama border; Anderson et al., 2004) and 0.1 to 5 mm/yr (central Texas; Anderson et al., 2004). The same observation is made along the eastern coast of China. The Yangtze River delivers 4.8 x 10^8 tons/yr of sediment to the ECS margin. On the inner shelf near the river mouth, subsidence rates vary between 1.6 and 4.4 mm/yr (Stanley and Chen, 1993). On the outer margin, the rates drop to 0.3 mm/yr (Berne et al., 2002). Along the coast, north and south of the Yangtze, regional uplift is reported as high as 3 mm/yr (Wang and Wang, 1982; Kim, 1987; Congxian et al., 1991).

De-coupling isostatic flexure from total basinal subsidence (i.e., tectonic or thermal) has been addressed by the application of differential equations with techniques such as backstripping using variables such as flexural rigidity, density of mantle, average stratal density, density of water column, gravity acceleration, and elastic thickness (e.g., Holt and Stern, 1991; Peper, 1993; Csato et al., 1994, Lavier et al., 2000; Lee, 2003). Backstripping is usually applied to basins on a much larger scale (kilometers-thick strata representing millions of years) and not considered appropriate for the thin successions and small time-scale of interest in this investigation. Similar to the fuzzy stratigraphic model FUZZIM (Nordlund and Silvfersparre, 1994; Nordlund, 1996; 1999a; 1999b), *fuzzy*PEACH applies a simple hydrostatic approach to simulate isostatic flexure (i.e., the compensating mass density is determined only by the topographic load directly above it; Airy, 1855; Li et al., 2004). The

quantification of values for each of the three subsidence components on various continental margins is lacking in the literature. However, some general ratios were observed using the regional seismic dataset from the ECS margin (see Figure 3.14), combined with published values for sediment accumulation and total subsidence. The FIS rules were written based on these relationships. During each time step, vertical displacement related to isostasy is simulated using a single FIS (Figure 3.12E) containing three rules to determine cumulative stratal thickness and vertical displacement.

IF thin THEN subside little
IF moderate THEN subside some
IF thick THEN subside a lot

The rule premise (left) defines the thickness of a stratal unit. The conclusion (right) simulates isostatic compensation by applying downward displacement of the sediment column for each 1-km-square grid cell at the end of each time step (after compaction). The two variables of the rules (i.e., stratal thickness and vertical displacement) contain multiple fuzzy sets. The boundary of each set is determined by a MF. The geological data and/or justification(s) for these sets (domain variables and set boundaries) are discussed below.

The results of load-driven subsidence are observed in the shallow strata of regional seismic profiles of the ECS margin. Subsidence rates between 1.6 and 4.4 mm/yr on the inner margin near the mouth of the Yangtze River (Stanley and Chen, 1993) are roughly 10% of sedimentation rates (between 10 and 54 mm/yr; DeMaster et al., 1985). The tectonic component of subsidence at this location is regarded as negligible due to its location near the tectonic hinge associated with regional uplift along the east coast of China (Wang, 1980; Congxian et al., 1991). This range of subsidence is similar to other marginal basins receiving a high sediment input, including the northern Gulf of Mexico from south Texas to western

Figure 3.14. A) Strike-oriented stratigraphic cross-section from the middle of the ECS margin. Inset shows estimate of tectonic (thermal) subsidence from a portion of the margin receiving little sediment. B) Estimation of isostatic adjustment based on stratal geometry and offset from the transgression between OIS 6 and 5.

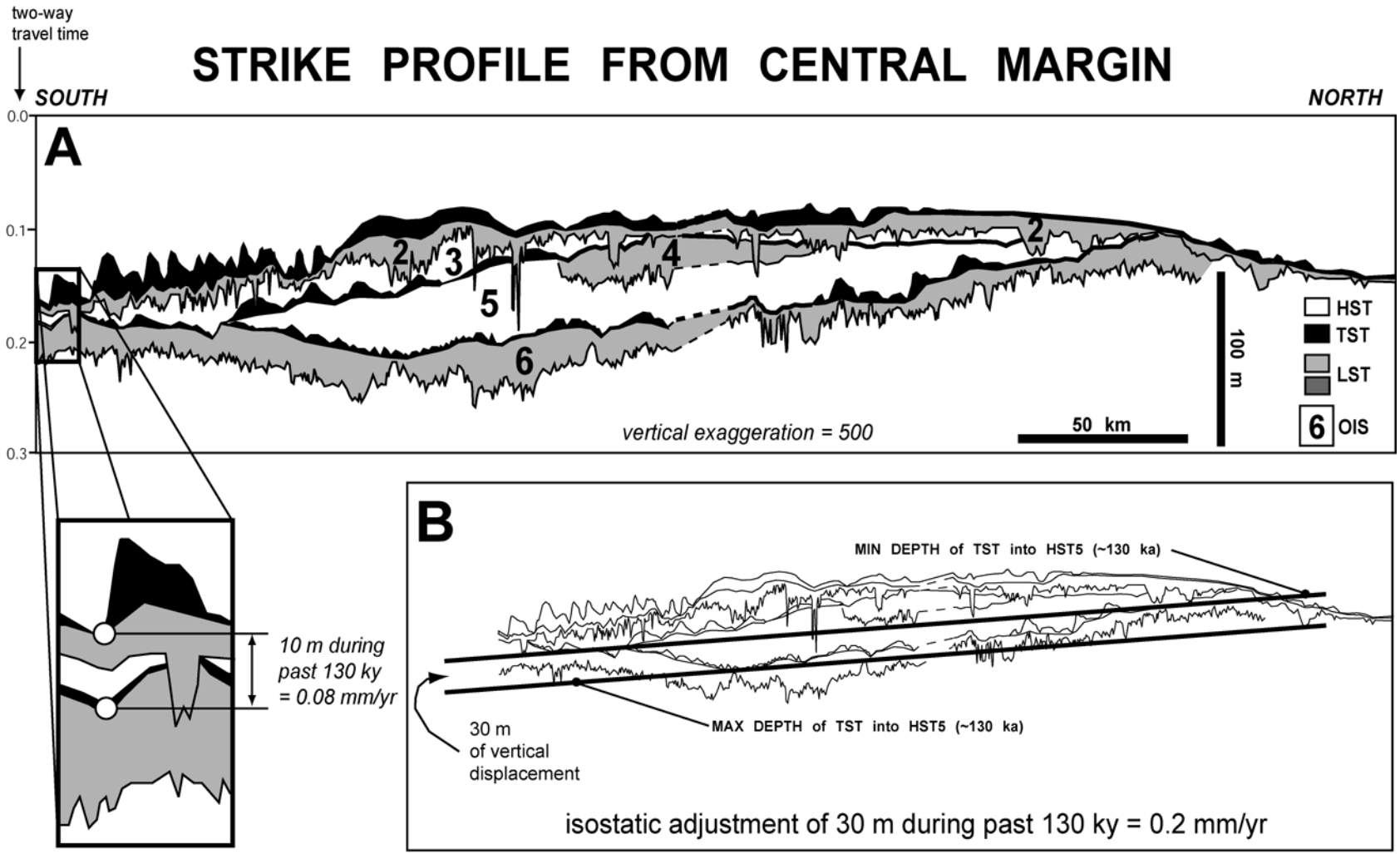
two-way
travel time
STRIKE PROFILE FROM CENTRAL MARGIN
SOUTH
NORTH
A
0.0
0.1
0.2
0.3
2
3
4
5
6
2
HST
TST
LST
6 OIS
100 m
vertical exaggeration = 500
50 km
10 m during
past 130 ky
= 0.08 mm/yr
B
MIN DEPTH of TST into HST5 (~130 ka)
MAX DEPTH of TST into HST5 (~130 ka)
30 m
of vertical
displacement
isostatic adjustment of 30 m during past 130 ky = 0.2 mm/yr

Louisiana (up to 5 mm/yr; Anderson et al., 2004), the northern Gulf of Mexico at the mouth of the Mississippi River (up to 8 mm/yr; Wells, 1996), the Ganges River delta plain in the Bengal Basin (up to 5.5 mm/yr; Alam, 1996), and the Canterbury Plains in New Zealand (up to 2 mm/yr; Browne and Naish, 2003). On the middle and outer ECS margin, the subsidence rate is 0.3 mm/yr (Berne et al., 2002). When corrected for tectonic subsidence (0.3 mm/yr - 0.1 mm/yr = 0.2 mm/yr; see Figure 3.14), this value is a little more than 5% of the sedimentation rate of 3 mm/yr (DeMaster et al., 1985). Elsewhere on the margin, sedimentation is negligible and isostatic loading is assumed to be zero.

Isostatic adjustment is simulated using the trends between sediment accumulation and isostatic adjustment observed on the ECS margin. These data, at least for this investigation, provide a range of coefficients ranging between 0 and 10% that determine the amount of vertical displacement, at the end of each time step, based on sediment accumulation rate (i.e., total thickness / time elapsed). Regional seismic profiles verify subsidence rates presented above by measuring total downward displacement in the strata relative to a structural datum (e.g., the transgressive surface between OIS 6 and OIS 5; Figure 3.14). This method is independent of compaction. Therefore, after correcting for tectonic displacement, this method is used as a proxy for isostatic flexure (at least for depositional conditions analogous to the ECS margin) and is incorporated easily into *fuzzy*PEACH. Based on this proxy of isostatic adjustment, sediment accumulation (stratal thickness) defines sediment loading (vertical adjustment of sediment column). At the end of each time step, sediment accumulation is determined for that particular time step. Three fuzzy sets define (in millimeters) stratal thickness: 1) “thin”, 2) “moderate”, and 3) “thick.” The ranges of ECS sediment accumulation (presented above) define these linguistic terms (i.e., sediment

accumulation about 0.2 mm on outer margin and up to 5 mm on inner margin). Therefore, full membership (MF=1) in each fuzzy set occurs at 0 mm ("thin"), 0.2 mm ("moderate") and 5 mm ("thick"). Partial membership (overlap in adjacent fuzzy sets where MF=1) is defined along the continuum of values between 0 and 0.2 mm (membership in both "thin" and "moderate") as well as 0.2 and 5 mm (membership in both "moderate" and "thick"). Based on these thicknesses, *fuzzy*PEACH calculates the approximate percentage of expected vertical displacement by multiplying the sediment accumulation rate with the appropriate coefficient (in this case, ≤10%). Simulated isostasy displaces the entire vertical sediment column at each of the model's 1-km-square grids. The percentage of downward adjustment is defined (in meters) using three fuzzy sets: 1) "subside little", 2) "subside some", and 3) "subside a lot" (Figure 3.12E). The values for these sets are defined by the rate of subsidence relative to sediment accumulation on the inner margin that, relative to the observations presented above, was higher on the inner margin (~10%), lower on the middle to outer margin proximal to the deltaic depocenter (~5%), and negligible on portions of the outer shelf distal to the deltaic depocenter (~0%). Therefore, full membership (MF=1) in each fuzzy set is set similarly at 0% ("subside little"), 5% ("subside some") and 10% ("subside a lot"). Partial membership (overlap in adjacent fuzzy sets where MF=1) is defined along the continuum of values between 0 and 5% (membership in both "subside little" and "subside some") as well as 5 and 10% (membership in both "subside some" and "subside a lot").

3.3 RESULTS

Sensitivity testing was used, in part, to define four of the 15 variables used in *fuzzy*PEACH, (fluvial sediment volume, fluvial grain size, deltaic sediment volume, and deltaic grain size); however, the primary purpose of the sensitivity tests was to investigate the relationship between stratigraphic architecture and variables associated with relative sea level (eustasy and tectonics), sediment influx, and margin physiography. A total of 18 sea level curves were analyzed using various magnitudes and periodicities (4 shapes x 2 magnitudes x 4 periodicities). Curve functions include simple sinusoids, sinusoid with asymmetry on falling limb, sinusoid with asymmetry on rising limb and complex, symmetric sinusoids with superimposed parasequences (Figure 3.10). Sea level periodicities varied between 1, 2, 3 and 4 sea level cycles (i.e., highstand to highstand) per model. Magnitudes of each curve were either 120 or 180 m below modern sea level. Multiple permutations of sedimentation rates ranging between 1 x 10^8 and 5 x 10^8 tons/yr and tectonic subsidence rates ranging between 0 and 2.4 mm/yr were applied to each sea level scenario described above. Although the geometry of the margin was held constant throughout these sensitivity tests, variations in sea level cycle periodicity changed the rate at which sea level rose and fell and, therefore, affected the speed of lateral shoreline translation across the margin. The rate of shoreline movement can also be affected by margin gradient (e.g., shoreline movement decreases as the margin gradient increases and vice versa). Sea level periodicity can, therefore, simulate stratigraphic response to different margin gradients with a constant geometry. Similarly, variations in sea level magnitude have the potential to either leave the shelf-slope break submerged or exposed. Sea level elevations below the shelf-slope break create the potential for incision and sedimentary bypass. Therefore, sea level magnitude can be used to simulate different depths for the shelf-slope break on a margin that has remained constant. Using this

approach, sensitivity testing was able to use sea level as a proxy for margin geometry to observe the stratigraphic response to numerous margin configurations while leaving the actual geometry unchanged.

General stratigraphic trends from the sensitivity testing were consistent with the general concepts of both seismic stratigraphy (e.g., Payton, 1977; Brown and Fisher, 1980; Berg and Woolverton, 1985) and sequence stratigraphy (e.g., Vail, 1987; Posamentier and Vail, 1988; Posamentier et al., 1988; Van Wagoner et al., 1988; Van Wagoner et al., 1990; Posamentier and Allen, 1999). Onlapping stratal patterns were formed during all conditions of both rises, falls, and stillstands of sea level. Downstepping stratal patterns were products of forced regressions (e.g., Hunt and Tucker, 1992; Catuneanu, 2003) as falling sea level forced a basinward shift in the shoreline. A combination of aggradational and progradational strata as well as downlapping stratal patterns are associated with periods of slow sea level rise (normal regression; e.g., Hunt and Tucker, 1992; Catuneneau, 2003). Retrogradation (backstepping) patterns dominate periods of faster rates of sea level rise. The general stratal response to increasing eustatic periodicity was thinner strata and faster rates of shoreline translation across the margin. This resulted in higher progradation rates and lower aggradation during sea level fall (forced regression) as well as higher rates of backstepping and lower rates of progradation and aggradation during eustatic rise. Therefore, normal regressions become less noticeable under increasing eustatic rate changes (but occurred as parasequences during eustatic slowdowns and stillstands). Exposure of the shelf-slope break during lowstands in sea level bypassed sediment from the exposed shelf basinward of the shelf-slope break and onto the continental slope. The initial *fuzzy*PEACH model did not simulate incision; however, subsequent versions of the model described here, tested the preliminary

development of an erosion component (not presented in this paper). These "incisions" constrained avulsion and led to limited floodplain sedimentation. Further development of a dedicated FIS for erosion and incision will continue and be included in future versions of *fuzzy*PEACH.

In addition to sea level fluctuations, strata also responded to changes in tectonic subsidence and sedimentation rate. Stratal thickness as well as rate of basinward translation of the shoreline was proportional to sediment influx (i.e., higher sedimentation led to quicker rates of accommodation infill and basinward translation of the shoreline). Where sedimentation rates were high, shoreline regression occurred during periods of rising sea level. Increased tectonic subsidence also created thicker strata by increasing accommodation and, therefore, limiting the basinward movement of the shoreline. As sedimentation rates were steadily increased, strata steadily moved basinward and eventually deposited sediment beyond the shelf-slope break. As subsidence rates steadily increased, strata were deposited farther from the shelf-slope break and strata become much thicker than simulations with the same sediment influx and lower, or no, subsidence. Shoreline translation rates increased with higher sediment input but decreased with increased tectonic subsidence. These results are analogous to the stratal geometry typical of passive continental margins (e.g., Burke and Drake, 1974; Weimer and Posamentier, 1990; Watkins et al., 1992).

3.3.1 Selected Examples of Sensitivity Testing

Hundreds of *fuzzy*PEACH simulations were completed during the course of this investigation. Each of these contributed to the general understanding of *fuzzy*PEACH's ability to produce reasonable stratigraphic architecture under various permutations of sea level, tectonic subsidence, and sedimentation. A subset of eight simulations is presented in

this section. These results demonstrate the model's capabilities and, more importantly, provide insight into the evolution of continental margin stratigraphy. The FIS controlling avulsions (Figure 3.12B) in the simulations was turned off during these particular simulations (i.e., avulsion did not occur during one complete sea level cycle). This was done to present an idealized, dip-oriented cross-section analogous to many other two- and three-dimensional stratigraphic models (e.g., Jervey, 1988; Kendall et al., 1991; Reynolds et al., 1991; Syvitski and Daughney, 1992; Steckler et al., 1993; Bowman and Vail, 1999; Penn and Harbough, 1999; Steckler, 1999; Goodbred et al., 2003). The fuzzy-logic-controlled avulsions create a more realistic stratigraphy; however, it is easier to establish process-relationship between the other modeled parameters (i.e., eustasy, tectonic subsidence, and sediment influx) under simplified conditions without high-frequency avulsions. For this reason, simulations without fuzzy avulsion control are presented here to demonstrate the overall utility of *fuzzy*PEACH (although simulations with fuzzy logic avulsion control are presented in the next section of this paper). Sensitivity testing throughout the investigation without avulsion control was able to create baseline data for comparison with simulations with an active avulsion FIS. Isolation of the fuzzy avulsion signal in simulated stratigraphy provided the ability to observe its effect on the overall stratigraphic architecture and determine its effectiveness (see *Discussion*).

The results of the eight sensitivity simulations presented in this section (i.e., two rates of sediment supply, two rates of subsidence, and two different eustatic curves) are presented in Table 3.1. Two different eustatic curves spanning 200 ky were used. One curve is a simple sinusoid spanning a single sea level cycle (highstand to highstand) chosen because of its simplicity. The other curve is a complex sinusoid with an asymmetry on the falling limb that

Table 3.1. Observations from eight simulations selected to illustrate the sensitivity of stratigraphic architecture generated by *fuzzy*PEACH to variable rates of sea level, tectonic subsidence, and sediment influx.

shape of sea level curve	simple sinusoid	simple sinusoid	simple sinusoid	simple sinusoid	asymmetric sinusoid	asymmetric sinusoid	asymmetric sinusoid	asymmetric sinusoid
frequency of sea level curve	195 ky	195 ky	195 ky	195 ky	195 ky	195 ky	195 ky	195 ky
magnitude of sea level curve	120 m	120 m	120 m	120 m	120 m	120 m	120 m	120 m
tectonic subsidence	0	0	2.4 mm/yr	2.4 mm/yr	0	0	1.2 mm/yr	1.2 mm/yr
sediment influx	160 million tons/yr	320 million tons/yr	160 million tons/yr	320 million tons/yr	160 million tons/yr	320 million tons/yr	160 million tons/yr	320 million tons/yr
width of delta plain	75 km	140 km	75 km	160 km	90 km	160 km	90 km	150 km
area of delta	2,210 km^2	7,710 km^2	2,210 km^2	10,050 km^2	3,180 km^2	10,050 km^2	3,180 km^2	8,836 km^2
shoreline @ lowstand *(distance from modern shoreline)*	500 km	500 km	280 km	350 km	500 km	500 km	370 km	430 km
shoreline @ end of model *(distance from modern shoreline)*	280 km	390 km	200 km	310 km	290 km	390 km	230 km	320 km
max stratal thickness on margin	80 m	125 m	120 m	175 m	90 m	125 m	115 m	145 m
location of max thickness *(distance from modern shoreline)*	275 km	400 km	200 km	310 km	290 km	400 km	240 km	320 km
max thickness @ shelf-slope break	50 m	75 m	<10 m	40 m	50 m	80 m	20 m	75 m
depth of shelf-slope break @ end of model	110 m	65 m	280 m	240 m	110 m	65 m	200 m	150 m

also spans a single sea level cycle (highstand to highstand). The asymmetry of the complex sinusoid causes a slowdown in the rate of sea level fall and represents the general trend from oxygen isotope stages 5 to 1 (Figure 3.11). Tectonic subsidence rates varied between zero, 1.2 and 2.4 mm/yr (considered as "none", "moderate", and "high", respectively). An intermediate value of 1.2 mm/yr was also chosen in order to observe the stratal response under conditions of lower subsidence. Two sedimentation rates were used in these specific simulations. "Moderate" sedimentation was defined at 1.6×10^8 tons/yr and "high" sedimentation rate was double the rate (3.2×10^8 tons/yr). These rates were chosen because one is twice the other, they are similar to rates of modern rivers (e.g., Mekong and Irrawaddy; Figure 3.9), and are both evenly distributed on either side of 2.4×10^8 tons/yr (the average rate of the world's top 25 rivers in terms of sediment load; Milliman and Meade, 1983; Milliman and Syvitski, 1992).

Simple Sinusoid. Four simulations included a comparison of stratigraphic response to moderate and high sediment rates as well as a rate of tectonic subsidence that was either zero or high (2 mm/yr). The four permutations were as follows: 1) high sediment supply and no tectonic subsidence, 2) high sediment supply and high tectonic subsidence, 3) moderate sediment supply and no tectonic subsidence, and 4) moderate sediment supply and high tectonic subsidence. Synthetic, dip-oriented cross-sections from the middle of the margin (down the axis of the channel) are presented in Figure 3.15. Observations from these cross-sections (including thickness of strata, basinward extent of shoreline, width and area of delta) are included in Table 3.1. Under conditions of no tectonic subsidence, doubling the rate of sediment influx (from moderate to high) almost doubled the longitudinal (shore-normal) width of the delta plain and increased the area by more than a factor of three. The maximum

Figure 3.15. Synthetic, dip-oriented cross sections from the middle margin simulating stratal evolution during a simple sinusoidal sea level cycle. Four sensitivity test results are shown: A) high sediment influx (320 million tons per year) and no tectonic subsidence, B) moderate sediment supply (160 million tons per year) and no tectonic subsidence, C) high sediment supply and high tectonic subsidence (2.4 mm/yr), and D) moderate sediment supply and high tectonic subsidence.

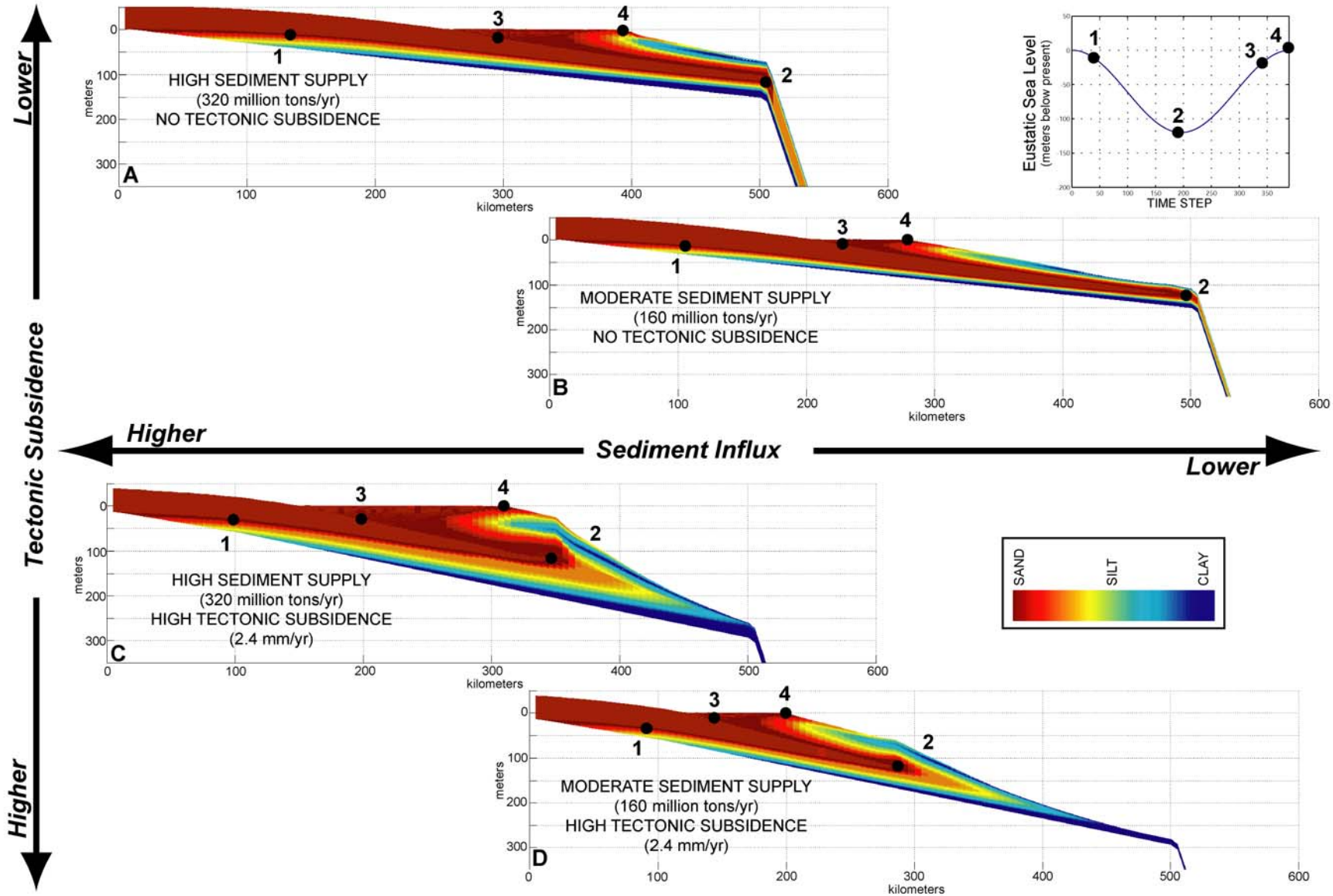
Lower
Tectonic Subsidence
Higher
Higher
Sediment Influx
Lower
HIGH SEDIMENT SUPPLY
(320 million tons/yr)
NO TECTONIC SUBSIDENCE
A
MODERATE SEDIMENT SUPPLY
(160 million tons/yr)
NO TECTONIC SUBSIDENCE
B
HIGH SEDIMENT SUPPLY
(320 million tons/yr)
HIGH TECTONIC SUBSIDENCE
(2.4 mm/yr)
C
MODERATE SEDIMENT SUPPLY
(160 million tons/yr)
HIGH TECTONIC SUBSIDENCE
(2.4 mm/yr)
D
meters
kilometers
Eustatic Sea Level
(meters below present)
TIME STEP
SAND
SILT
CLAY
1
2
3
4

stratal thickness increased significantly (between 40 and 50 m), was deposited farther basinward, and produced a shallower shelf-slope break (twice as shallow as the simulation with half the sediment influx). Under conditions of high subsidence, a high sediment influx also created a delta width twice as wide, with an area greater by over a factor of four. These values are similar to those in simulations without tectonic subsidence, however, neither the deltaic depocenters nor the lowstand shorelines extended as far basinward. As a result, minimal sediment was deposited on the outer margin and potentially bypassed to the deep basin. Tectonic subsidence also forced the shelf-slope break downward (into deeper water). In all four scenarios described above, the location of the shoreline at the end of the model run coincided with the thickest strata on the margin (Figure 3.15). Shoreline locations on the margin with respect to time step during the model are plotted, for all four simulations, in Figure 3.16. It is important to remember that avulsion control was not active during these simulations. The result was strata that were not as laterally extensive and, therefore, thicker.

A quantitative comparison of the synthetic, dip-oriented cross-section in Figure 3.15 is plotted in Figure 3.16 and makes rates of shoreline movement easier to identify. The most obvious trend in these data is that higher sedimentation rates placed the location of the shoreline farther basinward and, thus, increased the rate of translation of the shoreline across the margin. During tectonic subsidence, the rates of movement decreased because the shoreline did not make it to the outermost margin near the shelf-slope break (as it did during conditions without tectonic subsidence). During sea level rise, the rate of landward translation under conditions of tectonic subsidence were similar, although the shoreline was farther basinward under conditions of higher sediment influx. The rate of landward translation of the shoreline during high sediment influx and no tectonism was a little higher

Figure 3.16. Shoreline position on the simulated margin for each of the four scenarios presented in Figure 3.15. Points 1-4 on the graph correspond to points 1-4 on the sea level curve.

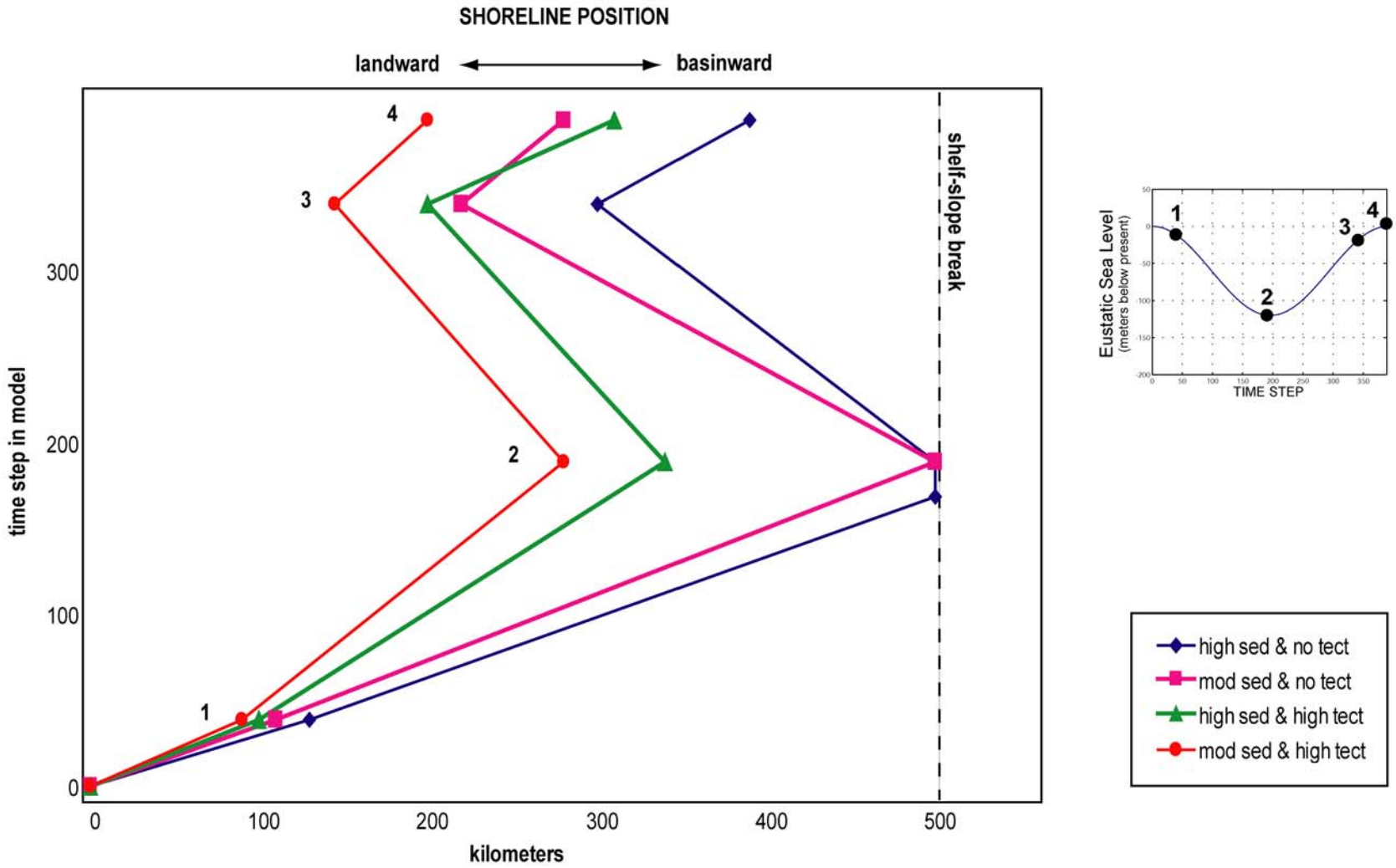
SHORELINE POSITION
landward
basinward
shelf-slope break
time step in model
kilometers
0
100
200
300
400
500
1
2
3
4
Eustatic Sea Level
(meters below present)
TIME STEP
high sed & no tect
mod sed & no tect
high sed & high tect
mod sed & high tect

but similar. The departure from this trend during rising sea level occurred with moderate sediment influx and no subsidence. The rate was much faster as the shoreline moved farther landward during the same amount of time. As the rate of sea level rise slowed down approaching highstand (point 3 on the sea level curve; Figures 3.15 and 3.16), the shoreline migrated basinward. Models with moderate sediment influx (with and without tectonic subsidence) had identical rates. Models with high sediment influx (with and without tectonic subsidence) also shared similar rates of shoreline movement, although these rates were higher with a higher sediment influx. At the end of the model, the landward-most shoreline was from moderate sediment input and tectonic subsidence and the most basinward shoreline was from high sediment conditions and no tectonic subsidence. The remaining shorelines were between these two endpoint locations, although the higher sediment supply with subsidence was farther basinward by about 20 km than the moderate sedimentation rate without subsidence.

Complex, Asymmetric Sinusoid. Four simulations included a comparison of stratigraphic response to moderate and high sediment rates as well as a rate of tectonic subsidence that was either zero or high (2 mm/yr). The four permutations were as follows: 1) high sediment supply and no tectonic subsidence, 2) high sediment supply and moderate tectonic subsidence, 3) moderate sediment supply and no tectonic subsidence, and 4) moderate sediment supply and moderate tectonic subsidence. Synthetic, dip-oriented cross-sections from the middle of the margin (down the axis of the channel) are presented in Figure 3.17. Observations from these cross-sections (including thickness of strata, basinward extent of shoreline, width and area of delta) are included in Table 3.1. Under conditions of no tectonic subsidence, doubling the rate of sediment influx (from moderate to high) almost

Figure 3.17. Synthetic, dip-oriented cross sections from the middle margin formed during an asymmetric (sawtooth) sinusoidal sea level cycle. Four sensitivity test results are shown: A) high sediment influx (320 million tons per year) and no tectonic subsidence, B) moderate sediment supply (160 million tons per year) and no tectonic subsidence, C) high sediment supply and high tectonic subsidence (2.4 mm/yr), and D) moderate sediment supply and high tectonic subsidence.

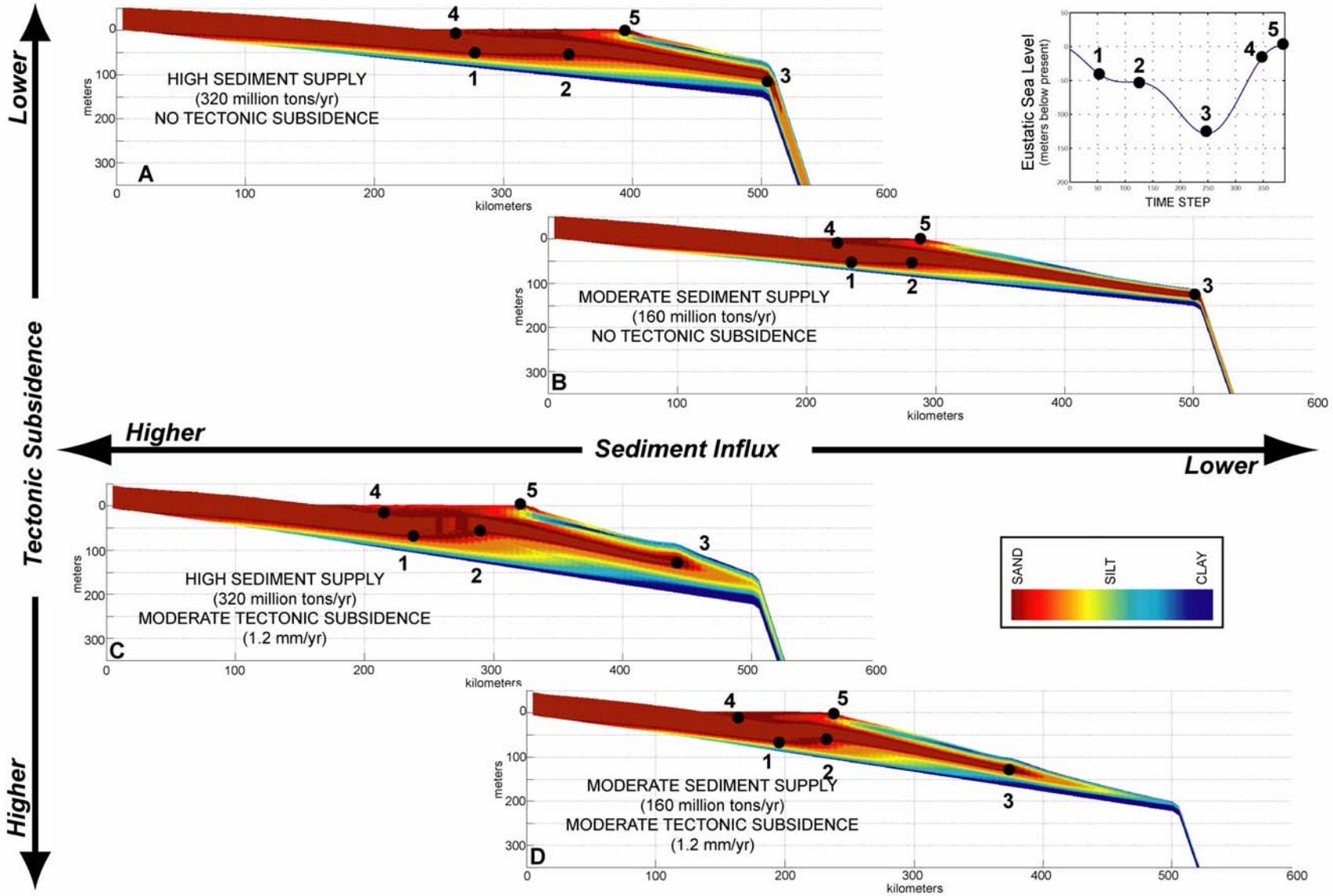
Lower
Tectonic Subsidence
Higher
HIGH SEDIMENT SUPPLY
(320 million tons/yr)
NO TECTONIC SUBSIDENCE
A
MODERATE SEDIMENT SUPPLY
(160 million tons/yr)
NO TECTONIC SUBSIDENCE
B
Higher
Sediment Influx
Lower
HIGH SEDIMENT SUPPLY
(320 million tons/yr)
MODERATE TECTONIC SUBSIDENCE
(1.2 mm/yr)
C
MODERATE SEDIMENT SUPPLY
(160 million tons/yr)
MODERATE TECTONIC SUBSIDENCE
(1.2 mm/yr)
D
meters
kilometers
Eustatic Sea Level
(meters below present)
TIME STEP
SAND
SILT
CLAY

doubled the longitudinal (shore-normal) width of the delta plain and increased the area by more than a factor of three. The maximum stratal thickness increased significantly (by about 20 m) and was deposited farther basinward under high sediment conditions. As a result, thicker strata at the shelf-slope break created an end-model elevation twice as shallow as the simulation with half the sediment influx. Under conditions of high subsidence, a high sediment influx also created a delta width almost twice as wide with an area twice as large. These values are similar to those in simulations without tectonic subsidence, however, neither the deltaic depocenters nor the lowstand shorelines extended as far basinward. As a result, minimal sediment was deposited on the outer margin. Tectonic subsidence also forced the shelf-slope break downward. Similar to the sinusoid sea level curve, the location of the shoreline at the end of the four model runs described above, coincided with the thickest strata on the margin (Figure 3.17). Shoreline locations on the margin with respect to time step during the model are plotted, for all four simulations, in Figure 3.18. It is important to remember that avulsion control was not active during these simulations. The result was strata that were not as laterally extensive and, therefore, thicker.

A quantitative comparison of the synthetic, dip-oriented cross-section in Figure 3.17 is plotted in Figure 3.18 and makes rates of shoreline movement easier to identify. The most obvious trend in these data is that higher sedimentation rates placed the location of the shoreline farther basinward and, thus, increased the rate of translation of the shoreline across the margin. With one exception, this occurred from the onset of sea level fall at the beginning of the model, through stillstand (between points 1 and 2 on the sea level curve; Figure 3.17 and 3.18) to the point of maximum regression (point 3). The exception to this trend was during moderate sediment influx and no tectonic subsidence when the

Figure 3.18. Shoreline position on the simulated margin for each of the four scenarios presented in Figure 3.17. Points 1-5 on the graph correspond to points 1-5 on the sea level curve.

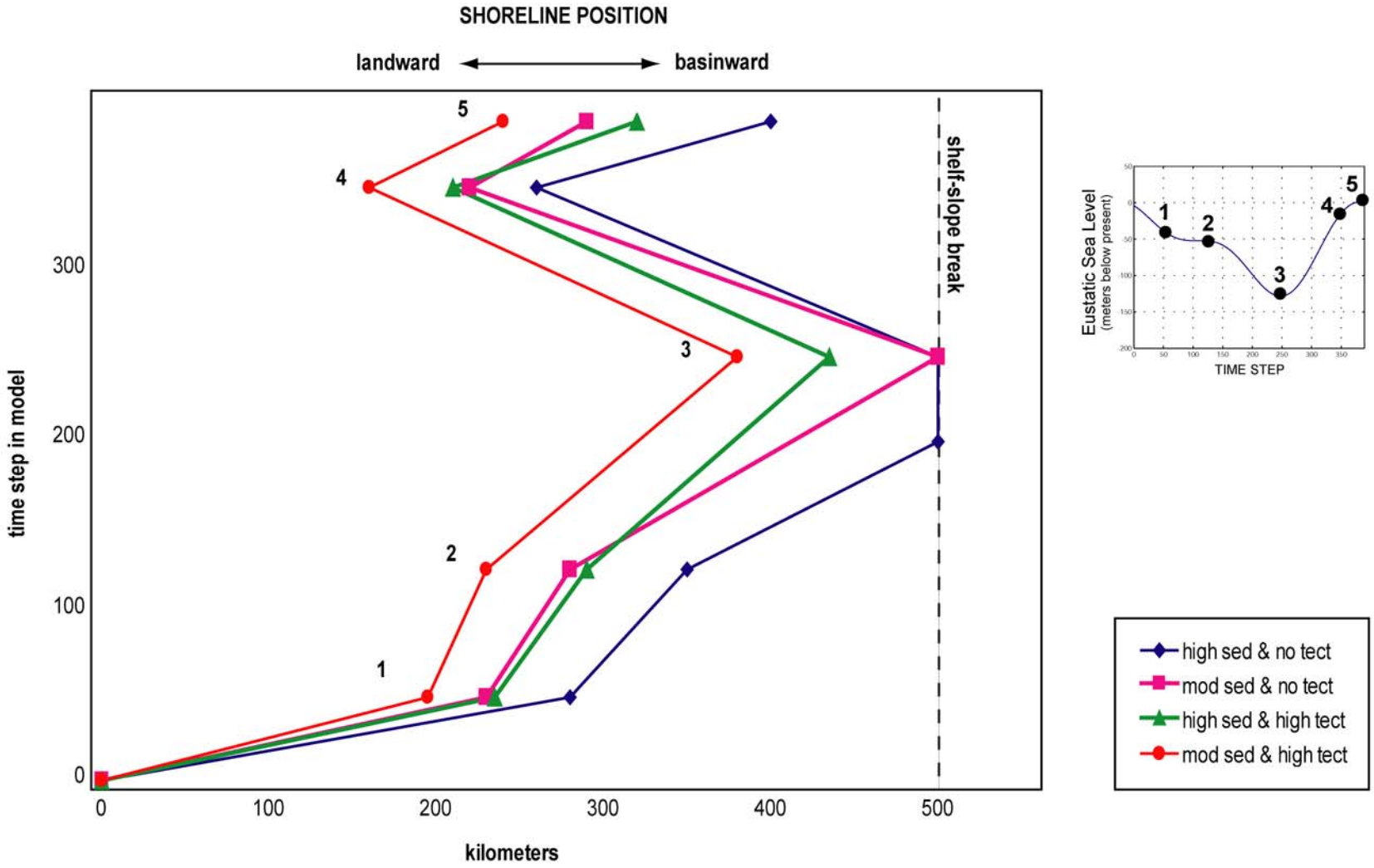
SHORELINE POSITION
landward
basinward
shelf-slope break
time step in model
kilometers
0
100
200
300
400
500
1
2
3
4
5
Eustatic Sea Level
(meters below present)
TIME STEP
high sed & no tect
mod sed & no tect
high sed & high tect
mod sed & high tect

shorelinewas located farther landward at the end of stillstand and covered more distance to reach the shelf-slope break at the point of maximum regression. During sea level rise, this same scenario (moderate sediment and no subsidence) moved across the margin at an even faster rate until the rate of sea level rise slowed as it approached highstand (point 4 on the sea level curve; Figure 3.17 and 3.18). The shorelines were translated basinward (normal regression) at a similar rate for all four simulations during this period of slower sea level rise (between points 4 and 5 on the sea level curve). At the end of the model, the landward-most shoreline was from moderate sediment input and tectonic subsidence and the most basinward shoreline was from high sediment conditions and no tectonic subsidence. The remaining shorelines were between these two endpoint locations, although the higher sediment supply with subsidence was farther basinward by about 20 km than the moderate sedimentation rate without subsidence.

3.3.2 Selected Examples of Models Constrained to the ECS Margin

The results of extensive sensitivity testing of *fuzzy*PEACH simulations, not all presented in this paper, establish the general response of a passive continental margin to multiple scenarios of sea level fluctuation and a range of tectonic subsidence variables and sediment influx common for passive margins. Previous work on numerous continental margins, both modern and ancient, constrained both the input and output of the model. The collective field of knowledge from these investigations provided the range of geologically reasonable variables that defined the fuzzy sets (i.e., the input). Results from these same studies (output) helped validate *fuzzy*PEACH simulations and determine if the model output produced stratigraphy observed (or expected) on continental margins. The extensive dataset from the ECS margin provides an opportunity to validate the results of *fuzzy*PEACH in an area where

relative sea level variables are well constrained. Margin physiography remained constant, eustatic fluctuation is well understood, and tectonic subsidence was negligible (0.1 mm/yr; Figure HMW4). Therefore, simulations run under conditions hypothesized to exist on the ECS margin during the last 195 ky (last highstand of OIS 7 to present) focus on stratigraphic response to different rates of sediment influx. Sedimentation rates were constrained by those of the modern Yangtze River (4.8×10^8 tons/yr ; Milliman and Meade, 1983; Milliman and Syvitski, 1992). Sedimentation rates, half as much, are suggested to represent conditions prior to 6 ka (Hori et al., 2001; Saito et al., 2001). For the purpose of these four simulations, a high sedimentation rate refers to 4.8×10^8 tons/yr and low to 2.4×10^8 tons/yr. The results from four of these models are presented in this paper. Two simulations applied 1) moderate and 2) high sediment supplies to the margin through a single fluvial system with limited avulsion (i.e., the FIS controlling avulsion was turned off). Two additional models used the same sediment moderate and high sediment inputs with avulsion controlled by the dedicated FIS (see *Fuzzy Variables, Fuzzy Sets, Fuzzy Inference Systems*).

A collection of synthetic dip- and strike-oriented cross-sections as well as isopach maps from each of the four simulations are presented in Figures 3.19 through 3.30. Observations from these cross-sections (including thickness of strata, basinward extent of shoreline, width and area of delta) as well as general conditions of each of the four models are included in Table 3.2. In general, strata in simulations receiving high sediment influx were about twice as thick as those using moderate sediment supply. Strata deposited during simulations using the FIS to drive avulsion were thinner than those where the fuzzy controller was turned off. However, the lateral extent of units associated with simulations in which avulsion was permitted, was greater during fuzzy avulsion events. This trend is observed in strike-oriented

profiles from each of the models (Figures 3.21, 3.24, 3.27, 3.30) as well as isopach maps (Figures 3.19, 3.22, 3.25, 3.28; Table R2). The location of shorelines during extreme lowstands (OIS 6 and OIS 2) is farther basinward, albeit by only 5 km, during conditions when the avulsion FIS is not operating. Regardless of avulsion, shorelines were located farther basinward under conditions of higher sediment supply. Two distinct, lobate depocenters are identified in dip-oriented profiles from simulations without fuzzy avulsion control (Figures 3.20 and 3.23). When avulsion was permitted, three lobes were formed (Figures 3.26 and 3.29). The geometry of these lobes is more pronounced under conditions of higher sediment supply (regardless of avulsion status).

Figure 3.19. Isopach maps (OIS 6-1) from *fuzzy*PEACH simulation using late Pleistocene sea level data (Figure 3.11A), minimal tectonic subsidence (Figure 3.14A), and a moderate sediment influx (240 million tons/yr). The FIS controlling avulsion (Figure 3.12B) was turned off during this simulation.

MODERATE SEDIMENT SUPPLY (240 tons/yr) and NO AVULSION FIS

ISOPACH MAP for OIS 1
(12 ka to present)

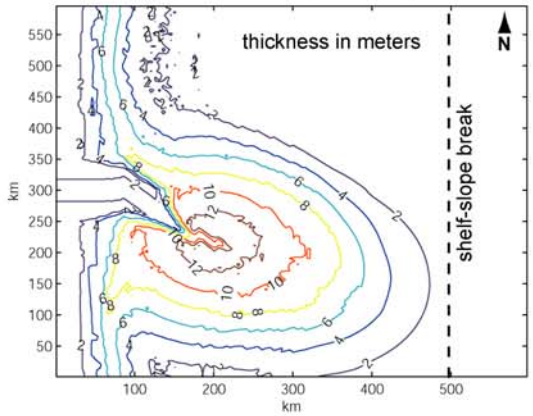

ISOPACH MAP for OIS 2
(24 to 12 ka)

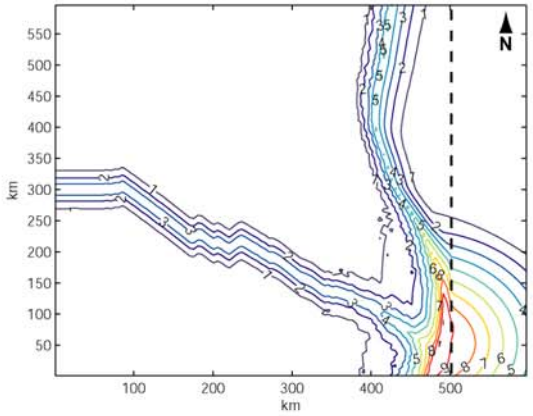

ISOPACH MAP for OIS 3
(59 to 24 ka)

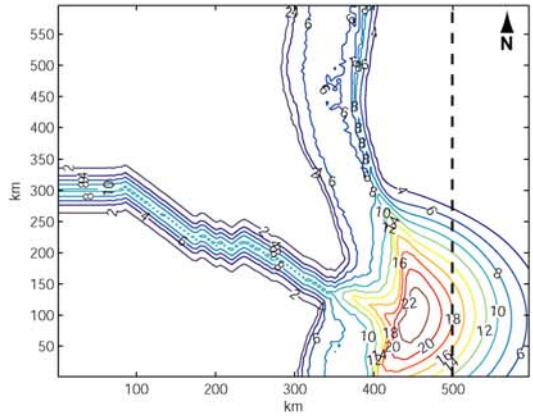

ISOPACH MAP for OIS 4
(71 to 59 ka)

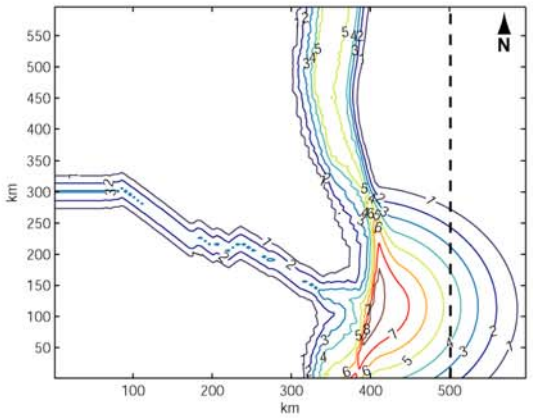

ISOPACH MAP for OIS 5
(128 to 71 ka)

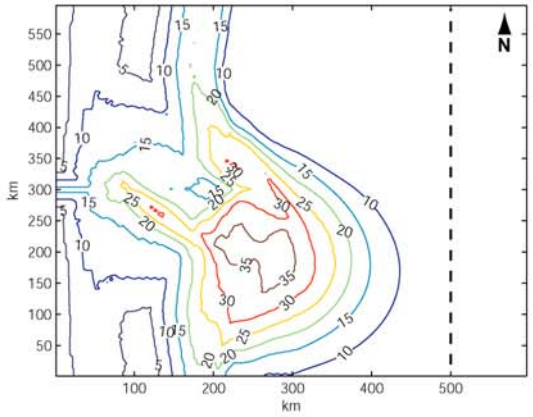

ISOPACH MAP for OIS 6
(186 to 128 ka)

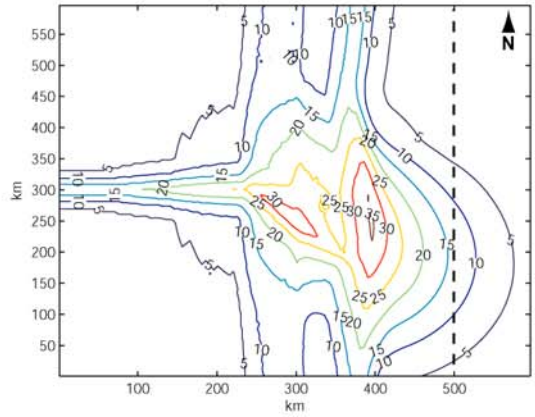

Figure 3.20. Dip-oriented synthetic cross-section from the middle margin simulating stratal evolution during the eustatic signal from the late Pleistocene (Figure 3.11A). Sediment influx was moderate (240 million tons per year), tectonic subsidence was low (<0.1 mm/yr), and the FIS controlling avulsion (Figure 3.12B) was turned off during this simulation.

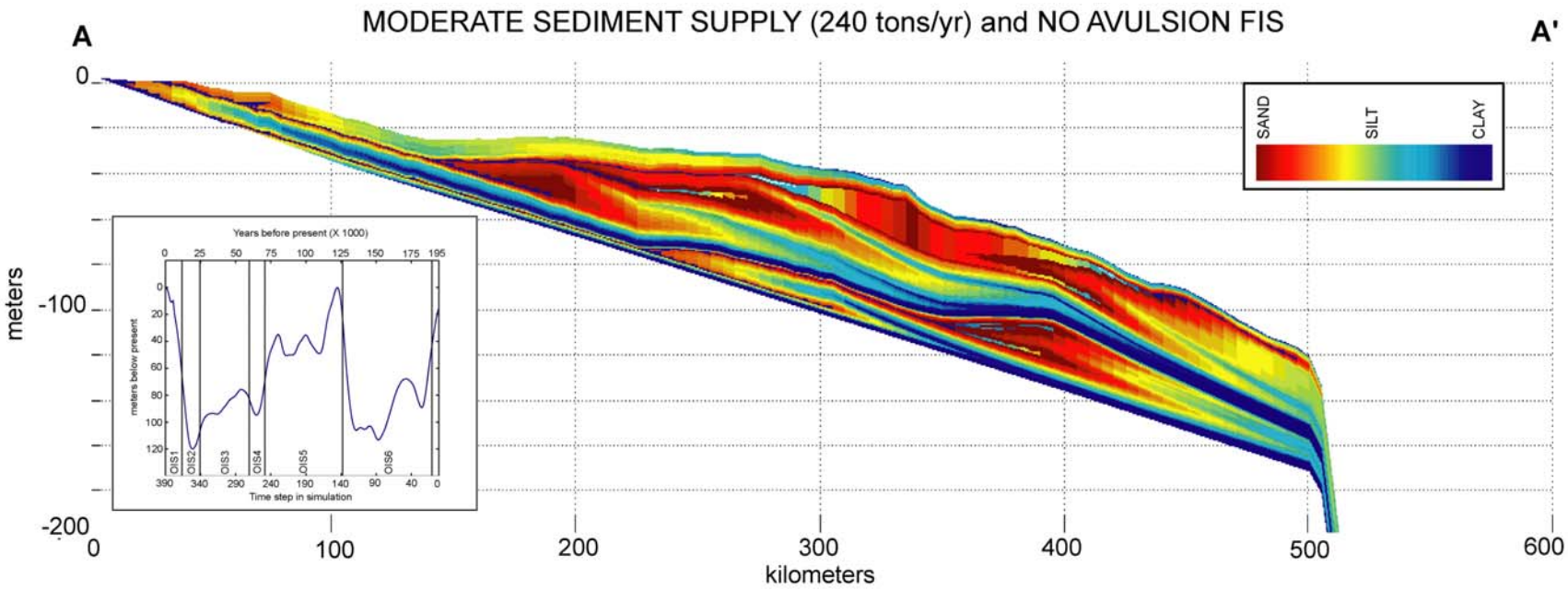
MODERATE SEDIMENT SUPPLY (240 tons/yr) and NO AVULSION FIS
A
A'
SAND
SILT
CLAY
meters
kilometers
Years before present (X 1000)
meters below present
Time step in simulation
OIS1
OIS2
OIS3
OIS4
OIS5
OIS6

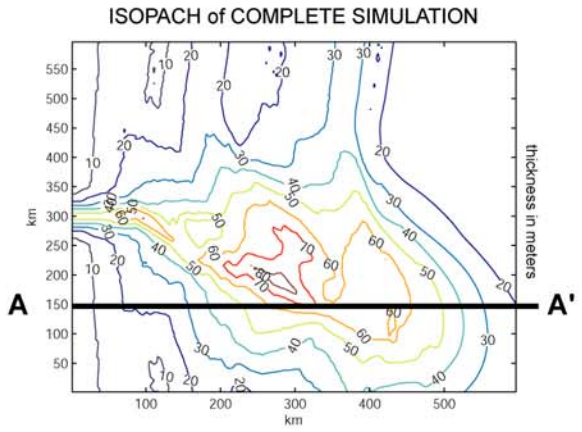
ISOPACH of COMPLETE SIMULATION
A
A'
km
thickness in meters

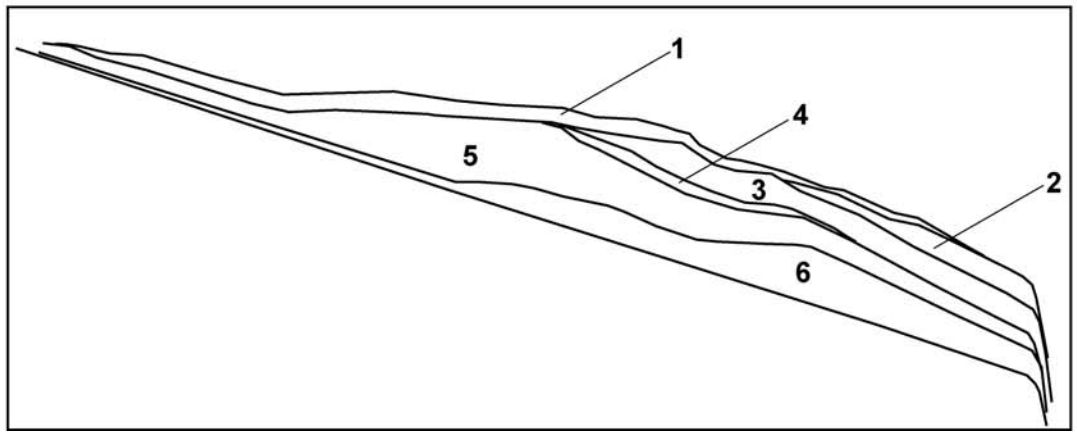
1
2
3
4
5
6

Figure 3.21. Strike-oriented synthetic cross-section from the middle margin simulating stratal evolution during the eustatic signal from the late Pleistocene (Figure 3.11A). Sediment influx was moderate (240 million tons per year), tectonic subsidence was low (<0.1 mm/yr), and the FIS controlling avulsion (Figure 3.12B) was turned off during this simulation.

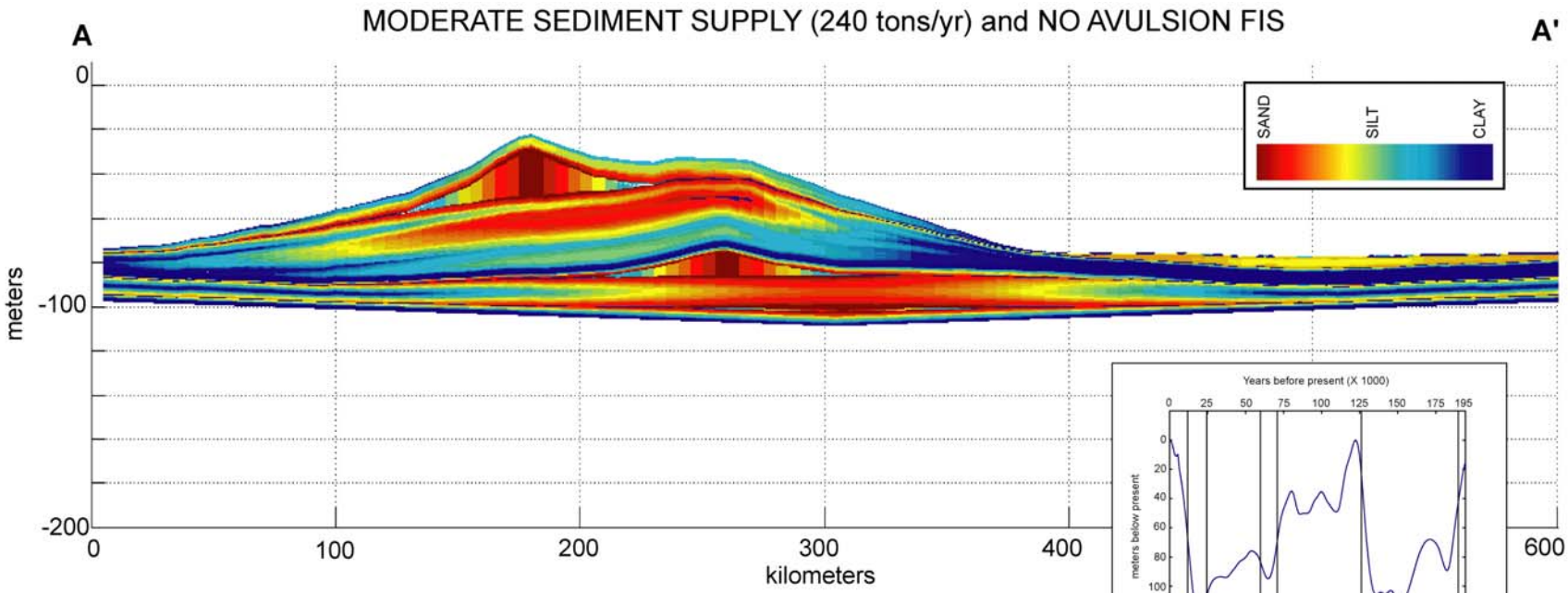
MODERATE SEDIMENT SUPPLY (240 tons/yr) and NO AVULSION FIS
A
A'
SAND
SILT
CLAY
meters
0
-100
-200
0
100
200
300
400
600
kilometers
Years before present (X 1000)
0 25 50 75 100 125 150 175 195
meters below present
0 20 40 60 80 100 120
OIS1
OIS2
OIS3
OIS4
OIS5
OIS6
390 340 290 240 190 140 90 40 0
Time step in simulation

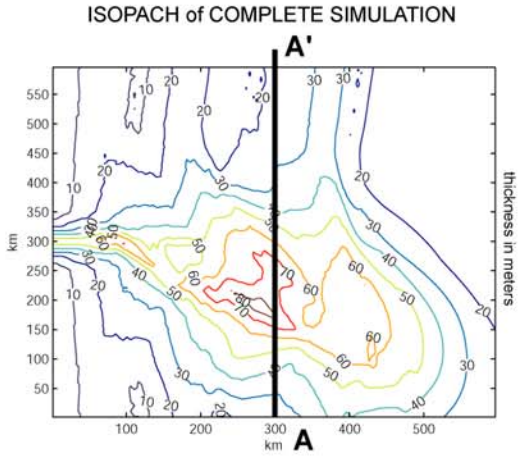
ISOPACH of COMPLETE SIMULATION
A'
A
km
km
thickness in meters
100 200 300 400 500
50 100 150 200 250 300 350 400 450 500 550

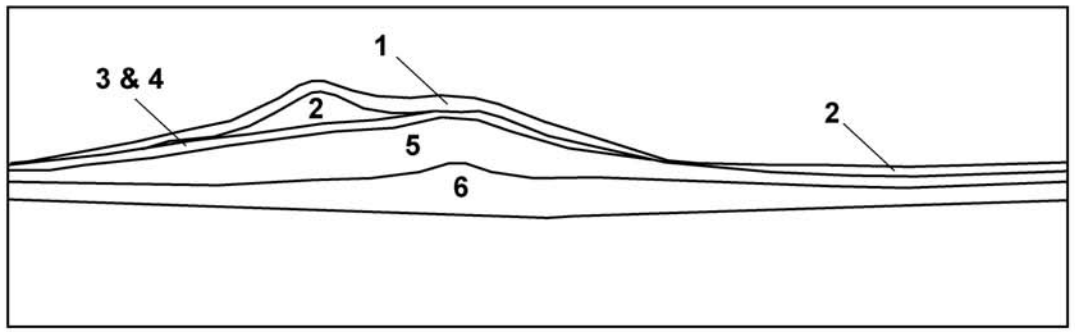
1
2
2
3 & 4
5
6

Figure 3.22. Isopach maps (OIS 6-1) from *fuzzy*PEACH simulation using late Pleistocene sea level data (Figure 3.11A), minimal tectonic subsidence (Figure 3.14A), and a high sediment influx (480 million tons/yr). The FIS controlling avulsion (Figure 3.12B) was turned off during this simulation.

HIGH SEDIMENT SUPPLY (480 tons/yr) and NO AVULSION FIS

ISOPACH MAP for OIS 1
(12 ka to present)

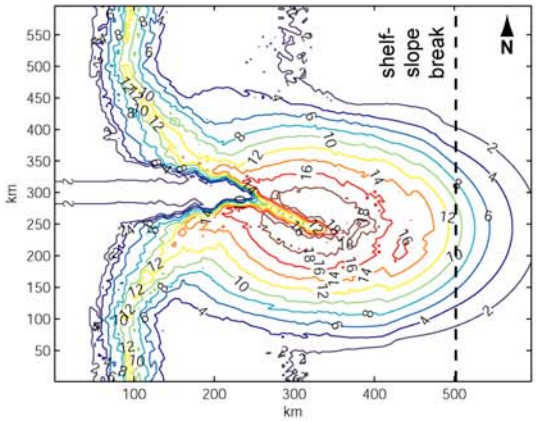

ISOPACH MAP for OIS 2
(24 to 12 ka)

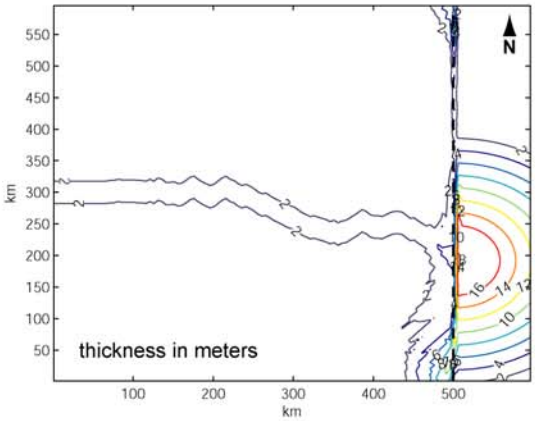

ISOPACH MAP for OIS 3
(59 to 24 ka)

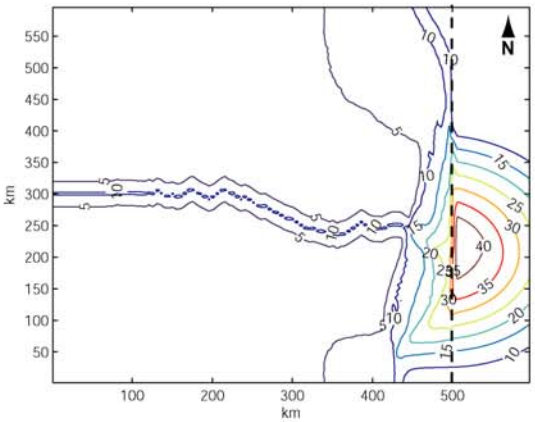

ISOPACH MAP for OIS 4
(71 to 59 ka)

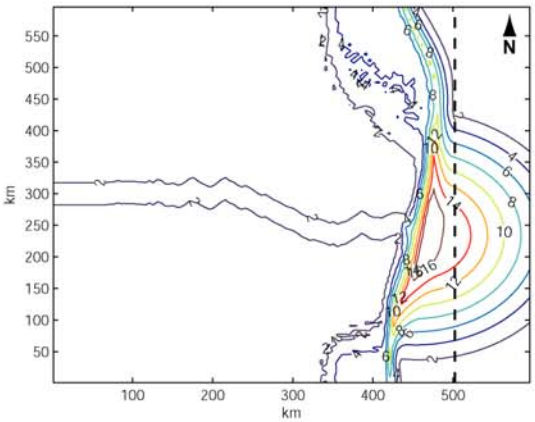

ISOPACH MAP for OIS 5
(128 to 71 ka)

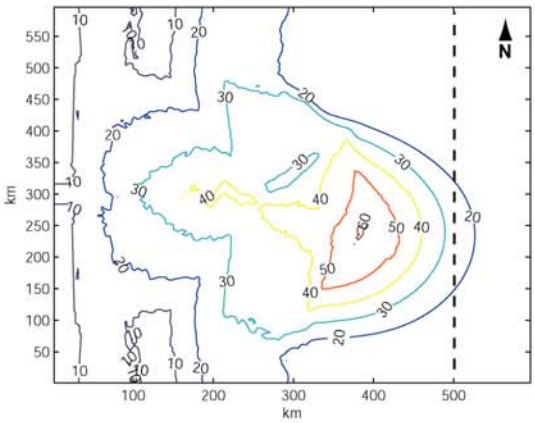

ISOPACH MAP for OIS 6
(186 to 128 ka)

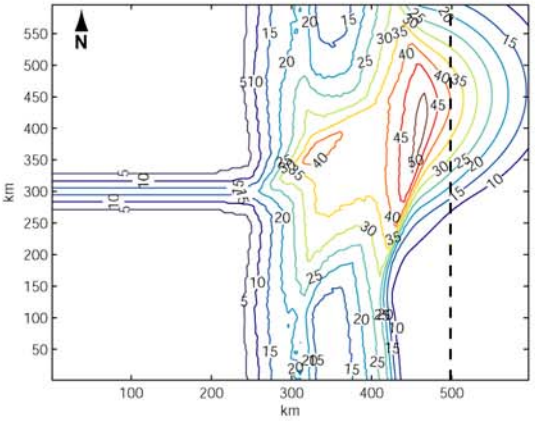

Figure 3.23. Dip-oriented synthetic cross-section from the middle margin simulating stratal evolution during the eustatic signal from the late Pleistocene (Figure 3.11A). Sediment influx was high (480 million tons per year), tectonic subsidence was low (<0.1 mm/yr), and the FIS controlling avulsion (Figure 3.12B) was turned off during this simulation.

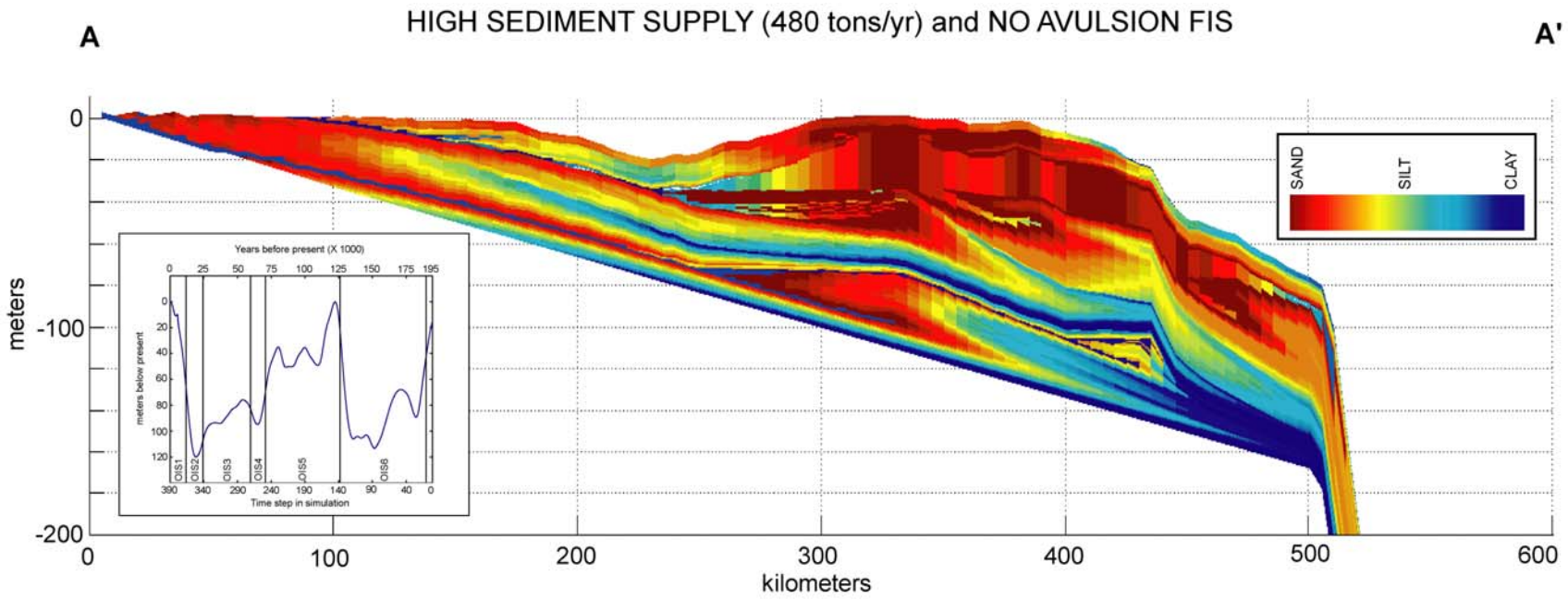
HIGH SEDIMENT SUPPLY (480 tons/yr) and NO AVULSION FIS
A
A'
meters
0
-100
-200
0
100
200
300
400
500
600
kilometers
SAND
SILT
CLAY
Years before present (X 1000)
meters below present
Time step in simulation
OIS1
OIS2
OIS3
OIS4
OIS5
OIS6

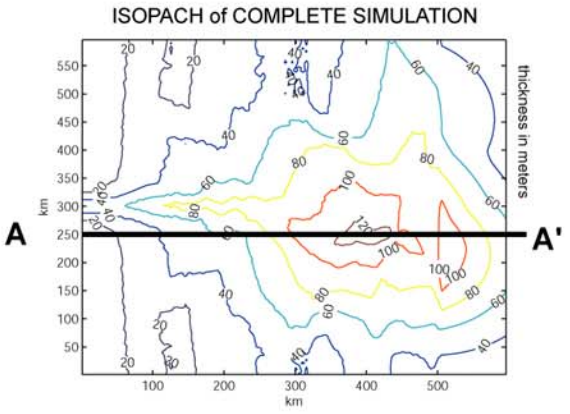
ISOPACH of COMPLETE SIMULATION
thickness in meters
A
A'
km
km

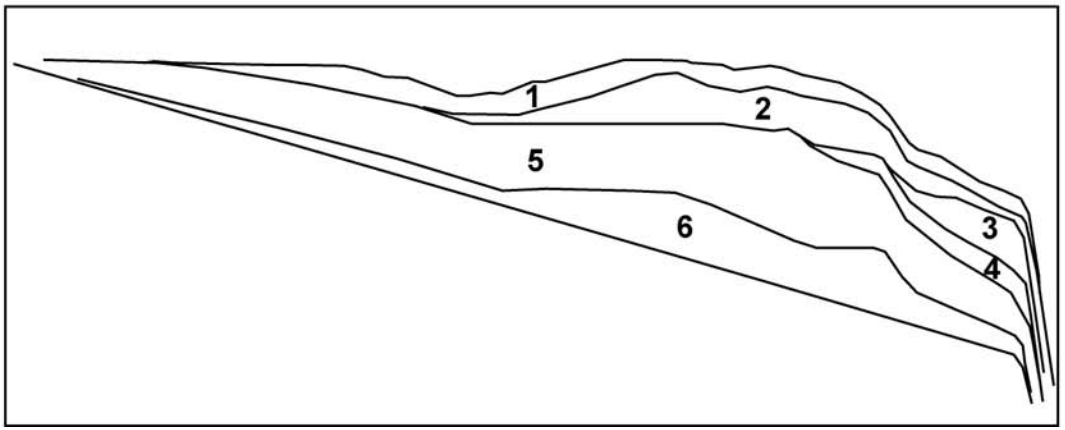
1
2
3
4
5
6

Figure 3.24. Strike-oriented synthetic cross-section from the middle margin simulating stratal evolution during the eustatic signal from the late Pleistocene (Figure 3.11A). Sediment influx was high (480 million tons per year), tectonic subsidence was low (<0.1 mm/yr), and the FIS controlling avulsion (Figure 3.12B) was turned off during this simulation.

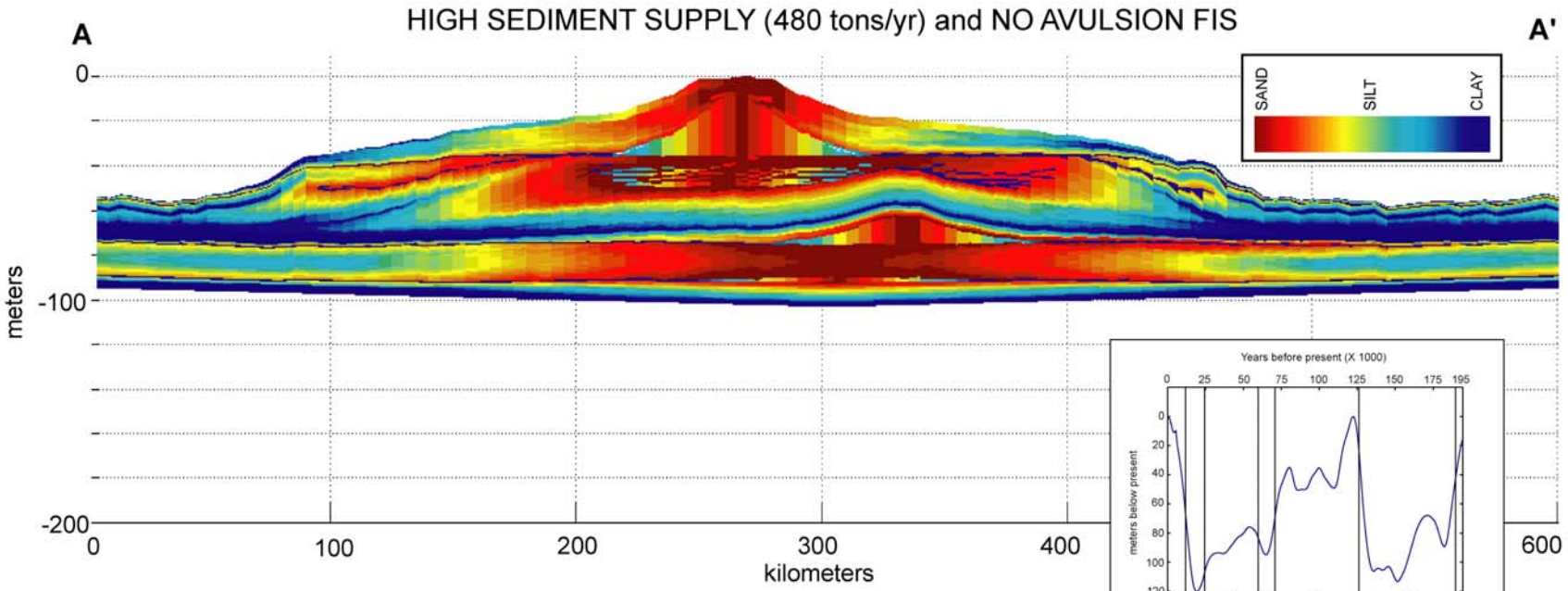
HIGH SEDIMENT SUPPLY (480 tons/yr) and NO AVULSION FIS
A
A'
SAND
SILT
CLAY
meters
0
-100
-200
0
100
200
300
400
600
kilometers
Years before present (X 1000)
0 25 50 75 100 125 150 175 195
meters below present
0 20 40 60 80 100 120
OIS1
OIS2
OIS3
OIS4
OIS5
OIS6
390 340 290 240 190 140 90 40 0
Time step in simulation

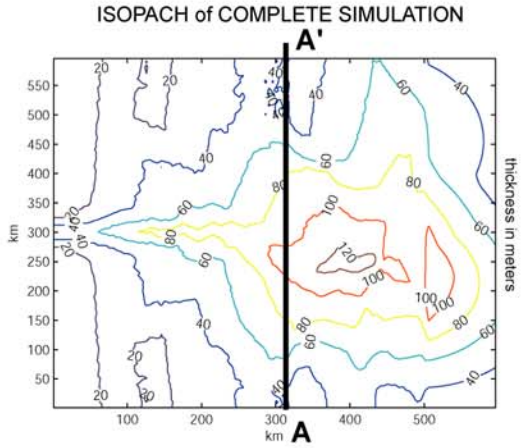
ISOPACH of COMPLETE SIMULATION
A'
A
km
thickness in meters
100 200 300 400 500
50 100 150 200 250 300 350 400 450 500 550

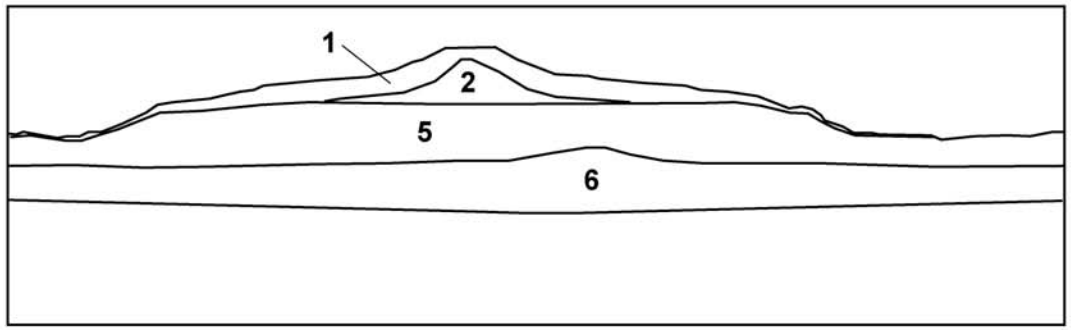
1
2
5
6

Figure 3.25. Isopach maps (OIS 6-1) from *fuzzy*PEACH simulation using late Pleistocene sea level data (Figure 3.11A), minimal tectonic subsidence (Figure 3.14A), and a moderate sediment influx (240 million tons/yr). Avulsion was controlled by a FIS (Figure 3.12B) during this simulation.

MODERATE SEDIMENT SUPPLY (240 tons/yr) and AVULSION FIS ON

ISOPACH MAP for OIS 1
(12 ka to present)

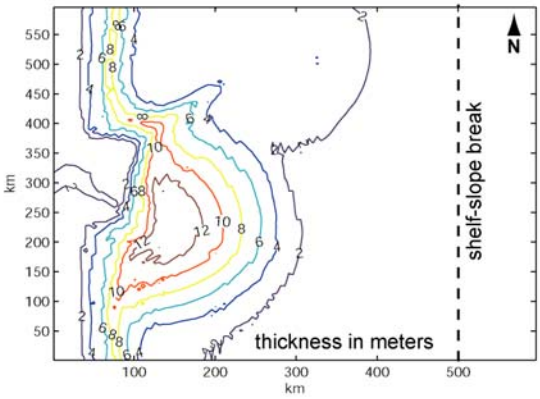

ISOPACH MAP for OIS 2
(24 to 12 ka)

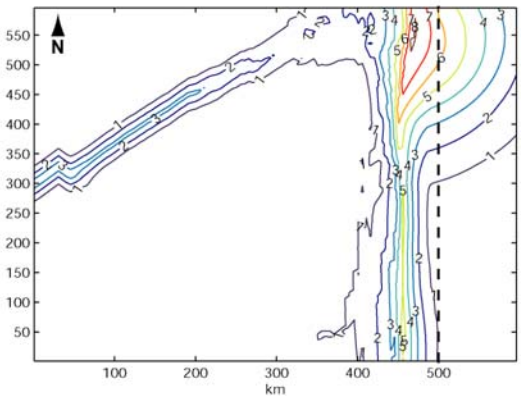

ISOPACH MAP for OIS 3
(59 to 24 ka)

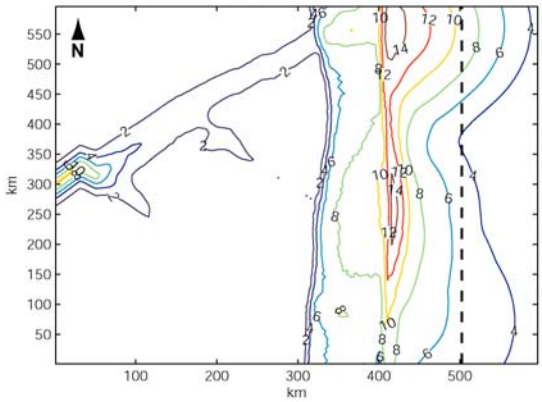

ISOPACH MAP for OIS 4
(71 to 59 ka)

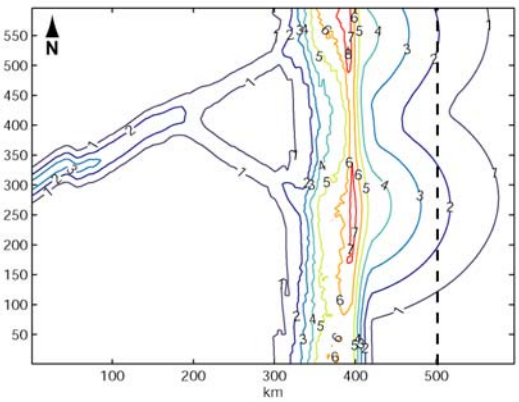

ISOPACH MAP for OIS 5
(128 to 71 ka)

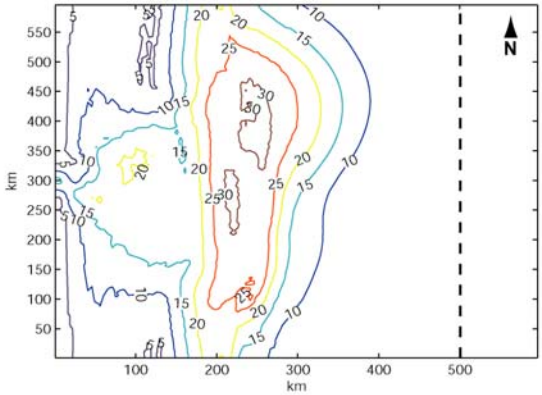

ISOPACH MAP for OIS 6
(186 to 128 ka)

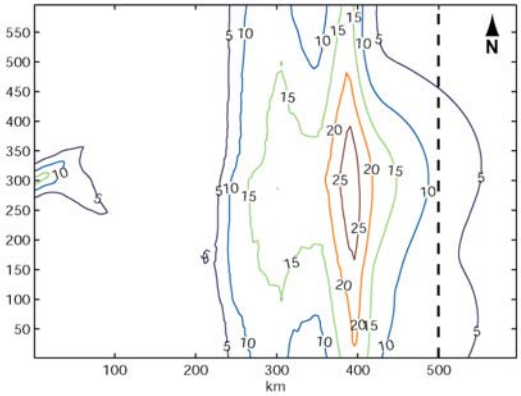

Figure 3.26. Dip-oriented synthetic cross-section from the middle margin simulating stratal evolution during the eustatic signal from the late Pleistocene (Figure 3.11A). Sediment influx was moderate (240 million tons per year), tectonic subsidence was low (<0.1 mm/yr), and avulsion was controlled by a FIS (Figure 3.12B) during this simulation.

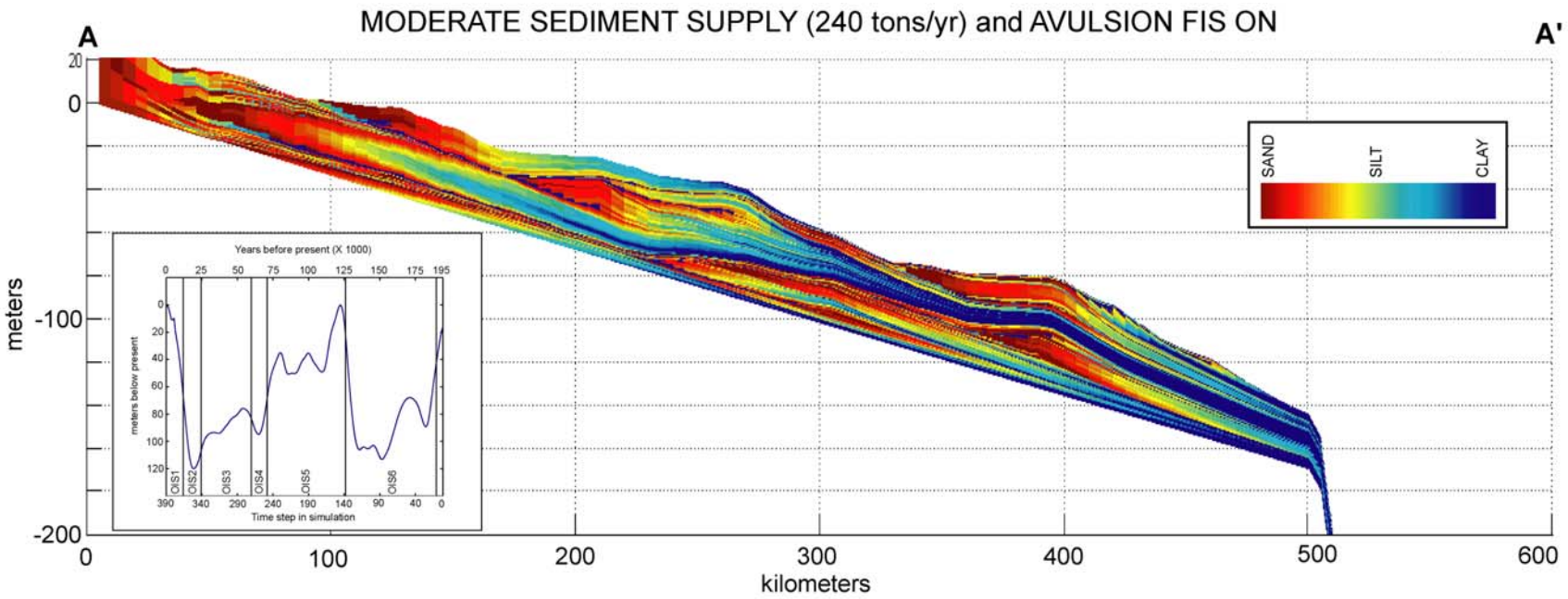
MODERATE SEDIMENT SUPPLY (240 tons/yr) and AVULSION FIS ON
A
A'
SAND
SILT
CLAY
meters
kilometers
Years before present (X 1000)
meters below present
Time step in simulation
OIS1
OIS2
OIS3
OIS4
OIS5
OIS6

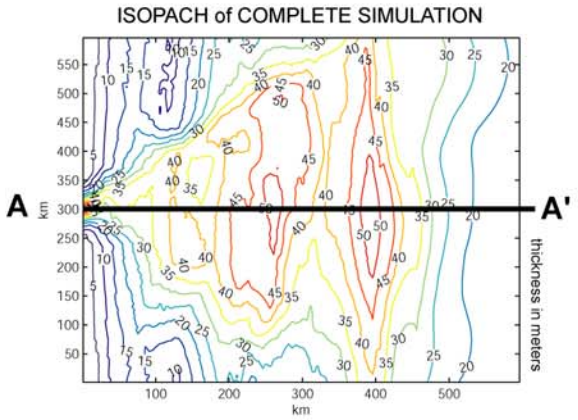
ISOPACH of COMPLETE SIMULATION
A
A'
km
thickness in meters

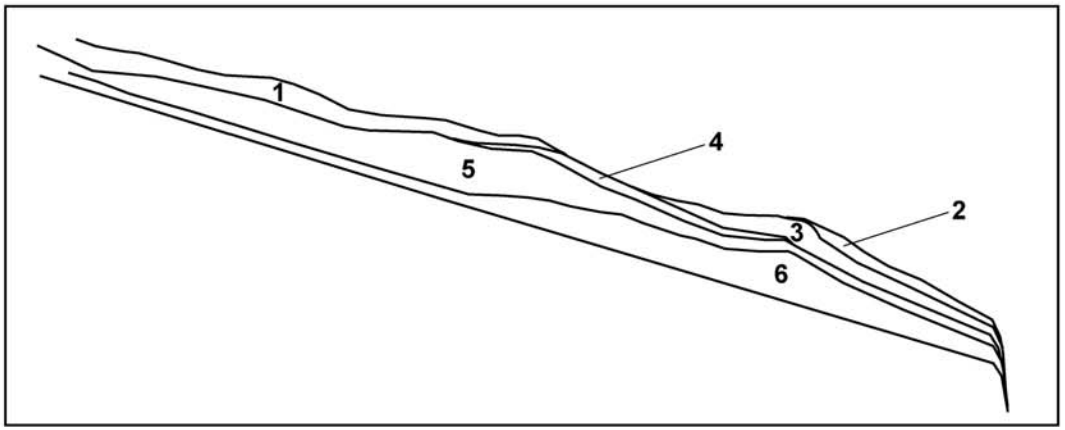
1
2
3
4
5
6

Figure 3.27. Dip-oriented synthetic cross-section from the middle margin simulating stratal evolution during the eustatic signal from the late Pleistocene (Figure 3.11A). Sediment influx was moderate (240 million tons per year), tectonic subsidence was low (<0.1 mm/yr), and avulsion was controlled by a FIS (Figure 3.12B) during this simulation.

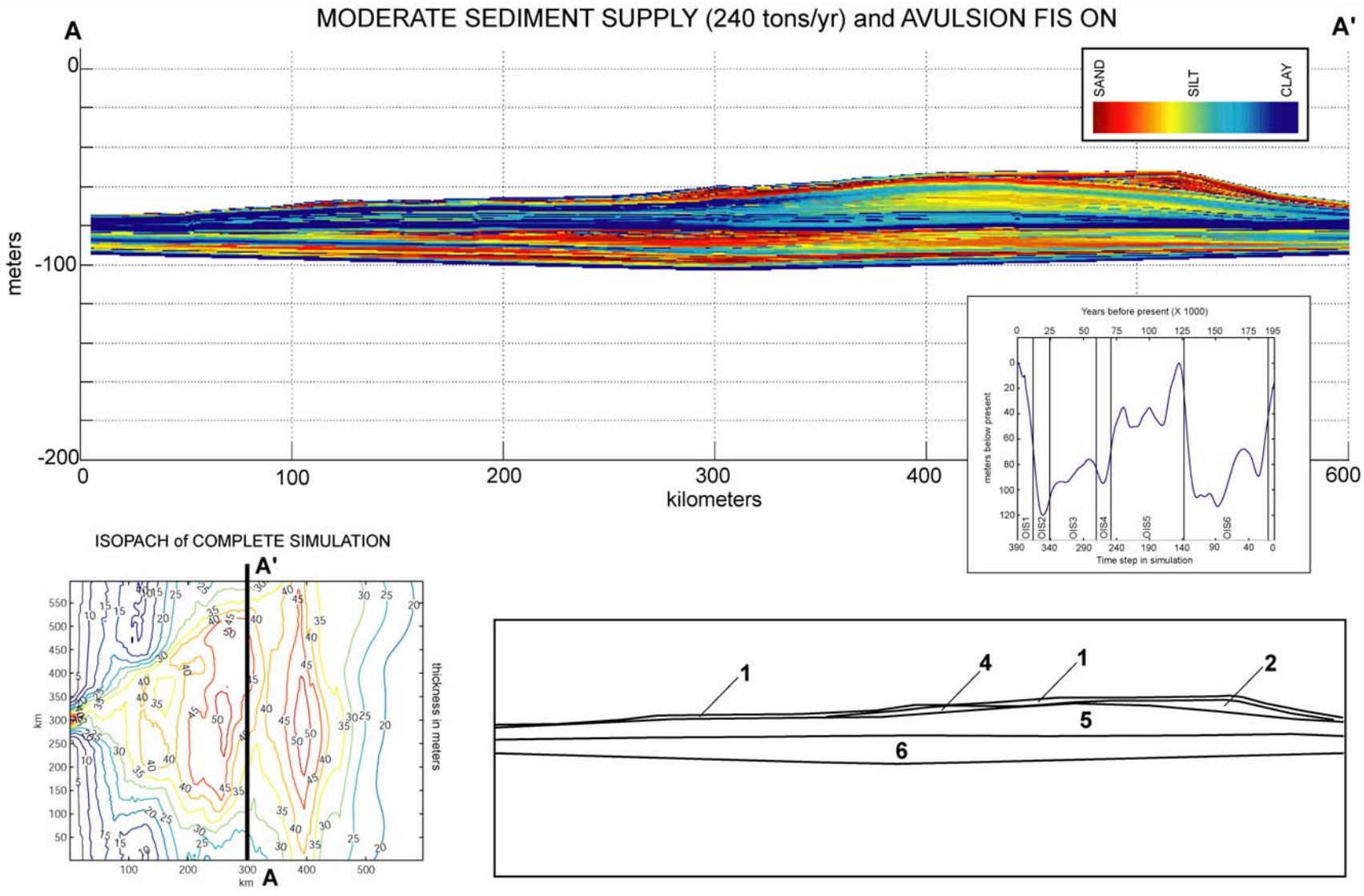
MODERATE SEDIMENT SUPPLY (240 tons/yr) and AVULSION FIS ON
A
A'
SAND
SILT
CLAY
meters
0
-100
-200
0
100
200
300
400
600
kilometers
Years before present (X 1000)
meters below present
OIS1
OIS2
OIS3
OIS4
OIS5
OIS6
Time step in simulation
ISOPACH of COMPLETE SIMULATION
km
thickness in meters
1
4
1
2
5
6

Figure 3.28. Isopach maps (OIS 6-1) from *fuzzy*PEACH simulation using late Pleistocene sea level data (Figure 3.11A), minimal tectonic subsidence (Figure 3.14A), and a high sediment influx (480 million tons/yr). Avulsion was controlled by a FIS (Figure 3.12B) during this simulation.

HIGH SEDIMENT SUPPLY (480 tons/yr) and AVULSION FIS ON

ISOPACH MAP for OIS 1
(12 ka to present)

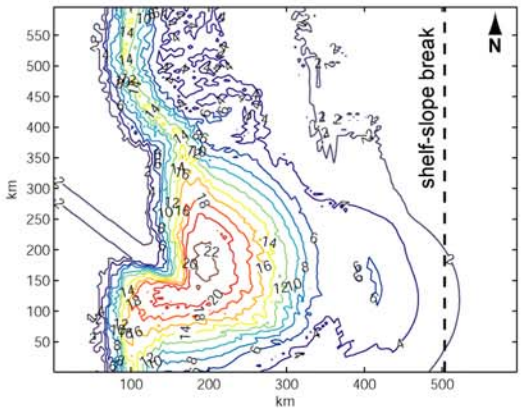

ISOPACH MAP for OIS 2
(24 to 12 ka)

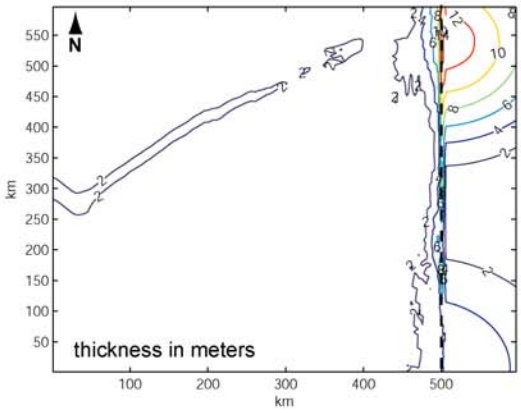

ISOPACH MAP for OIS 3
(59 to 24 ka)

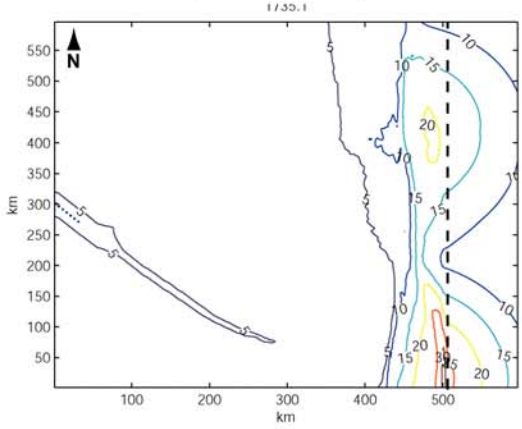

ISOPACH MAP for OIS 4
(71 to 59 ka)

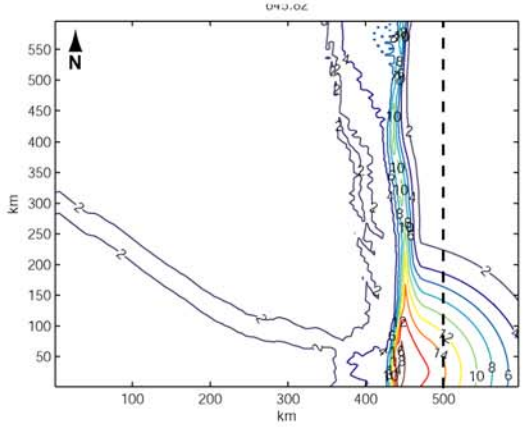

ISOPACH MAP for OIS 5
(128 to 71 ka)

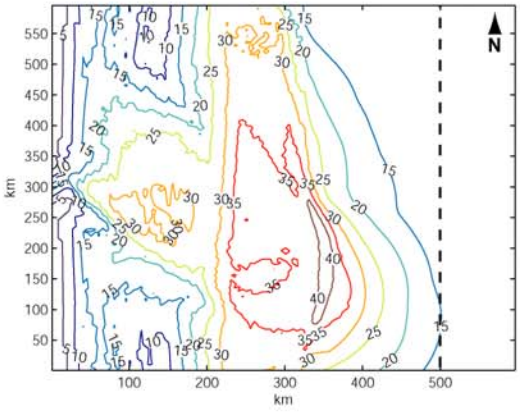

ISOPACH MAP for OIS 6
(186 to 128 ka)

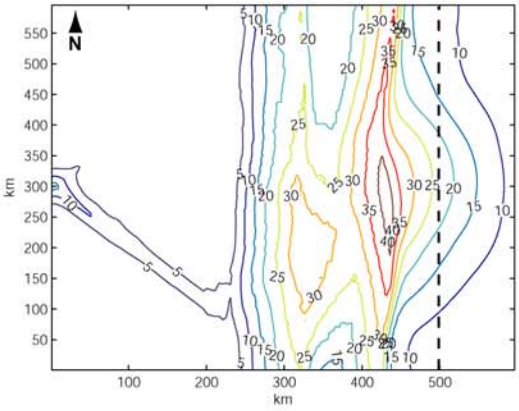

Figure 3.29. Dip-oriented synthetic cross-section from the middle margin simulating stratal evolution during the eustatic signal from the late Pleistocene (Figure 3.11A). Sediment influx was high (480 million tons per year), tectonic subsidence was low (<0.1 mm/yr), and avulsion was controlled by a FIS (Figure 3.12B) during this simulation.

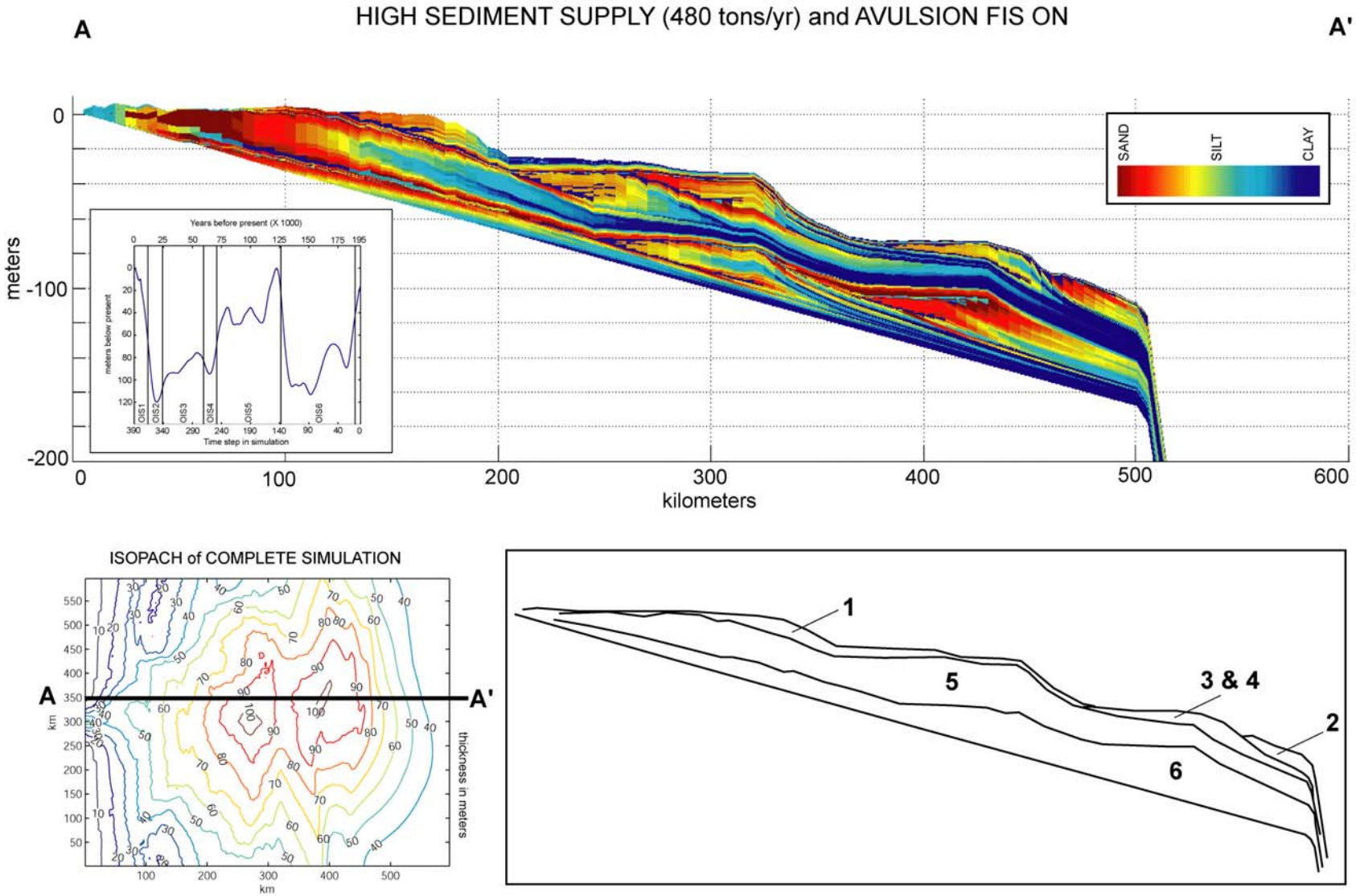
HIGH SEDIMENT SUPPLY (480 tons/yr) and AVULSION FIS ON
A
A'
meters
kilometers
SAND
SILT
CLAY
Years before present (X 1000)
meters below present
Time step in simulation
OIS1
OIS2
OIS3
OIS4
OIS5
OIS6
ISOPACH of COMPLETE SIMULATION
km
thickness in meters
1
5
3 & 4
2
6

Figure 3.30. Strike-oriented synthetic cross-section from the middle margin simulating stratal evolution during the eustatic signal from the late Pleistocene (Figure 3.11A). Sediment influx was high (480 million tons per year), tectonic subsidence was low (<0.1 mm/yr), and avulsion was controlled by a FIS (Figure 3.12B) during this simulation.

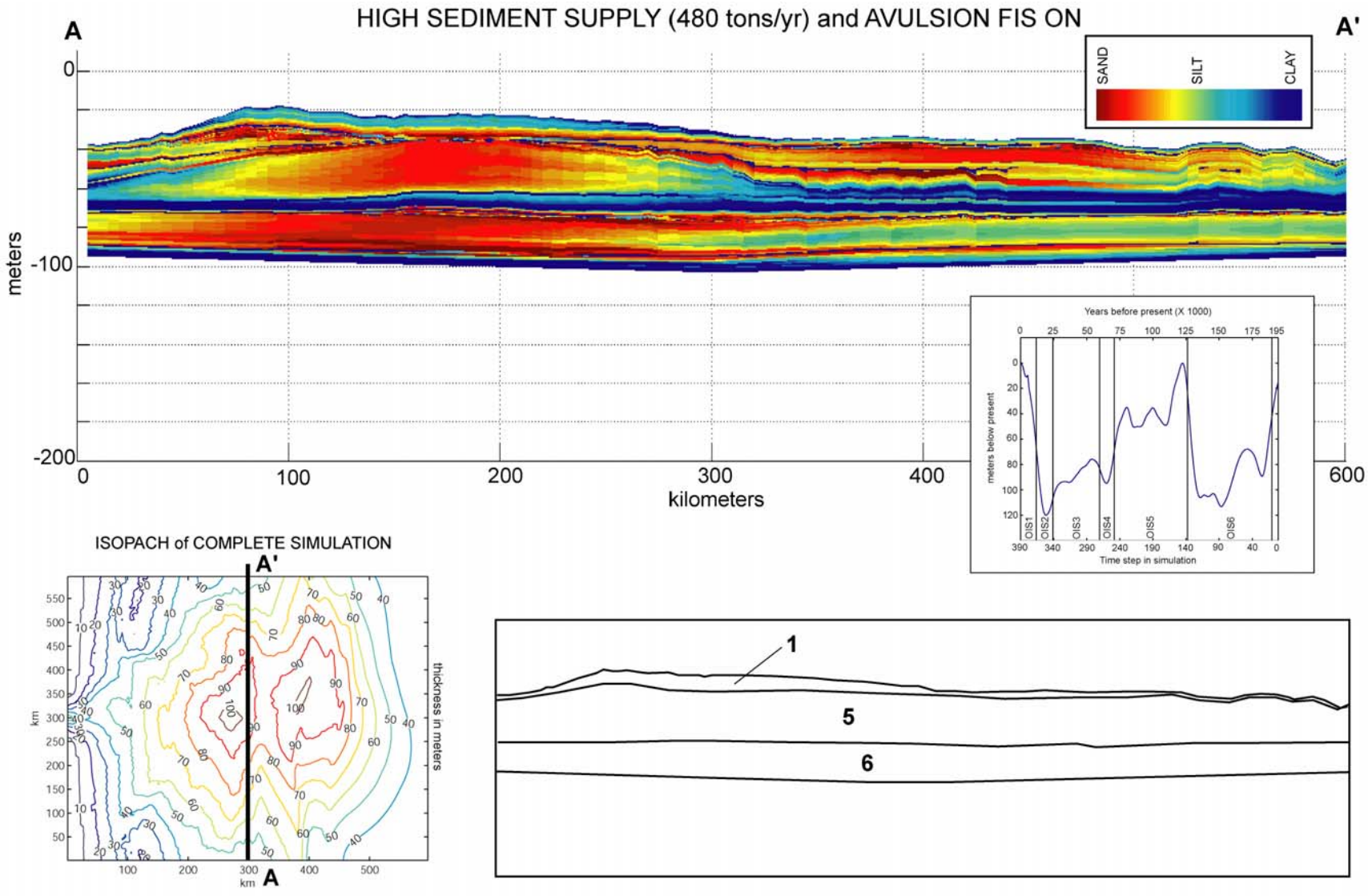
HIGH SEDIMENT SUPPLY (480 tons/yr) and AVULSION FIS ON
A
A'
SAND
SILT
CLAY
meters
0
-100
-200
0
100
200
300
400
600
kilometers
Years before present (X 1000)
0 25 50 75 100 125 150 175 195
meters below present
0 20 40 60 80 100 120
OIS1
OIS2
OIS3
OIS4
OIS5
OIS6
390 340 290 240 190 140 90 40 0
Time step in simulation
ISOPACH of COMPLETE SIMULATION
A'
A
km
thickness in meters
1
5
6

Table 3.2. Observations from four *fuzzy*PEACH simulations constrained by sea level, tectonic subsidence, and sediment influx variables hypothesized to have existed on the ECS margin during the past 195 ky. Observations from the ECS seismic dataset are also presented for comparison.

DATA from ECS MARGIN

shape of sea level curve	SPECMAP	SPECMAP	SPECMAP	SPECMAP	___
Fuzzy Inference System for avulsion	OFF	OFF	ON	ON	___
magnitude of sea level curve	120 m	120 m	120 m	120 m	___
tectonic subsidence	0.1 mm/yr	0.1 mm/yr	0.1 mm/yr	0.1 mm/yr	___
sediment influx	240 million tons/yr	480 million tons/yr	240 million tons/yr	480 million tons/yr	___
width of delta plains	375 km	375 km	350 km	350 km	200 km *(OIS 5)*
length-to-width ratio of deltas *(length is measured shore parallel)*	1:2 *(OIS 1 = 1:1)*	1:2 *(OIS 1 = 1:1.5)*	between 1:2 to 1:4	between 1:2 to 1:4	1:1 *(OIS 5)*
shoreline @ OIS 2 lowstand *(distance from modern shoreline)*	490 km	500 km	460 km	490 km	~475 km
shoreline @ OIS 6 lowstand *(distance from modern shoreline)*	410 km	430 km	405 km	425 km	~450 km
max stratal thickness OIS 1	12 m	18 m	12 m	22 m	20m
max stratal thickness OIS 2	9 m	18 m	8 m	14 m	30 m
max stratal thickness OIS 3	22 m	40 m	14 m	30 m	50 m
max stratal thickness OIS 4	8 m	16 m	7 m	18 m	8 m
max stratal thickness OIS 5	35 m	60 m	30 m	40 m	50 m
max stratal thickness OIS 6	35 m	50 m	25 m	40 m	40 m
max stratal thickness on margin *(all strata)*	60 m	120 m	50 m	100 m	112 m
location of max thickness *(distance from modern shoreline)*	300 to 450 km	350 to 450 km	110, 250 and 375 km	150, 300 and 450 km	300 km
max thickness @ shelf-slope break	50 m	90 m	28 m	60 m	80 m
depth of shelf-slope break @ end of model	120 m	80 m	142 m	110 m	150 m

3.4 DISCUSSION

This investigation occurred in two phases. The first phase of the study, described in this paper, assessed the ability of fuzzy logic to model complex stratigraphy under various depositional conditions on an idealized, passive continental margin. Fuzzy logic was chosen because it is simple to use and understand. Fuzzy logic provides the ability to quantify subjectivity by capturing the vagueness of linguistics terms, thus making it flexible and tolerant of imprecise data (Demicco and Klir, 2004b). General concepts and expert knowledge assembled *fuzzy*PEACH, a MATLAB-based model that used five FISs to simulate the complicated, nonlinear relationships of stratal evolution on a passive continental margin. No special knowledge, apart from basic mathematical logic, was required for this application (Nordlund, 1999b). Similar to previous fuzzy-logic-based stratigraphic simulations (Nordlund and Silvfersparre, 1994; Nordlund, 1996; 1999a; 1999b; Parcel, 2000; Demicco and Klir, 2001; Parcell, 2003a; 2003b; Demicco, 2004), the goal of *fuzzy*PEACH was to describe, in simplistic terms, the complexity of a fluvial system and its delta. The general instructions defining fluvial deposition are straightforward: the highest volume and coarsest sediments are deposited closest to the channel and the lowest volume and finest sediments are deposited farther away. The same concept is used for the delta (i.e., high volume and coarse sediment at the river mouth transitioning to low volume and fine sediment farther away). User-defined variables such as sediment influx, margin geometry, and tectonic subsidence may be altered for any given simulation, but the rules, variables, fuzzy sets, and fuzzy set boundaries are "hard coded" and remained constant for all simulations. With the exception of avulsion, which is based on sea level elevation as a proxy for gradient, no special instructions are included within *fuzzy*PEACH to define how stratal geometry should be built during numerous permutations of eustasy, tectonic subsidence, and sediment influx.

Instead, stratal geometries are based solely on sediment distribution (how much, what type, and where) and available accommodation. Accomodation is determined by relative sea level, eustasy, tectonic subsidence, and sediment influx.

The second phase of this investigation, also described in this paper, used *fuzzy*PEACH to simulate the physical conditions associated with low-gradient margins. Phase II was justified because Phase I showed that the stratigraphic architecture generated during variable conditions of eustasy, tectonic subsidence, and sediment influx is consistent with the general concepts of both seismic stratigraphy and sequence stratigraphy. The evaluation of phase II uses an extensive, regional dataset from the ECS margin that provides the constraints needed to assess the accuracy of *fuzzy*PEACH simulations and validates output. Low-gradient margins were studied because the traditional sequence stratigraphic model predicts incision at the shelf-slope break as well as sedimentary bypass across the continental margin during sea level lowstands. When the shelf-slope break of the margin remains submerged during lowstand, fluvial systems under low-gradient conditions are unconfined, laterally extensive, and do not bypass the majority of sediments beyond the shelf-slope break and into deeper water. Although these margins are rare in the modern and recent geologic record, examples include northeastern Australia (Woolfe et al., 1998), New Zealand (Canterbury Plains; Browne and Naish, 2003), northern Java (Posamentier, 2001), and the ECS (Bartek et al., 2001; Bartek and Warren 2002; Warren and Bartek, 2002a; 2002b; Warren et al., 2002a).

The regional extent of the large seismic dataset from the ECS margin used in this study provides a unique set of observations that were not available to previous investigations. Interpretations of the stratigraphic architecture of the ECS margin, derived from the seismic data set, combined with numerous published studies, provide a good understanding of the

depositional conditions under which the stratigraphy was formed. There appears to be a good correlation between *fuzzy*PEACH simulations constrained by these same conditions (i.e., margin physiography, eustatic curve, tectonic subsidence rate, sediment influx). Therefore, in areas with similar depositional conditions, but with little or no data, strataigraphic trends can be inferred from *fuzzy*PEACH simulations. Potential analogs to these depositional conditions in the ancient record are foreland basins, which generally exhibit a low-gradient ramp morphology, a high volume of sediment delivered as a line source (rather than a point source), and unconfined fluvial systems with minimal incision. Examples of these strata are found in the Bowen Basin in eastern Queensland, Australia (Permian; Fiedling et al., 1993), the Devonian Catskill Delta, U.S. Appalachian Basin (Devonian; Ettensohn, 1985; Woodrow, 1985); the Castlegate Formation (Van Wagoner et al., 1990; Van Wagoner and Bertram, 1995; Miall and Arush, 2001) and the Mesa Rica Sandstone (Holbrook and Dunbar, 1992; Holbrook, 1996) from the Cretaceous U.S. western interior; the Alaska Range (Miocene; Lesh et al., 2001), the Pakistani foreland (Miocene; Pivnik and Johnson, 1995), the Ganga Megafan, India (Miocene; Shukla et al., 2001), and the Spanish Pyrenees foreland basin (Eocene; Bentham et al., 1993; Miocene; Jones et al., 2001).

3.4.1 Evaluation of Model with Regional Dataset from ECS Margin

Previous stratigraphic simulations based on fuzzy logic were constrained and validated by limited geologic data. For example, FUZZIM (Nordlund and Silvfersparre, 1994; Nordlund, 1996; 1999a; 1999b) simulated a Miocene carbonate platform from Mallorca, Spain with a 25 x 25 km grid over 70 ky. Demicco and Klir (2001) used a 150 km x 300 km ramp margin to model 10 ky of tidal flat deposition in the Bahamas, and Demicco (2004) modeled a 15 x 65 km basin from Death Valley, CA over a period of 191 ky. Parcel (2000;

2003a; 2003b) developed FUZZYREEF to simulate 4 millions years of carbonate production and deposition on a 5 km x 5 km ramp margin from the US Gulf coast during the Jurassic. In comparison, the modeled universe of *fuzzy*PEACH is larger than previous studies (600 x 600 km), as is the regional dataset from the ECS margin. These data provide a thorough understanding of the stratal geometry preserved on the ECS margin during the past 200 ky. The ability to use these data, combined with observations from previous studies (e.g., Yang, 1989; Saito et al., 1998; Liu et al., 2000; Berne et al., 2002; Yoo et al., 2002), to develop a detailed seismic- and sequence-stratigraphic framework on the ECS margin allows a regional understanding of the stratal architecture and the geoloigic processes that created it. This body of knowledge provides a validation extent for *fuzzy*PEACH that was not available in earlier fuzzy logic studies.

Regional Dataset used for Constraining Model. The seismic data utilized in this investigation were acquired in the ECS during the past decade as part of a broader investigation (Bartek and Warren, 1995; Bartek et al., 2001; Bartek and Warren, 2002; Warren and Bartek, 2002a; 2002b; Warren et al., 2002a; Wellner and Bartek, 2003; Bartek et al., 2004; Bartek and Warren, 2005). These surveys consist of an overlapping grid of approximately 14,000 km of 2-D, high-resolution (~1 m vertical resolution), single-channel seismic profiles and cover a 300,000 km^2 study area extending from 28° to 33° N latitude and 123° to 128° 30' E longitude (Figure 3.31). Survey geometries consist of an even distribution of strike- and dip-oriented profiles where strike is considered to trend parallel to the shelf-slope break (approximately N 12° E). Survey lines are spaced between 10 and 20 km on the inner margin and between 20 and 50 km on the outer margin. In addition to seismic data, approximately 10,000 km of higher-frequency chirp sonar profiles were

Figure 3.31. Geographic map from the ECS identifying the study area in which the regional seismic dataset, discussed in this paper, was acquired. The location of the two cores used to chronologically constrain the seismic profiles (cores DZQ4 and YQ1) are shown in the inset. Fluvial input data compiled from: a) Milliman and Meade, 1983; b) Qian and Dai, 1980; c) Wang and Aubrey, 1987; d) Zhang and Li, 1996; e) Congxian et al., 1991; f) Milliman and Syvitski, 1992; g) Chough and Kim, 1981; h) Lee and Chough, 1989. Bathymetry modified from Quanxing (1990).

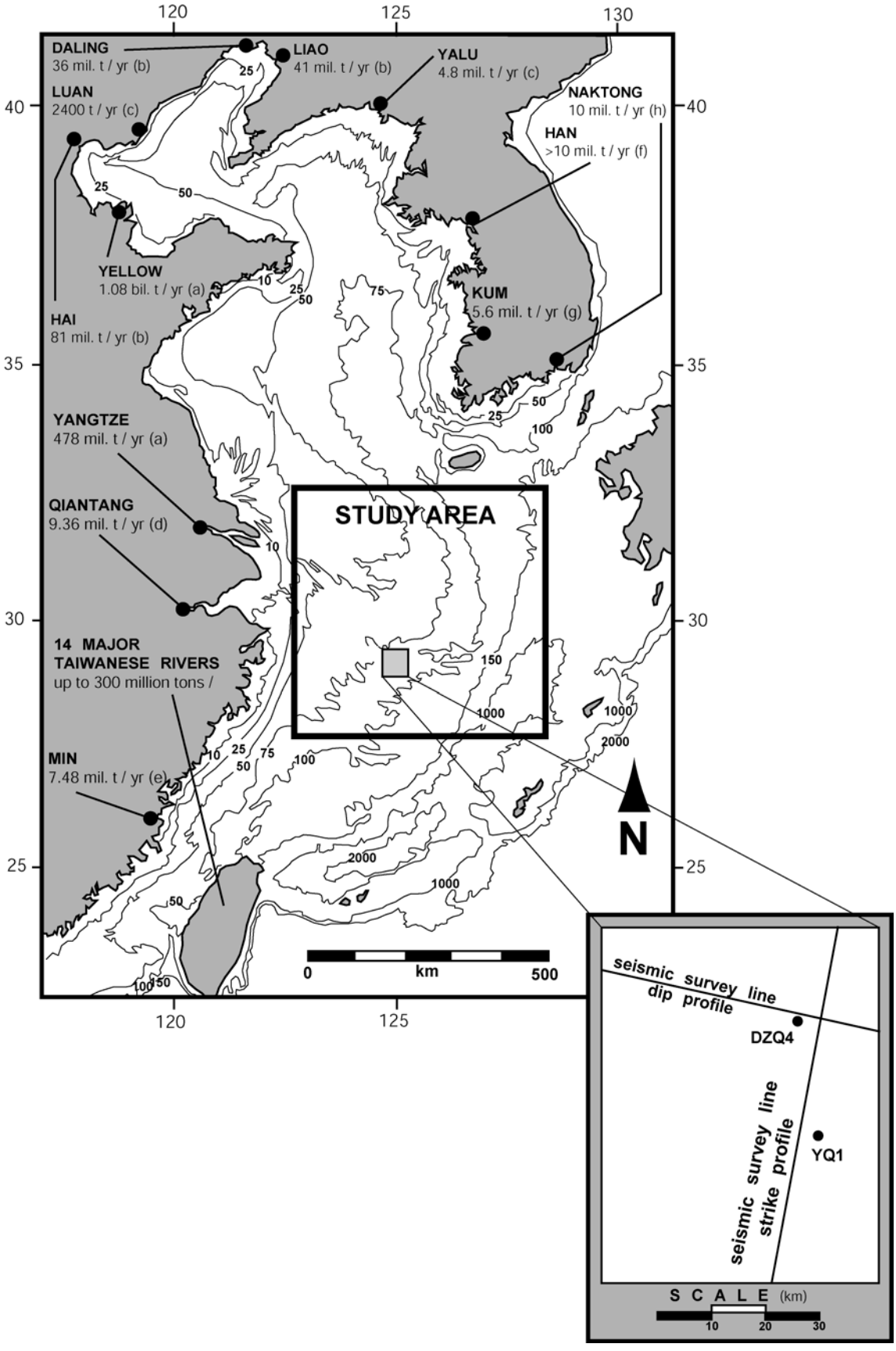
120
125
130
40
35
30
25
DALING
36 mil. t / yr (b)
LIAO
41 mil. t / yr (b)
YALU
4.8 mil. t / yr (c)
LUAN
2400 t / yr (c)
NAKTONG
10 mil. t / yr (h)
HAN
>10 mil. t / yr (f)
YELLOW
1.08 bil. t / yr (a)
KUM
5.6 mil. t / yr (g)
HAI
81 mil. t / yr (b)
YANGTZE
478 mil. t / yr (a)
QIANTANG
9.36 mil. t / yr (d)
STUDY AREA
14 MAJOR
TAIWANESE RIVERS
up to 300 million tons /
MIN
7.48 mil. t / yr (e)
N
0
km
500
seismic survey line
dip profile
DZQ4
seismic survey line
strike profile
YQ1
SCALE (km)
10
20
30

collected concurrently over portions of the same grid. These data provide sub-meter resolution of the uppermost strata that are often masked in seismic profiles by the acoustic source signature (i.e., bubble pulse). This extensive, nested-frequency dataset (i.e., 100 to 2,000 Hz for seismic and 2,000 to 16,000 Hz for chirp) facilitates a regional, seismic- and sequence-stratigraphic analysis of shallow subsurface strata (up to 150 m deep) deposited during the Holocene and late Pleistocene back to OIS 12 (approximately 500 ka). However, this investigation primarily focuses on the strata from the sea level lowstand associated with the glacial period during OIS 6.

Chronostratigraphic data (thermoluminescence and ^{14}C dates) and paleoclimate indicators (sporo-pollen and foraminiferal assemblages) from cores DZQ4 (Figure 3.32) and YQ1 (Figure 3.33) permitted correlations of the sequence stratigraphy if the seismic profiles to both the sea level and oxygen isotope curves (e.g., Shackleton, 1987; Winograd et al., 1988, 1992; Pillans et al, 1998; Saito et al., 1998). Stratigraphic units were, therefore, divided into their respective oxygen isotope stages from six to present (i.e., OIS 6 to OIS 1) to allow direct comparison between model simulations and real data. A summary of ECS seismic data is presented as a collection of isopach maps (Figure 3.34) and dip- and strike-oriented cross-sections (Figures 3.35 and 3.36, respectively).

Similarity of *fuzzy*PEACH to Conditions on the ECS Margin. Numerous conditions were simulated with *fuzzy*PEACH, including the user-defined parameters for margin geometry, eustasy, tectonic subsidence, and sediment influx. These values were based on a combination of general geologic conditions (deltaic deposition, avulsion, compaction, subsidence) with a few being specific to low-gradient margins in general (fluvial deposition). The values used to constrain the fuzzy sets used in the five FISs driving the fuzzy logic

Figure 3.32. The correlation between the six units from core DZQ4 projected less than 1 km into a nearby, dip-oriented seismic profile. The location of this profile, with respect to the ECS margin, is identified in Figure 3.31.

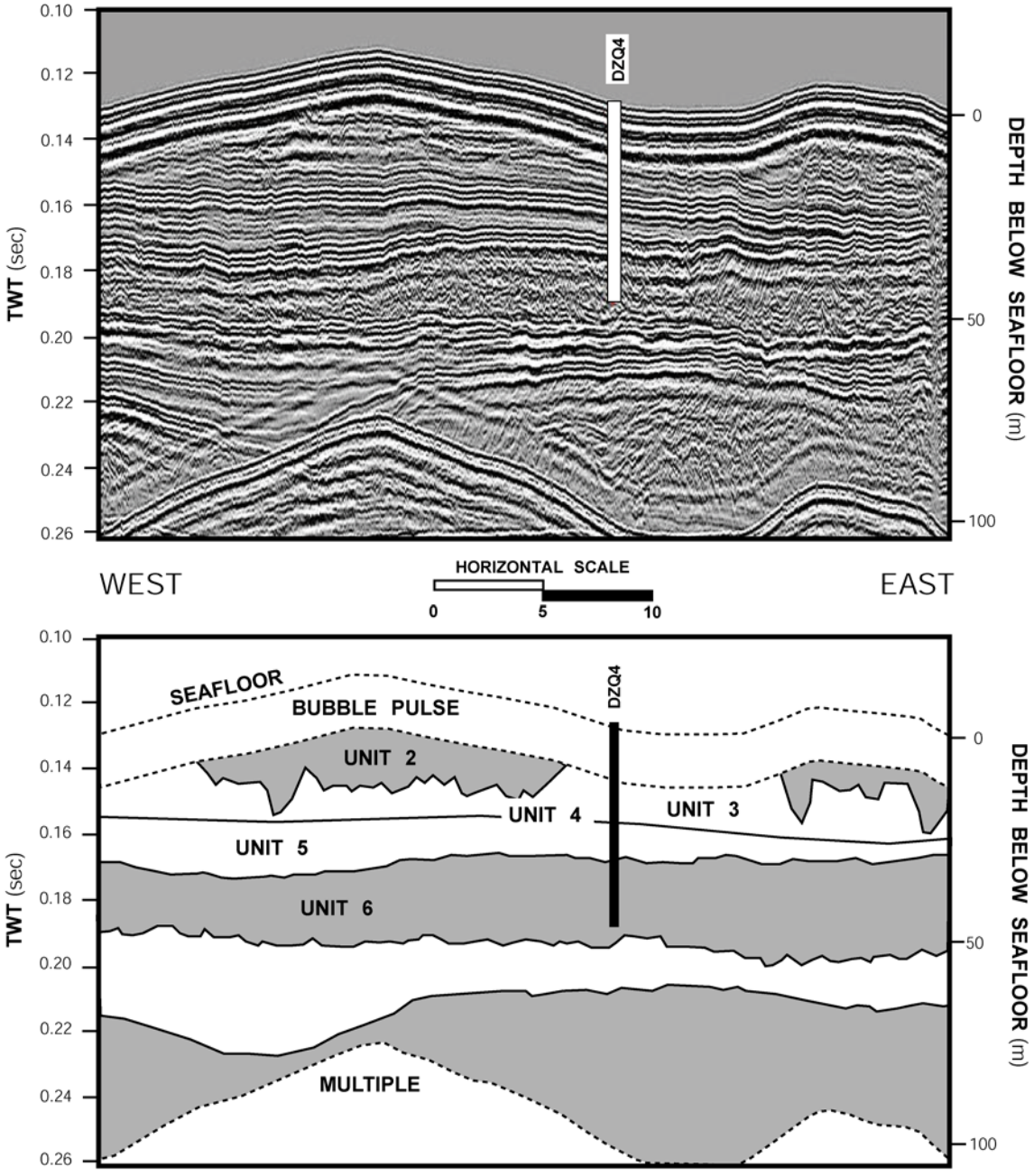
0.10
0.12
0.14
0.16
0.18
0.20
0.22
0.24
0.26
TWT (sec)
DZQ4
0
50
100
DEPTH BELOW SEAFLOOR (m)
WEST
HORIZONTAL SCALE
0
5
10
EAST
SEAFLOOR
BUBBLE PULSE
UNIT 2
UNIT 4
UNIT 3
UNIT 5
UNIT 6
MULTIPLE

Figure 3.33. Summarized core description of core YQ1 from Yang (1989) with interpretive comparisons from this paper and Berne et al. (2002). The location of this profile, with respect to the ECS margin, is identified in Figure 3.31.

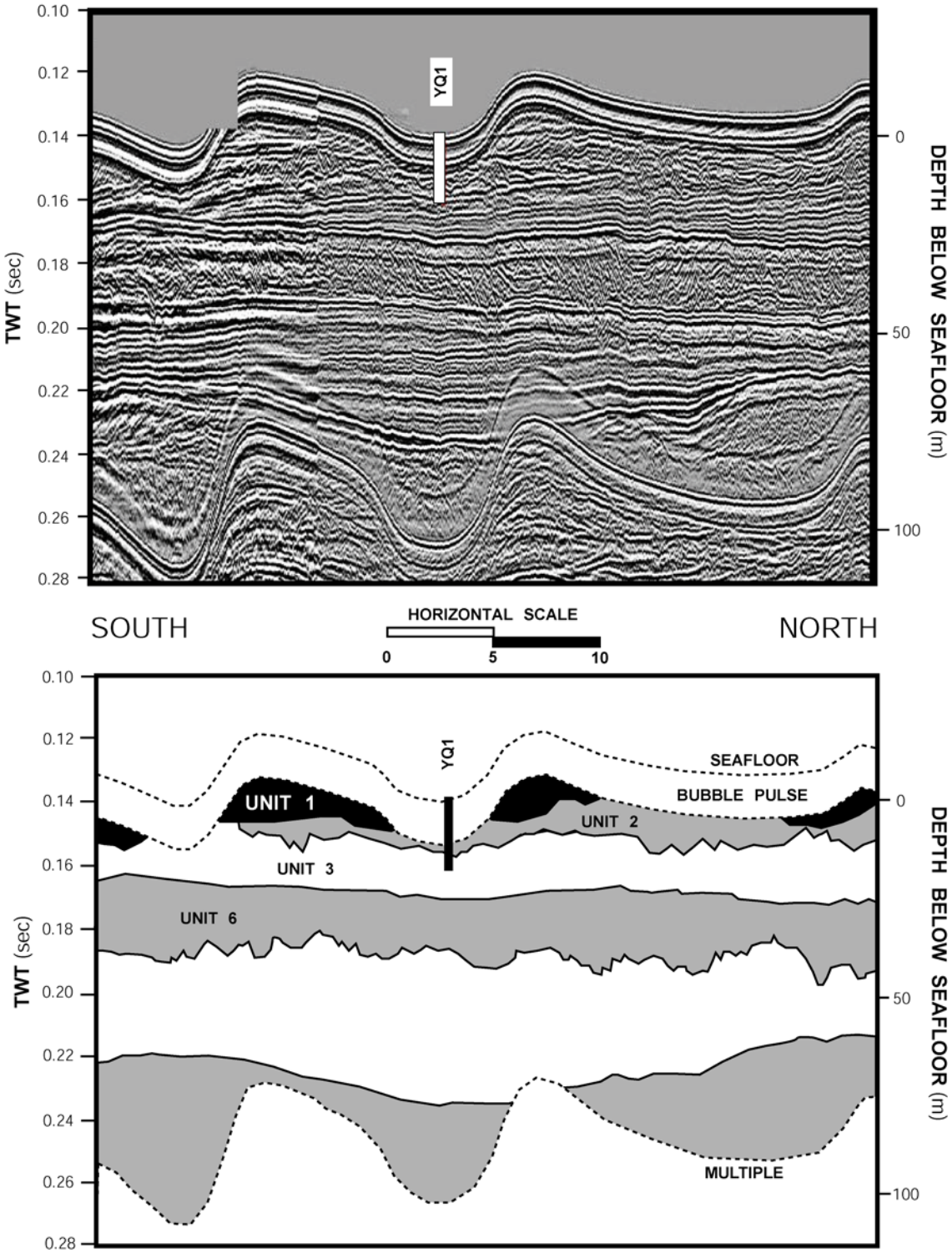
0.10
0.12
0.14
0.16
0.18
0.20
0.22
0.24
0.26
0.28
TWT (sec)
YQ1
0
50
100
DEPTH BELOW SEAFLOOR (m)
SOUTH
HORIZONTAL SCALE
0
5
10
NORTH
SEAFLOOR
BUBBLE PULSE
UNIT 1
UNIT 2
UNIT 3
UNIT 6
MULTIPLE

Figure 3.34. Isoapch maps for OIS 6-1 generated from ECS seismic data.

ISOPACH MAPS FROM EAST CHINA SEA SEISMIC DATA

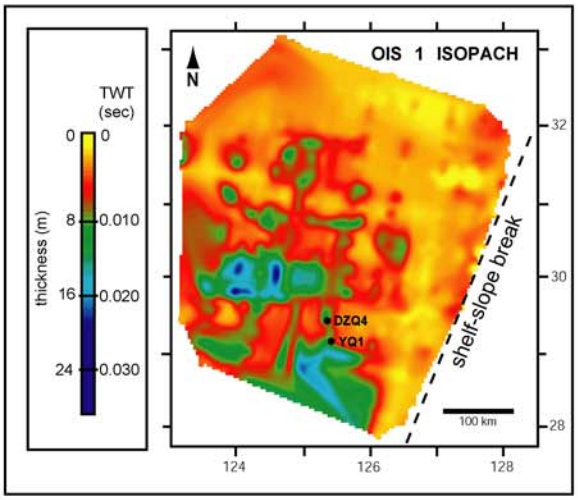

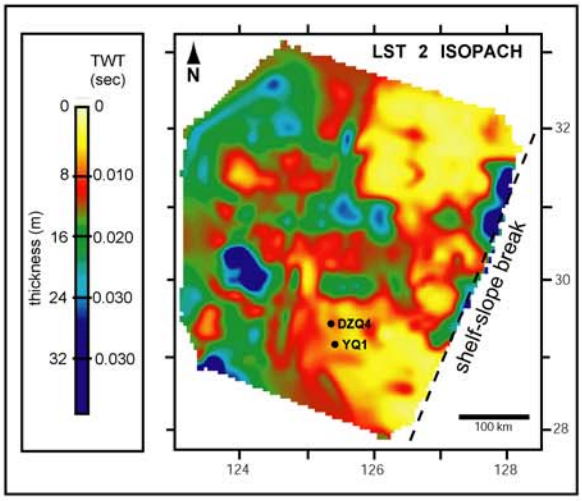

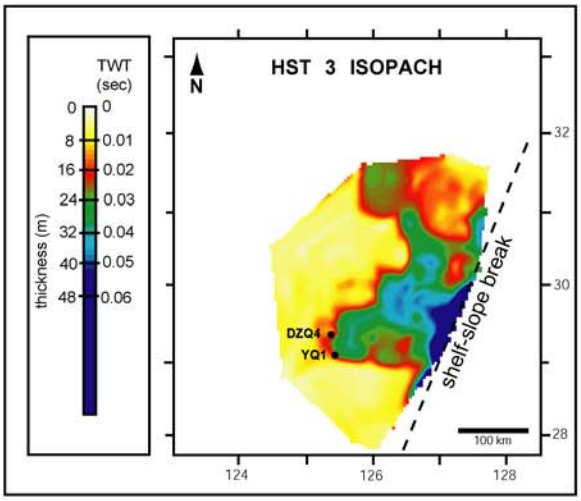

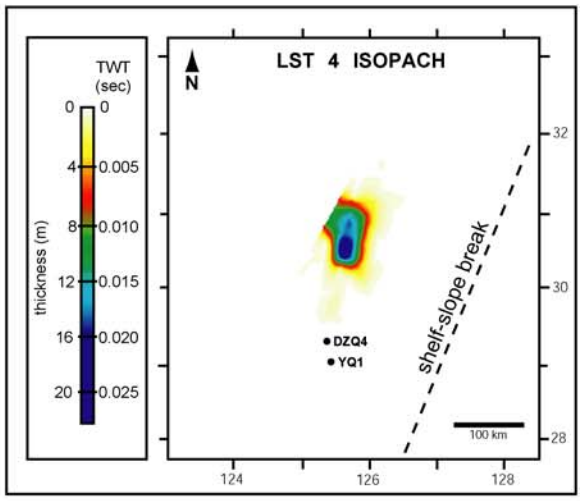

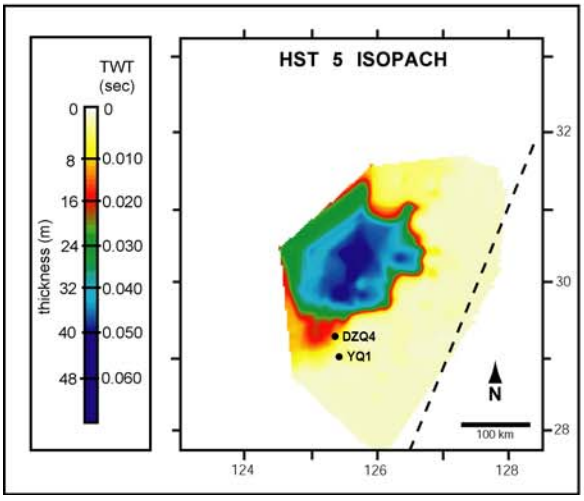

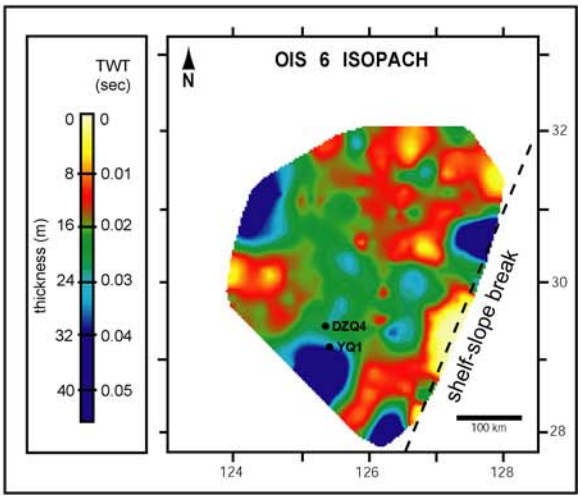

Figure 3.35. A dip-oriented stratigraphic cross-section generated from seismic profiles from the southern portion of the ECS margin.

DIP-ORIENTED SEISMIC PROFILE from EAST CHINA SEA

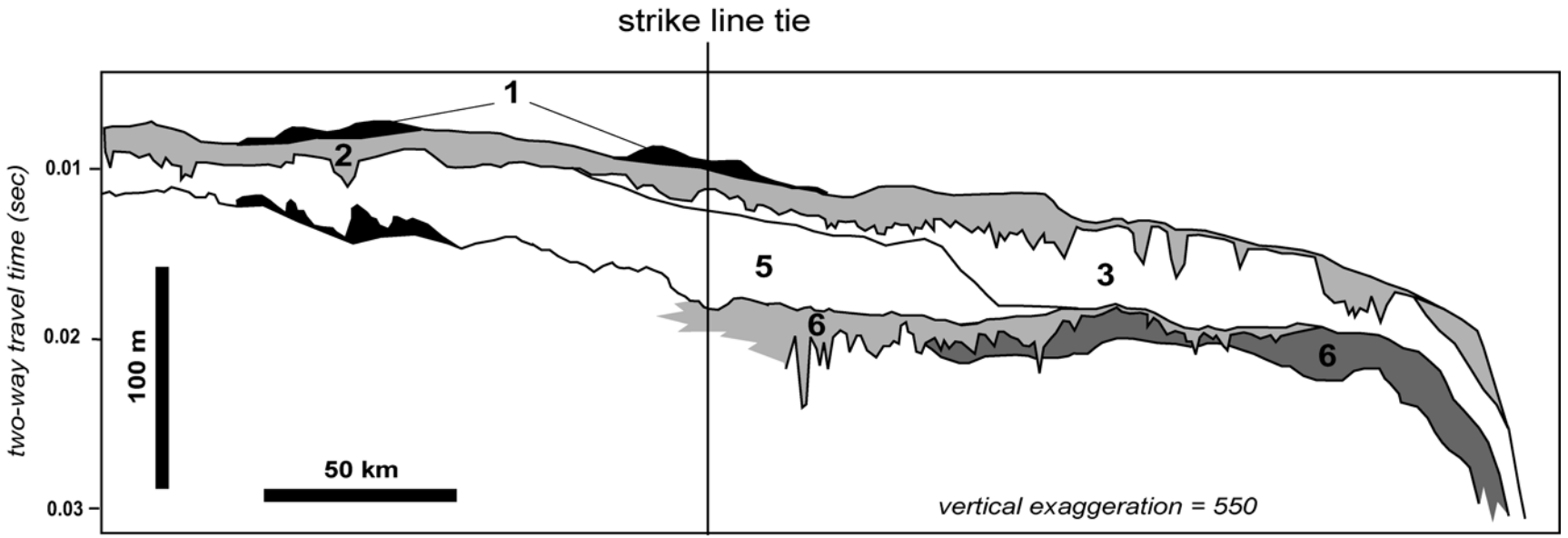

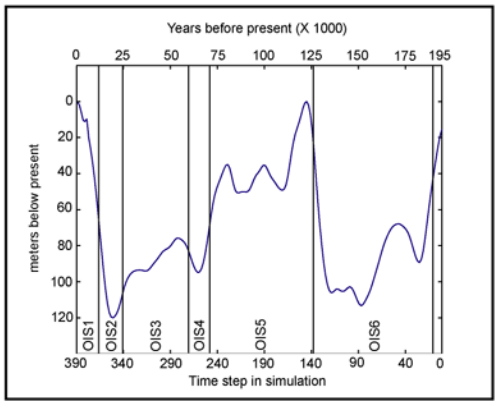

SEISMIC LINE LOCATION

Figure 3.36. A strike-oriented startigraphic cross-section generated from seismic profiles from the middle portion of the ECS margin.

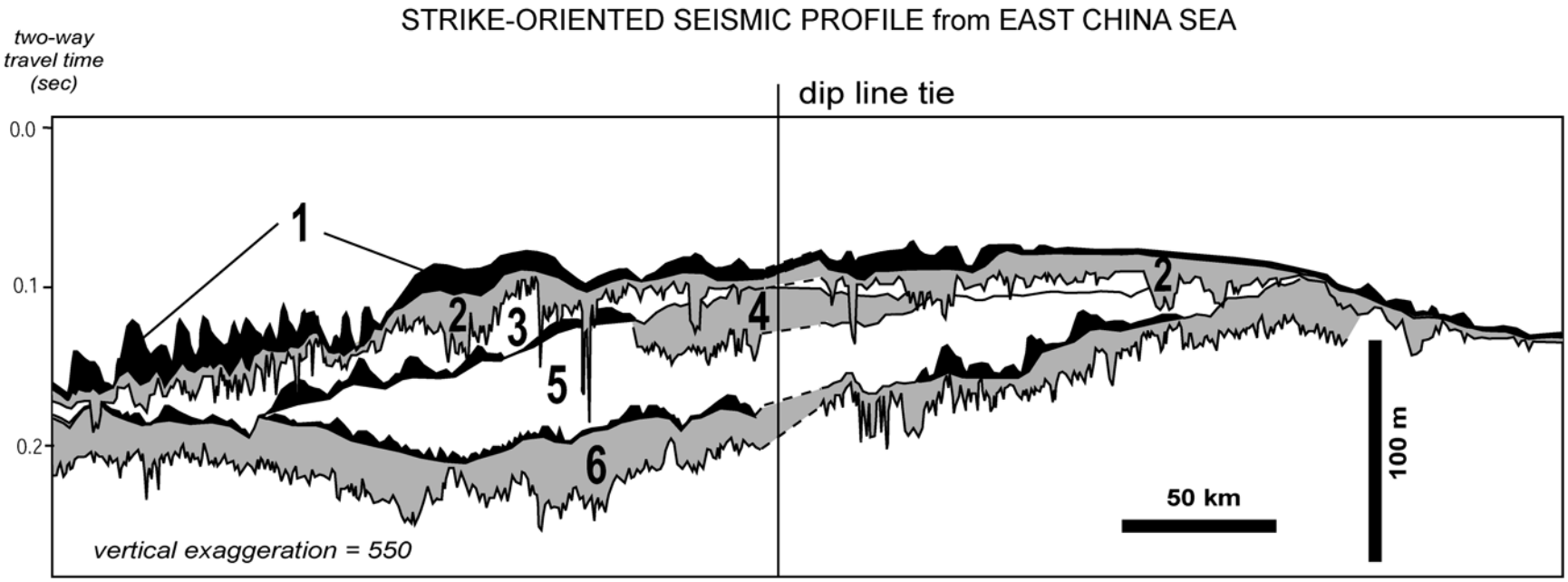
STRIKE-ORIENTED SEISMIC PROFILE from EAST CHINA SEA
two-way travel time (sec)
dip line tie
0.0
0.1
0.2
1
2
3
4
5
6
2
100 m
50 km
vertical exaggeration = 550

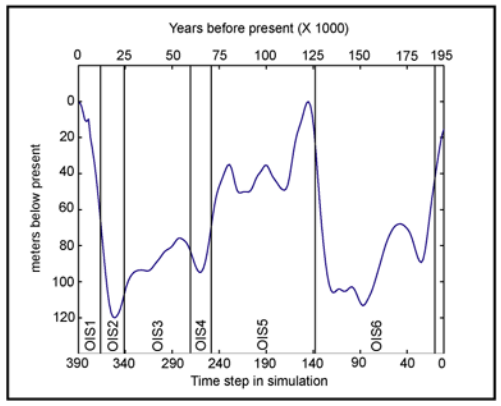
Years before present (X 1000)
0 25 50 75 100 125 150 175 195
meters below present
0 20 40 60 80 100 120
OIS1
OIS2
OIS3
OIS4
OIS5
OIS6
390 340 290 240 190 140 90 40 0
Time step in simulation

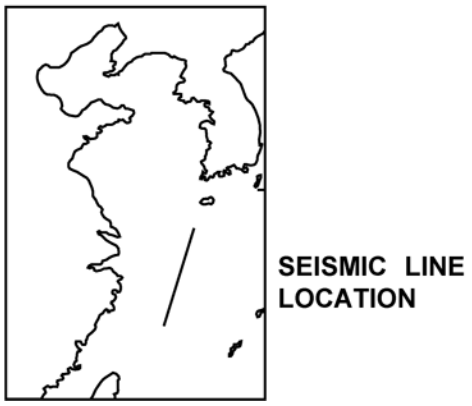
SEISMIC LINE LOCATION

engine of *fuzzy*PEACH were also established based primarily on general geologic conditions. Evaluation of model skill includes comparing the geologic variables used in *fuzzy*PEACH simulations to those observed, inferred, or expected on the ECS margin. This process is summarized here.

The simulated margin geometry at the first time step lacks antecedent topography, has a length (shore parallel) of 600 km and a shelf width (shore normal) of 500 km. The shelf-slope break is shore parallel at 150 m below modern sea level and creates a shelf gradient of 0.017° (Figure 3.8). Comparatively, ECS margin physiography is defined by a low gradient (0.23 m/km or 0.013°) and a deep shelf-slope break that occurs in present water depths between 150 and 192 m deep (average = 170 m; Wong et al., 2000). The ECS has maximum dimensions of 1,300 km (north-south) by 740 km (east-west) making the underlying continental margin one of the broadest shelves in the world. Stratal architecture observed in seismic profiles from the ECS margin indicates that similar physiographic conditions existed throughout the late Pleistocene and Holocene (i.e., similar width, depth of shelf-slope break). Paleo-shelf breaks are within 10 km of the modern shelf edge and the lack of major incision along the shelf-slope break signifies that the margin edge remained submerged during the high magnitude lowstands (-120 m below present) of OIS 2 and OIS 6. Simulations assumed a margin without topographic relief at the first time step. Seismic profiles indicate that antecedent topography (lobes = positive relief, incision = negative relief) was not present at the onset of OIS 6 (186 ka).

Core DZQ4 extends into fluvial strata deposited during OIS 6 (186 ka) and provides chronological constraints for the seismic profiles (Figure 3.32). A local, ECS-specific sea level curve was developed by Saito et al. (1998), but it only extends to 80 ka. The regional

curve from the western Pacific (offshore Papua, New Guinea; Shackleton, 1987; Pillans et al., 1998) is also temporally restrictive, spanning only the past 150 ky. Establishing a eustatic signal back to OIS 6 requires a longer record. The SPECMAP data (Winograd et al., 1988; 1992) matches the trends of both local and regional curves above and is used to define the eustatic signal back to the last highstand of OIS 7 (approximately 195 ka).

In order to create a more accurate stratigraphic mode, and therefore, a better understanding of stratigraphic response to relative sea level, an attempt was made in this investigation to de-couple the three major components of subsidence: tectonics, isostatic flexure and compaction. Tectonic subsidence, while varied during sensitivity tests between 0 and 4 mm/yr, was assumed to be minimal during passive margin conditions, and was therefore set at 0.1 mm/yr for all simulations. Seismic profiles were used to determine the specific tectonic subsidence rate for the ECS margin. To minimize the effect of sediment loading, tectonic subsidence was measured from seismic profiles in the southern portion of the outer margin. In this region, the strata contain a condensed section between OIS 5 and OIS 2 (130 ky) with no major unconformities. A basic calculation (thickness divided by time) between the transgressive surface between OIS6 and OIS 5 (approximately 130 ka) and the modern seafloor yields a subsidence rate that did not exceed 0.1 mm/yr (Figure 3.14). Therefore, *fuzzy*PEACH simulations from this investigation assume tectonic subsidence rate to be no more than 0.1 mm/yr at the shelf-slope break. This rate remained constant for each time step and decreased linearly landward (along dip) to zero along the coast (the landward most edge of the 600 km x 600 km modeled universe). This hinge corresponds to the general region of uplift along China's eastern coast (Wang, 1980; Congxian et al., 1991). A low rate of tectonic subsidence is consistent with previous investigations. The geometry of the ECS

shelf and the Okinawa Trough exhibits the fundamental shelf-slope-rise morphology that is typical of most passive continental margins (*sensu* Heezen et al., 1959). Many have classified the ECS as tectonically inactive throughout the Quaternary (Desheng, 1984; Weiling and Junying, 1989; Yu, 1991). However, the abundance of sediment on the margin (between 8 and 10 km thick; Wang and Aubrey, 1987; Shanshu et al., 1990; Yunshan et al., 1996) has been considered by others to be greater than the subsidence, if the subsidence was driven solely by compaction. Consequently, others (Emery and Aubrey, 1986; Wang and Aubrey, 1987; Chen and Stanley, 1993; Stanley and Chen, 1993) attributed the subsidence to a combination of tectonic down-warping and isostatic compensation during all of the Cenozoic.

The *fuzzy*PEACH uses a single fluvial system to deliver sediment to the simulated margin. Because fluvial influx was a user-defined variable, sensitivity testing used sedimentation rates spanning 1 x 10^8 to 5 x 10^8 tons/yr. Values associated with the Yangtze River (past and present) were used for simulations being constrained by the overall ECS dataset. The Yangtze River presently contributes 4.8 x 10^8 tons of sediment per year to the ECS margin and is the fourth largest river in the world, in terms of sediment discharge (Milliman and Meade, 1983; Milliman and Syvitski, 1992). This current rate reflects changes in climate regime, patterns of erosion and deposition, and anthropogenic influences (primarily cultivation and deforestation) that did not exist during the past 6 ky. Prior to this period, sediment influx rate is estimated to be 50% lower (Hori et al., 2001; Saito et al., 2001). To observe the stratigraphic response to variable sedimentation, this investigation used both rates (which remained constant for each time step): modern rate at 4.8 x 10^8 t/yr (2.4 x 10^{11} tons per 500-year time step) and paleo rate approximation at 2.4 x 10^8 t/yr (1.2 x

10^{11} tons per 500-year time step). These two rates are similar to many other modern river systems, a comparison of which is presented in Figure 3.9. An assumption of constant sediment influx for each time step followed one of the general assumptions of the sequence stratigraphic model. Based on precipitation rates associated with the high-frequency glacio-eustatic signal throughout the Pleistocene (Figure 3.39), sedimentation rates were probably not constant. Challenges associated with this variability are addressed later in this discussion.

The rest of the geologic variables, used to define the boundaries of the fuzzy sets defining the five FISs, were not user defined and remained constant throughout all simulations. These included, the average porosity used in mass balance, the variables used to define and calculate compaction and isostatic compensation (e.g., grain size, depth, and volume of sediment deposited), and specific values for fuzzy sets defining distances from channel (fluvial deposition) and river mouth (deltaic deposition). The mass balance algorithm embedded within the *fuzzy*PEACH ensures depositional volume of sediment deposited in both the fluvial and deltaic systems is equal to sediment influx for each time step. A mass-to-volume conversion algorithm assumes a clastic-dominated, silica-rich sediment load (density of quartz = ρ_{qtz} = 2643 kg/m^3) and an average porosity (Φ) of 50% (although ρ and Φ can be user-defined variables with *fuzzy*PEACH). Average porosities of shallow ($\leq$ 3 m) silty clays (<11% sand) in the ECS range from 62% to 72% (Keller and Yincan, 1985). Porosities of shallow ($\leq$ 3.5 m) fine-grained sediments from the YS exhibit Φ values as high as 70% and sands were as low as 40% (Lee et al., 1987). An average porosity set at 50% for mass balance compares well to ECS core data (cores DZQ4 and YQ1 discussed above). If anything, based on the dominance of silt-sized sediment on the seafloor

at and near the mouth of the Yangtze (e.g., Milliman et al., 1985b; Chen et al., 2000; Hori et al., 2001; 2002c), the porosity used for mass balance may be a little low. These core data generally agree with numerous curves presented by Baldwin and Butler (1985) that bracketed values ranging from 80 to 50% at the surface (Figure 3.13). However, in this case, the compaction values may be somewhat high.

The FIS controlling deltaic deposition (grain size and volume) used water depth to define the general depth at which the physical processes affecting depositional processes are no longer affected by surface waves. The depth of fair-weather wave base has been reported as deep as 60 m for specific locations (Ebro Delta; Puig et al., 2001) to as shallow as 10 m for modern, high-energy coasts in general (Clifton, 2000). Therefore, "shallow" was defined for water depths less than 10 m and "deep" for depths greater than 60 m. The range between 10 and 60 m was a combination of both "shallow" and "deep" to varying degrees with equal membership (MF=0.5) at 35 m (Figure 3.12C). In the ECS, the 10 m isobath defines the boundary of maximum turbidity (Hori et al., 2002c; their Figure 3) and the seaward boundary of the Yangtze depocenter (Chen et al., 2000; their Figure 8). Fluvial and coastal processes dominate the areas shoreward of this position and a combination of fluvial and marine processes occur seaward of the 10 m depth. The 30 m isobath defines the general boundary dividing coarse- and finer-grained sediment fractions near the mouth of the Yangtze River (Milliman et al., 1985b; their Figure 3). The grain size distribution is widespread and represents a potential boundary between depositional processes (e.g., where the influence of coastal currents and fluvial processes on deltaic deposition cease to dominate). Thus, the boundary between the fuzzy sets "shallow" and "deep" defined at 35 mare taken to be a

reasonable proxy for the ECS to define the boundary between dominant processes affecting seafloor deposition.

The determination of isostatic flexure was based on the general premise that higher sediment loads require higher amounts of isostatic compensation. This isostatic reponse of the earth's crust via subsidence has been observed on continental margins receiving a high sediment load, including the Ganges-Brahmaputra delta (Alam, 1996), the Mobile River delta (Fillon et al., 2004), and the Mississippi River (Törnqvist et al., 2005). The geometry of the ECS shelf and the Okinawa Trough exhibits the fundamental shelf-slope-rise pattern that is typical of most passive continental margins (*sensu* Heezen et al., 1959). Many have classified the ECS as tectonically inactive throughout the Quaternary (Desheng, 1984; Weiling and Junying, 1989; Yu, 1991). However, the abundance of sediment on the margin (between 8 and 10 km thick; Wang and Aubrey, 1987; Shanshu et al., 1990; Yunshan et al., 1996) has been considered by others to be greater than the subsidence if it was driven solely by compaction. Consequently, others (Emery and Aubrey, 1986; Wang and Aubrey, 1987; Chen and Stanley, 1993; Stanley and Chen, 1993) attributed the subsidence to a combination of tectonic down-warping and isostatic compensation during all of the Cenozoic. The general relationship for isostatic compensation, presented by Bitzer and Pflug (1990) and Turcotte and Schubert (2002), is

$$S = [(\rho_m - \rho_w) / (\rho_m - \rho_s)] \cdot (D - d)$$

where S = is the change if thickness of the sedimentary column to which the the crust responds isostatically, ρ_m is mantle density (3300 kg/m^3), ρ_w is density of ocean water (1027 kg/m^3), ρ_s is the density of the sediment load (2643 kg/m^3), D is water depth before deposition, and d is the water depth after deposition. This calculation overestimates the

amount of subsidence observed on the ECS margin based on published rates and observed trends in the seismic data. Therefore, ranges for the fuzzy variables "subside a little", "subside a lot", "thick", and "thin" were defined. Subsidence rates between 1.6 and 4.4 mm/yr on the inner margin near the mouth of the Yangtze River (Stanley and Chen, 1993) are roughly 10% of sedimentation rates (between 10 and 54 mm/yr; DeMaster et al., 1985). The tectonic component of subsidence at this location is regarded as negligible due to its location near the tectonic hinge that is associated with regional uplift along the east coast of China (Wang, 1980; Congxian et al., 1991). On the middle and outer ECS margin, the subsidence rate is 0.3 mm/yr (Berne et al., 2002). When corrected for tectonic subsidence (0.3 mm/yr - 0.1 mm/yr = 0.2 mm/yr; see Figure 3.14), this value is a little more than 5% of the sedimentation rate of 3 mm/yr (DeMaster et al., 1985). Elsewhere on the margin, sedimentation is negligible and isostatic loading is assumed to be zero.

Results of Simulations Compared to Regional ECS Dataset. A stage-by-stage (i.e., oxygen isotope stage) comparison of seismic data to model results is presented below. The 195 ka simulation included the last 9 ky of OIS 7, however, core data were only deep enough to constrain strata back through OIS 6. The shallow nature of the ECS (average depth = 72 m; Yunshan et al., 1996) also limited the observation of the geologic record formed during this time by creating a shallow seafloor multiple that often obscured seismic reflections from strata deeper than OIS 6. The initial simulation was constrained by estimates of the paleo sedimentation rate (50% of modern or 2.4×10^8 tons/yr; Hori et al., 2001; Saito et al., 2001). Wellner and Bartek (2003) suggested that sediment delivery to the margin was abundant during warm and wet conditions and minor during cool, dry climates (at least since OIS 2). Therefore, to consider large potential shifts in sediment supply (i.e., higher precipitation rate

than present during HST 5), another simulation was designed to incorporate higher sedimentation influx (equal to modern rates in the Yangtze River). In addition, two models were also run under these two sediment conditions (moderate and high, respectively) to determine the accuracy of the rules governing avulsion (Figure 3.12B). To do this, high and moderate sediment conditions were also simulated with the avulsion FIS deactivated. Fluvial avulsion that was not governed by fuzzy logic still occurred, but with less frequency. As accommodation was filled, the fluvial system shifted in order to re-establish the lowest elevation pathway to base level.

Output for each of these four simulations is presented graphically in this paper as a set of isopach maps for each OIS, as well as two synthetic cross-sections in both dip and strike orientation. The results for moderate sediment influx, under FIS-controlled avulsion, are presented in Figures 3.19, 3.20, and 3.21. The results for high sediment influx under FIS-controlled avulsion are presented in Figures 3.22, 3.23, and 3.24. The results for moderate sediment influx with a deactivated avulsion FIS are presented in Figures 3.25, 3.26, and 3.27. The results for high sediment influx with a deactivated avulsion FIS are presented in Figures 3.28, 3.29, and 3.30. Isopach maps for each OIS generated from ECS margin seismic profiles are included in Figure 3.34. Dip- and strike-oriented cross section assembled from seismic profiles are presented in Figures 3.35 and 3.36, respectively. Observations from all of these data, simulations and ECS seismic surveys, are summarized in Table 3.2.

OIS 6 (186 to 128 ka). This stratal unit extends more than 500 km along strike of the ECS margin and upwards of 200 km along dip, with an average thickness of 20 m. A distinct seismic facies of chaotic reflections is associated with most of OIS 6 (Figure 3.32). At DZQ4, OIS 6 contains cross-bedded sands with terrestrial components such as pollen from

land plants and wood debris. Pollen assemblages indicate a warm and humid climate transitioning to a colder and drier climate toward the top of the interval. Nannofossil assemblages (coccolithophores), however, are indicative of cold environments throughout the entire interval (Liu et al., 2000; Berne et al., 2002). The depositional environment has been interpreted as a sand sheet formed by an unconfined, fluvial braid plain (Warren et al., 2002a; Bartek and Warren, 2002; Warren and Bartek, 2002a; 2002b). Three lobate, depocenters on the middle to outer margin (Figure 3.34) are considered the downdip, deltaic equivalent of the fluvial facies (Figure 3.35) (Berne et al., 2002; Warren and Bartek, 2002a, 2002b). These small lobes are approximately 50 km in diameter and upwards of 40 m thick. Simulations using a high sedimentation rate (4.8×10^8 tons/yr), and an active avulsion FIS, also produced strata with a maximum thickness of 40 m. (Table 3.2). The simulation produced a delta complex on the outer margin with a length-to-width ratio (length = shore perpendicular) of approximately 1:3. Length-to-width ratios greater than 1:2 are produced with an operational avulsion FIS (Table 3.2). However, even high length-to-width ratios for a highly avulsive system created two distinct depocenters (Figure 3.28). The lateral extent and consistent thickness, of this depositional unit is also observed in the synthetic, strike-oriented cross-section from the middle margin (Figure 3.30). The simulated grain size of this unit primarily is coarser material (sand and silt) similar to the silty sands observed in core DZQ4.

OIS 5 (128 to 71 ka). The major feature of this stratal unit is the lobate morphology observed on the middle of the ECS margin (Figure 3.34 and 3.35). Strata exceed 40 m thickness in the central portion of this lobe and pinch-out, basinward on the outer margin, about 125 km from the shelf-slope break. This lobe is about 200 km wide, composed of clays and silts, and interpreted as deltaic in origin (Saito et al., 1998; Liu et al., 2000; Berne

et al., 2002). Similar thickness, between 30 and 60 m, is observed in each of the four model runs (Table 3.2). However, the synthetic isopach map of modeling results for OIS 5 (Figure 3.19), under moderate sedimentation rates (2.4 x 10^8 tons/yr) and a deactivated avulsion FIS, most strongly resembles the seismic data (Figure 3.34), in both morphology and thickness (single lobe with maximum thickness of 35 m). The prominent, single lobe in the simulation was formed during a period that did not experience avulsion. The finer-grained material from the middle-to-outer margin observed in synthetic cross-sections (both strike and dip; Figure 3.20 and 3.21) is similar to the fine-grained material in core DZQ4.

OIS 4 (71 to 59 ka). The only substantially thick (i.e., >1 m) portion of OIS 4 is observed on the middle margin in two seismic profiles (Figure 3.34, 3.35, and 3.36). At this location, it extends for less than 100 km along strike and, on average, is 8 m thick. Elsewhere on the margin, the strata are thin and resolved by a single seismic reflection that correlates to a 3-cm interval in core DZQ4 (Liu et al., 1998; Berne et al., 2002). The thicker portion of the unit that is observed in seismic profiles is not constrained by core data, and actual lithologies are unknown. Based on sequence stratigraphic framework (a lowstand systems tract) and seismic facies (chaotic reflections), the lithology of OIS 4 is inferred to be fluvial sands. The chaotic seismic facies is identical to that defining the fluvial sands of OIS 6 (Figure 3.32). Stratigraphy simulated under conditions of moderate sediment influx generated similar thickness to the thicker portions of OIS 4 on the ECS margin (Table 3.2). The avulsion FIS caused lobe shifting that created mutliple depocenters (Figure 3.25). Cross-sections generated from a few seismic profiles, particularly strike-oriented profiles on the middle shelf (Figure 3.36), indicate that minor incision occurred during OIS 4. Incision was not included in the preliminary version of *fuzzy*PEACH, so the data indicate that this

stage is not accurately simulated. The observed incision, however, is not associated with exposure and incision at the shelf-slope break. It occurs in the middle portion of the margin, and is associated with the depocenter of the delta lobe from the preceding highstand (OIS 5).

OIS 3 (59 to 24 ka). Seismic profiles and the isopach map from OIS 3 indicate that the majority of deposition occurred on the outer margin basinward of the OIS 5 lobe (Figure 3.34 and 3.35). These strata, on average, are between 30 and 50 m thick. A large volume of sediment from OIS 3 is observed in seismic data to offlap over the shelf-slope break and onto the continental slope (Figure 3.35). This unit is interpreted as deltaic and is dominated by silts and clays (Saito et al., 1998; Liu et al., 2000; Berne et al., 2002). The depocenter locations, for all four *fuzzy*PEACH simulations (i.e., high and moderate sediment input with avulsion FIS active and inactive), also occured on the outermost portion on the margin (Figure 3.19, 3.22, 3.25, 3.28). The two *fuzzy*PEACH simulations using high sedimentation rates (4.8×10^8 tons/yr), both with and without FIS avulsion control, have thicknesses that are most similar to the ECS seismic data (Table 3.2; Figure 3.22 and 3.28). Two distinct depocenters were produced when the avulsion FIS was activated (during both moderate and high sedimentation) (Figure 3.22-3.24 and 3.28-3.30). Therefore, the high sediment simulation without fuzzy avulsion control share the most similarities with the seismic data from OIS 3. The synthetic unit is coarser than the overall grain size observed in core DZQ4.

OIS 2 (24 to 12 ka). Lobate units composed of offlapping reflections are perched at the shelf-slope break and a laterally extensive unit consisting of chaotic reflections of variable thickness was deposited on the inner margin, all over 30 m thick, are the major features associated with the OIS 2 isopach from the ECS dataset (Figure 3.34). Both of these features are also observed on dip- and strike-oriented cross-sections (Figure 3.35 and 3.36). The thick

deposits on the inner margin are associated with overbank and an incised valley system (e.g., Hori et al., 2001, 2002a, 2002b; Warren and Bartek, 2002b; Wellner and Bartek, 2003). The incision occurred on the middle portion of the margin rather than at the shelf-slope break, which remained submerged during the lowstand of OIS 2. The prominent lobes (> 30 m thick), that are perched on the outermost margin at the shelf-slope break, are interpreted as lowstand deltas (Warren and Bartek, 2002b). Excluding the incised valley deposits and deltaic lobes, the unit, while laterally continuous, is thin (on average, it is less than 4 m thick). The thickness of modeled strata during high sediment influx (4.8×10^8 tons/yr) was more similar to ECS data than moderate sediment models (Table 3.2). However, the incised nature of OIS 2 on the ECS margin was not simulated by *fuzzy*PEACH. Simulated incision was partially addressed during model development but still under development at the time this paper was prepared. While the simulated lowstand deltas on the outermost margin correlate to seismic profiles, the fluvial components of *fuzzy*PEACH strata from OIS2 do not accurately represented the stratal geometry observed on the margin. Continued development of erosion and incision for future inclusion into *fuzzy*PEACH is planned.

OIS 1 (12 ka to present). The average thickness of this unit in seismic profiles proximal to boreholes DZQ4 and YQ1 was about 3 m (Yang, 1989; Liu et al., 2000; Berne et al., 2002). The upper surface of this unit is the present-day seafloor of the ECS. Strata from OIS 1 are either a thin unit (<1 m) or discrete ridges up to 20 m thick. The thicker ridges are interpreted as mounds of sediment reworked by tidal currents (e.g., Yang, 1989; Saito et al., 1998; Liu et al., 2000; Li et al., 2001; Berne et al., 2002; Zhu and Chen, 2005). Where tidal ridges do not exist, the unit is a thin (<2 m) sand veneer (Bartek and Wellner, 1995; Wellner and Bartek, 2003). One exception exists on the inner margin where strata are associated with

incised valley fill (Figure 3.34). Unlike the strata observed in seismic profiles, prominent deltas were formed during this time period in each of the four models (Figure 3.19, 3.22, 3.25, 3.28). This morphology is not consitent with trends observed in the seismic data.

Summary of ECS Margin Simulations. A high sedimentation rate (4.8 x 10^8 tons/yr) during FIS-controlled avulsion was most similar to the laterally extensive strata preserved on the ECS margin during OIS 6. Distinct depocenters observed in seismic data were also observed in model output. Output from a simulation using a moderate sediment influx (2.4 x 10^8 tons/yr) and avulsion conditions not governed by fuzzy logic produced a single-dominant deltaic lobe formed on the middle margin during OIS 5. This unit shared the most similarities to the strata observed in seismic profiles. The minor incision that occurred on the ECS margin during OIS 4 was not simulated by *fuzzy*PEACH, and the distinct deltas observed in all model output for OIS 4 were not identified in seismic profiles. However, the condensed nature of this unit away from the fluvial source (<3 cm in core DZQ4 and a single reflection in seismic profiles) was similar to a lack of deposition on portions of the margin distal to the fluvio-deltaic system. The strata simulated during OIS 3, with a high sediment influx (4.8 x 10^8 tons/yr) deposited under conditions not controlled by the avulsion FIS, were most similar to the strata deposited on the outermost portion of the ECS margin. The deltas simulated during OIS 2, in all models, were similar to the those observed on the outermost shelf of the ECS. However, the lack of incision in the version of fuzzyPEACH discussed in this paper did not allow the model to create strata similar to OIS 2 and OIS 1 observed in ECS seismic profiles.

In addition to comparing the simulated strata as individual units, it is also necessary to compare the entire succession of stratigraphy for the entire time period. The model output

most similar to the cross-sections from the ECS were formed with a moderate sediment supply (2.4 x 10^8 tons/yr) and avulsion not governed by fuzzy logic. The depth of the shelf-slope break at the end of this particular simulation was 120 m deep (Figure 3.20). Moderate sediment influx, with avulsion controlled by the FIS, produced an even deeper shelf-slope break at 142 m (Figure 3.26). While closer to that of the modern ECS margin (on average 170 m deep; Wong et al., 2000), this average thickness and overall cross-sectional geometry were not similar to ECS data (Figure 3.35 and 3.36). In order to provide a more detailed comparison to actual borehole data from the ECS margin, a synthetic core was extracted from the results of the simulation that used moderate sediment supply and no fuzzy avulsion control. The location of DZQ4, is 400 km from the modern shoreline (measured radially from the mouth of the Yangtze River). Therefore, a synthetic core was extracted from the same location on the middle to outer margin (Figure 3.37). The summary of core DZQ4 is from Liu et al. (2000) and Berne et al. (2002), but stratigraphic units have been re-defined during the broader ECS investigation (Bartek et al., 2001; Bartek and Warren, 2002; Warren and Bartek, 2002a; 2002b; Warren et al., 2002; Bartek et al., 2004). Thickness correlates well with the exception of OIS 3 and OIS 5, where thickness values are inversely proportional (i.e., synthetic OIS 5 thickness closer to DZQ4 OIS 3 and vice versa). A synthetic core from a position that is closer to the shelf-slope break has a thinner OIS 5 and thicker OIS 3 that is more consistent with DZQ4. Decreasing the sediment influx and/or increasing the rate of tectonic subsidence, while leaving the synthetic core in its original location (Figure D1b), would also simulate thinner strata in OIS 5 and thicker strata in OIS 3 and make it more consistent with DZQ4.

Figure 3.37. Synthetic core extracted on the outer margin approximately 400 km basinward from the simulated river mouth at sea level highstand. Core DZQ 4 is approximately the same distance from the mouth of the Yangtze River (Figure 3.31). Synthetic strata are compared to those found in core DZQ4 (Berne et al., 2002).

INTERPRETATION of CORE DZQ4
DEPTH in SECTION
0 m
20 m
40 m
60 m
~67 m
OIS 1
OIS 2
OIS 3
OIS 4
OIS 5
OIS 6
OIS 7
SYNTHETIC CORE
DEPTH (m)
HST 1
TST 2/1
LST 2
HST 3
TST 4/3
LST 4
HST 6
TST 6/5
LST 6
0.13
3.2
11.85
28.1
30.3
30.6
37.4
39.4
51.6
SAND
SILT
CLAY
SYNTHETIC CORE
meters
kilometers
CORE DZQ4
Berne et al., 2002
clay
silt
sand
TL DATE 46903 +/-2313
TL DATE 50246 +/-2512
Ehux acme
TL DATE 87764 +/-4388
shell debris
foram debris
mud clasts
wood debris
corals
bioturbation
horizontal bedding
cross bedding
undulated bedding
DEPTH (m)

3.4.2 Assessment of fuzzyPEACH Performance

The extensive, regional seismic dataset from the ECS margin provides the opportunity to assess the skill of stratigraphic simulations. Based on these data and other published studies, the variables affecting relative sea level, eustasy, tectonic subsidence, sediment influx, and margin physiography during the past 195 ky were established. The overall performance of the *fuzzy*PEACH, based on these conditions, simulates reasonable stratigraphic architecture. A minor issue with the model may be related to the assumption that sedimentation rate is constant for every time step. Even though this is an assumption of the general sequence stratigraphic model, as well as many numerical simulations (e.g., Strobel et al., 1989; Lawrence et al., 1990; Carey et al., 1999; Ritchie et al., 2004a; 2004b), the thickness and distribution of model output, under modern rates of sedimentation (4.8 x 10^8 tons/yr) is most similar to OIS 6. However, model output from OIS 5 to present more closely resembles the simulation using 50% less sediment influx. The simulation of fluvial avulsion also provided results that are not consistent with ECS stratigraphy (i.e., the avulsion FIS created similar strata only during OIS 6). A major exception to the model's overall accuracy, though, is the inability of *fuzzy*PEACH to simulate erosion. Although erosion is minimized on the ECS margin, due to the high influx of sediment, and incision is not associated with the shelf-slope break, the result of incision was observed in seismic profiles from the middle portion of the margin. Therefore, with the exception of lowstand deltas during OIS 2, strata simulated from OIS 4 to present are not an accurate predictor of the stratigraphic architecture of the ECS margin. Incision will be incorporated into subsequent versions of *fuzzy*PEACH.

Sediment supply. One inconsistency between *fuzzy*PEACH simulations and ECS stratigraphy is stratal thickness. This is either a product of incorrect sedimentation rate or incorrect sediment distribution (i.e., avulsion). The avulsion frequency controlled with fuzzy logic is able to distribute sediment in a manner that is similar to the distribution of OIS 6 (i.e., consistent thickness extending laterally across the margin). This unit is interpreted as a sand sheet formed by an unconfined, fluvial braid plain (Warren et al., 2002a; Bartek and Warren, 2002; Warren and Bartek, 2002a, 2002b). Park (1987) presented a hypothesis of the numerous, braided fluvial systems active on the subaerially exposed ECS margin during sea level lowstand (Figure 3.38). In addition to these braid plain hypotheses, it is also possible that the Yangtze remained the dominant river, capturing smaller tributaries into the main trunk. A similar dominant-river hypothesis is presented by Hanebuth et al. (2003) for the Sunda Shelf during extreme lowstands. The two distinct deltas from OIS 6, observed in seismic data on the outermost margin, suggest one main fluvial system rather than multiple systems flowing across the margin (Figure 3.34). Younger units in the ECS have single depocenters representative of a stable (non-avulsive) delta (Saito et al., 19998; Liu et al., 2000; Berne et al., 2002), but these strata are not laterally extensive across the margin. They represent a point source rather than a line source. The avulsion FIS does not produce similar stratigraphy during these periods of lobe stability. There are two potential scenarios for this. First, the avulsion rules in the FIS might not accurately represent avulsion rates under all conditions (e.g., periods of higher sea level). Second, the minor incision noted in OIS 4, as well as the major incision during OIS 2, could have prevented the river from avulsing under conditions during which it otherwise might have avulsed at a frequency similar to hose

Figure 3.38. Potential analog for fluvial system distribution across subaerially exposed East China Sea continental margin during extreme lowstands (adapted from Park, 1987).

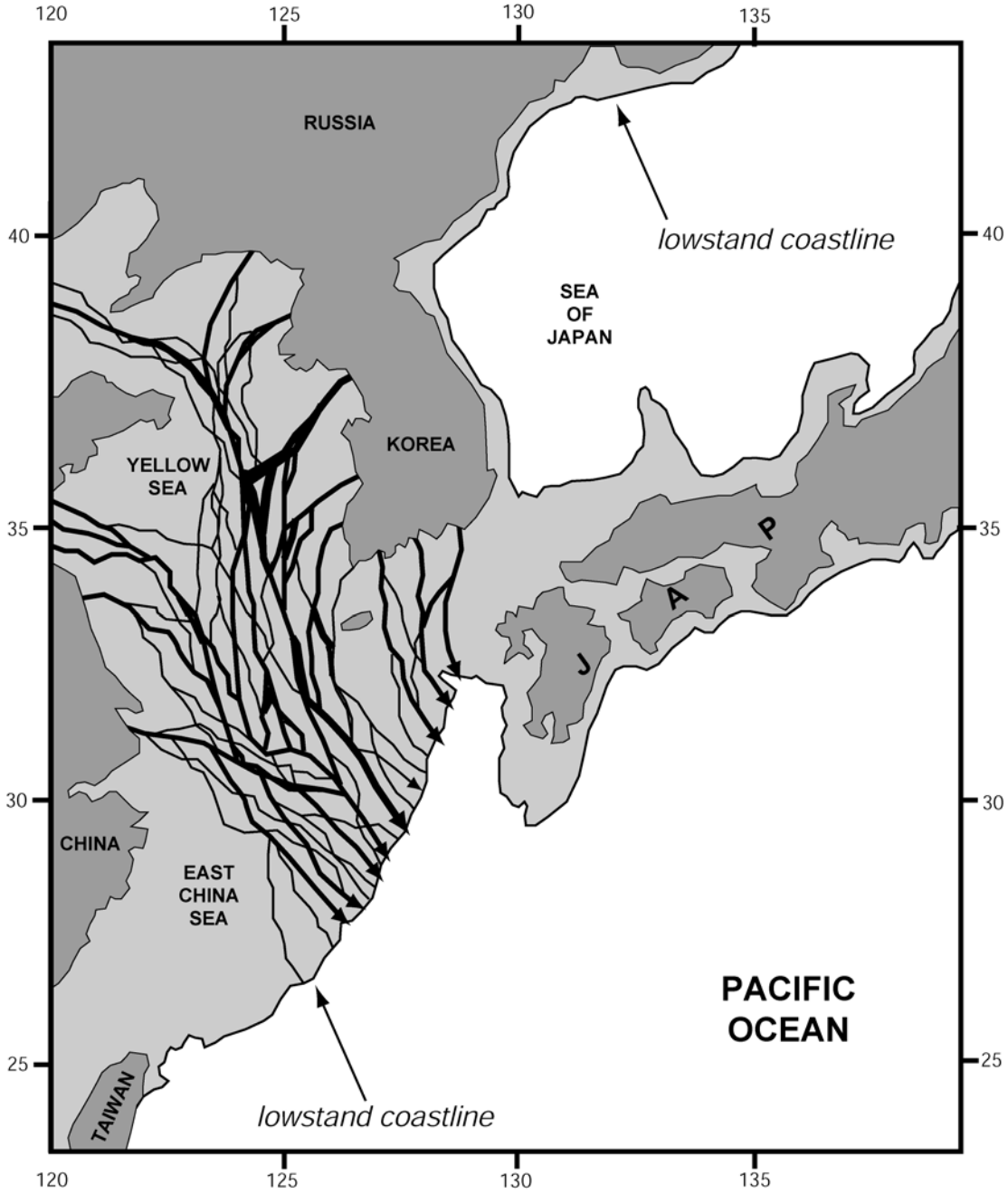
120
125
130
135
40
35
30
25
RUSSIA
lowstand coastline
SEA
OF
JAPAN
KOREA
YELLOW
SEA
P
A
J
CHINA
EAST
CHINA
SEA
PACIFIC
OCEAN
TAIWAN
lowstand coastline

described in the fuzzy rules. The extent that incision may have controlled fluvial deposition is discussed in more detail below.

A third possibility that could have impacted avulsion, and certainly stratal thickness and sediment distribution, on the ECS margin is temporal variation in sediment influx. This scenario is not included in *fuzzy*PEACH simulations. An assumption of the general sequence stratigraphic model is a constant sedimentation rate (*sensu* Posamentier et al., 1988). *Fuzzy*PEACH also makes this assumption by delivering a constant influx to the margin during each time step. Based on the high-frequency, glacio-eustatic fluctuations during the Pleistocene, and the climate changes driven by these cycles (e.g., Winkler and Wang, 1993; Sarnthein and Wang, 1999; Xiao et al., 1999; An, 2000; Stocker, 2000), this may be an incorrect assumption (at least during short-term, high-resolution periods). Climate changes, in turn, control precipitation. Evans and Heller (2001) compiled multiple datasets from the Luochuan section of the Loess Plateau that indicate somewhat higher paleoprecipitation rates during OIS 6 (between 300 and 400 mm/yr), but still much less than present day for this region (i.e., 650 mm/yr; Figure 3.39). With the paleo precipitation rates for this region fairly well established, the effect of decreased precipitation on the sediment yield in fluvial systems bordering the ECS is not well documented. It has been assumed in past studies of the ECS (e.g., Hori et al., 2001; Saito et al., 2001; Wellner and Bartek, 2003) that decreased precipitation during glacial maxima, and a subsequent decrease in runoff and erosion, also yielded a decrease in fluvial sedimentation rates, at least in the two major systems flowing into the ECS/YS/BS from the Asian continent (i.e., the Yellow and Yangtze rivers). On the other hand, during OIS 2, deposition rates on the exposed Sunda Shelf (South China Sea)

Figure 3.39. A) High resolution paleoprecipitation data from the Xifeng section on the Loess Plateau of China (from Liu et al. 1995). B) Low resolution paleoprecipitation from the Luochuan section of the Loess Plateau of China as compiled in Evans and Heller (2001).

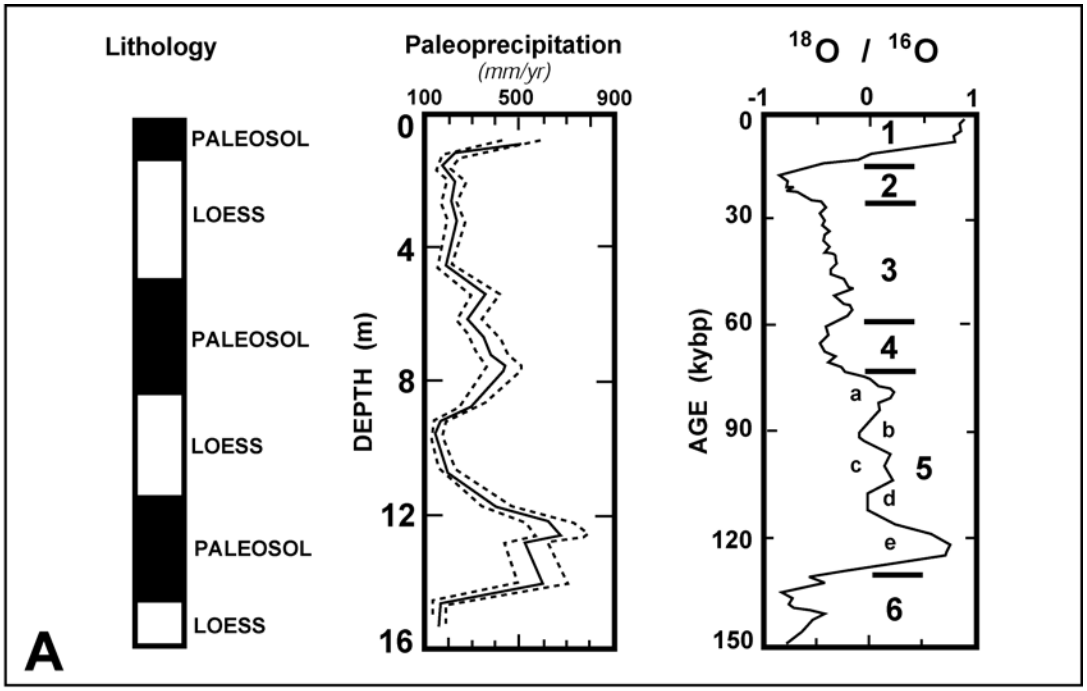
Lithology
PALEOSOL
LOESS
PALEOSOL
LOESS
PALEOSOL
LOESS
Paleoprecipitation
(mm/yr)
100
500
900
0
4
8
12
16
DEPTH (m)
18O / 16O
-1
0
1
0
30
60
90
120
150
AGE (kybp)
1
2
3
4
a
b
c
d
5
e
6
A

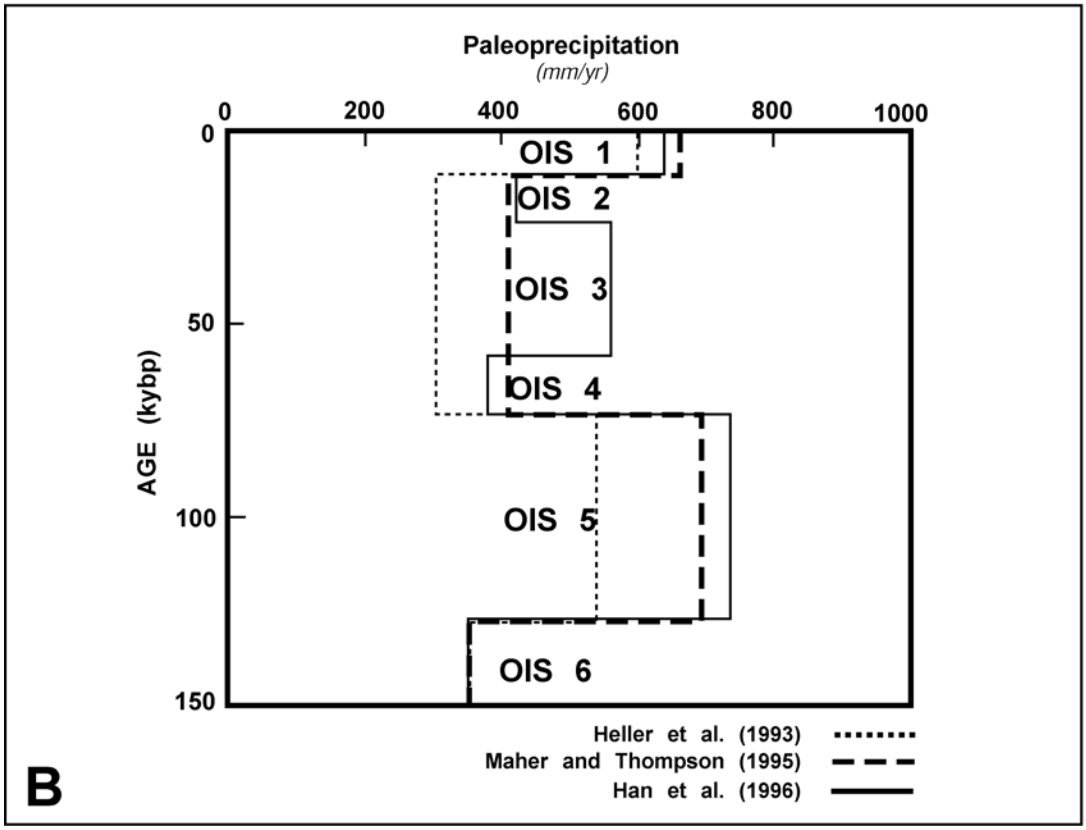
Paleoprecipitation
(mm/yr)
0
200
400
600
800
1000
0
50
100
150
AGE (kybp)
OIS 1
OIS 2
OIS 3
OIS 4
OIS 5
OIS 6
Heller et al. (1993)
Maher and Thompson (1995)
Han et al. (1996)
B

were twice as high as during the post-glacial times attributed, in part, to the erosion of the subaerially exposed Sunda Shelf (Wang et al., 1995).

Additional factors that could change sediment delivery to the margin, and stratal thickness, are independent of sediment supply from the drainage basin. These factors include the impact of subaerial exposure on fluvial gradient and the reduction of oceanic currents in the area during lowstands. As the wide ECS margin became subaerially exposed, the widening coastal plain could have created a lower fluvial gradient resulting in overextended fluvial systems. The resultant power loss could have increased bed load and rates of deposition (i.e., reduced velocity leading to higher deposition rates on the exposed shelf). This idea is presented by Holbrook (1996) to explain the broad, fluvial sand sheet of the Cretaceous Mesa Rica Sandstone (Dakota Group, late Albian) of the U.S. Western Interior Basin. The Mesa Rica Sandstone, which is similar to the MFSS presented by Warren and Bartek (2002a; 2002b), experienced frequent avulsion in conjunction with a low gradient that, in turn, caused regional scouring of a flat, planar, sequence-bounding unconformity (Holbrook and Dunbar, 1992; Holbrook, 1996). It is not unreasonable to expect these conditions of fluvial overextension preserved in the ancient record on the ECS margin during lowstand. However, sediment delivery to the margin, also unrelated to fluvial input from the drainage basin, can also be explained during highstand conditions. Presently, the ECS has an extensive current system related to the Kuroshio western boundary current (Figure 3.40) (e.g., Hung and Chung, 1994; Chung and Chang, 1995; Tamburini et al., 2003). Of the 4.78 x 10^8 tons of sediment presently transported by the Yangtze River each year, 40% (1.91 x 10^8 tons/year) is deposited at the river mouth and 30% (1.46 x 10^8 tons/year) is carried south by the Changjiang (Yangtze) Coastal Water current (Milliman et al., 1985a). During high-

Figure 3.40. Major ocean currents found in the modern ECS and adjacent basins (modified from Bingxian, 1994).

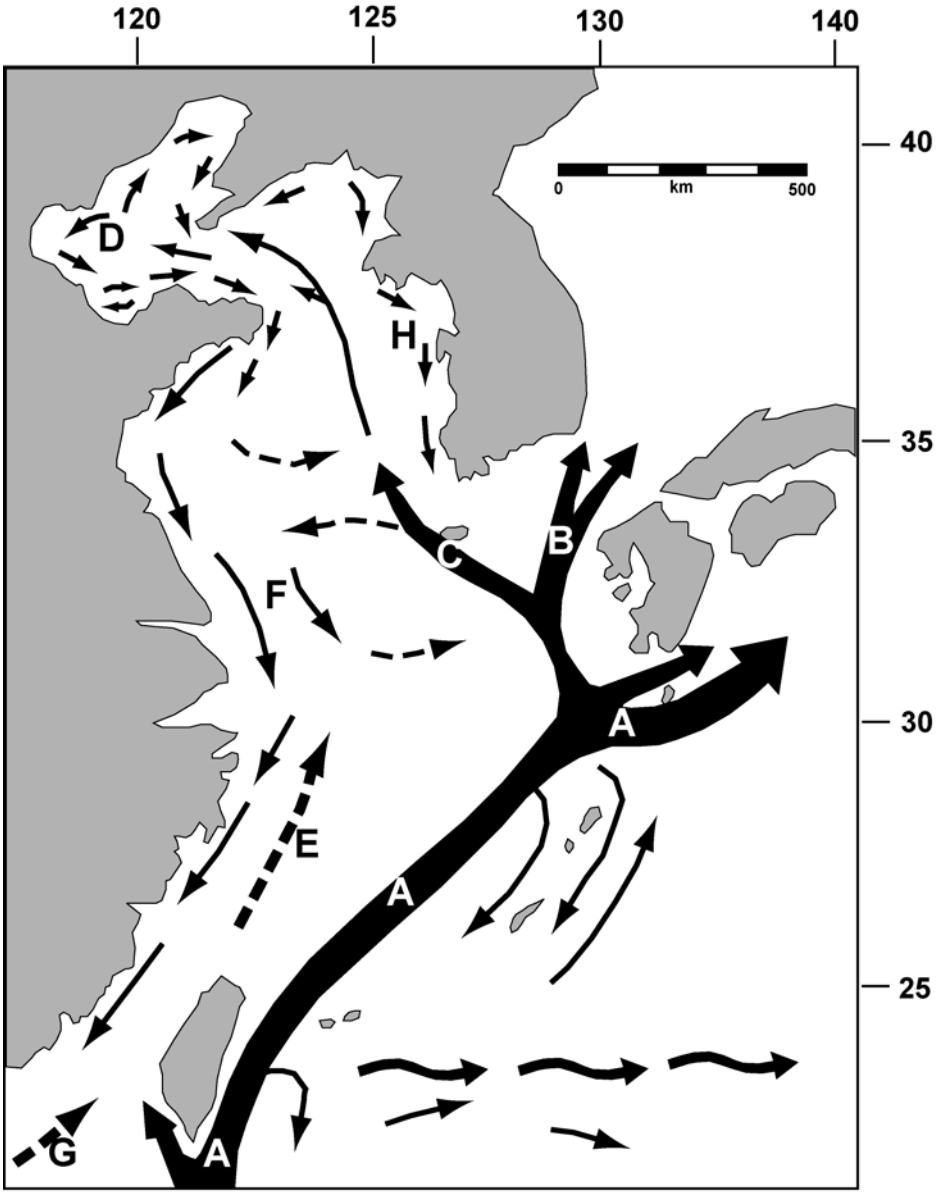

MAJOR OCEANIC CURRENTS

A = Kuroshio
B = Tsushima Warm Current
C = Yellow Sea Warm Current
D = Bohai Circulation
E = Taiwan Warm Current
F = China Coastal Current
G = South China Sea Warm Current
H = West Korea Coastal Current

magnitude lowstands (>100 m drop), these currents are attenuated or non-existent (Jun et al., 1995). Shieh and Chen (1995) and Ujiié and Uiijé (1999) suggested a land bridge between the Ryukyu Islands and Taiwan prohibited the Kuroshio Current, during periods of lowered sea level, from its present course on the western side of the Ryukyu Island chain through the Okinawa Trough. Without the Kuroshio's influence on the ECS margin, the entire fluvial sediment load is available for depositions on the exposed margin.

It is even plausible that conditions in the Pacific Ocean during highstand could pull the Kuroshio eastward and away from the ECS margin, thereby increasing rates of sediment delivery to the margin. Therefore, the scenario exists for a net increase in sediment delivery to the margin without major shifts in sea level and/or climate. However, seismic profiles provide evidence that this was not the case. For example, stratigraphic features such as tidal ridges are observed on the modern seafloor of the ECS. These ridges occur throughout the shallow stratigraphic record in the ECS (see Figure 3.35 and 3.36), are the focus of many recent investigations (e.g., Yang, 1989; Saito et al., 1998; Liu et al., 2000; Li et al., 2001; Berne et al., 2002), and are considered to represent concentrations of sediments reworked by the flow field of tidal currents during marine transgressions. The youngest of these ridges, observed on the present-day seafloor of the ECS are linked to shallow-water tidal currents. Ridges on the outer and middle portions of the present-day shelf are moribund while those on the inner shelf in the ECS as well as the YS are presently active and in equilibrium with current oceanographic conditions (Yang and Sun, 1988; Yang, 1989; Bartek and Wellner, 1995). The vertical repetition of these ridges throughout the seismic profiles, at least as far back as 200 ky, suggests that oceanographic conditions were similar to present.

Of all the depositional variables used in *fuzzy*PEACH simulations, sediment influx is certainly the one with the highest level of uncertainty. Comparisons between individual stratal units in existing simulation output (i.e., sediment thickness and distribution during different rates of sediment influx), with the exception of higher sedimentation rates during OIS 6, do not suggest variable sedimentation rates from the drainage basin between OIS 5 to OIS 3. The comparisons of simulation output become more difficult during OIS 2 to present because the incision observed in the seismic data from the ECS margin certainly increased the sediment influx to the outer margin and beyond the shelf-slope break into deeper water. Therefore, it is hypothesized here that the simulation of constant sediment supply may be too simplistic. While it is unclear whether all, some, or none of the sediment-supply scenarios discussed above might have affected sediment supply (and if so, by how much?), it would be easy to modify *fuzzy*PEACH with an additional FIS containing rules that vary sediment supply based on parameters such sea level (ocean currents, fluvial gradient) and precipitation (suspended load, runoff, discharge, etc.). Rules and sets could easily be varied to test multiple hypotheses in relatively short order (i.e., higher or lower sediment supply with high precipitation, higher or lower sediment supply with submerged versus exposed margin). Based on relative relationships, some potential rules might be:

IF precipitation high THEN sed rate high
IF precipitation low THEN sed rate low
IF sea level high THEN coastal current removal high AND sed rate to margin moderate
IF sea level low THEN no coastal current removal AND sed rate high

Further, it may be prudent to explore more sediment influx scenarios than just the modern Yangtze rate (4.8×10^8 tons/yr) versus the paleo rate estimate of 2.4×10^8 tons/yr (Hori et al., 2001; Saito et al., 2001). The Yellow River's frequent avulsions (eight since 2278 BC) were partially responsible for the Yangtze/Yellow paleo delta complex north of the

modern Yangtze River mouth (Yunshan and Fan, 1983; Wang and Aubrey, 1987; Saito et al., 2001). The Yellow River is presently the second largest river in the world, in terms of sediment supply (1.08×10^9 tons/yr; Milliman and Meade, 1983; Milliman and Syvitski, 1992). Therefore, the Yellow River was certainly a contributing factor to stratigraphic evolution when it entered the ECS from the north. Future simulations of *fuzzy*PEACH may need to incorporate multiple fluvial systems with different sedimentation rates in order to more accurately simulate stratigraphic architecture not only in on the ECS margin but in general.

Incision. The simulated strata of the *fuzzy*PEACH, during moderate sediment influx (2.4×10^8 tons/yr) and no FIS controlling avulsion, resemble the ECS strata preserved during OIS 5 and 3. As discussed briefly above, the avulsion rules in the FIS appear to accurately control stratal formation during OIS 6, but might not accurately represent avulsion rates under all conditions (e.g., periods of higher sea level such as OIS 5 and 3). Second, the minor incision noted in OIS 4, as well as the major incision during OIS 2, could have prevented the river from avulsing during conditions where it otherwise might have avulsed at a frequency similar to those described in the fuzzy rules.

The complete exposure of the margin during OIS 6 was quickly followed by the complete submergence during OIS 5. During this subsequent highstand, the Yangtze River delta shifted to a nearshore depocenter. During the fall of sea level during OIS 5, there was a rapid drop of 40 m (Figure 3.11) that subaerially exposed nearshore deltaic sediments. The exposure of this lobate unit created an abrupt gradient change between the initial delta plain and delta front. An increase in slope can cause channel incision (e.g., Talling, 1998; Posamentier et al., 1992; Schumm, 1993; Wescott, 1993; Leeder and Stewart, 1996;

Posamentier and Allen, 1999). The incision of exposed topographic relief related to highstand deltas has been observed in the geologic record (Talling, 1998) and modeled numerically (Ritchie et al., 2002a; 2002b). Once incised, fluvial systems become further entrenched, migrate headward, and commonly capture other active channels (e.g., Wood et al., 1993; Koss et al., 1994; Ritchie et al., 2004a; 2004b). Once captured, avulsion is limited and sediment transport is focused basinward. Such a scenario can produce a single, dominant delta. Fluvial capture, early in OIS 5, as well as subsequent capture of distributaries and other fluvial systems further upstream, throughout the overall falling trend of base level into the maximum lowstand in OIS 2 is consistent with the regional seismic stratigraphic profiles. For example, the thickest portion of OIS 4 is incised into OIS 5 (Figure 3.35). The large accumulation of OIS 3 sediments directly basinward of this OIS 4 incision (and the preceding OIS 5 lobe) (Figure 3.34) and support the hypothesis that the Yangtze River remained captured as it incised into antecedent topography, while the continental margin became exposed during rapid sea level fall. A cartoon of this sequence of events is presented in Figure 3.41. The funneling of sediment through this incision produced the concentrated depocenters of OIS 3 and OIS 2 on the outer margin and at the shelf-slope break (Figure 3.34). Incision continued to become deeper, wider and more extensive heading into the maximum lowstand. Seismic data indicate that multiple incised valleys formed on the ECS margin during this period (OIS 2) (Figure 3.42). Widths of incised portions of the paleo Yangtze River (OIS 2) were between 70 km (Hori et al., 2002b) and in excess of 300 km (Wellner and Bartek, 2003). While the southern incised system was attributed to the Yangtze River, it is hypothesized here that the lowstand deltas on the northern margin and much of the sediment from the north-central portion of the margin was deposited by the Yellow River

Figure 3.41. Hypothetical geologic history of the ECS strata since OIS 5 (128 ka) presented in this paper. Note the incision of antecedent topography that forms during the exposure of major gradient differential from deltaic lobes. It is hypothesized that incision such as this limited the avulsion of the Yangtze River into the ECS during since OIS 5.

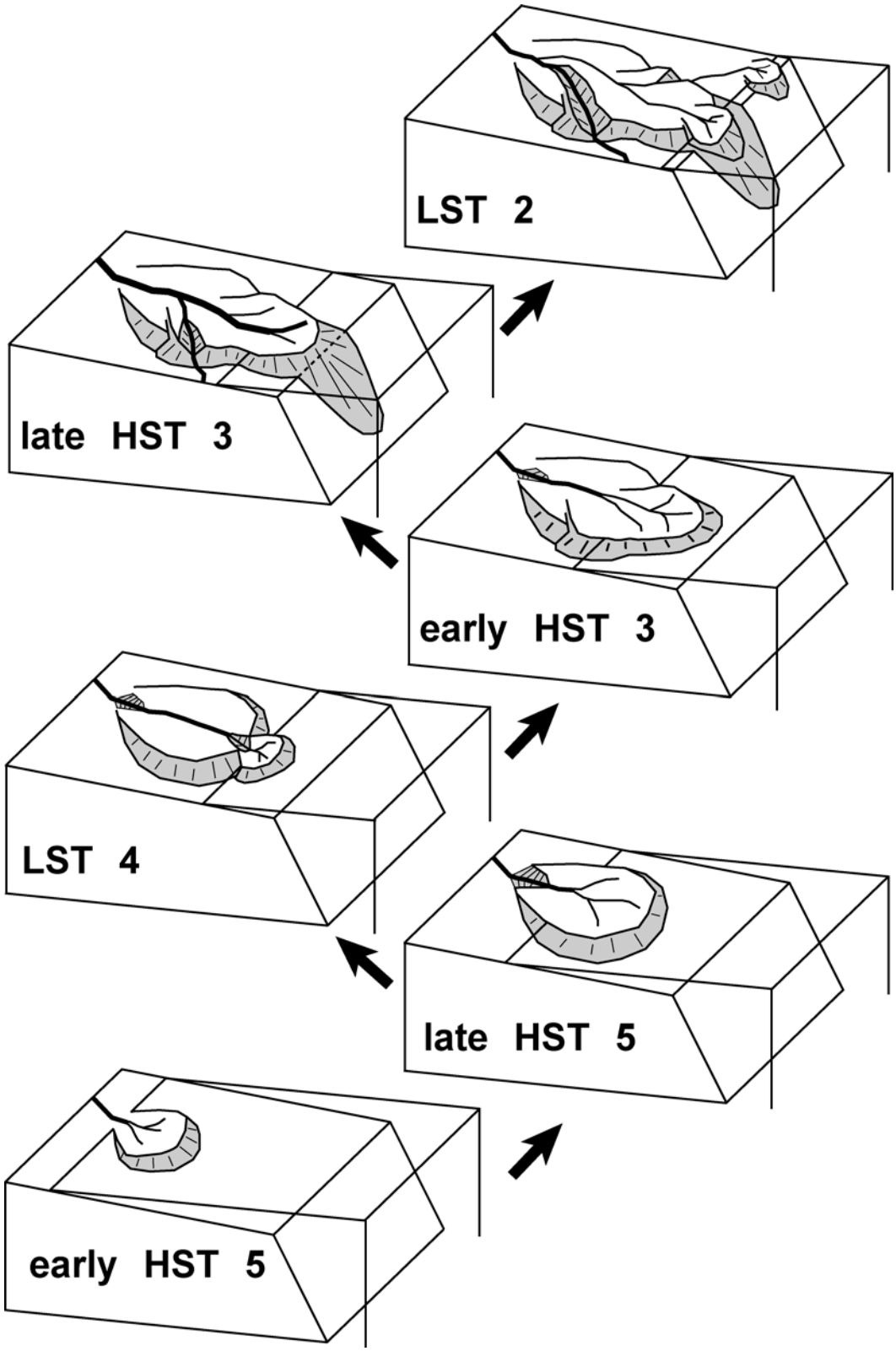
LST 2
late HST 3
early HST 3
LST 4
late HST 5
early HST 5

Figure 3.42. A) Structure map generated from the regional seismic dataset from the ECS margin showing the sequence boundary at the base of OIS 2 formed during the last glacial maximum. Arrows denote locations of incision. B) Isopach map from ECSl seismic data. Arrows identify depocenters on the outermost margin attributed to lowstand deltas.

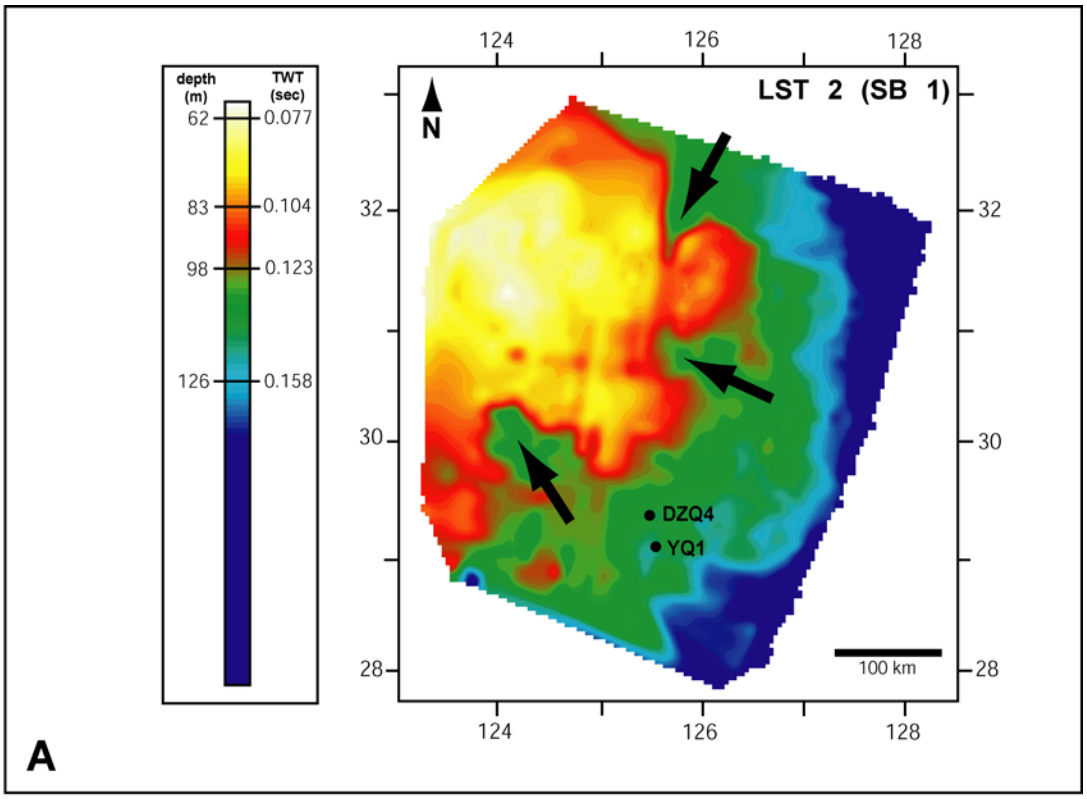
depth (m)
TWT (sec)
62
0.077
83
0.104
98
0.123
126
0.158
LST 2 (SB 1)
N
124
126
128
32
30
28
DZQ4
YQ1
100 km
A

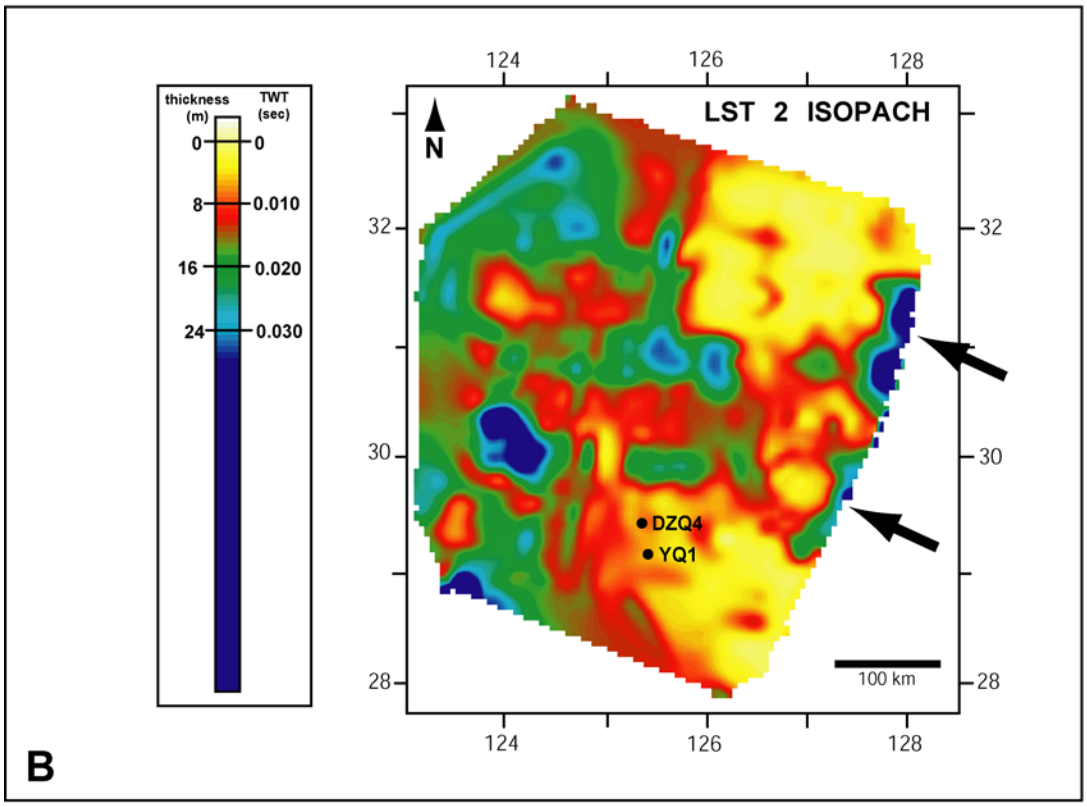
thickness (m)
TWT (sec)
0
0
8
0.010
16
0.020
24
0.030
LST 2 ISOPACH
N
124
126
128
32
30
28
DZQ4
YQ1
100 km
B

or a combination of rivers that included the Yellow. The Loess Plateau gives Yellow River sediments an overwhelming carbonate signature and makes them easily distinguishable from the Yangtze (Milliman et al., 1985b). Provenance investigations to test this hypothesis have not been conducted but seem warranted.

The initial version of *fuzzy*PEACH presented in this paper did not incise. An initial erosion component has been developed as a separate FIS, but is still under development. Similar to fluvial the FIS controlling fluvial deposition (Figure 3.12A), there are three rules of the prototype FIS.

IF in channel THEN erode a lot
IF near channel THEN erode some
IF far from channel THEN erode little

Preliminary results are promising (Figure 3.43), however, there are additional challenges to be overcome with erosion and re-distribution of sediment as well as knickpoint migration (instead of wholesale erosion at all points along the fluvial axis, as depicted in the rules above). Just as the incised valleys from the ECS data remove and focus sediment, an accurate FIS will certainly create a more realistic simulation that is able to produce the stratigraphic architecture that is similar to that observed in OIS 4, 2, and 1.

Physical Oceanographic Conditions. Physical oceanographic conditions were not incorporated explicity into *fuzzy*PEACH. The high-energy environment of the present-day ECS is a complex interaction of oceanic and tidal currents as well as frequent and intense storm events. There is no doubt that sediment distribution, deposition, and stratigraphic architecture has been affected by these high-energy oceanographic processes. The general oceanic circulation pattern of the ECS and the adjoining Yellow Sea (YS) and Bohai Sea (BS) is driven by the warm (T=20° to 27° C; Yu and Hong, 1992) and highly saline

Figure 3.43. Preliminary efforts for simulation of erosion in *fuzzy*PEACH stratigraphic simulations show incision in A) three dimensions and B) two dimensions.

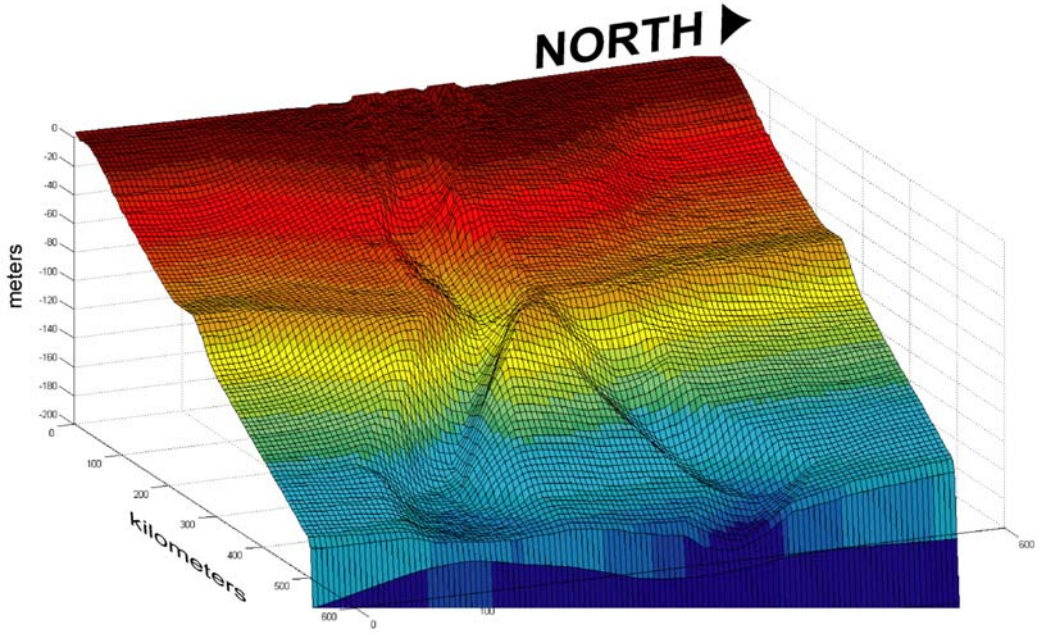

STRUCTURE MAP

(bathymetry at end of simulation)

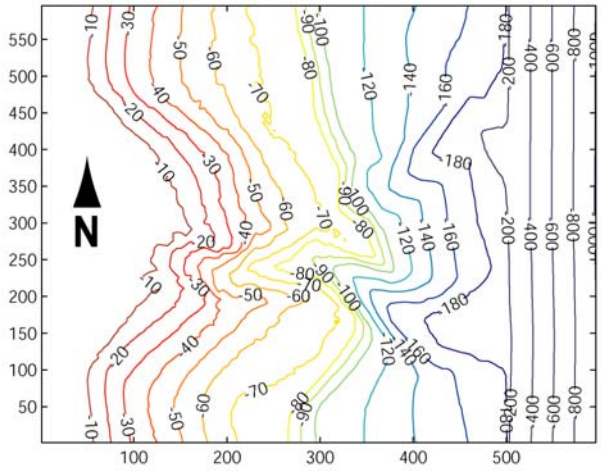

contour values indicate depth below sea level in meters at last time step

(S=33 ‰ ; Yu and Hong, 1992) Kuroshio western boundary current, its offspring (e.g., Taiwan Warm Current, Tsushima Current, Jiangsu Warm or Yellow Sea Warm Current, Shandong Coastal Current, Jiangsu or Yellow Sea Coastal Current, and Changjiang Coastal Current), and a minor thermohaline component from the colder, sediment-laden freshwater discharge of the Yellow and Yangtze Rivers (Figure 3.40). The ECS, YS, and BS are geographically and hydrodynamically inseparable and are, therefore, considered one system (Bingxian and Hanli, 1982). Semidiurnal tidal currents between 20 cm/sec (weakest in BS) and 100 cm/sec (strongest near mouth of Yangtze River) are sufficiently strong in some areas to cause localized resuspension or bedload transport (Choi, 1980; Milliman et al., 1985a). Approximately 7% of the global dissipation of tidal energy presently occurs in the shallow ECS/YS/BS system (Choi, 1980) and causes sea level fluctuations from 5 to 6 m in Taiwan and up to 11 m in Hangchow Bay southwest of Shanghai (Fairbridge, 1966). Without these physical processes, the simulation of the ECS margin did not remove sediment from the ECS system via coastal currents (as mentioned above) nor did it remove, rework, and redistribute sediment around the margin. For this reason, features such as the tidal ridges observed on the modern seafloor, as well as deeper in the seismic record (see Figure 3.35 and 3.36), were not simulated by *fuzzy*PEACH. Because these strata are relatively thin and a minor component of the shallow seismic record, the lack of simulated oceanographic conditions, relative to conditions of sea level and sediment influx, is considered to be of minor importance.

3.4.3 General Stratigraphic Response of Model

Although the discussion thus far has focused on validating the model to the ECS margin dataset and low-gradient margins in general, the results and observations of these stratigraphic simulations are generally applicable to the stratigraphic evolution of a wide

range of depositional systems. The three-dimensional stratal geometries, stratal termination patterns, and rates of shoreline change produced by *fuzzy*PEACH are similar to those observed in natural systems. Therefore, understanding this complex strtatigraphic architecture as it relates eustatic sea level, tectonic (thermal) subsidence, and sediment influx has important implications. Without this understanding, it is difficult to relate these variables to outcrops and subsurface data (or lack thereof) throughout the geologic record.

General Trends. Variables used in *fuzzy*PEACH were established using general fluvio-deltaic parameters (e.g., sedimentation rate, width of channel, radius of delta, etc.), so the overall simulations are applicable to continental margins under all conditions of relative sea level (eustasy, tectonic subsidence) and sediment influx. Numerous permutations of these variables, with a wide range of values, were used to test the sensitivity of the stratal response. The margin remained constant for continuity throughout the sensitivity testing, however, the alteration of magnitude and periodicity of the eustatic curves can be used as a proxy of different margin geometries (e.g., margin width and depth of shelf-slope break). A sea level curve with periodicities of 100, 40, and 20 ky approximate Milankovitch cycles of eccentricity, obliquity, and precession, respectively (Imbrie et al., 1984). Using a period of 100 ky, and assuming a sea level magnitude similar to the Quaternary (i.e., 120 meters below present; Figure 3.11) and a low-gradient margin (0.01°), the rate of shoreline translation across the margin is 14 m/yr. Increasing the gradient leads to a slower rate of shoreline movement (i.e., 0.1° = 1.4 m/yr and 1° = 0.14 m/yr). Therefore, stratigraphic response to lowering margin gradient, while maintaining a constant margin physiography, can be accomplished by increasing the frequency of sea level oscillations. For example, the rate of shoreline translation during a 20 ky precession cycle (120 m magnitude, 0.01° margin) is 68

m/yr. This rate slows to 34 m/yr during obliquity and 14 m/yr during eccentricity. In addition to altering sea level cycle periodicity, the magnitude can also be used as a proxy for changing margin geometry (when margin physiography is kept constant). For example, the deep shelf-slope breaks associated with the low-gradient basin discussed in this paper (Australia, Java, New Zealand, and ECS) can be exposed by increasing the magnitude of sea level fall. The general stratal response to increasing eustatic periodicity was thinner strata and faster rates of shoreline translation across the margin. Higher rates of eustatic change resulted in higher progradation rates and lower aggradation during sea level fall (forced regression) as well as higher rates of backstepping and lower rates of progradation and aggradation during eustatic rise. Therefore, normal regressions became less noticeable under increasing rates of eustatic change (but occurred as parasequences during eustatic slowdowns and stillstands). Because erosion and incision were not included in this preliminary version of *fuzzy*PEACH, incision at the shelf-slope break did not occur. However, when the shelf edge was exposed, sediment was deposited beyond the shelf-slope break (thus bypassing the exposed margin).

Different rates and magnitude of sea level fall have a major impact on sequence development and the character of sequence boundaries. Because margin geometry was held constant throughout this study (although it can be changed since it is user-defined), it is important to point out that the modification of rates and amplitude of eustatic change can be used to simulate stratigraphic response to variation in margin physiography. More important, though, is the translation of this concept to traditional stratigraphic models in order to simulate conditions on low-gradient margins with deep shelf-slope breaks by increasing eustatic rates of rise and fall, as well as decreasing magnitude of sea level change, to keep the

shelf-slope break submerged during lowstands. Using this approach to augment existing techniques that have been validated for typical passive margins potentially allows a direct comparison to, and potentially further validation of, the overall accuracy of the relatively new fuzzy logic approach used in this investigation. Rapid rates of sea level rise result in highly retrogradational deltaic deposits that are thin and backstep a long way towards the sediment source. Slower rates of sea level rise results in little to no retrogradation. Relatively early in the rising limb of the sea level curve, strata are dominated by normal regressions. Strata are largely aggradational but become strongly progradational. However, there may be some limitations to this approach. For example, the rate of shoreline translation across a higher-gradient margin with slower rates of sea level change may equal that of a lower gradient margin with faster rates of eustatic change. However, the stratal signatures will not be identical. Regardless of the rate, lower-gradient margins have less accomodation, and the extent of progradation basinward and retrogradation (and onlap) landward will be greater for the lower gradient margin. Therefore, strata will tend to be thinner and more poorly developed. In contrast, strata on a more steeply dipping margin will tend to be thicker and have steeper dipping clinoforms. The depth of wave base in a natural system, a process not simulated with *fuzzy*PEACH, will be the same, but the basinward extent (shore-perpendicular) of seafloor affected by wave interaction (e.g., scouring and reworking), the width of transgressive/regressive processes will be narrower on a margin with a steeper gradient, regardless of the rate of sea level change.

Previous numerical models suggest that stratigraphic response is most sensitive to eustatic fluctuations and, to a lesser degree, subsidence (e.g., Steckler et al., 1993; Steckler, 1999; Ritchie et al., 2004a; 2004b). Simulations from *fuzzy*PEACH suggest that, at least on a

low-gradient margin, stratal geometry is most sensitive to sediment influx. It should be noted that sediment influx in all simulations, while variable, was between 1 x 10^9 and 5 x 10^9 tons/yr. Admittedly, these rates are extremely high (the world's top 12 rivers, in terms of sediment discharge, are equal to or greater than 1 x 10^9 tons per year; Milliman and Meade, 1983; Milliman and Syvitski, 1992). Abundant sediment influx rapidly fills accommodation. The low-gradient nature of the margin modeled (0.017°), regardless of rate of sea level, has less accommodation than a typical continental margin (≥ 0.1°). Similar to increased rates of sea level rise and fall, increased sediment influx produces thicker strata, greater rates of progradation, and faster rates of shoreline translation. A threshold may exist for fluvial influx, below which the stratigraphy is not as sensitive to sedimentation rate. It may also exist as a continuum. For example, at some point, a low enough rate of sediment influx, combined with a high enough rate of sea level fall, will produce a series of forced regressive wedges that are not well connected (Posamentier et al., 1992; Hunt and Tucker, 1995; Plint and Nummedal, 2000; Catuneaunu, 2003).

Accommodation. Sediment accommodation (*sensu* Jervey, 1988) decreases during periods of eustatic fall and deposition is focused progressively into the basin as the shoreline is forced downward and basinward (forced regressive systems tract of Hunt and Tucker, 1995; falling stage systems tract of Plint and Nummedal, 2000). Shorelines with higher sedimentation rates, also decreasing accommodation by filling available space at a faster rate, should move basinward at a faster rate compared to scenarios with lower sediment influx (all other variables being equal). The creation of additional accomodation by tectonic subsidence should, at least in part, decrease the rate of shoreline movement because net accomodation is not being filled as fast. However, higher sediment influx during identical subsidence

conditions should theoretically move the shoreline basinward faster. These trends were observed in *fuzzy*PEACH output (Figure 3.15, 3.16, 3.17, 3.18).

Multiple simulations with different rates of subsidence and sediment influx experienced similar rates of shoreline translation across the margin during both rising and falling sea level conditions. Conditions of no tectonic subsidence (both moderate and high sedimentation rate) during a simple, sinusoidal sea level oscillation, had similar rates of shoreline translation during transgression (Figure 3.15 and 3.16). Simulations that included tectonic subsidence were translated basinward at a slower rate that those without tectonic subsidence simply because accommodation was being created by the subsidence component. The rate of accommodation decrease was the same between high and moderate sediment influx (with subsidence) because tectonic subsidence increased basinward. Therefore, the shoreline associated with a moderate sedimentation rate had not prograded as far into the basinward at the point of maximum regression (point 2 on the sea level curve; Figure 3.15). The two sedimentation rates (high and moderate), under conditions of no subsidence, had similar shoreline progradation rates because the shoreline associated with higher sediment influx was farther basinward in an area of greater accomodation than the shoreline nearer to shore associated with a lower sedimentation rate. The simulated shoreline under conditions of high sediment influx and no subsidence was translated landward at a similar rate because of the greater amount of accommodation associated with the deeper water on the outer margin. During sea level fall, all three of these shorelines prograded basinward at different rates (faster rate of movement during sea level fall equating to a faster decrease in accomodation)(Figure 3.15 and 3.16). Conditions of moderate sediment influx without tectonic subsidence translated basinward at a rate similar to high sediment influx (and no

subsidence). However, during sea level rise, the moderate sediment influx shoreline moved landward faster than all other scenarios because accommodation was decreasing least and, therefore, basinward progradation of the shoreline was limited. At the slowdown in sea level rise (point 3 on the sea level curve; Figure 3.16), all four simulations prograded basinward, although high sediment influx with subsidence prograded faster than moderate sediment without subsidence. This is an indication that, at least at this point in time, accommodation was decreasing more rapidly by sediment influx rather than tectonic subsidence. In this situation, strata were more sensitive to sediment influx.

Similar shoreline trends were also observed in the same four sediment and subsidence scenarios controlled by an asymmetric sea level curve that incorporated a stillstand on the falling limb (Figure 3.17 and 3.18). At point 1 on the sea level curve, a shift from progradational strata to a combination of progradation and aggradation occurred. Rates of basinward translation of the shoreline were similar for conditions with high sediment influx (with and without subsidence). These rates were also higher a little higher than those under moderate sediment influx (with and without subsidence). Similar rates for simulations without subsidence, as well as those for conditions with tectonic subsidence (although at a lower overall rate), continued as the rate of sea level fall increased (point 2 on the sea level curve; Figure 3.17 and 3.18). During sea level rise (points 3 to 4 on sea level curve), the shoreline during conditions of moderate sediment influx (no subsidence) moved landward faster than all other scenarios because accommodation was decreasing least and, therefore, basinward progradation of the shoreline was limited. At the slowdown in sea level rise (point 4 on the sea level curve; Figure 3.18), all four simulations prograded basinward, although high sediment influx with subsidence prograded faster than moderate sediment without

subsidence. This is an indication that, at least at this point in time, accommodation was decreasing more rapidly by sediment influx rather than tectonic subsidence. In this situation, strata were more sensitive to sediment influx.

3.5 CONCLUSIONS

As part of a broader investigation, a detailed seismic- and sequence-stratigraphic framework was developed for the ECS margin (a low-gradient margin with a deep shelf-slope break and an abundant sediment influx) based on a regional seismic dataset from the ECS margin. Numerous quantitative models have simulated the stratigraphic response of continental margins throughout the geologic record. These quantitative models, and sequence stratigraphy in general, predict incision and sedimentary bypass across a continental margin during sea level lowstand. On the other hand, low-gradient margins, such as the ECS, have not been addressed by the modeling community. The response of a fluvial system across a low-gradient margin (especially one that is lower than the fluvial gradient) is deposition and avulsion throughout the basin, with little sedimentary bypass beyond the shelf-slope break. There is no incision at the shelf-slope break, which remains submerged.

The *fuzzy*PEACH is a three-dimensional, forward simulator that uses fuzzy logic to model the stratigraphic response of low-gradient margins as well as continental margins in general. In this investigation, *fuzzy*PEACH simulated numerous scenarios of eustasy, tectonic subsidence, and sediment influx onto a continental margin. The various rates and magnitudes of eustatic fluctuations may also be used as a proxy for the effect of margin physiography on stratal geometry, although *fuzzy*PEACH allows the geometry to be user defined. Fuzzy logic was chosen because it is simple yet powerful. General concepts and expert knowledge assembled a set of robust fuzzy logic inference systems that were able to describe complicated, nonlinear relationships. *Fuzzy*PEACH simulations collectively uses only five FISs containing a total of 21 separate rules. These rules incorporate 15 variables and are defined by 47 fuzzy sets.

Visual comparison of model output compares well with the stratigraphic trends observed in the ECS seismic dataset. The laterally extensive fluvial deposits from OIS 6 were similar to *fuzzy*PEACH simulations with higher sediment influx (i.e., rates similar to the modern Yangtze River) and avulsion controlled by a set of fuzzy rules. The more defined deltaic lobes of OIS 5 and OIS 3 shared trends simulated with moderate sediment influx (half the rate of the modern Yangtze River) and less frequent avulsions. Seismic data and simulation output support a hypothesis of variable sedimentation rates, and the current sediment delivery method in fuzzyPEACH (i.e., constant for each time step) will be redesigned with additional fuzzy logic rules that define trends between sedimentation rate, climatic, and physical conditions of the margin. The incised nature of OIS 2 on the ECS margin was not simulated by *fuzzy*PEACH. Simulated incision was partially addressed during model development and will continue to be developed for inclusion into future versions of *fuzzy*PEACH.

Although a portion of this study focused on the validation of the model output against the ECS seismic dataset, the results and observations of these stratigraphic simulations are generally applicable to the stratigraphic evolution of a wide range of depositional systems. The three-dimensional stratal geometries, stratal termination patterns, and rates of shoreline change produced by *fuzzy*PEACH are similar to those observed in natural systems. Therefore, understanding this complex strtatigraphic architecture as it relates eustatic sea level, tectonic (thermal) subsidence, and sediment influx has important implications. Simulation data suggest that previous theories of stratal geometry being most sensitive to tectonic subsidence and sea level change may not be accurate in basins with rates of high sediment influx. Without this understanding, it is difficult to relate these variables to outcrops and subsurface data (or lack thereof) throughout the geologic record.

3.6 REFERENCES CITED

Airy, G.B., 1855, On the computation of the effect of the attraction of mountain-masses as disturbing the apparent astronomical latitude of stations in geodetic surveys. Philosophical Transactions of the Royal Society of London, v. 145, p. 101-104.

Alam, M., 1996, Subsidence of the Ganges-Brahmaputra delta of Bangladesh and associated drainage, sedimentation and salinity problems. In Milliman, J.D. and Haq, B.U., (eds.), Sea-level Rise and Coastal Subsidence: Causes, Consequences, and Strategies, Coastal Systems and Continental Margins, v. 2, Kluwer Academic Publishers, Dordrecht, The Netherlands, p. 169-192.

An, Z., 2000, The history and variability of the East Asian paleomonsoon climate. Quaternary Science Reviews, v. 19, p. 171-187.

Anderson, J.B., Rodriguez, A., Abdulah, K.C., Fillon, R.F., Banfield, L.A., McKeown, H.A., Wellner, J.S., 2004, Late Quaternary stratigraphic evolution of the northern Gulf of Mexico margin: A synthesis. In Anderson, J.B. and Fillon, R.H., (eds.), Late Quaternary Stratigraphic Evolution of the Northern Gulf of Mexico Margin, SEPM Special Publication no. 79, Society for Sedimentary Geology, Tulsa, OK, p. 1-23.

Ashworth, P.J., Best, J.L., Jones, M., 2004, Relationship between sediment supply and avulsion frequency in braided rivers. Geology, v. 32, p. 21-24.

Athy, L.F., 1930, Density, porosity, and compaction of sedimentary rocks. AAPG Bulletin, v. 65, p. 2433-2436.

Baeteman, C., Bodemans, F., Govaert, E., Huanzhong, H., Jingxin, L., 1992, The Quaternary deposits of the Changjiang coastal plain (Shanghai area). Bulletin of the International Association of Engineering Geology, no. 46, p. 7-23.

Baldwin, B. and Butler, C.O., 1985, Compaction curves. AAPG Bulletin, v. 69, p. 622-626.

Bartek, L.R. and Warren, J.D., 2002, Concurrent incised and unincised valley systems and their geomorphic control during Quaternary lowstands on the East China Sea continental margin. SEPM Research Conference: Incised Valleys: Images and Processes, August 18-23, 2002, Casper and Newcastle, WY.

Bartek, L.R. and Warren, J.D., 2005, Comparison of the fill of high and low sediment supply incised valley systems. Abstracts Volume 14, AAPG Annual Convention, Calgary, Alberta, Canada, June 19-22, p. A12.

Bartek, L.B., Warren, J.D., and Miller, K.L., 2001, Perched lowstand stratigraphy on the East China Sea continental margin: AGU Chapman Conference on Formation of Sedimentary Strata on Continental Margins, June 17-19, Ponce, Puerto Rico.

Bartek, L.R., Wellner, R.W., Warren, J.D., 2004, Climate change and shelf physiography – their role in shaping sequence architecture: An example from the East China Sea. AAPG Annual Meeting Program, April 18-21, Dallas, TX, p. A185.

Beard, D.C. and Weyl, P.K., 1973, Influence of texture on porosity and permeability. AAPG Bulletin, v. 57, p. 349-369.

Berg, O.R. and Woolverton, D.G., (eds.), Seismic Stratigraphy II – An integrated approach to hydrocarbon exploration. AAPG Memoir 26, American Association of Petroleum Geologists, Tulsa, OK, 276 pp.

Berne, S., Vagner, P., Guichard, F., Lericolais, G., Liu, Z., Trentesaux, A., Yin, P., and Yi, H.I., 2002, Pleistocene forced regressions and tidal sand ridges in the East China Sea: Marine Geology, v. 188, p. 293-315.

Bingxian, G. and Hanli, M, 1982, A note on the circulation of the East China Sea. Chinese Journal of Oceanology and Limnology, v. 1, p. 5-16.

Bitzer, K. and Pflug, R., 1990, DEPO3D: A three-dimensional model for simulating clastic sedimentation and isostatic compensation in sedimentary basins. In Cross, T.A., (ed.), Quantitative Dynamic Stratigraphy, Prentice Hall, Englewood Cliffs, NJ, p. 335-348.

Boole, G., 1951, The Mathematical Analysis of Logic. B. Blackwell, Oxford, 82 pp.

Borg, I., Friedman, M., Handin, J., Higgs, D.V., 1960, Experimental deformation of St. Peter Sand: A study of cataclastic flow. In Griggs, D. and Handin, J., (eds.), Rock Deformation (A Symposium), Geological Society of America Memori 79, New York, p. 133-191.

Brice, J.S., 1985, Planform properties of meandering river. In Elliott, C.M. (ed.), River Meandering, Proceedings from the Conference on Rivers, 1983, New Orleans, LA, p. 1-15.

Bridge, J.S. and Leeder, M.R., 1979, A simulation model of alluvial stratigraphy. Sedimentology, v. 26, p. 617-644.

Brown, L.F., Jr. and Fisher, W.L., 1980, Seismic Stratigraphic Interpretation and Petroleum Exploration. Continuing Education Course Note Series #16, American Association of Petroleum Geologists, Tulsa, 191 pp.

Browne, G.H. and Naish, T.R., 2003, Facies development and sequence architecture of a late Quaternary fluvial-marine transition, Canterbury Plains and shelf, New Zealand: implications for forced regressive deposits. Sedimentary Geology, v. 158, p. 57-86.

Bryant, M., Falk, P., Paola, C., 1995, Experimental study of avulsion frequency and rate of deposition. Geology, v. 23, p. 365-368.

Carey, J.S., Swift, D.J.P., Steckler, M., Reed, C.W., Niedoroda, A., 1999, High-resolution sequence stratigraphic modeling 2: Effects of sedimentation processes. In Harbaugh, J.W., Watney, W.L., Rankey, E.C., Slingerland, R., Goldstein, R.H., Franseen, E.K. (eds.), Numerical Experiemnts in Stratigraphy: Recent Advances in Stratigraphic and Sedimentologic Computer Simulations. SEPM Special Publication #62, Tulsa, OK, p. 151-164.

Carson, M.A., 1984, Observations on the meandering-braided river transition, the Canterbury Plains, New Zealand: Part one. New Zealand Geographer, v. 40, p. 12-17.

Catuneanu, O., 2003, Sequence Stratigraphy of Clastic Systems. Short Course Notes v. 16, Geological Association of Canada, Newfoundland, 248 pp.

Chappaz, R.J., 1977, Application of the fuzzy sets theory to the interpretation of seismic sections. Geophysics, v. 42, p. 1499.

Chen, Z. and Stanley, D.J., 1993, Yangtze delta, eastern China: 2. Late Quaternary subsidence and deformation. Marine Geology, v. 112, p. 13-21.

Chen, Z., Song, B., Wang, Z., Cai, Y., 2000, Late Quaternary evolution of the sub-aqueous Yangtze Delta, China: Sedimentation, stratigraphy, palynology, and deformation. Marine Geology, v. 162, p. 423-441.

Chough, S.K. and Kim, D.C., 1981, Dispersal of fine-grained sediments in the southeastern Yellow Sea: A steady-state model: Journal of Sedimentary Petrology, v. 51, no. 3, p. 721-728.

Clifton, E.H., 2000, Shoreface myths and misconceptions. Annual Meeting Extended Abtsratcs, v. 2000, American Association of Petroleum Geologists, p. 29.

Coleman, J.M., 1981, Deltas: Processes of Deposition and Models for Exploration. Burgess Publishing Company, CEPCO Division, Minneapolis, 124 pp.

Congxian, L., Gang, C., Ming, Y., Ping, W., 1991, The influence of suspended load on the sedimentation in the coastal zones and continental shelves of China. Marine Geology, v. 96, p. 341-352.

Csato, I., Cao, S., Petersen, K., Lerche, I., Sullivan, N., Lowrie, A., 1994, Basement motion and sediment loading: A quantitative study in northern Louisiana, Gulf of Mexico. American Association of Petroleum Geologists Bulletin, v. 78, p. 1453.

Curry, C.W., Bennett, R.H., Hulbert, M.H., Curry, K.J., Faas, R.W., 2004, Comparative study of sand porosity and a technique for determining porosity of undisturbed marine sediment. Marine Georesources and Geotechnology, v. 22, p, 231-252.

Dalrymple, R.W., Zaitlin, B.A., Boyd, R., 1992, Estuarine facies models: Conceptual basis and stratigraphic implications. Journal of Sedimentary Petrology, v. 62, p. 1130-1146.

DeMaster, D.J., McKee, B.A., Nittrouer, C.A., Qian, J., Cheng, G., 1985, rates of sediment accumulation and particle reworking based on radiochemical measurements from continental shelf deposits in the East China Sea. Continental Shelf Research, v. 4, p. 143-158.

Demicco, R.V., 2004a, Fuzzy logic and earth science: An overview. In Demicco, R.V. and Klir, G.J. (eds.), Fuzzy Logic in Geology. Elsevier, Amsterdam, p. 63-102.

Demicco, R.V., 2004b, Applications of fuzzy logic to stratigraphic modeling. In Demicco, R.V. and Klir, G.J. (eds.), Fuzzy Logic in Geology. Elsevier, Amsterdam, p. 121-151.

Demicco, R.V., 2004c, Fuzzy logic in geological Sciences: A literature review. In Demicco, R.V. and Klir, G.J. (eds.), Fuzzy Logic in Geology. Elsevier, Amsterdam, p. 103-120.

Demicco, R.V. and Klir, G.J., 2001, Stratigraphic simulations using fuzzy logic to model sediment dispersal. Journal of Petroleum Science and Engineering, v. 31, p. 135-155.

Demicco R.V. and Klir, G.J., 2004a, Fuzzy Logic in Geology. Elsevier, Amsterdam, 347 pp.

Demicco R.V. and Klir, G.J., 2004b, Introduction. In Demicco, R.V. and Klir, G.J. (eds.), Fuzzy Logic in Geology. Elsevier, Amsterdam, p. 1-9.

Desheng, L., 1984, Geologic evolution of petroliferous basins on continental shelf of China. AAPG Bulletin, v. 68, p. 993-1003.

Dickinson, G., 1953, Geological aspects of abnormal reservoir pressures in Gulf Coast Louisiana. American Association of Petroleum Geologists Bulletin, v. 37, p. 410-432.

Domenico, S.N., 1977, Elastic properties of unconsolidated sand reservoirs. Geophysics, v. 42, p. 1339-1368.

du Fornel, E., Joseph, P., Guillocheau, F., Euzen, T., Granjeon, D., 2003, Regional outcrop study and 3-D stratigraphic modeling ina foreland basin setting: The example of the Gres d'Annot Turbidite Formation (French Alps). American Association of Petroleum Geologists Annual Meeting Expanded Abstracts, v. 12, p. 44.

Dymond, J. and Lyle, M., 1994, Particle fluxes in the ocean and implications for sources and preservation of ocean sediments. In Material Fluxes on the Surface of the Earth, Studies in Geophysics series, National Research Council, Washington, DC, p. 125-142.

Evans, M.E. and Heller, F., 2001, Magnetism of loess/paleosol sequences: recent developments. Earth-Science Reviews, v. 54, p. 129-144.

Fagan, S.D. and Nanson, G.C., 2004, The morphology and formation of floodplain-surface channels, Cooper Creek, Australia. Geomorphology, v. 60, p. 107-126.

Fairbridge, R.W. and Krebs, O.A., 1962, Sea-level and the southern oscillation. Geophysical Journal, v. 6, p. 532-545.

Fang, J.H., 1987, Toward fuzzy expert systems in geology. Acta Geologica Taiwanica, no. 25, p. 85-96.

Fang, J.H., 1997, Fuzzy logic and geology. Geotimes, v. 42, p. 23-26.

Ferguson, R.I., 1981, Channel Form and channel changes. In Lewin, J. (ed.), British Rivers. Geroge Allen and Unwin, London, p. 90-125.

Fillon, R.H., Kohl, B., Roberts, H.H., 2004, Late Quaternary deposition and paleobathymetry at the shelf-slope transition, ancestral Mobile River delta complex, northeastern Gulf of Mexico. In Anderson, J.B. and Fillon, R.B., (eds.), Late Quaternary stratigraphic evolution of the northern Gulf of Mexico margin, SEPM Special Publication no. 79, Society for Sedimentary Geology, Tulsa, OK, p. 111-141.

Galloway, W.E., 1975, Process framework for describing the morphologic and stratigraphic evolution of deltaic depositional systems. In Broussard, M.L. (ed.), Deltas: Models for Exploration, Houston Geological Society, p. 87-98.

Garcia-Castellanos, D., Fernandez, M., Torne, M., 2002, Modeling the evolution of the Guadalquivir foreland basin (southern Spain). Tectonics, v. 21, no. 3, 17 pp.

Giles, M.R., Indrelid, S.L., James, D.M.D., 1998, Compaction – the great unknown in basin modeling. In Düppenbecker, S.J. and Iliffe, J.E. (eds.), Basin Modelling: Practice and Progress. Geological Society, London, Special Publication 141, p. 15-43.

Goodbred, S.L., Jt., Kuehl, S.A., Steckler, M.S., Sarker, M.H., 2003, Controls on facies distribution and stratigraphic preservation in the Ganges-Brahmaputra delta sequence. Sedimentary Geology, v. 155, p. 301-316.

Gornitz, V., Lebedeff, S., Hansen, J., 1982, Global sea-level trend in the past century. Science, v. 215, p. 1611-1614.

Gutenberg, B., 1941, Changes in sea-level, postglacial uplift, and mobility of the earth's interior. Geological Society of America Bulletin, v. 52, p. 721-772.

Han, J.M., Lu, H.Y., Wu, N.Q., Guo, Z.T., 1996, The magnetic susceptibility of moern soils in China and its use for paleclimate reconstruction. Stduies in Geophysics and Geodesy, v. 40, p. 262-275.

Hanebuth, T.J.J., Stattegger, K., Schimanski, A., Lüdmann, T., Wong, H.W., 2003, Late Pleistocene forced-regressive deposits on the Sunda Shelf (Southeast Asia). Marine Geology, v. 199, p. 139-157.

Heezen, B., Tharp, M., and Ewing, M., 1959, The floors of the oceans: I. The North Atlantic. Geological Society of America Special Paper 65, 122 p.

Heller, F., Shen, C.D., Beer, J., Liu, X.M., Liu, T.S., Bronger, A., Suter, M., Bonani, G., 1993, Quantitative estimates and paleoclimatic implications of pedogenic ferromagnetic mineral formation in Chinese loess. Earth and Planetary Science Letters, v. 114, p. 385-390.

Heritage, G.L., Charlton, M.E., O'Regan, S., 2001, Morphological classification of fluvial environments: An investigation of the continuum of channel types. The Journal of Geology, v. 109, p. 21-33.

Hicks, S.D., 1978, An average geopotential sea-level series for the United States. Journal of Geophysical Research, v. 83, p. 1377-1379.

Holbrook, J., 1996, Complex fluvial response to low gradients at maximum regression: A genetic link between smooth sequence-boundary morphology and architecture of overlying sheet sandstone. Journal of Sedimentary Research, v. 66, p. 713-722.

Holbrook, P., 2002, The primary controls over sediment compaction. In Huffman, A.R. and Bowers, G.L. (eds.), Pressure Regimes in Sedimentary Basins and their Prediction, American Association of Petroleum Geologists Memoir 76, Tusla, OK, p. 21-32.

Holbrook, J.M. and Dunbar, R.W., 1992, Depositional history of Lower Cretaceous strata in northeastern New Mexico; implications for regional tectonics and depositional sequences. Geological Society of America Bulletin, v. 104, p. 802-813.

Holt, W.E. and Stern, T.A., 1991, Sediment loading on the Western Platform of New Zealand continent: Implcations for the strength of a continental margin. Earth and Planetary Science Letters, v. 107, p. 523-538.

Hori, K., Saito, Y., Zhao, Q., Cheng, X., Wang, P., Sato, Y., Li, C., 2001, Sedimentary facies of the tide-dominated paleo-Changjiang (Yangtze) estuary during the last transgression. Marine Geology, v. 177, p. 331-351.

Hori, K., Saito, Y., Zhao, Q., Wang, P., 2002a, Control of incised-valley fill stacking patterns by accelerated and decelerated sea-level rise: the Changjiang example during the last deglaciation. Geo-Marine Letters, v. 22, p. 127-132.

Hori, K., Saito, Y., Zhao, Q., Wang, P., 2002b, Architecture and evolution of the tide-dominated Changjiang (Yangtze) River delta, China. Sedimentary Geology, v. 146, p. 249-264.

Hori, K., Saito, Y., Zhao, Q., Wang, P., 2002c, Architecture and evolution of the tide-dominated Changjiang (Yangtze) River delta, China. Sedimentary Geology, v. 146, p. 249-264.

Hunt, D. and Tucker, M.E., 1992, Stranded parasequences and the forced regressive wedge systems tract: Deposition during base-level fall. Sedimentary Geology, v. 81, p. 1-9.

Imbrie, J., Hayes, J.D., Martinson, D.G., McIntyre, A., Mix, A.C., Morley, J.J., Pisias, N.G., Prell, W.L., Shackleton, N.J., 1984, The orbital theory of Pleistocene climate: Support from a revised chronology of the marine $\delta^{18}O$ record. In Berger, A.L., Imbrie, J., Hays, J., Kukla, G., Saltzman, B. (eds.), D. Reidel Publishing Company, Dordrecht, Holland, pp. 269-305.

Jervey, M.T., Quantitative geologic modeling of siliciclastic rock sequences and their seismic expression. In Wilgus, C.K., Hastings, B.S., Kendall, C.G.St.C., Posamentier, H.W., Ross, C.A., Van Wagoner, J.C. (eds.), Sea-Level Changes: An Integrated Approach. SEPM Special Publication 42, Society of Exonomic Paleontologists and Mineralogists, Tulsa, p. 47-69.

Journal of Petroleum Geology, 2001, v. 24, no. 4, p. 381-484.

Jun, Y., Shuxi, C., and Healy-Williams, N., 1995, Evolution of the paleo-Kuroshio system and its relation to climate changes since the last interglacial. Marine Geology and Quaternary Geology (Haiyang Dizhi Yu Disiji Dizhi), v. 15, p. 26-40.

Kandel, A., Matins, A., Pacheco, R., 1995, Discussion: On the very real distinction between fuzzy and statistical methods. Technometrics, v. 37, p. 276-281.

Karner, S.L., Chester, F.M., Kronenberg, A.K., Chester, J.S., 2003, Subcritical compaction and yielding of granular quartz sand. Tectonophysics, v. 377, p. 357-381.

Karner, S.L., Chester, J.S., Chester, F.M., Kronenberg, A.K., Hajash, A., Jr., 2005, Laboratory deformation of granular quartz sand: Implications for the burial of clastic rocks. AAPG Bulletin, v. 89, p. 603-625.

Keller, G.H. and Yincan, Y., 1985, Geotechnical properties of surface and near-surface deposits in the East China Sea. Continental Shelf Research, v. 4, p. 159-174.

Kendall, C.G.St.C., Moore, P., Strobel, J., Cannon, R., Perlmutter, M., Bezdek, J., Biswas, G., 1991a, Simulation of the sedimentary fill of basins. In Franseen, E.K., Watney, W.L., Kendall, C.G.St.C., Ross, W. (eds.), Sedimentary Modeling: Computer Simulations and Methods for Improved Parameter Definition, Bulletin 223, Kansas Geological Survey, Lawrence, KS, p. 9-30.

Kendall, C.G.St.C., Strobel, J., Cannon, R., Bezdek, J., Biswas, G., 1991b, The simulation of the sedimentary fill of basins. Journal of Geophysical Research, v. 96, no. B4, p. 6911-6929.

Klir, G.J., 2004, Fuzzy Logic: A specialized tutorial. In Fuzzy Logic in Geology, Elsevier, Amsterdam, p. 11-61.

Knighton, D.A. and Nanson, G.C., 1993, Anastamosis and the continuum of channel pattern. Earth Surface Processes and Lanforms, v. 18, p. 613-625.

Koss, J.E., Ethridge, F.G., and Schumm, S.A., 1994, An experimental study of the effects of baselevel change on fluvial, coastal plain and shelf systems. Journal of Sedimentary Research, v. B64, p. 90-98.

Kukal, Z., 1971, Geology of Recent Sediments. Academic Press, London, 490 pp.

Lavier, L.L., Steckler, M.S., Brigaud, F., 2000, An improved method for reconstructing the stratigraphy and bathymetry of continental margins: Applications to the Cenozoic tectonic and sedimentary history of the Congo margin. American Association of Petroleum Geologists Bulletin, v. 84, p. 923-939.

Laviolette, M., Seaman, J.W., Jr., Barrett, J.D., Woodall, W.H., 1995, A probabilistic and statistical view of fuzzy methods. Technometrics, v. 37, p. 249-261.

Leckie, D.A., 1994, Canterbury Plains, New Zealand – implications for sequence stratigraphic models. American Association of Petroleum Geologists Bulletin, v. 78, p. 1240-1256.

Lee, H.J. and Chough, S.K., 1989, Sediment distribution, dispersal and budget in the Yellow Sea. Marine Geology, v. 87, p. 195-205.

Lee, H.J., Chough, S.K., Jeong, K.S., Han, S.J., 1987, Geotechnical properties of sediment cores from the southeastern Yellow Sea: Effects of depositional processes. Marine Geotechnology, v. 7, p. 37-52.

Lee, S-.M., Kim, J-.W., Baag, C.-E., 2003, 2-D flexural analysis of the Ulleung back-arc basin, East Sea (Sea of Japan). Terrestrial, Atmospheric and Oceanic Sciences, v. 14, no. 4, p. 431-444.

Leeder, M.R. and Stewart, M.D., 1996, Fluvial incision and sequence stratigraphy: Alluvial responses to relative sea-level fall and their detection in the geological record. In Hesselbo, S.P. and Parkinson, D.N. (eds.), Sequence Stratigraphy in British Geology. Geological Society of London, Special Publication 103, p. 25-39.

Leopold, L.B. and Wolman, M.G., 1957, River Channel Patterns: Braided, Meandering and Straight. Geological Survey Professional Paper 282-B, US Government Printing Office, Washington, 85 pp.

Li, F., Dyt, C., Griffiths, C., 2004, 3D modeling of flexural isostatic deformation. Computers and Geosciences, v. 30, p. 1105-1115.

Lisitzin, A.P., 1972, Sedimentation in the world ocean. SEPM Special Publication 17, Society for Economic Paleontologists and Mineralogists, Tulsa, OK, 218 pp.

Liu, X., Rolph, T., Bloemendal, J., Shaw, J., Liu, T., 1995, Quantitative estimates of paleoprecipitation at Xifeng, in the Loess plateau of China. Palaeogeography, Palaeoclimatology, Palaeoecology, v. 113, p. 243-248.

Liu, Z.X., Berne, S., Saito, Y., Lericolais, G., Marsset, T., 2000, Quaternary seismic stratigraphy and paleoenvironments on the continental shelf of the East China Sea: Journal of Asian Earth Sciences, v. 18, p. 441-452.

Lotfi, A. and Tsoi, A.C., 1994, Importance of membership functions: A comparative study on different learning methods for fuzzy inference systems. Proceedings of the Third IEEE Conference on Fuzzy Systems, v. 3, IEEE World Congress on Computational Intelligence, p. 1791-1796.

Lukasiewicz, J., 1957, Aristotle's Syllogistic from the Standpoint of Modern Formal Logic. Clarendon Press, Oxford, 222 pp.

Maher, B.A., and Thompson, R., 1995, Paleorainfall reconstructions from pedogenic magnetic susceptibility variations in the Chinese loess and paleosols. Quaternary Research, v. 44, p. 383-391.

Mamdani, E.H. and Assilian, S., 1975, An experiment in linguistic synthesis with fuzzy logic controller. International Journal of Man-Machine Studies, v. 7, p. 1-13.

Maxwell, J.C., 1960, Experiments on compaction and cementation of sand. In Griggs, D. and Handin, J., (eds.), Rock Deformation (A Symposium), Geological Society of America Memori 79, New York, p. 105-132.

Miall, A.D., 1977, A review of the braided-river depositional environment. Earth-Science Reviews, v. 13, p. 1-62.

Miall, A.D. and Arush, M., 2001, The Castlegate Sandstone of the Book Cliffs, Utah: sequence stratigraphy, paleogeography, and tectonic controls. Journal of Sedimentary Research, v. 71, p. 537-548.

Miller, J.H., Bartek, L.R., Potty, G.R., Tang, D., Na, J. and Qi, Y., 2004, Sediments in the East China Sea. IEEE Journal of Oceanic Engineering, v. 29, p. 940-951.

Milliman, J.D. and Syvitski, J.P.M., 1992, Geomorphic/tectonic control of sediment discharge to the ocean: The importance of small mountainous rivers. The Journal of Geology, v. 100, p. 525-544.

Milliman, J.D., Shen, H-.T., Yang, Z-.S., Meade, R.H., 1985a, Transport and deposition of river sediment in the Changjiang estuary and adjacent continental shelf. Continental Shelf Research, v. 4, p. 37-45.

Milliman, J.D., Beardsley, R.C., Yang, Z-.S., Limeburner, R., 1985b, Modern Huamghe-derived muds on the outer shelf of the East China Sea: Identification and potential transport mechanisms. Continental Shelf Research, v. 4, p. 175-188.

Moore, D.G., Curray, J.R., Raitt, R.W., and Emmel, F.J., 1974, Stratigraphic-seismic section correlations and implications to Bengal Fan history. In von der Borch, C.C., Sclater, J.G., (eds.), Initial Reports of the Deep Sea Drilling Project, US Government Printing Office, Washington, DC, p. 403-412.

Morozova, G.S. and Smith, N.D., 1999, Holocene avulsion history of the lower Saskatchewan fluvial system, Cumberland marshes, Saskatchewan-Manitoba, Canada. *In* Smith, N.D. and Rogers, J. (eds.), 1999, Fluvial Sedimentology VI. Special Publication No. 28 of the International Association of Sedimentologists, Blackwell Science, Oxford, p. 231-249.

Niino, H. and Emery, K.O., 1961, Sediments of shallow portions of the East China Sea and South China Sea. GSA Bulletin, v. 72, p. 731-762.

Nikravesh, M., Aminzadeh, F., Zadeh, L. (eds.), 2003, Soft Computing and Intelligent Data Analysis in Oil Exploration. Developments in Petroleum Science, no. 51, Elsevier, Amsterdam, 744 pp.

Nordlund, U., 1996, Formalizing geological knowledge – with an example of modeling stratigraphy using fuzzy logic. Journal of Sedimentary Research, v. 66, p. 689-698.

Nordlund, U., 1999a, Stratigraphic modeling using common-sense rules. In Harbaugh, J.W., Watney, W.L., Rankey, E.C., Slingerland, R., Goldstein, R.H., Franseen, E.K. (eds.), Numerical Experiemnts in Stratigraphy: Recent Advances in Stratigraphic and Sedimentologic Computer Simulations. SEPM Special Publication #62, Tulsa, OK, p. 245-251.

Nordlund, U., 1999b, FUZZIM: forward stratigraphic modeling made simple. Computers and Geosciences, v. 25, p. 449-456.

Nordlund, U. and Silfversparre, M., 1994, Fuzzy logic – a means for incorporating qualitative data in dynamic stratigraphic modeling. International Association for Mathematical Geology Annual Conference, Proceedings, p. 265-266.

Novak, V. and Perfilieva, I. (eds.), 2000, Discovering the World with Fuzzy Logic. Studies in Fuzziness and Soft Computing, v. 57, Heidelberg,

Orton, G.J. and Reading, H.G., 1993, Variability of deltaic processes in terms of sediment supply, with particular emphasis on grain size. Sedimentology, v. 40, p. 475-51.

Parcell, W.C., 2000, 3D computer simulation of carbonate depositional facies distribution and productivity rates using continuous set theory to mimic geologists' reasoning. Gulf Coast Association of Geological Societies Transactions, v. 50, p. 439-449.

Parcell, W.C., 2003a, Examining the definition and significance of the maximum flooding surface through fuzzy logic modeling. Gulf Coast Association of Geological Societies Transactions, v. 53, p. 659-667.

Parcell, W.C., 2003b, Evaluating the development of Upper Jurassic reefs in the Smackover Formation, eastern Gulf Coast, USA through fuzzy logic computer modeling. Journal of Sedimentary Research, v. 73, p. 498-515.

Park, Y.A., 1987, Continental shelf sedimentation (chapter 25). In, Lee, D. (ed.), Geology of Korea, Kyohak-sa Publishing Company, Geological Society of Korea, Seoul, p. 406-426.

Payton, C.E. (ed.), 1977, Seismic Stratigraphy – Applications to Hydrocarbon Exploration. AAPG Memoir 26, American Association of Petroleum Geologists, Tulsa, 516 pp.

Peper, T., 1993, Quantitative subsidence analysis of the Western Canada foreland basin with implications for short-term facies change. Tectonophysics, v. 226, p. 301-318

Pillans, B., Chappell, J., Naish, T.R., 1998, A review of the Milankovitch climatic beat: template for Plio-Pleistocene sea level changes and sequence stratigraphy. Sedimentary Geology, v. 122, p. 5-21.

Plint, A.G., and Nummedal, D., 2000, The falling stage systems tract: Recognition and importance in sequence stratigraphy. In: Hunt, D., Gawthorpe, R.L. (eds.), Sedimentary Responses to Forced regressions. Geolgoical Society, London, p. 1-17.

Posamentier, H.W., 2001, Lowstand alluvial bypass systems: Incised vs. unincised. AAPG Bulletin, v. 85, p. 1771-1793.

Posamentier, H.W. and Vail, P.R., 1988, Eustatic controls on clastic deposition II – sequence and systems tracts models. In Wilgus, C.K., Hastings, B.S., Kendall, C.G.St.C., Posamentier, H.W., Ross, C.A., Van Wagoner, J.C. (eds.), Sea-Level Changes: An Integrated Approach. SEPM Special Publication 42, Society of Exonomic Paleontologists and Mineralogists, Tulsa, p. 125-154.

Posamentier, H.W. and Allen, G.P., 1999, Siliciclastic Sequence Stratigraphy – Concepts and Applications. SEPM Concepts in Sedimentology and Paleontology #7, Tulsa, 210 p.

Posamentier, H.W., Jervey, M.T., Vail, P.R., 1988, Eustatic controls on clastic deposition I – conceptual framework. In Wilgus, C.K., Hastings, B.S., Kendall, C.G.St.C., Posamentier, H.W., Ross, C.A., Van Wagoner, J.C. (eds.), Sea-Level Changes: An Integrated Approach. SEPM Special Publication 42, Society of Exonomic Paleontologists and Mineralogists, Tulsa, p. 109-124.

Posamentier, H.W., Allen, G.P., James, D.P., Tesson, M., 1992, Forced regressions in a sequence stratigraphic framework: Concepts, examples, and exploration significance. American Association of Petroleum Geologists Bulletin, v. 11, p. 1687-1709.

Pritchard, D.W., 1967, Observations of circulation in coastal plain estuaries. In: Lauff, G.H. (ed.), Estuaries, American Association for the Advancement of Science, Publication 83, Washington, D.C., p. 3-5.

Puig, P., Palanques, A., Guillen, J., 2001, Near bottom suspended variability caused by storms and near-intertidal internal waves on the Ebro mid continental shelf (NW Mediterranean). Marine Geology, v. 178, p. 81-93.

Qian, N. and Dai, D.-Z., 1980, Problems of river sedimentation and the present status of its research in China: Chinese Society Hydraulic Engineers, Proceedings of the International Symposium on River Sedimentation, v. 1, p. 1-39.

Reynolds, D.J., Steckler, M.S., Coakley, B.J., 1991, The role of the sediment load in sequence stratigraphy: The influence of flexural and isostatic compaction. Journal of Geophysical Research, v. 96, no. B4, p. 6931-6949.

Rieke, H.H., III and Chilangarian, G.V., 1974, Compaction of Argillaceous Sediments. Developments in Sedimentology 16, Elsevier, Amsterdam, 424 p.

Ritchie, B.D., Gawthorpe, R.L., Hardy, S., 2004a, Three-dimensional numerical modeling of deltaic depositional sequences 1: Influence of the rate and magnitude of sea-level change. Journal of Sedimentary Research, v. 74, p. 203-220.

Ritchie, B.D., Gawthorpe, R.L., Hardy, S., 2004b, Three-dimensional numerical modeling of deltaic depositional sequences 2: Influence of local controls. Journal of Sedimentary Research, v. 74, p. 221-238.

Rondeau, L., Levrat, E., Brémont, J., 1996, An analytical formulation of the influence of membership functions shape. Proceedings of the Fifth IEEE International Conference on Fuzzy Systems, v. 2, Sept. 8-11, New Orleans, LA, p. 1314-1319.

Rust, B.R., 1978, A classification of alluvial channels. In Miall, A.D., (ed.), Fluvial Sedimentology, Canadian Society of Petroleum Geology Memoir 5, p. 187-198.

Saggaf, M.M. and Nebrija, E.L., 2003, A fuzzy logic approach for the estimation of facies from wire-line logs. AAPG Bulletin, v. 87, p. 1223-1240.

Saito, Y., Katayama, H., Ikehara, K., Kato, Y., Matsumoto, E., Oguri, K., Oda, M., Yumoto, M., 1998, Transgressive and highstand systems tracts and post-glacial transgression, the East China Sea: Sedimentary Geology, v. 122, p. 217-232.

Saito, Y., Yang, Z., Hori, K., 2001, The Huanghe (Yellow River) and Changjiang (Yangtze River) deltas: A review on their characteristics, evolution and sediment discharge during the Holocene. Geomorphology, v. 41, p. 219-231.

Sancho-Royo, A. and Verdegay, J.L., 1999, Methods for the construction of membership functions. International Journal of Intelligent Systems, v. 14, p. 1213-1230.

Sandham, W. and Leggett, M., 2003, Geophysical Applications of Artificial Neural Networks and Fuzzy Logic. Kluwer Academic Publishers, Dordrecht, The Netherlands, 324 pp.

Sarnthein, M. and Wang, P., 1999, Response of West Pacific marginal seas to global climatic change. Marine Geology, v. 156, p. 1-3.

Saucier, R.T., 1994, Geomorphology and Quaternary geologic history of the Lower Mississippi Valley, volume 1. US Army Corps of Engineers, Waterways Experiment Station, Geotechnical Laboratory, Vicksburg, MS, 418 pp.

Schindel, D.E., 1980, Microstratigraphic sampling and the limits of paleontologic resolution. Paleobiology, v. 6, p. 408-426.

Schumm, S.A., 1968, Speculations concerning paleohydraulic controls on terrestrial sedimentation. Geological Society of America Bulletin, v. 79, p. 1573-1588.

Schumm, S.A., 1972, Fluvial paleochannels. *In* Rigby, J.K. and Hamblin, W.K. (eds.), Recognition of Ancient Sedimentary Environments, Society of Economic Paleontologists and Mineralogists Special Publication No. 16, Tulsa, p. 98-107.

Schumm, S.A., 1981, Evolution and response of the fluvial system, sedimentologic implications. SEPM Special Publication 31, p. 19-29.

Schumm, S.A., 1993, River response to base level changes: Implications for sequence stratigraphy. Journal of Geology, v. 101, p. 279-294.

Schumm, S.A., 1999, Causes and controls of incision. In, Darby, S.E. and Andrew, S. (eds.), Incised River Channels: Processes, Forms, Engineering and Management, John Wiley & Sons, Chichester, United Kingdom, p. 19-33.

Schumm, S.A. and Khan, H.R., 1972, Experimental study of channel patterns. GSA Bulletin, v. 83, p. 1755-1770.

Sclater, J.G. and Christie, P.A.F., 1980, Continental stretching: An explanation of the post-mid-Cretaceous subsidence of the central North Sea basin. Journal of Geophysical Research, v. 85, p. 3711-3739.

Shackleton, N.J., 1987, Oxygen isotopes, ice volume and sea level. Quaternary Science reviews, v. 6, p. 183-190.

Shanshu, W., Zuobin, Y., Libin, L., 1990, Hydrocarbon accumulations on China's continental shelf. China Earth Sciences, v. 1, p. 93-109.

Shieh, Y. and Chen, M., 1995, The Ancient Kuroshio Current in the Okinawa Trough during the Holocene. Acta Oceanographica Taiwanica, v. 34, p. 73-80.

Stanley, D.J. and Chen, Z., 1993, Yangtze delta, eastern China: 1. Geometry and subsidence of Holocene depocenter. Marine Geology, v. 112, p. 1-11.

Steckler, M.S., 1999, High-resolution sequence stratigraphic modeling 1: The interplay of sedimentation, erosion, and subsidence. In Harbaugh, J.W., Watney, W.L., Rankey, E.C., Slingerland, R., Goldstein, R.H., Franseen, E.K. (eds.), Numerical Experiemnts in Stratigraphy: Recent Advances in Stratigraphic and Sedimentologic Computer Simulations. SEPM Special Publication #62, Tulsa, OK, p. 139-149.

Steckler, M.S., Reynolds, D.J., Coakley, B.J., Swift, B.A., Jarrard, R., 1993, Modeling passive margin sequence stratigraphy. In Posamentier, H.W., Summerhayes, C.P., Haq, B.U., Allen, G.P., (eds.), Sequence Stratigraphy and Facies Associations, Special Publication no. 18 of the International Association of Sedimentologists, Blackwell Scientific, Oxford, England, p. 19-41.

Stocker, T., 2000, Past and future reorganizations in the climate system. Quaternary Science Reviews, v. 19, p. 301-319.

Stouthamer, E. and Berendsen, H.J.A., 2001, Avulsion frequency, avulsion duration, and interavulsion period of Holocene channel belts in the Rhine-Meuse delta, the Netherlands. Journal of Sedimentary Research, v. 71, p. 589-598.

Syvitski, J.P.M. and Daughney, S., 1992, Delta2: Delta progradation and basin filling. Computers and Geosciences, v. 18, p. 839-897.

Takagi, T. and Sugeno, H., 1985, Fuzzy identification of systems and its application for modeling and control. IEEE Transactions on Systems, Man and Cybernetics, v. 15, p. 116-132.

Talling, P.J., 1998, How and where do incised valleys form if sea level remains above the shelf edge? Geology, v. 26, p. 87-90.

Thorne, J., 1994, Constraints on riverine valley incision and the response to sea-level change based on fluid mechanics. In: Dalrymple, R.W., Boyd, R., Zaitlin, B.A. (eds.), Incised-Valley Systems: Origin and Sedimentary Sequences, SEPM Special Publication no. 51, Society for Sedimentary Geology, Tulsa, p. 29-43.

Törnqvist, T.E., 1994, Middle and late Holocene avulsion history of the River Rhine (Rhine-Meuse delta, Netherlands), Geology, v. 22, p. 711-714.

Törnqvist, T.E. and Bridge, J.S., 2002, Spatial variation of overbank aggradation rate and its influence on avulsion frequency. Sedimentology, v. 49, p. 891-905.

Törnqvist, T.E., Blick, S.J., van der Borg, K., de Jong, A.F.M., Greenberg, J., 2005, Using Holocene relative sea-level data for high-precision measurement of tectonic subsidence rates in the Mississippi Delta. Abstracts with Programs, v. 37, no. 5, Geological Society of America, North-Central Section, 39th Annual Meeting, p. 90.

Turcotte, D.L. and Schubert, G., 2002, Geodynamics. Cambridge University Press, United Kingdom, 456 pp.

Uiijé, H. and Uiijé, Y., 1999, Late Quaternary course changes of the Kuroshio Current in the Ryukyu Arc region, northwestern Pacific Ocean. Marine Micropaleontology, v. 37, p. 23-40.

Vail, P.R., 1987, Seismic stratigraphic interpretation procedure. In: Bally, A.W., (ed.), Atlas of Seismic Stratigraphy: AAPG Studies in Geology no. 27, p. 1-10.

van den Berg, J.H., 1995, Prediction of alluvial channel pattern of perennial rivers. Geomorphology, v. 12, p. 259-279.

van Gelder, A., van den Berg, J.H., Cheng, G., Xue, C., 1994, Overbank and channelfill deposits of the modern Yellow River delta. Sedimentary Geology, v. 90, p. 293-305.

Van Wagoner, J.C., Posamentier, H.W., Mitchum, R.M., Vail, P.R., Sarg, J.F., Loutit, T.S., and Hardenbol, J., 1988, An overview of the fundamentals of sequence stratigraphy and key definitions. In: Wilgus, C.K., Hastings, B.S., Kendall, C.G.S.C., Posamentier, H.W., Ross, C.A., Van Wagoner, J.C. (eds.), Sea-Level Changes: An Integrated Approach, SEPM Special Publication no. 42, Tulsa, p. 39-46.

Van Wagoner, J.C., Mitchum, R.M., Campion, K.M., Rahmanian, V.D. (eds.), 1990, Siliciclastic Sequence Stratigraphy in Well Logs, Cores, and Outcrops: Concepts for High-Resolution Correlation of Time and Facies. AAPG Methods in Exploration Series #7, American Association of Petroleum Geologists, Tulsa, 55 p.

Wageman, J.M., Hilde, T.W.C., Emery, K.O., 1970, Structural framework of the East China Sea and Yellow Sea: AAPG Bulletin, v. 54, no. 9, p. 1611-1643.

Wang, P.P. (ed.), 2001, Computing with Words. John Wiley and Sons, New York, 451 pp.

Wang, Y., 1980, The coast of China. Geoscience Canda, v. 7, p. 109-113.

Wang, J. and Wang, P., 1982, Relationship between sea-level changes and climatic fluctuations in East China since last Pleistocene. The Quaternary Research, v. 21, p. 101-114 (in Japanese).

Wang, Y. and Aubrey, D.G., 1987, The characteristics of the China coastline: Continental Shelf Research, v. 7, no. 4, p. 329-349.

Wang, P., Wang, L., Bian, Y., Jian, Z., 1995, Late Quaternary paleoceanography of the South China Sea: surface circulation and carbonate cycles. Marine Geology, v. 127, p. 145-165.

Warren, J.D. and Bartek, L.R., 2002a, The Metastable Fluvial Shelf System (MFSS): An alternative hypothesis to lowstand unincised fluvial bypass on the East China Sea continental margin. SEPM Research Conference: Incised Valleys: Images and Processes, August 18-23, 2002, Casper and Newcastle, WY.

Warren, J.D. and Bartek, L.R., 2002b, The Sequence Stratigraphy of the East China Sea: Where are the incised valleys? GCSSEPM Foundation Bob F. Perkins Research Conference: Sequence Stratigraphic Models for Exploration and Production: Evolving Methodology, Emerging Models and Applications History, December 8-11, Houston, TX, p. 729-738.

Warren, J.D., Bartek, L.R., and Miller, K.L., 2002, Stratigraphic architecture of the East China Sea continental margin: a case study of eustacy and sediment supply: AAPG Annual Meeting Program, March 10-14, Houston, TX, p. A185.

Warren, J.D., Bartek, L.R., Wang, P.P., and Ramsey, H.N., 2002, Fuzzy logic applied to the geological sciences: an emerging application for seismic interpretation. Proceedings from the Joint Conference on Information Science, March 9-14, Durham, NC, p. 128-132.

Warren, J.D., Bartek, L.R., Wang, P.P., and Ramsey, H.R., 2003, Relative sea-level modeling using fuzzy logic: Proceedings from the Joint Conference on Information Science, September 26-30, 2003, Research Triangle Park, NC, p. 117-120.

Watkins, J.S., Zhiqiang, F., McMillen, K.J., (eds.), 1992, Geology and Geophysics of Continental Margins. Memoir 53, American Association of Petroleum Geologists, Tulsa, 373 pp.

Watney, W.L., Rankey, E.C., Harbaugh, J., 1999, Perspectives on stratigraphic simulation models: Current approaches and future opportunities. In Harbaugh, J.W., Watney, W.L., Rankey, E.C., Slingerland, R., Goldstein, R.H., Franseen, E.K. (eds.), Numerical Experiemnts in Stratigraphy: Recent Advances in Stratigraphic and Sedimentologic Computer Simulations. SEPM Special Publication #62, Tulsa, OK, p. 3-21.

Watts, A.B., Karner, G.D., Steckler, M.S., 1982, Lithospheric flexure and the evolution of sedimentary basins. Philosophical Transactions of the Royal Society of London, Mathematical and Physical Sciences, v. 305, p. 249-281.

Weedon, G.P., 1991, The spectral analysis of stratigraphic time seris. In Einsele, G., Ricken, W., and Seilacher, A., (eds.), Cycles and Events in Stratigraphy, Springer-Verlag, Berlin, p. 840-854.

Weiling, X. and Junying, L., 1989, Structural history of the East China Sea. China Earth Sciences, v. 1, no. 1, p. 59-73.

Weimer, P. and Posamentier, H.W. (eds.), 1990, Siliciclastic Sequence Stratigraphy: Recent Developments and Applications. AAPG Memoir 58, American Association of Petroleum Geologists, Tulsa, 492 pp.

Wellman, H.W., 1979, An uplift map for the South Island of New Zealand and a model for uplift of the Southern Alps. In Walcott, R.I., Cresswell, M.M. (eds.), The Origin of the Southern Alps, Royal Society of New Zealand Bulletin 18, pp. 13-20.

Wellner, R.W. and Bartek, L.R., 2003, The effect of sea level, climate, and shelf physiography on the development of incised valley complexes: a modern example from the East China Sea. Journal of Sedimentary Research., v. 73, p. 926-940.

Wells, J.T., 1996, Subsidence, sea-level rise, and wetlands loss in the lower Mississippi River delta. In Milliman, J.D. and Haq, B.U., (eds.), Sea-level Rise and Coastal Subsidence: Causes, Consequences, and Strategies, Coastal Systems and Continental Margins, v. 2, Kluwer Academic Publishers, Dordrecht, The Netherlands, p. 281-311.

Wells, J.T. and Coleman, J.M., 1984, Deltaic morphology and sedimentology, with special reference to the Indus River Delta. In Haq, B.U. and Milliman, J.D. (eds.), Marine Geology and Oceanography of Arabian Sea and Coastal Pakistan, Van Nostrand Reinhold Company, New York, p. 85-100.

Wentworth, C.K., 1922, A scale of grade and class terms for clastic sediments. Journal of Geology, v. 30, p. 377-392.

Wescott, W.A., 1993, Geomorphic thresholds and complex response to fluvial systems – some implications for sequence stratigraphy. American Association of Petroleum Geology Bulletin, v. 77, p. 1208-1218.

Winkler, M.G. and Wang, P.K., 1993, The late-Quaternary vegetation and climate of China. In Wright, H.E., Jr., Kutbach, J.E., Webb, T., III, Ruddiman, W.F., Street-Perrott, F.A., Bartlein, P.J. (eds.), Global Climates since the Last Glacial Maximum. University of Minnesota Press, Minneapolis, p. 221-261.

Winograd, I.J., Szabo, B.J., Coplen, T.B., Riggs, A.G., 1988, A 250,000-year climatic record from Great Basin vein calcite: Implications for Milankovitch theory. Science, v. 242, p. 1275-1280.

Winograd, I.J., Coplen, T.B., Landwehr, J.M., Riggs, A.C., Ludwig, K.R., Szabo, B.K., 1992, Continuous 500,000-year climate record from vein calcite in devils hole Nevada. Science, v. 258, p. 255-260.

Wolkenhauer, O., 1998, Possibility Theory with Applications to Data Analysis. Research Studies Press Ltd., Taunton, Somerset, England, 261 pp.

Wong, G.T.F., Chao, S.-Y., Li, Y.-L., Shiah, F.-K., 2000, The Kuroshio edge exchange process (KEEP) study – an introduction to hypotheses and highlights. Continental Shelf Research, v. 20, p. 335-347.

Wong, P., Aminzadeh, F., Mikravesh, M. (eds.), 2002, Soft Computing for Reservoir Characterization and Modeling. Studies in Fuzziness and Soft Computing, no. 80, Physica-Verlag, Heidelberg, 586 pp.

Woolfe, K.J. and Balzary, J.R., 1996, Fields in the spectrum of channel style. Sedimentology, v. 43, p. 797-805.

Yang, C.S., 1989, Active, moribund and buried tidal sand ridges in the East China Sea and the southern Yellow Sea: Marine Geology, v. 88, p. 97-116.

Yoshida, S., 2000, Sequence and facies architecture of the upper Blackhawk Formation and the Lower Castlegate Sandstone (Upper Cretaceous), Book Cliffs, Utah. Sedimentary Geology, v. 136, p. 239-276.

Yu, H-.S., 1991, East China Sea Basin revisited: Basin architecture and petroleum potential. Petroleum Geology of Taiwan, v. 26, p. 33-44.

Yunshan, Q. and Fan, L., 1983, Study of influence of sediment loads discharged from the Hunaghe River on sedimentation in the Bohai Sea and the Hunaghai Sea. In Proceedings of International Symposium on Sedimentation on the Continental Shelf with Special Reference to the East China Sea, April 12-16, Hangzhou, China, China Ocean Press, Beijing, p. 83-92.

Yunshan, Q., Yiyang, Z., Lirong, C., Songling, Z. (eds.), 1996, Geology of the East China Sea. Science Press, Beijing, China. 357 pp

Zadeh, L.A., 1965, Fuzzy sets. Information and Control, v. 8, p. 338-353

Zadeh, L.A., 1975, Fuzzy logic and approximate reasoning. Synthese, v. 30, p. 407-428.

Zadeh, L.A., 1985, Syllogistic reasoning in fuzzy logic and its application to usuality and reasoning with dispositions. IEEE Transactions on Systems, Man, and Cybernetics, v. SMC-15, p. 754-763.

Zadeh, L.A., 1995, Discussion: probability theory and fuzzy logic are complementary rather than competitive. Technometrics, v. 37, p. 271-276.

Zhang, G. and Li, C., 1996, The fills and stratigraphic sequences in the Qiantangjiang incised paleovalley, China. Journal of Sedimentary Research, v. 66, p. 406-414.

Zhou, D., Yu, H-.S., Xu, H-.H, Shi, X-.B., Chou, Y-.W., 2003, Modeling of thermo-rheological structure of lithosphere under the foreland basin and mountain belt of Taiwan. Tectonophysics, v. 374, p. 115-134.

Zhu, Y. and Chen, Q., 2005, On the origin of the radial sand ridges in the southern Yellow Sea: Results from the modeling of the paleoradial tidal current fields off the paleo-Yangtze River estuary and northern Jiangsu Coast. Journal of Coastal Research, v. 21, p. 1245-1256.

APPENDIX A

MATLAB CODE FOR *FUZZY*PEACH

```
clear

%  WELCOME TO THE FUZZY PEACH MODEL version February 6, 2005
%  Written by Robert V. Demicco and Jeffrey D. Warren

% Fuzzy Logic Inference Systems must be built using the
% MATLAB Fuzzy Logic Toolbox.  These files have a *.fis
% extension and are needed to run this model.

subsidence = zeros(600,600);
mass_per_time_step = 12e13;

% mass of sediment delta system has in it for a 500 year time
% step units = square km. FOR EXAMPLE: 12e13 = 240 tons/yr

total_tectonic_subsidence =  50

% units = meters, external subsidence max at center of deepest
% part of basin – linearly interpolated away from that point
% SET TO 0 FOR NO EXTERNAL SUBSIDENCE

% ************DATA LOADING*****************************

%data = xlsread('junk_1.xls')
%uncomment this line if reading dataset from Excel

load setup_2.mat

% THERE MAY BE MORE THAN ONE SETUP FILE, BE SURE TO LOAD THE
% ONE YOU WANT.

load sealevel.mat % THIS IS THE DIGITIZED SPECMAP CURVE
sedsurface = Z1;

%************DATA ENTRY AND SETUP*****************

store = zeros(120,120,200,2);

% this command sets up a matrix to store all the values for
% the matrix calculations for points in the X and Y axes of
% matrix storing only 100 points instead of 500 and
% undersampling by 1/5
```

```
grainsize_2=readfis('river_grainsize');

% FIS of sed relative to lateral distance from subaerial
% channel

dump_2 = readfis('river_dump');

% FIS of sed amount relative to lateral distance from
% subaerial channel

compact = readfis('compaction');

% compaction routine read in here

sub_2=readfis('subsidence');
AA = readfis('avulsion');

total_thickness_of_deposit = zeros(600,600);

grd = gradient(sea_level);  %will be used to define gradient
of SPECMAP curve (+ or -)


%********MAIN PROGRAM DO LOOP STARTS HERE***************

for numbertimesteps = 1:389;

% change second variable in ratio for total number of time
% steps (389 MAX)

% next part of code determines delta FIS based on sea level
% movement(up, down or % neutral).  The final model made both
% the rising and falling delta FISs the same by simulating a
% shoreface

     if grd(numbertimesteps) <= 0
     % this means if sea level is falling or neutral

        dump = readfis('delta_dump_shoreface');

% FIS that creates amount of sed deposited in delta relative
% to river mouth

        grainsize = readfis('delta_grainsize_shoreface');

%FIS codes grain size across delta with respect to river mouth
```

```
     else
        dump = readfis('delta_dump_rising');

% FIS that creates amount of sed deposited in delta relative
% to river mouth

        grainsize = readfis('delta_grainsize_rising');

% FIS codes grain size across delta with respect to
% river mouth

      end
         numbertimesteps

% END FIS decision based on sea level movement

% This next block of code controls river incision which is
% still in a prototype format.  Uncommenting thelines below
% will allow erosion to occur between user-defined time steps.
% In this case, erosion is simply negative deposition
% (deposition in a downward direction).

       dump_2 = readfis('river_dump');

       %if numbertimesteps > 250
       %   if sea_level(numbertimesteps)<(-100)
       %     if grd(numbertimesteps)<=0
       %         dump_2 = readfis('river_erode');
       %     end
       %   end
       %end

       %if numbertimesteps >= 340;
       %    if numbertimesteps <= 360;
       %        avulsion_flag = 0
       %        if grd(numbertimesteps)>=0
       %            dump_2 = readfis('river_erode');
       %        end
       %    end
       %end

% END INCISION CONTROL

       depth = sea_level(numbertimesteps) - sedsurface;

% THIS LINE CALCULATES WATER DEPTH OVER THE PLATFORM
```

```
% *******START INITIAL RIVER CHANNEL SETUP*******************


% SET UP initial channel to start in the center of the model
% tells model not to avulse on first time step

  if numbertimesteps == 1;
        avulsion_flag = 0;
        scoop_1 = sedsurface(:,1);
        [value index] = min(scoop_1);
        river_x(1) = index;
        river_y(1) = 1;
        river_z(1) = sedsurface(index,1);
        for n = 2:600;
            river_y(n) = n;
            foo(1) = sedsurface(river_x(n-1)+1,n);
            foo(2) = sedsurface(river_x(n-1),n);
            foo(3) = sedsurface(river_x(n-1)-1,n);
            [value,index]= min(foo);
                if index == 1;
                    river_x(n) = river_x(n-1)+1;
                    river_z(n) = sedsurface(river_x(n-1)+1,n);
                elseif index == 2;
                    river_x(n) = river_x(n-1);
                     river_z(n) = sedsurface(river_x(n-1),n);
                elseif index == 3;
                    river_x(n) = river_x(n-1)-1;
                    river_z(n) = sedsurface(river_x(n-1)-1,n);
                end
                if river_z(n) <= sea_level(numbertimesteps);
                    river_mouth_x = river_x(n)
                    river_mouth_y = river_y(n)
                break
                end
        end

   end

% ********END INITIAL RIVER CHANNEL SETUP*************

% **** THIS NEXT BLOCK OF CODE CHANGES THE LOCATION OF THE
% RIVER MOUTH AND THE RIVER CHANNEL **********

if avulsion_flag == 0;
    depth_at_river_mouth = depth(river_mouth_x,river_mouth_y);
```

```
            if depth_at_river_mouth >= 0;
                for s = (river_mouth_y):-1:1
                  s;
                  foo_1 = depth(river_x(s),river_y(s));
                   if foo_1 <= 0;
                     river_mouth_x = river_x(s);
                     river_mouth_y = river_y(s);
                     river_x = river_x(1:river_mouth_y);
                     river_y = river_y(1:river_mouth_y);
                     river_z = river_z(1:river_mouth_y);
                     break
                   end
                end
            elseif depth_at_river_mouth < 0
             for n = river_mouth_y+1:600;

% these next two if-then statements keep the river from
% avulsing outside of the model

            river_y(n) = n;
                if river_x(n-1) == 600;
                    river_x(n-1) = 599;
                end
                if river_x(n-1) == 1;
                    river_x(n-1) = 2;
                end

            foo(1) = sedsurface(river_x(n-1)+1,n);
            foo(2) = sedsurface(river_x(n-1),n);
            foo(3) = sedsurface(river_x(n-1)-1,n);
            [value,index]= min(foo);
                if index == 1;
                     river_x(n) = river_x(n-1)+1;
                     river_z(n) = sedsurface(river_x(n-1)+1,n);
                elseif index == 2;
                     river_x(n) = river_x(n-1);
                      river_z(n) = sedsurface(river_x(n-1),n);
                elseif index == 3;
                     river_x(n) = river_x(n-1)-1;
                     river_z(n) = sedsurface(river_x(n-1)-1,n);
                end
                if river_z(n) <= sea_level(numbertimesteps);
                     river_mouth_x = river_x(n);
                     river_mouth_y = river_y(n);
                 break
                 end
             end
```

```
            end

% here is where river breaks and follows low points if
% avulsion is called for

elseif avulsion_flag == 1
          length = size(river_y);
          length(2);
          break_point = round(rand*(length(2) - 10));
          if break_point < 2;
              break_point = 2;
          end

          junk_1 = river_x(1:break_point);
          junk_2 = river_y(1:break_point);
          junk_3 = river_z(1:break_point);
          clear river_x;
          clear river_y;
          clear river_z;
          river_x(1:break_point) = junk_1;
          river_y(1:break_point) = junk_2;
          river_z(1:break_point) = junk_3;


     for n = break_point+1:600;
          river_y(n) = n;
          if river_x(n-1) == 600;
                     river_x(n-1) = 599;

% keeps break point of river from getting to edge of model

                end
                if river_x(n-1) == 1;
                    river_x(n-1) = 2;
                end

            foo(1) = sedsurface(river_x(n-1)+1,n);
            foo(2) = sedsurface(river_x(n-1),n);
            foo(3) = sedsurface(river_x(n-1)-1,n);

            [value,index]= min(foo);
                if index == 1;
                    river_x(n) = river_x(n-1)+1;
                    river_z(n) = sedsurface(river_x(n-1)+1,n);
                elseif index == 2;
                    river_x(n) = river_x(n-1);
                     river_z(n) = sedsurface(river_x(n-1),n);
```

```
                elseif index == 3;
                    river_x(n) = river_x(n-1)-1;
                    river_z(n) = sedsurface(river_x(n-1)-1,n);
                end
                if river_z(n) <= sea_level(numbertimesteps);
                    river_mouth_x = river_x(n)
                    river_mouth_y = river_y(n)
                break
                end
        end

        end


% These next 6 lines of code will calculate the
% radial distance of every point on the sedsurface with
% respect to the river mouth site x and y

x_33 = river_mouth_y;
y_33 = river_mouth_x;
x_new = ((-x_33+1:1:(600-x_33)));
y_new = ((-y_33+1:1:(600-y_33)));
[X_pol,Y_pol] = meshgrid(x_new,y_new);
[TH,R] = cart2pol(X_pol,Y_pol);

% converts to polar coordinates to get radial distance

screen_1 = R <= 400;

% setting up logical matrices if distance in R is less than
% or equal to 100 km from the river mouth then value in
% screen_1 = 1, if further than 100 km value = 0;

screen_2 = R>400;

% screen set for distances > 100, screen_2 will equal 1 for
% all values >100 and 0 for all values <= 100

R_1 = ones(600,600)*400;
R = R.*screen_1 + R_1.*screen_2;

screen_1 = depth <= 200;

% screen set up for depth, screen_1 = 1 where statement is
% true, 0 where false

screen_2 = depth > 200;
```

```
% screen set up for depth, screen_2 = 1 where statement is
% true, 0 where false

depth_1 = ones(600,600)*200;
depth  = depth.*screen_1 + depth_1.*screen_2;

% makes all values >200 equal to 200 for FIS

% uncomment the two lines below to save a movie file of model
% view(-120,80)
% M(numbertimesteps) = getframe;

dude_1 = reshape(depth,600*600,1);

% reshapes X values from matrix array to a single column,
% running columns of data through an FIS is much more
% efficient

dude_2 = reshape(R,600*600,1);

tic

% starts timing how long the calculation below will take

thickness = evalfis([dude_1 dude_2 ], dump);
color_1   = evalfis([dude_1 dude_2 ], grainsize);

toc

% stops timing and reports length of the above calculation

screen = depth>=0;
screen_2 = depth<0;

AAA = reshape(thickness,600,600);
color_1 = reshape(color_1,600,600);
B = AAA.*screen;
C = color_1.*screen;

warning off

for j=1:600
    if j<= river_mouth_y

        R(:,j) = abs(Y1(:,j) - river_x(j));
    else
```

```
        R(:,j) = abs(Y1(:,j)- river_mouth_x);
    end
  end

dude_1 = reshape(R,600*600,1);

% reshapes X values from matrix array to a single column,
% running columns of data through an FIS is more efficient

   tic
   thickness_2 = evalfis([dude_1  ], dump_2);
   color_2   = evalfis([dude_1  ], grainsize_2);
   toc
   thickness_2 = reshape(thickness_2,600,600);
   %.*maxchannelsedrate;
   color_2 = reshape(color_2,600,600);

   thickness_2 = thickness_2.*screen_2;

   color_2 = color_2.*screen_2;

%MASS BALANCE CALCULATION

    volume_sed = sum(sum(AAA))*10^6
    mass_sed = volume_sed*1322

%assumes 2643 density * .50 porosity

    multiplier = mass_per_time_step/mass_sed
    B = B.*multiplier;

    AAA = thickness_2 + B;

% AAA contains the values for the amount of sediment deposited
% at every 500X500 point of the matrix at this
% time step in both the river and the delta.


    color = C + color_2;

% AAA contains the values for the type of sediment deposited
% at every 600 x 600 point of the matrix at this
% time step in both the river and the delta.

%END OF MASS BALANCE CODE

%Draws the sediment type for each time step in window
```

```
sedsurface = sedsurface + AAA;
subplot(2,2,1),
surf(X1(1:5:600,20:5:600),Y1(1:5:600,20:5:600), ...
sedsurface(1:5:600,20:5:600),color(1:5:600,20:5:600), ...
'edgecolor', 'none')

view(60,60)
axis([1 600 1 600 -1000 200])
title((194.5-numbertimesteps*.5)*1000)
%counts backwards in time for each time step


% remove comment from line below to save a MOVIE file of the
% model run

%M(numbertimesteps) = getframe;
drawnow

%Draws the sea level curve in window

subplot(2,2,2),
plot(1:numbertimesteps,sea_level(1:numbertimesteps),'.')
axis([1 389 -210 10])
grid on
title('IDEALIZED SEA LEVEL CURVE');
drawnow

% If needed, this code below will draw the longitudinal river
% profile

%subplot(2,2,3), plot(river_y,river_z);
%title('LONGITUDINAL RIVER PROFILE');
%drawnow
%subplot(2,2,4), surf(AAA(1:5:600,1:5:600)'edgecolor',...
%'none'));
%axis([1 120 1 120 0 4])
%view(60,60)

store(:,:,numbertimesteps,1) =  AAA(1:5:600,1:5:600);
%stores thickness for every 5th grid node

store(:,:,numbertimesteps,2) =  color(1:5:600,1:5:600);
%stores sediment type for every 5th grid node

% These few lines allow tectonic subsidence set in line 13
% to occur only during OIS 6
```

```
if numbertimesteps < 140
      sedsurface = sedsurface + ...
      subsidence.*(total_tectonic_subsidence/389);
      Z1 = Z1 + subsidence.*(total_tectonic_subsidence/389);
end

%  Implementation of FIS for compaction-type subsidence
%  junk_1 = reshape(AAA,600*600,1);
%  junk_2 = evalfis([junk_1], sub_2);
%  junk_2 = reshape(junk_2,600,600);
%  sedsurface = sedsurface - junk_2;

% Draws isopach map in window

total_thickness_of_deposit = total_thickness_of_deposit + AAA;
subplot(2,2,3),...
surf(total_thickness_of_deposit(1:10:600,1:10:600));
title('CUMULATIVE ISOPACH');
axis([0 60 0 60 0 150]);
view(60,60);
drawnow

% Draws structure map in window

subplot(2,2,4),surf(sedsurface(1:10:600,1:10:600));
axis([5 60 0 60 -150 50]);
title('STRUCTURE MAP');
view (60,60);
drawnow

% THE NEXT 5 LINES OF CODE HANDLE AVULSION WITH A FIS

foo_2 = rand*100;
probabil = evalfis([sea_level(numbertimesteps)
grd(numbertimesteps)], AA)
avulsion_flag = 0
if foo_2< probabil
     avulsion_flag =1;
end

end

%**** MAIN PROGRAM DO LOOP ENDS HERE ***************

why(round(rand.*1000))
```

```
% This last comment returns a random answer to the
% philosophical question "Why?" in order to let the user
% know the model has completed the simulation.
```

APPENDIX B

MATLAB CODE FOR MARGIN GEOMETRY SETUP FOR *fuzzy*PEACH

```
clear

% The following values establish an x-y matrix that creates
% the margin idealized margin used in fuzzyPEACH simulations.
% The units are in km and the dimensions are 600 x 600 km^2.

x = [1 100 200 300 400 500 600; ...
1 100 200 300 400 500 600; ...
1 100 200 300 400 500 600; ...
1 100 200 300 400 500 600; ...
1 100 200 300 400 500 600; ...
1 100 200 300 400 500 600 ];

y = [1  1  1  1   1   1   1; ...
100 100 100 100 100 100 100; ...
200 200 200 200 200 200 200; ...
300 300 300 300 300 300 300; ...
400 400 400 400 400 400 400; ...
500 500 500 500 500 500 500; ...
600 600 600 600 600 600 600 ];

% The folling values are the elevation of the margin surface
% relative to modern sea level.

z = [ 3  -30 -60 -90 -120 -150 -1000; ...
      2  -31 -61  -91 -121 -151 -1001; ...
      1  -32 -62 -92  -122 -152 -1002; ...
      0  -33 -63  -93 -123 -153 -1003; ...
      1  -32 -62 -92  -122 -152 -1002; ...
      2  -31 -61  -91 -121 -151 -1001; ...
      3  -30 -60 -90 -120 -150 -1000];

[X1, Y1] = meshgrid(1:600,1:600);
Z1 = interp2(x,y,z,X1,Y1);
surf(X1(1:5:600,1:5:600),Y1(1:5:600,1:5:600), ...
Z1(1:5:600,1:5:600))
view(60,60)
clear x, clear y, clear z;
save setup_2.mat
% saves data to be used as input by fuzzyPEACH
```

APPENDIX C

MATLAB CODE FOR SEA LEVEL CURVE FOR *fuzzy*PEACH

```
clear

% ***********************************************************
% THIS PROGRAM GENERATES GENERIC SINE WAVES TO MIMIC
% IDEALIZED PLEISTOCENE EUSTASY BASED ON MILANKOVITCH BANDS
% 21 ka = precession, 40 ka = obliquity, 100 ka = eccentricity
%***********************************************************

time_step  = 500;
run_duration =  195000;   %set in years

sin_1_height    =  60;%2.5;  %in meters
sin_1_period    =  195000; % in years
sin_1_phase_lag =  .25 %betweein 0 and 2

sin_2_height    =  0;  %in meters  9
sin_2_period    =  20000; % in years
sin_2_phase_lag =  0.35; %between 0 and 2

sin_3_height    =  0;  %really amplitude in meters
sin_3_period    =  2000000; % in years
sin_3_phase_lag =  0.0 ;%between 0 and 2

sin_4_height    =  0;%4.00;  %in meters
sin_4_period    =  20000; % in years
sin_4_phase_lag =  0; %between 0 and 2

sin_5_height    =  0;  %in meters
sin_5_period    =  210000; % in years
sin_5_phase_lag =  0; %between 0 and 2

saw_tooth_height =  0;%2;% 25
saw_tooth_period = 100000;
saw_tooth_max    =  0.25;

n=1:time_step:run_duration;

C_level_1 = sin_1_height*sin( (2.0*pi) *
(n./sin_1_period)+(2*pi*sin_1_phase_lag));
C_level_2 = sin_2_height*sin( (2.0*pi) *
(n./sin_2_period)+(2*pi*sin_2_phase_lag));
C_level_3 = sin_3_height*sin( (2.0*pi) *
(n./sin_3_period)+(2*pi*sin_3_phase_lag));
```

```
C_level_4 = sin_4_height*sin( (2.0*pi) *
(n./sin_4_period)+(2*pi*sin_4_phase_lag));
C_level_5 = sin_5_height*sin( (2.0*pi) *
(n./sin_5_period)+(2*pi*sin_5_phase_lag));


complete_saw_teeth = ceil(run_duration/saw_tooth_period);
inter_times = zeros(1,complete_saw_teeth*2+2);
inter_heights = zeros(1,complete_saw_teeth*2+2);
inter_times(1) = 1;
inter_heights(1) = -saw_tooth_height/2;

counter = 2;

for q=2:complete_saw_teeth+1;
    inter_times(counter) = ((q-1)*saw_tooth_period) -
saw_tooth_period*(1-saw_tooth_max);
    inter_heights(counter) = saw_tooth_height/2;
    counter = counter+1 ;
    inter_times(counter) = (q-1)*saw_tooth_period;
    inter_heights(counter) = -saw_tooth_height/2 ;
    counter = counter+1;
end
C_level_6 = interp1(inter_times,inter_heights,n,'linear');
C_level  = C_level_1 + C_level_2 + C_level_3 + C_level_4 +
C_level_5 + C_level_6;
sea_level = C_level - 60;
%figure
plot(sea_level)
title('Idealized Regular Amplitude Sea Level');
axis([0 389 -200 50]);
grid on;

save sealevel.mat
return

% The sealevel.mat file is needed for input in the fuzzyPEACH
```

APPENDIX D

MATLAB CODE FOR CREATION OF ISOPACH MAPS

```
clear

% this isopach program is interactive, you will be prompted
% for the time step to start the isopach and the time step to
% end the isopach.  You will need to load a mat file for a
% saved run with the following lines

% step 1 - load the file you wish to isopach
% type: load <filename>.mat (run_1.mat is the model data file)

% if there is already a loaded file in MATLAB, just keep those
% lines commented out

thickness_all = store(:,:,:,1);
color_all = store(:,:,:,2);

% step 2 - rearrange the data sets so that time steps
% are first dimension

rearranged_thickness = permute(thickness_all,[3 2 1 ]);
rearranged_color = permute(color_all, [3 2 1]);

% you will be prompted for the start and stop times.

start_timestep = input('ENTER TIME STEP FOR START OF ...
ISOPACH \n \n');
end_timestep = input('ENTER TIME STEP FOR END OF ...
ISOPACH \n \n');

junk = sum(rearranged_thickness...
(start_timestep:end_timestep,:,:));
junk = permute(junk, [2 3 1]);
[X,Y] = meshgrid(1:5:600,1:5:600);
[c,h]= contour(X,Y,junk);
clabel(c,h);
view(90,270)
xlabel('km')
ylabel('km')
volume = sum(sum(abs(junk)))*25;
volume = volume*10^(-3);
title(volume);
```

APPENDIX E

MATLAB CODE FOR DIP-ORIENTED CROSS-SECTION VIEWER

```
%need to load the data for the run you want

tic
% load <filename>.mat (file name is generic)
toc

% clear only selected data files from simulation
clear specmap, clear new_dope, clear index;
clear avulsion_flag

% step 1 - break out all thickness and all color data
% from storage array
thickness_all = store(:,:,:,1);
color_all = store(:,:,:,2);

% step 2 - rearrange the data sets so that time steps are
% first dimension
rearranged_thickness = permute(thickness_all,[3 2 1 ]);
rearranged_color = permute(color_all, [3 2 1]);

% step 3 - pull out a strike line to plot.
% Note that the data in fuzzyPEACH only saves every 5th column

dip_line_location =  300
% enter integer for dip line you want from dataset (in km)

model_line_location = round(dip_line_location/5);
dip_line_thickness_data =  rearranged_thickness...
(:,:,model_line_location);
dip_line_color_data = rearranged_color...
(:,:,model_line_location);


% step 4 - find the topo line of the surface at the
% location in question
base_profile = Z1(dip_line_location,1:5:600);
reshaped_base_profile = reshape(base_profile,1,120);

% step 5 accumulate the thickness data
z = cumsum(dip_line_thickness_data);
z_2 = sum(dip_line_thickness_data);
for n=1:(numbertimesteps);
```

```
    for m=1:120;
       z_in_depth(n,m) = z(n,m) + reshaped_base_profile(m);
  end
end

% set up the x and y coordinate grids to plot the data on
y = ones(numbertimesteps,120);
%.*strike_line_location here to plot multiple strike lines;
x = meshgrid(1:120,1:numbertimesteps);2

surf(z_in_depth,strike_line_color_data,'EdgeColor','none');
view(0, 0)
```

APPENDIX F

MATLAB CODE FOR STRIKE-ORIENTED CROSS-SECTION VIEWER

```
% need to load the file into memory
tic
%load <filename>.mat
toc

clear specmap, clear new_dope, clear index, ...
clear avulsion_flag
% step 1 - break out all thickness and all color data from
% storage array
thickness_all = store(:,:,:,1);
color_all = store(:,:,:,2);

% step 2 - rearrange the data sets so that time steps are
% first dimension
rearranged_thickness = permute(thickness_all,[3 1 2 ]);
rearranged_color = permute(color_all, [3 1 2]);

% step 3 - pull out a dip line to plot.
% Note that the data only saves every fifth column.

strike_line_location =  500
% enter integer for line you want from original model

model_line_location = round(strike_line_location/5);
strike_line_thickness_data =
rearranged_thickness(:,:,model_line_location);
strike_line_color_data =
rearranged_color(:,:,model_line_location);

% step 4 - find the topo line of the surface at the location
% in question
base_profile = Z1(1:5:600,dip_line_location);
reshaped_base_profile = reshape(base_profile,1,120);

% step 5 accumulate the thickness data
z = cumsum(strike_line_thickness_data);
z_2 = sum(strike_line_thickness_data);

for n=1:(numbertimesteps);
    for m=1:120;
      z_in_depth(n,m) = z(n,m) + reshaped_base_profile(m);
  end
```

```
end

% set up the x and y coordinate grids to plot the data on
y = ones(numbertimesteps,120);

%.*dip_line_location here to plot multiple strike lines;
x = meshgrid(1:120,1:numbertimesteps);2

surf(z_in_depth,strike_line_color_data,'EdgeColor','none');
view(0, 0)
```